ANNUAL REVIEW

INSTITUTE FOR MOLECULAR SCIENCE

OKAZAKI, JAPAN

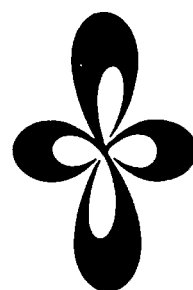## 1979

ANNUAL REVIEW

INSTITUTE FOR MOLECULAR SCIENCE

OKAZAKI, JAPAN

1979

IMS 1979

It is our pleasure to publish the Annual Review 1979 which is the report on the state and activity of IMS during a year since August 1978. IMS which was established in 1975 has attained to its fifth year. This year, supported by the government funds, the construction of buildings made progress as favorably as expected. The Computer Center started to work as soon as it became ready for occupancy in January. At the end of March, Administration Office, Library and Low-Temperature Center were brought to completion. The Main Laboratory was also completed. The total area of buildings is now 24,020 m^2.

Two Research Laboratories have been newly established. Laboratory of Excited State Dynamics was initiated by Prof. I. Hanazaki who moved from Osaka Univ., with Assoc. Prof. N. Nishi. Laboratory of Photochemistry started in March when Prof. K. Kimura transfered from Hokkaido Univ. to the chair of the Laboratory. Dr. K. Shobatake came to the same Laboratory as Assoc. Professor.

It is an important role of IMS to work effectively as the inter-university research institute. A progress has been made on this aspect. The Computer Center with powerful computers can offer exciting opportunities to the scientists. The Instrument Center was enriched with the preparation of equipments and instruments which are ready for common use. The Low-Temperature Center came into operation. The role of iner-university research institute is not only just the service but also activities which encourage research in the related fields on the basis of molecular aspects and stimulate collaborative work to develop new methods of molecular science. The joint studies and symposia in IMS are now widely known and highly appreciated among the scientists. It is hoped that such an activity could be extended to the international collaboration.

The research at IMS is basic studies concerned with molecular structure and their functions. The subjects of investigation are not restricted, but can be selected by individuals according to the internal demands of their own scientific interest. Needless to say, the members of the institute are bound together with their common scientific interests. There is a tendency that they make a research program spontaneously putting together their scientific demands. It is a merit of research institute. However, scientific studies of today are highly institutionalized. Under such a condition, there is general trend that a fruitful progress can be expected in the region where the internal demand of scientists contacts with the demand of human society. We have the special research programs which are concerned with the molecular process of energy conversion and the molecular designing for useful materials. These subjects are believed to be at the contact point between scientific interest and world needs of today.

(August, 1979)

Hideo Akamatu
Director

i

CONTENTS

ORGANIZATION AND STAFF

Organization

The Institute for Molecular Science, upon completion, will comprise 15 research laboratories—each staffed by a professor, an associate professor, two research associates and a few technical associates—and five research facilities. The laboratories are grouped into five divisions as follows:

Division of Theoretical Studies	Theoretical Studies I
	Theoretical Studies II[1]
	Theoretical Studies III[2]
Division of Molecular Structure	Molecular Structure I
	Molecular Structure II[2]
	Molecular Dynamics[3]
Division of Electronic Structure	Excited State Chemistry
	Excited State Dynamics
	Electronic Structure[2]
Division of Molecular Assemblies	Solid State Chemistry
	Photochemistry
	Molecular Assemblies Dynamics[1]
	Molecular Assemblies[2]
Division of Applied Molecular Science	Applied Molecular Science I
	Applied Molecular Science II[2]
Five Research Facilities are:	Computer Center
	Instrument Center
	Low-Temperature Center
	Chemical Materials Center
	Development Workshop

[1] To be established.
[2] Professors and associate professors are adjunct professors from universities.
[3] Established in 1979.

COUNCIL

Hideo AKAMATU, Director-General

Counsellors

Chairman   Masao KOTANI, President, The Science University of Tokyo
Vice-Chairman   Saburo NAGAKURA, Professor, The University of Tokyo
Melvin CALVIN, Professor, University of California, U.S.A.
Kenichi FUKUI, Professor, Kyoto University
Heinz GERISCHER, Director, Fritz-Haber Institut der Max-Planck-Gesellschaft
Kodi HUSIMI, President, Japan Science Council
Naotaka ISHIZUKA, President, Nagoya University
Keiya KANDA, President, Kyushu University
Yonezo MORINO, Professor Emeritus, The University of Tokyo
Sogo OKAMURA, Professor Emeritus, The University of Tokyo
Kazuo SAITO, Professor, Tohoku University
Shoji SHIBATA, Professor Emeritus, The University of Tokyo
Yataro TAJIMA, Director-General, National Institute of Genetics
Yasutada UEMURA, Professor, The University of Tokyo
Tadao UMESAO, Director-General, National Museum of Ethnology
Itaru WATANABE, Professor, Keio University
Yasuhide YUKAWA, Professor Emeritus, Osaka University

The Council is the advisory board for the Director-General. Two of the counsellors are selected among distinguished foreign scientists.

STAFF

Hideo AKAMATU, Director-General
Misaku MATSUZAWA, Administrative Director

Scientific Staff

Division of Theoretical Studies
   Theoretical Studies I

Keiji MOROKUMA	Professor
Masaru TSUKADA	Associate Professor
Shigeki KATO	Research Associate
Chikatoshi SATOKO	Research Associate
Shigeru NAGASE	Technical Associate
Iwao OHMINE	Research Fellow
Setsuko NAKAGAWA	Visiting Scholar from Kitasato Univ. (-March 79)
Masami KUSUNOKI	Visiting Scholar from Meiji Univ. (April 79-)
Keiichi YANO	Graduate Student from Waseda Univ. (October 78-)
Mitsuyasu HANAMURA	Graduate Student from Tohoku Univ. (April 79-)

   Theoretical Studies II

Katsunori HIJIKATA	Adjunct Professor from Univ. of Electro-Communications (-March 79)
Teijiro YONEZAWA	Adjunct Professor from Kyoto Univ. (April 79-)

2

Haruo HOSOYA	Adjunct Associate Professor from Ochanomizu Univ. (-March 79)
Suehiro IWATA	Adjunct Associate Professor from the Inst. for Phys. Chem. Res. (April 79-)
Kazuo KITAURA	Research Associate

Division of Molecular Structure
Molecular Structure I

Eizi HIROTA	Professor
Shuji SAITO	Associate Professor
Chikashi YAMADA	Research Associate
Yasuki ENDO	Research Associate
Kentarou KAWAGUCHI	Technical Associate
Masao KAKIMOTO	Research Fellow
Keiichi NAGAI	Research Fellow
Nobukimi OHASHI	Visiting Scholar from Kanazawa Univ. (-March 79)
Kazuhiko YOSHIDA	Graduate Student from Sophia Univ. (-March 79)
Keiji MATSUMURA	Graduate Student from Kyushu Univ. (-March 79)

Molecular Structure II

Kozo KUCHITSU	Adjunct Professor from the Univ. of Tokyo (-March 79)
Masamichi TSUBOI	Adjunct Professor from the Univ. of Tokyo (April 79-)
Michio TAKAMI	Adjunct Associate Professor from the Inst. for Phys. Chem. Res. (April 78-)

Division of Electronic Structure
Excited State Chemistry

Keitaro YOSHIHARA	Professor
Tadayoshi SAKATA	Associate Professor
Nobuaki NAKASHIMA	Research Associate
Tomoji KAWAI	Research Associate
Keiji KAMOGAWA	Research Fellow

Excited State Dynamics

Ichiro HANAZAKI	Professor
Nobuyuki NISHI	Associate Professor
Iwao NISHIYAMA	Research Associate
Hisanori SHINOHARA	Research Associate
Susumu KUWABARA	Graduate Student from Osaka Univ. (April 79-)

Electronic Structure

Mitsuo ITO	Adjunct Professor from Tohoku Univ. (June 78-)
Masahiro MATSUOKA	Adjunct Associate Professor from Kyoto Univ. (June 78-)

Division of Molecular Assemblies
Solid State Chemistry

Hiroo INOKUCHI	Professor
Inosuke KOYANO	Associate Professor
Kenichiro TANAKA	Research Associate
Kazuhiko SEKI	Research Associate
Naoki SATO	Technical Associate
Tatsuhisa KATO	Technical Associate
Kazumichi NAKAGAWA	Research fellow
Kiyoshi TAKAGI	Graduate Student from Nagoya Univ. (-March 79)

Photochemistry

Katsumi KIMURA	Professor
Kosuke SHOBATAKE	Associate Professor
Yohji ACHIBA	Research Associate
Kiyohiko TABAYASHI	Research Associate
Katsunori NOMOTO	Graduate Student from Hokkaido Univ. (April 79 - June 79)
Yoshinori KAKUTA	Graduate Student from Hokkaido Univ. (April 79-)

Molecular Assemblies

Ikuji TSUJIKAWA	Adjunct Professor from Kyoto Univ. (-March 79)
Yuji MORI	Adjunct Professor from Tokyo Inst. of Tech. (April 79-)
Mizuka SANO	Adjunct Associate Professor from Univ. of Electro-Communications (April 78-)
Gunji SAITO	Research Associate

Division of Applied Molecular Science
Applied Molecular Science I

Hiizu IWAMURA	Professor
Tasuku ITO	Associate Professor
Tadashi SUGAWARA	Research Associate
Koshiro TORIUMI	Research Associate
Yuzo KAWADA	Technical Associate
Yoshinori NISHIZAWA	Research Fellow
Morimatsu KATOH	Graduate Student from Nagoya Inst. of Tech. (October 78-)
Takahiko OOSUMI	Graduate Student from Ehime Univ. (April 79-)

Applied Molecular Science II

Yoshihiko SAITO	Adjunct Professor from the Univ. of Tokyo (-March 79)
Junnosuke FUJITA	Adjunct Professor from Nagoya Univ. (April 79-)
Teruyoshi SAKATA	Adjunct Associate Professor from Osaka Univ. (April 78-)

Research Facilities
Computer Center

Hiroshi KASHIWAGI	Associate Professor
Shigeru OBARA	Graduate Student from Hokkaido Univ. (October 78-)

Instrument Center

Gen SODA	Associate Professor
Keisaku KIMURA	Research Associate
Toshiro MURAO	Technical Associate

Low-Temperature Center

Toshiaki ENOKI	Research Associate

Chemical Materials Center

Hidemasa TAKAYA	Associate Professor
Akira MIYASHITA	Research Associate
Arata YASUDA	Technical Associate

Development Workshop

Makoto WATANABE	Associate Professor
Yoshihiro TAKAGI	Research Associate

Technical Staff

Shigetoshi TAKAHASHI	Technical Chief
Kusuo SAKAI	Technical Manager
Akira UCHIDA	Technical Manager
Satoshi INA	Computer Center
Fumio NISHIMOTO	Computer Center
Kenichi IMAEDA	Low-Temperature Center
Kazuo HAYAKAWA	Electronic Shop
Masaaki NAGATA	Glassblowing Shop
Katsumi KATO	Machine Shop
Nobuo MIZUTANI	Machine Shop
Norio OKADA	Machine Shop
Mitsukazu SUZUI	Machine Shop

Foreign Visiting Staff

Jon T. Hougen (NBS, Washington, D. C., USA)	July 17, 1978 — Feb. 28, 1979
Harry F. King (State Univ. of New York, Buffalo, USA)	Dec. 27, 1978 — Mar. 31, 1979
C. Bradley Moore (Univ. of California, Berkeley, USA)	May 14, 1979 — Aug. 13, 1979
Jean Durup (Univ. de Paris-Sud, Orsay, France)	Aug. 25, 1979 — Dec. 24, 1979
Anton Rieker (Univ. Tubingen, Germany)	Sept. 1, 1979 — Nov. 30, 1979

BUILDINGS AND CAMPUS

The IMS campus covering 62,561 m² is located on a low hill in the middle of Okazaki City. The inequality in the surface of the hill and growing trees are preserved as much as possible, and low-storied buildings are adopted for conservation of the environment. The buildings of IMS are separated according to their functions as shown in the map. The Research Office Building and all Research Facilities except for the Computer Center are linked organically to the Main Laboratory Building by corridors. Computer Center, Library, and Administration Buildings are situated between IMS and the neighboring National Institute for Basic Biology and National Institute for Physiological Sciences, because the latter two facilities are common to these three institutes.

The lodging facility of IMS called Yamate Lodge, located within 10 min. walk, has sleeping accommodations for 20 guests. Scientists who visit IMS can make use of this facility. Foreign visiting scientists can also live at this lodge with their families during their stay.

The Institute for Molecular Science

To Meitetsu Higashiokazaki Station

To National Institute for Basic Biology and National Institute for Physiological Science

1. Research Office Building
2. Main Laboratory Building
3. Development Workshop
4. Instrument Center
5. Chemical Materials Center
6. Low-Temperature Center
7. Computer Center
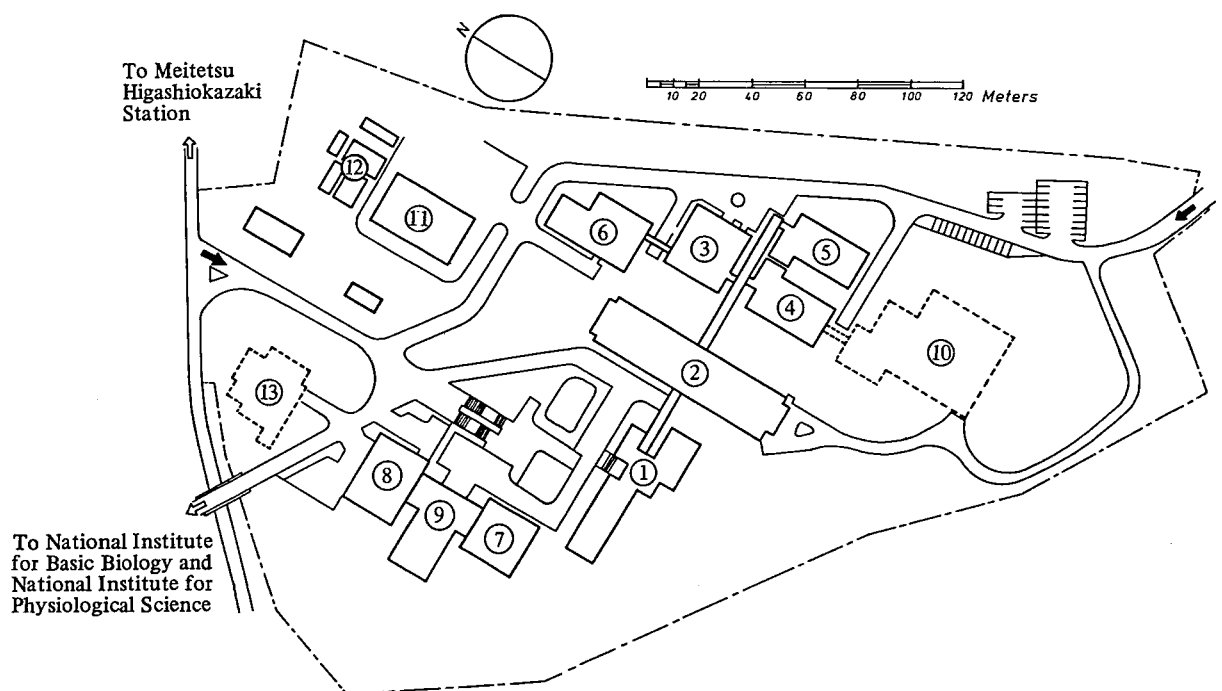
8. Library
9. Central Administration
10. Special Experiment Building†
11. Power Station
12. Waste-Water Disposition Facilities
13. Faculty Club†

† In the planning stage
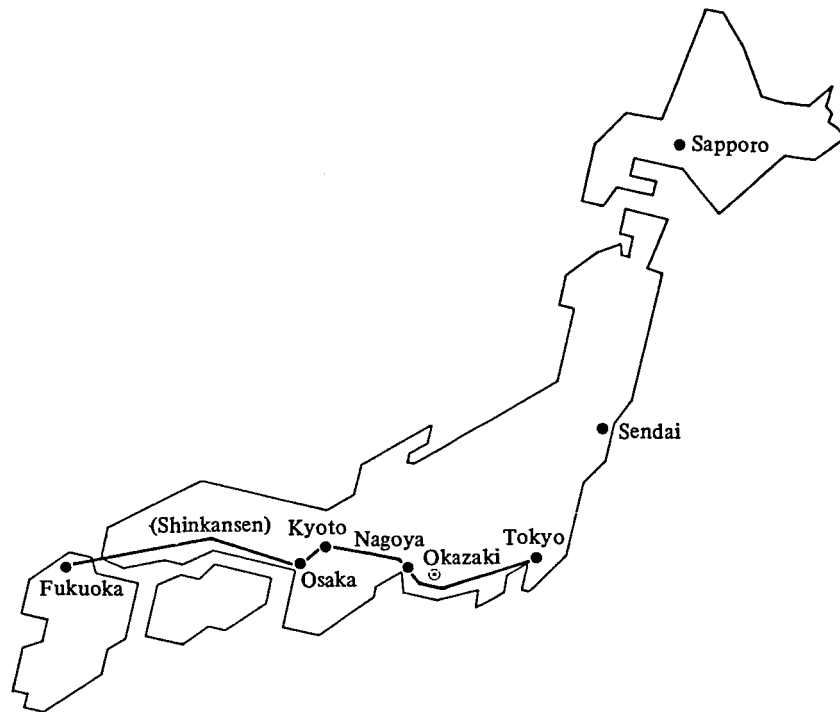
Okazaki (population 250,000) is 260 km southwest of Tokyo, and can be reached by train in about 3 hours from Tokyo via New Tokaido Line (Shinkansen) and Meitetsu Line.
The nearest large city is Nagoya, about 40 km west of Okazaki

RESEARCH ACTIVITIES I

Division of Theoretical Studies

Research in our Division in its first two years (1977–8) of existence has suffered much from the lack of computational facility. At last, on January 4, 1979, the Computer Center started its service and provides several thousand hours per annum of CPU time for molecular science calculation. (See RESEARCH FACILITIES for detail.) We are now making a very heavy use of the facility.

In many fronts of our research effort, we have been fortunate to find people outside as well as inside of IMS, who actively collaborate in planning and actual execution of research or who provide new and interesting experimental data as well as helpful advices.

Our research projects continue to be organized around two groups. One, often called the ab initio group, is interested in theoretical investigation of chemical reactions, transition metal complexes as well as other problems of molecular and electronic structure. They carry out research projects I-B to I-E in the following. The other group, internally called the Xα group, is mainly working on the electronic structure of solid surfaces and on their interactions with adsorbates. This group is involved in projects I-F to I-I. The grouping, however, is rather conventional now that the groups share rooms, have heated discussion, and sometimes work together as in the project I-A.

I—A Total Energies of Molecules with the Local Density Functional Approximation and Gaussian Basis Sets

Kazuo KITAURA, Chikatoshi SATOKO and Keiji MOROKUMA

Total energies of small molecules were calculated with a local density functional (LDF) approximation within the LCAO-MO-SCF scheme. The local spin density functional (LSD) of Gunnarsson and Lundqvist[1] was used. The method and detailed numerical procedures for solving the LDF one-electron equation have been already reported.[2] The basis sets used are of contracted Gaussian type such as the 4-31G, which allow a direct comparison of the LSD results with the ab initio Hartree-Fock (HF) results. Through the comparison the applicability of LDF to calculation of molecular electronic structures was demonstrated.

In Table I are shown the calculated LSD spectroscopic constants along with the HF results and experiments for first row diatomic molecules. The same basis set (4-31G with standard scale factors) was used for both the LSD and the HF calculations. Results of calculation with the extended basis set, 4-31G* (a d-type Gaussian with the exponent 0.8 is

Table I. Calculated spectroscopic constants.[a]

		R_e (Bohr)			ω_e (cm^{-1})			D_e (eV)		
		LSD	HF	exp.	LSD	HF	exp.	LSD	HF	exp.
H$_2$	($^1\Sigma_g^+$)	1.44	1.38	1.40	4280	4760	4403	4.74	3.55	4.75
C$_2$	($^1\Sigma_g^+$)	2.35	2.37	2.35	1830	1900	1856	7.13	0.00	6.35
N$_2$	($^1\Sigma_g^+$)	2.11 (2.09)	2.05 (2.03)	2.07	2390 (2420)	2710 (2730)	2358	10.20 (11.86)	2.71 (4.76)	9.91
O$_2$	($^3\Sigma_g^-$)	2.34	2.26	2.28	1590	1710	1580	6.42	−0.46	5.22
F$_2$	($^1\Sigma_g^+$)	2.69 (2.64)	2.67 (2.54)	2.68	1120 (1930)	1200 (1230)	892	3.02 (4.20)	−1.97 (−1.38)	1.67
CO	($^1\Sigma^+$)	2.18	2.08	2.13	2200	2430	2170	11.94	7.89	11.22
LiF	($^1\Sigma^+$)	2.96	2.95	2.96	970	960	910	6.21	3.47	6.01
HF	($^1\Sigma^+$)	1.76	1.74	1.73	4110	4090	4139	6.06	3.36	6.10

[a] The 4-31G basis set is used for both the LSD and HF calculations. For Li, the 5-21G basis set is used. The results with the 4-31G* basis set are given in the parentheses for N$_2$ and F$_2$. All LSD calculations are performed with 2,000 sample points per atom.

added to 4-31G), are shown in parentheses for N_2 and F_2 to see the basis set dependence of the results.

The LSD equilibrium distances are very close to those of HF and compares well with experiments. A tendency is found that LSD gives a little longer R_e than HF. The LSD vibrational frequencies are in good agreement with experiments. It is seen that the LSD approximation has also a trend to give smaller values of ω_e than HF, in accordance with the fact that LSD has a correct asymptotic dissociation limit, while HF does not. The LSD binding energy is larger than the HF energy and is in better agreement with experiments. The LSD results with the 4-31G* basis set show the same tendency as those of HF except the ω_e value of F_2.

The optimized geometries for the H_2O, NH_3 and C_2H_4 molecules are shown in Table II. The calculated results of NH_3 with the 4-31G** basis set (a set of d-type functions with the exponent 0.8 on N and a set of p-type functions with the exponent 1.1 on H) are given in the parentheses. The LSD results agree well with the HF results and experiments.

Our results suggests that the LSD approximation within the LCAO-MO scheme gives reliable results for molecular properties provided that the LSD total energy is calculated numerically acculately.

Table II. Calculated equilibrium geometries[a]

		LSD	HF	exp.
H_2O	R_{OH}	1.85	1.78	1.809
	$\angle HOH$	111	111	104.7
NH_3	R_{NH}	1.93	1.87	1.914
	$\angle HNH$	120 (106)	116 (105)	106.67
C_2H_4[b]	R_{CC}	2.53	2.49	2.531
	$\angle HCH$	117	116	117.6

[a] Bond lengths are in Bohr and angles in degrees. The calculated values are obtained with the 4-31G basis set for both LSD and HF except the values in the parentheses (4-31G**).

[b] The C-H bond length is fixed at the experimental value of 2.053 Bohr.

References

1) O. Gunnarsson and B. I. Lundqvist, *Phys. Rev.* B13, 4274 (1976).
2) K. Kitaura, C. Satoko and K. Morokuma, *IMS Ann. Rev.* 7 (1978)

I—B   Potential Energy Surfaces for Chemical Reactions

In our continuing effort in characterizing potential energy surfaces on which chemical reactions take place, we have relied heavily on the energy gradient technique in the ab initio molecular orbital method. The technique, which let one calculate all the energy gradient components as well as the energy in a single SCF calculation, has made possible a hitherto prohibitive full optimization of the equilibrium and saddle point geometries of molecules with many degrees of freedom. It turns out that the full geometry optimization is often crucial in characterizing potential energy surfaces.

We have also made the first extension of the gradient technique, beyond the single configuration SCF, to the multi-configuration (MC)-SCF method. This extension expands the applicability of the technique to such states as diradicals.

I-B-1   Energy Gradient in A Multi-Configurational SCF Formalism and Its Application to Geometry Optimization of Trimethylene Diradicals

Shigeki KATO and Keiji MOROKUMA

The energy gradient approach is already proving to be a powerful tool for theoretical studies of molecular structure and reactivity. Its most serious deficiency, however, has been its practical limitation to single-determinant Hartree-Fock (HF) wavefunctions. This precludes its application to many chemically significant systems such as the diradical electronic structures which appear in molecular dissociation processes and in certain types of reaction intermediates.

Our purpose here is to overcome this difficulty. We present an efficient method for calculating the energy gradient in the multi-configurational (MC) SCF theory and apply it to the geometry optimization of trimethylene reaction intermediates. The total energy for MCSCF wavefunctions including pair type two-, four-, six-, . . ., electron excitations from the originally doubly occupied orbitals is expressed by

$$E = \sum_i f_i <i|h|i> + \sum_{i,j} (a_{ij}J_{ij} + b_{ij}K_{ij}) + V_{nn} \tag{1}$$

where f_i is the occupation number of the i-th MO,

and J_{ij} and K_{ij} are the Coulomb and the exchange integral, respectively. The vector coupling coefficients are given by a_{ij} and b_{ij}. The generalized-valence-bond (GVB) method[1] and various types of open shell SCF theories[2] also fall into this class. The energy gradient for eq. (1) is given in an analytic form as in the case of single determinant HF wavefunctions.

We have performred 5-configuration MCSCF gradient calculations with the 4-31G basis set to determine the optimized geometries of the three forms of trimethylene, that is, the edge-to-edge (EE), the edge-to-face (EF) and the face-to-face (FF) trimethylene. There was no local minimum on the MCSCF potential energy surface corresponding to FF trimethylene. The optimized geometries as well as the energies of EF and EE trimethylenes are shown in Figure 1. The energy of EF trimethylene is lower than that of EE trimethylene by about 1.0 kcal/mol.
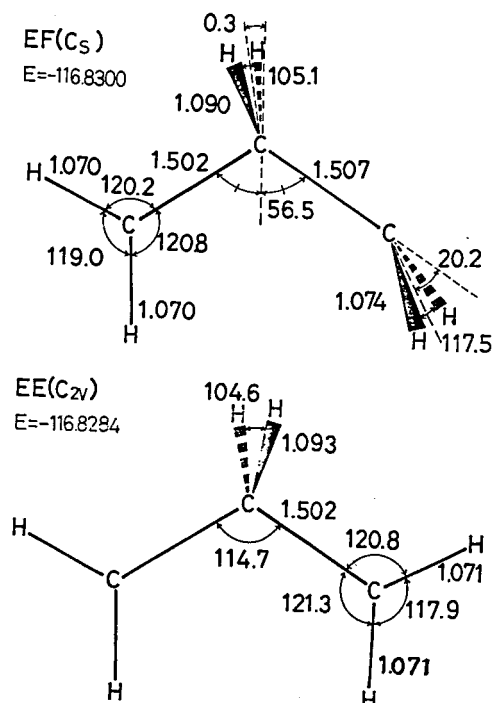
Figure 1. Optimized geometries and energies of EF and EE trimethylene. Engines are in hartree, bond distances are in Å, and bond angles are in degrees.

References

1) W. J. Hunt, P. H. Hay and W. A. Goddard III, *J. Chem. Phys.*, **57**, 738 (1972).
2) C. C. J. Roothaan, *Rev. Mod. Phys.*, **32**, 179 (1960).

I-B-2 Three and Four-Centered Transition State in HF Elimination Reaction of $CH_2 = CHF$

Shigeki KATO and Keiji MOROKUMA

Unimolecular dissociation reactions of haloethylenes have been extensively studied by means of mercury-photosensitizer[1] and infrared multiphoton techniques.[2] Some possible reaction routes to the product, hydrogen halide and acetylene, have been proposed.

In the present work, we have performed ab initio MO calculations to examine favorable reaction paths of unimolecular dissociation of fluoroethylene, $CH_2=CHF$. The geometries and energies of the transition states and the reaction intermediates involved in the following elementary steps both on the triplet and the singlet surfaces were determined by the use of the energy gradient method with the 4-31G basis set.

For the triplet state:

$^3CH_2CHF \rightarrow$ $^3CHCH_2F$ (1,2-hydrogen migration) (a)
$\rightarrow$ $^3CH_3CF$ (1,2-hydrogen migration) (b)
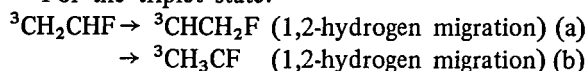
and for the singlet state:

$^1CH_2CHF \rightarrow$ CHCH + HF (α, β-elimination)   (c)
$\rightarrow$ CH_2C + HF (α, α-elimination)   (d)
$\rightarrow$ CHCH + HF (1,2-hydrogen migration) (d')
$\rightarrow$ $CHCH_2F$ (1,2-hydrogen migration) (e)
$\rightarrow$ CHCH + HF (α, α-elimination) (e')
$\rightarrow$ CH_3CF (1,2-hydrogen mitration) (f)
$\rightarrow$ CH_2CHF (cis-trans isomerization) (g)
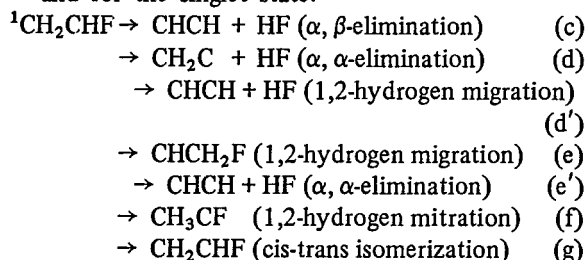
The results of our MO calculations can be summarized as follows.

1) On the triplet surface, the barrier heights for 1,2-hydrogen migration reactions, (a) and (b), are calculated to be ~85 kcal/mol measured from the equilibrium geometry of twisted $^3CH_2CHF$. Thus these reactions are not likely to occur in the mercury sensitized experiment. 2) There are three reaction paths to produce HF and CHCH on the singlet surface. The α,α-elimination path from $CHCH_2F$ carbene, (e'), has a higher barrier than the remaining two by ~30 kcal/mol., though the hydrogen migration, (e), is feasible. 3) The geometries of the transition states in the α,α- and the α,β-elimination reactions from CH_2CHF, (c) and (d), are shown in Figure 1. The barrier heights for these processes were calcualted to be nearly the same. Although we are not certain which route has the lower barrier, both reactions are likely to take place. In this connection, it would be interesting if one can measure the energy disposed in the internal modes of the product molecules; the pattern of energy partitioning is expected to be quite different between the two reaction paths.
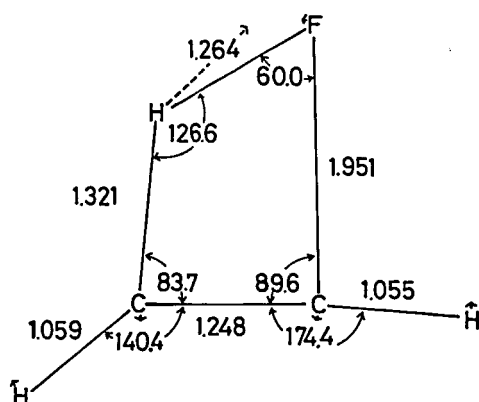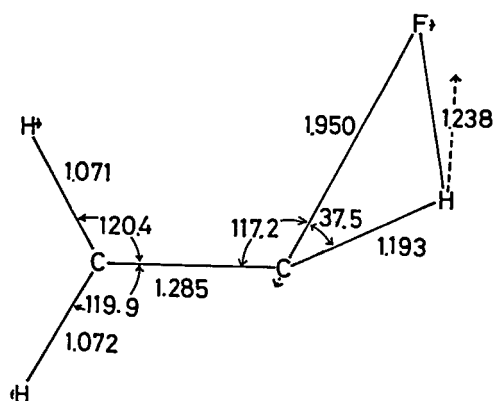
Figure 1. Geometries of Transition States of α, α- and α, β-Elimination Reactions.

References

1) S. Tsunashima, H. E. Gunning and O. P. Strausx, *J. Am. Chem. Soc.*, **98**, 1690 (1976).
2) C. Reiser, F. M. Lussier, C. C. Jensen and J. I. Steinfeld, *J. Am. Chem. Soc.*, **101**, 350 (1979).

I-B-3 An Ab Initio Approach to Organic Reaction Rates. Kinetic Isotope Effects in the Reaction H + C_2H_4 → C_2H_5

Shigeru NAGASE *(Osaka Univ.)*, Takayuki FUENO *(Osaka Univ.)* and Keiji MOROKUMA

It is of general interest to predict rate constants of organic reactions entirely from a nonempirical standpoint. Recent advances in the ab initio energy gradient method are expected to provide a reliable assistance to such predictions. We here present the results of a transition state theoretical (TST) study, reinforced by the relevant ab initio molecular orbital computation, of the addition reaction H + C_2H_4 → C_2H_5. The TST procedure, which would otherwise entail a considerable extent of empiricism on the transition state characteristics, has proved to be valuable indeed as a quantitative tool for kinetic considerations.

The geometries, energies and vibrational frequencies of the reactant as well as the transition state were determined with the 4-31G unrestricted Hartree-Fock method. As Table I shows, the TST rate constants calculated in the temperature range 198-320K are found to be in excellent agreement with the

Table I. Comparison of the Experimental and the Present Theoretical Rate Constants k for the H + C_2H_4 Reaction

Temperature T, K	k (10^{-13} cm^3 molecule^{-1} sec^{-1})	
	Expt.	Theory, this work
320	14.5 ± 1.1	16.9
298	11.3 ± 0.5	12.7
283	9.4 ± 0.6	10.3
258	6.3 ± 0.4	6.8
234	4.1 ± 0.2	4.3
216	3.0 ± 0.3	2.9
198	2.0 ± 0.1	1.8

Table II. Calculated Rate Constants k (cm^3 molecule^{-1} sec^{-1}) for the Additions of H or D Atom toward a Series of Deuterated Ethylenes[a]

Ethylene	10^{15} k(100 K)		10^{13} k (200 K)		10^{13} k (295 K)[b]		10^{12} k (400 K)	
	H	D	H	D	H	D	H	D
CH_2=CH_2	0.70	1.19	1.87	1.84	12.2[b]	10.4[d]	3.80	3.03
CHD=CH_2	0.66	1.77	1.77	2.18	11.7	11.6	3.67	3.30
CD_2=CH_2	0.61	1.13	1.67	1.70	11.2	9.8	3.55	2.90
CHD=CHD (cis)	0.60	1.10	1.67	1.69	11.2	9.8	3.56	2.91
CHD=CHD (trans)	0.58	1.06	1.65	1.67	11.1	9.7	3.54	2.89
CD_2=CHD	0.54	1.00	1.56	1.54	10.6	9.3	3.44	2.82
CD_2=CD_2	0.47	0.90	1.45	1.48	10.1[c]	8.9[e]	3.33	2.72

[a] All the entires are the total rate constants, i.e., the sum of the rate constants for the both ends of the ethylenic bond. The experimental values[3] are [b] 12.5 ± 0.4 [c] 11.5 ± 0.4, [d] 8.7 ± 0.3, and [e] 8.5 ± 0.5.

recent experimental data.[2] We have also examined kinetic isotope effects, both primary and secondary, in the title reaction. Experimental rate constants are available only for the addition of H and D to C_2H_4 and C_2D_4 at a few temperatures.[2] It is hoped that the results given in Table II constitute a comprehensive prediction.

References

1) J. H. Lee, J. V. Michael, W. A. Payne, and L. J. Stief, *J. Chem. Phys.*, 68, 1817 (1978).
2) D. Mihelcic, V. Schubert, F. Hofler, and P. Potzinger, Ber. Bunsenges. *Phys. Chem.*, 79, 1230 (1975).

I-B-4 Ab Initio Mechanistic Study of Radical Reactions. Substituent Effects in Addition Reactions

Shigeru NAGASE *(Osaka Univ.)*, Shigeki KATO, Keiji MOROKUMA and Takayuki FUENO *(Osaka Univ.)*

Radical additions to unsaturated organic molecules are among the most important processes in a variety of free-radical reactions. Current interests in reactions of radicals with olefins are focused mainly on two questions[1]: (i) how readily does a given radical add to the double bond of a given olefin, and (ii) at which end of the double bond does addition occur preferentially? At present, there is hardly any unified and satisfactory explanation for these questions.

Our purpose here is to examine, using an ab initio MO theory, how an introduction of substituents into radicals or olefins influences the geometry and energy of the transition state, and thereby to shed a theoretical insight on the above questions. For this, the transition state geometries for several addition reactions are calculated with the energy gradient technique, while the potential barriers are analyzed in terms of chemically interpretable energy components.

Table II. Potential Barriers ΔE (kcal/mol) for Addition of Atomic Hydrogen to Olefins

Olefin[a]	ΔE	Olefin	ΔE
C*H$_2$=CH (Me)	2.4	CH$_2$=C*H (Me)	4.2
C*H$_2$=CHF	3.1	CH$_2$=C*HF	5.5
C*H$_2$=CF$_2$	4.1	CH$_2$=C*F$_2$	8.0

[a] Point of addition of H Atom is denoted by *

All computations are performed within the framework of ab initio unrestricted Hartree-Fock SCF theory with the 4-31G basis set.

In Table I are given energy component analyses for the addition of alkyl radicals to ethylene. The potential barrier (ΔE) decreases with the increase in the number of F atoms in the CH$_3$ radical. The reduction in ΔE by the F substitution is due to the decrease in the molecular deformation and exchange repulsion energies. This observation is contrasting to the fact that the importance of charge transfer interaction has been often implicated. In this connection, it is worth noting that the course of reaction up to the transition state is often controlled by the balance between the deformation and exchange interactions.[2]

The effect of introduction of substituents into olefins is shown in Table II. The barrier ΔE decreases (increases) with the introduction of a CH$_3$ group (F atoms) into olefins. ΔE for addition onto the less substituted end of the double bond is smaller than ΔE onto the more substituted end. These are in agreement with the experimental data.[1] The positional selectivity has also been interpreted in terms of the molecular deformation and exchange repulsion energies.

References

1) J. M. Tedder and J. C. Walton, *Adv. Phys. Org. Chem.*, 16, 51 (1978).
2) S. Nagase and C. W. Kern, *J. Am. Chem. Soc.*, 101, 2544 (1979).

Table I. Energy Component Analysis for the Transition State in Addition of Alkyl Radicals to Ethylene

	Alkyl radical		
	CH$_3$	CH$_2$H	CF$_3$
ΔE (kcal/mol)[a]	8.7	6.1	0.7
Deformation energy	8.0	6.1	3.1
Interaction energy	0.7	0.0	−2.4
Electrostatic term	−17.7	−18.0	−11.2
Exchange term	44.4	43.0	25.7
Polarization term	−1.5	−1.9	−1.9
Charge transfer term	−13.0	−13.2	−9.0
Mixing term	−11.5	−9.9	−6.0

[a] ΔE = (Deformation energy) + (Interaction energy), where the latter energy consists of five interaction terms.

I-B-5 Geometry Optimization of Eight Different Diradical States of Ring-Opened Oxirane (CH$_2$CH$_2$O): Mechanism of Addition Reactions of Triplet Oxygen Atom (^{3}P) to Olefins

Kizashi YAMAGUCHI*, Satoshi YABUSHITA*, Takayuki FUENO*, Shigeki KATO and Keiji MOROKUMA *(*Osaka Univ.)*

A geometry optimization for eight different diradical states of the ring-opened oxirane (·CH$_2$CH$_2$O·) has been carried out with the ab initio unrestricted

Table I. Total Energies (eV) of Eight Diradical States of Ring-Opened Oxirane

Table I. Total Energies (eV) of Eight Diradical States of Ring-Opened Oxirane

	MINDO/3	4-31G
$^1\pi\pi$	0.4	1.3
$^3\pi\pi$	−1.2	0.6
$^1\sigma\pi$	1.3	2.2
$^3\sigma\pi$	0.0	0.0
$^1\sigma\sigma$	0.1^a	1.2
$^3\sigma\sigma$	−0.6	1.8
$^1\pi\sigma$	1.9	3.6
$^3\pi\sigma$	−1.1	1.9

^{a} The ring-closure reaction takes place. This energy is for an intermediate state.

Hartree-Fock (UHF) method (basis set: 4-31G) as well as with the semiempirical MINDO/3 UHF method. The energy gradient technique has been u :f for geometry optimization. The optimized geometry for a triplet state is similar to that for the corresponding singlet state. However, there is a considerable difference between the MINDO/3 and 4-31G results, as shown in Table I. For instance, the configuration energy defined as the average of the singlet and triplet energies increases in the following order: $\pi\pi$ (2π) $<$ $\sigma\pi$ (1π) $<$ $\sigma\sigma$ (2π) $<$ $\pi\sigma$ (3π) in the 4-31G results and $\pi\pi$ (2π) $<$ $\pi\pi$ (2π) $<$ $\pi\sigma$ (3π) $<$ $\sigma\pi$ (1π) in the MINDO/3 results. Here, for instance, the notation $\pi\sigma$ (3π) indicates that the odd electron on the CH_2 and the O end is in a π orbital and a σ orbital, respectively, with a total of three π electrons. The 4-31G results are in accord with the generalized valence bond (GVB)-CI results for the isoelectronic methylene peroxide diradical ($\cdot CH_2OO\cdot$).[1]

The triplet $\sigma\pi$ state is the most stable in energy among the eight diradical states, and has to go over a very small positive barrier at the $^3\pi\pi$ state for the internal rotation of its terminal methylene group around the C-C bond. Thus the large value (26 kcal/mol)[2] of this barrier obtained by a partial geometry optimization in the restricted Hartree-Fock (RHF) calculation appears to be unrealistic. The intersystem cossing between $^3\sigma\pi$ and $^1\sigma\sigma$ should be rather easy because of the favorable directionality of orbitals and of the small energy gap. These findings suggest the following mechanism:

$$H_2C=CH_2 + {}^3O \rightarrow {}^3\sigma\pi \begin{cases} {}^1\sigma\sigma \rightarrow \text{epoxide} \\ {}^3\pi\pi \rightarrow \text{isomerization} \end{cases}$$
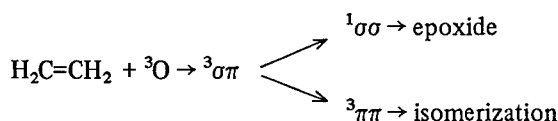
Thus the present results lend support to the side attack model[3] for addition reactions of a triplet oxygen atom to olefins.

References

1) L. B. Harding and W. A. Goddard III, *J. Am. Chem. Soc.*, 100, 7180 (1978).

2) O. P. Strauss, R. K. Gosavi, G. R. Demare, and I. G. Csizmadia, *Chem. Phys. Lett.* 62, 339 (1979).

3) R. J. Dvetanovic, *J. Phys. Chem.* 74, 2730 (1970).

I-B-6 Geometry Optimizations of Methylene Peroxide Diradicals (CH_2OO)

Kizashi YAMAGUCHI*, Satoshi YABUSHITA*, Takayuki FUENO*, Shigeki KATO and Keiji MOROKUMA (*Osaka Univ.)

The ab initio unrestricted Hartree-Fock (UHF) method with the 4-31G basis set with the energy gradient technique has been applied for elucidation of geometries and electronic structures of the ring and the open form of methylene peroxide. The O-O bond length of the ring form CH_2OO is calculated to be 1.534Å, in good agreement with the experimental value 1.519Å.[1] The optimized geometries of the singlet and the triplet $\pi\pi$- and the singlet $\sigma\pi$-diradical states of the open form $\cdot CH_2OO\cdot$ agree well with the partially optimized geometries by the GVB-CI method[2] except for the bending angle of the terminal methylene group. However, no local
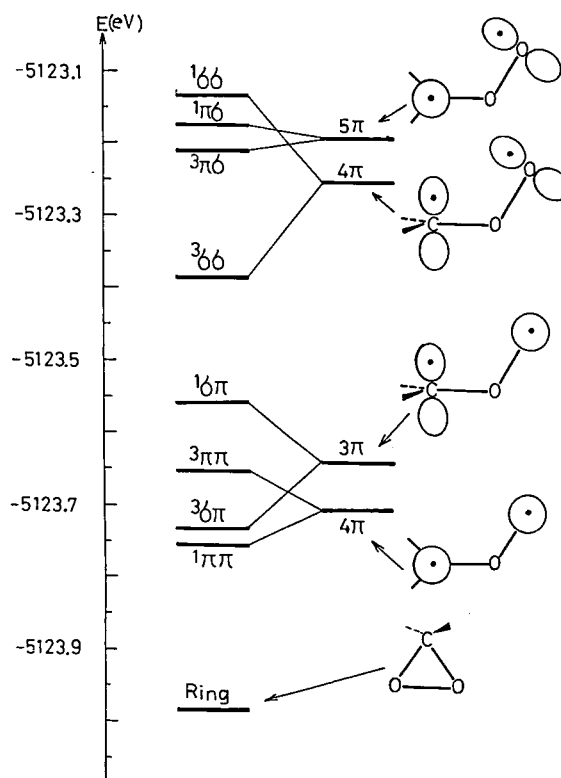
Figure 1. The relative energy of the closed shell ring form and eight diradical states of CH_2OO. On the right are shown the average of triplet and singlet energies as well as schematic diagrams of odd electrons.

13

potential energy minima were found for $^3\sigma\pi$-, $^{1,3}\sigma\sigma$- or $^{1,3}\pi\sigma$-diradicals in contradiction to the partially optimized GVB-CI results.[2] The present calculation indicates that these excited states are dissociative to CH_2O + O. The full geometry optimization appears to be essential for a quantitative discussion of geometries of these transient species. The relative energies of various diradical states are shown in Figure 1, where for planar ($\pi\pi$ and $\pi\sigma$) diradicals the optimized geometry of $^1\pi\pi$ and for nonplaner ($\sigma\pi$ and $\sigma\sigma$) diradicals that of $^1\sigma\pi$ were used. The configuration energy defined as the average of corresponding singlet and triplet energies increases in the order $\pi\pi$ (4π) $<\sigma\pi$ (3π)$<\sigma\sigma$ (4π) $<\pi\sigma$ (5π), in accord with the GVB and GVB-CI results.[2]

References

1) F. J. Lovas and R. D. Suenram, *Chem. Phys. Lett.*, 51, 453 (1977).

2) L. B. Harding and W. A. Goddard III, *J. Am. Chem. Soc.*, 100, 7180 (1978).

I-B-7 Ab Initio Molecular Orbital Calculations on Geometries of Reaction Intermediates Involved in the Rearrangement of Phenylcarbene to Cycloheptatrienacarbene

Keiichi YANO[1], Shigeki KATO and Keiji MOROKUMA

Studies of electronic structure of carbenes have
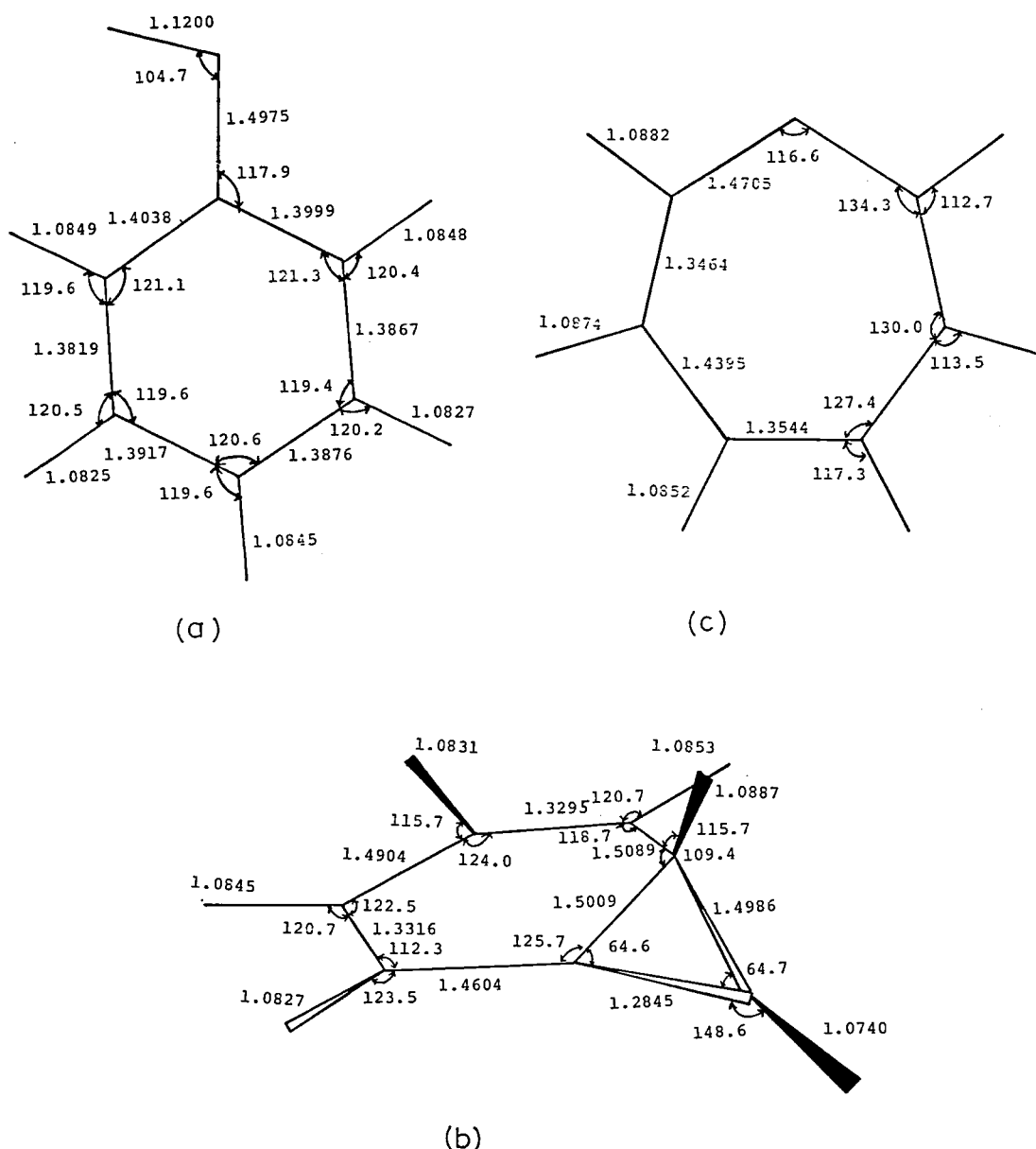
Figure 1. Optimized geometries for singlet carbenes: (a) phenylcarbene (planar); (b) bicyclo[4,1,0]heptatriene; (c) cycloheptatrienacarbene(C_{2v}).

14

been one of important contributions of theoretical chemistry to organic chemistry where carbenes play a key role in certain types of organic reactions. The rearrangement of phenylcarbene to cycloheptatriena-carbene is known to be involved in reactions such as the pyrolysis of the sodium salts of aromatic alde-hyde tosylhydrazones.[2] Details of mechanism of this interconversion, however, have not been well established. Dewer and Landman[3] have calculated the potential energy surfaces of the rearrangement process of phenylcarbene by the semiempirical MINDO/3 method and concluded that the reaction takes place in the two steps on the singlet potential energy surface via bicyclo[4.1.0]-heptatriene inter-mediate.

In the present study we have carried out ab initio closed shell SCF calculations with the minimal STO-3G basis set to determine the geometries and energies of reaction intermediates involved in this rearrange-ment reaction. The geometries were optimized with the energy gradient method. The optimized ge-ometries of the singlet phenylcarbene, bicyclo[4.1.0] heptatriene and cycloheptatrienacarbene are shown in Figure 1. The relative energies of these inter-mediates are also shown in Table I and compared with the MINDO/3 values of Dewer and Landman. The results of our calculations are very different from the MINDO/3 results. The STO-3G calculation gives the singlet rearrangement process to be endothermic in contrast with MINDO/3 calculation. The STO-3G geometries of intermediates are similar to the MINDO/3 geometries except for cycloheptatrienacarbene; the ab initio calculation makes cycloheptatrienacarbene have a nearly planar configuration.

Table I. Relative Energies (kcal/mole) at Optimized Ge-ometries

Molecule	RHF/STO-3G	RHF/4-31G	MINDO/3
Phenylcarbene	0.0	0.0	0.0
Bicyclo[4,1,0]hepta-triene	5.7	22.4	−12.9
Cycloheptatriena-carbene	23.3	17.0	−27.0

References

1) IMS Graduate Student 1978–9 from Waseda Univ.
2) W. J. Baron, M. Jones and P. P. Gaspar, J. Am. Chem. Soc., 92, 4739 (1970), W. D. Crow and M. N. Paddon-Row, ibid., 94, 4746 (1972).
3) M. J. S. Dewer and D. Landman, J. Am. Chem. Soc., 99, 6179 (1977).

I-B-8 Potential Energy Surface of the Chemi-cal Reaction $H_2^+ + H_2 \rightarrow H_3^+ + H$

Shogo SAKAI (Kansai Univ.), Shigeki KATO and Keiji MOROKUMA

The reaction $H_2^+ + H_2 \rightarrow H_3^+ + H$ is one of the simplest ion-molecule reactions, and has attracted much experimental and theoretical interest in the past several years. Our attention is mainly focused on the minimum energy reaction path and the resonance charge transfer in the neighborhood of the path. We have calculated the ground and excited state potential energy surfaces for the H_4^+ system by the ab initio UHF (unrestricted Hartree-Fock) and the complete configuration interaction (CI) method with a triple-zeta-plus polarization basis set.

A scan of the ground state surface with the UHF method has shown that the minimum energy reac-tion path has a T shape structure with the H_2^+ mole-cule approaching head on to the side of the H_2 mole-cule. The ground and the excited state potential energy surfaces are then calculated with the CI method for this T shape structure with three degrees of freedom. The ground state surface has no barrier going down from $H_2^+ + H_2$ to $H_3^+ + H$, but has a shallow well (about 3 kcal/mol.) at a geometry cor-responding to a complex between H_3^+ and H.

In order to see the possibility of resonance charge transfer, i.e., the positive charge hopping from one H_2 to another H_2, we show in Figure 1 the potential energy surfaces at the center-of-mass distance of R= 3.5Å. One sees a well defined avoided crossing; the ground state has two minima with a small barrier inbetween and the low lying excited state has a minimum just above the ground state barrier. The
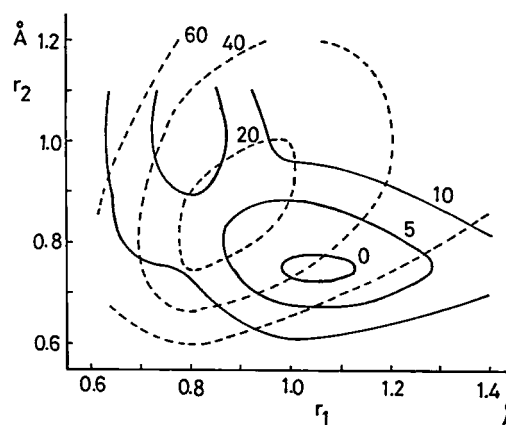
Figure 1. The potential energy surface of the ground (solid line) and the excited (dotted line) state. Energy is in kcal/mol. and is relative to the sum of energies of H_2 and H_2^+. R is fixed at 3.5Å. r_1 and r_2 are the intramolecular distances of the vertical and horizontal molecules, respectively.

15

deeper minimum has H_2^+ as the stem of the T shape and the shallower minimum as the bar of T. However, as R becomes smaller, the barrier becomes larger and the shallow minimum rapidly disappears. Therefore, we expect a repeated resonance charge transfer when the vibrational amplitude of the reactant molecule(s) is large, but only in the very early stage of the reaction.

I—C Mechanism of Photochemical Reactions

Our interest in the mechanism of photochemical reactions continues. In the polyene isomerization project we have evaluated the Franck-Condon type overlap integral between the triplet and the ground state and analyzed which normal modes can act as accepting modes during isomerization. We also found a classical trajectory on the triplet surface in which the torsional energy is transferred from one C-C bond to another, resulting in a double torsional isomerization, e.g. trans-trans to cis-cis, in a single elementary process. We are presently working on the isomerization mechanism in singlet excited states.

Despite its apparent simplicity and numerous experimental and theoretical studies photodissociation of formaldehyde remains to be a mystery. Hydroxycarbene has been implicated as an intermediate. In our work on HFCO we are proposing an experiment at a low energy which would exclude hydroxycarbene from being an intermediate.

I-C-1 Radiationless Transition in the Photo-isomerization Processes of Polyenes

Iwao OHMINE and Keiji MOROKUMA

To understand the mechanism of radiationless transition concomitant with photoisomerization process of polyene, we have analized the normal modes at the transition region and evaluated the Franck-Condon type overlap integrals between the excited and ground states.[1],[2] We have chosen the photoisomerization of butadiene in the triplet mechanism as an example. The ab initio unrestricted Hartree-Fock method with the STO-3G basis set was used for the calculation. The diagonal and offdiagonal force constants were obtained by the numerical differentiation of the analytically evaluated energy gradients.

Table I presents the calculated normal mode frequencies of butadiene. We can see that the corresponding normal mode frequencies are very similar between the two states. Exceptions are for torsional motion of the isomerizing C_1-C_2 bond and the flapping motion of terminal methylene group as well as the skeletal wagging motion. Except for the C-C torsional motions overlap integrals of these triplet and ground state normal modes are all small for the non(0-0) transition. This indicates that these modes do not act as major energy acceptors in the radiationless transition from the lowest triplet state to the ground state. For C-C torsional motions, we have used a two-dimensional Mathieu function to represent the coupled C_1-C_2 and C_3-C_4 torsional motions on each electronic state and evaluated its overlap integrals. The results are shown in Figure 1, where we can see that the highly excited C_1-C_2 torsional motion of the ground electronic state yields a large overlap with the ground torsional state of the triplet electronic state.[3] Therefore, the triplet state electronic energy is mainly converted into the torsional energy of the C_1-C_2 bond in the deactivation process of butadiene.

We have performed similar analyses for larger polyenes by using the MINDO/3 approximation. It has been found that for larger polyenes not only the isomerizing C-C bond is the major energy acceptor but also some other modes such as H-flapping and

Table I. Butadiene Normal Mode Analysis for Twisted Conformations[a]

Vibrational frequency		Description[b]
Ground	Triplet	
212 cm^{-1}	208 cm^{-1}	
300	271	(H)$_2$C-flap + skel wag
364	601 i	C_1-C_2 torsion
506	368	(H)$_2$C-flap + skel wag
568	564	C_3-C_4 torsion
618	556	(H)$_2$C-flap + skel wag
722	734	H$_2$ flap
739	649	—C(H)$_2$ flap
1028	1025	
1044	1025	H$_3$ falp
1135	1115	
1230	1231	
1301	1306	
1388	1372	
1511	1500	
1696	1678	
1734	1715	
1746	1747	
3616–3813	3596–3813	C-H st

[a] Equilibrium geometry for triplet state and the transition state for ground state.
[b] Flap stands for flapping(wagging), skel wag for skeletal wagging, and st for stretching.

16
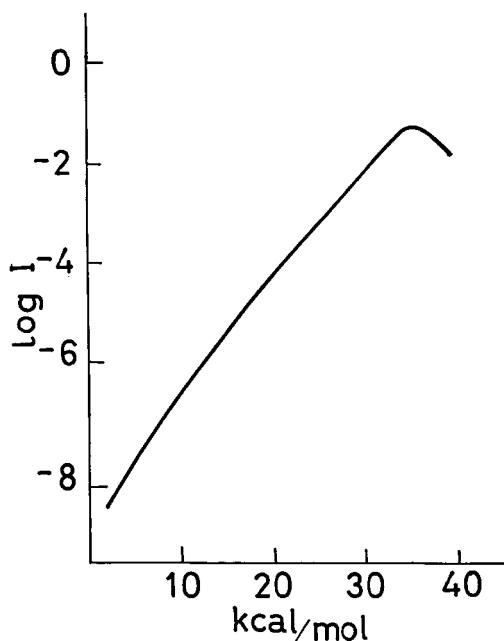
Figure 1. Overlap integral of Mathieu function as a function of torsional excitation energy of the ground state.

Figure 1. A trajectory of the butadiene triplet potential surface, starting from the saddle point near the planar conformation with the initial kinetic energy of 1.84 kcal/mol to the direction of the normal mode with an imaginary frequency. R. and BL. are for rotation(torsion) and bond length, respectively.

torsion of other C-C bonds act as minor but not negligible energy acceptors.

References

1) W. M. Gelbart, K. F. Freed and S. A. Rice, *J. Chem. Phys.* 52, 2460 (1970).

2) T. E. Sharp and H. M. Rosenstock, *J. Chem. Phys.* 41, 3453 (1964).

3) J. N. Kushick and S. A. Rice, *J. Chem. Phys.* 64, 1612 (1976).

I-C-2 Dynamical Double Torsion in Photo-isomerization of Polyenes

Iwao OHMINE and Keiji MOROKUMA

For a detailed interpretation of photoisomerization process of polyene, a knowledge of not only the potential surfaces involved but also the dynamics of the system on these surfaces is required. We focus here on the dynamical aspects of photoisomerization and present the results of trajectory calculations on the butadiene triplet surface. Preliminary results were already reported in the previous review.[1] Here we found new dynamical behaviors of polyenes, such as dynamical double torsion, which did not exist in small molecules.

We have analytically calculated the energy gradient with the MINDO/3 approximation and integrated the classical equation of motion, where the force is given as the negative of the energy gradient at each nuclear conformation. We have found that certain trajectories involve the transfer of torsional distorsion from one

bond to another. An example is shown in Figure 1. We can see in this trajectory that for the time less than 3000 a.u. (1 a.u. = 2.42×10^{-17} sec.) the C_1-C_2 torsion is the principal torsional motion. At t≈3200 a.u. the torsional kinetic energy is transfered from the C_1-C_2 bond to the C_3-C_4 bond and up to t≈5600 a.u. the system isomerizes around C_3-C_4 bond, while the C_1-C_2 torsional angle θ_{12} is confined in the region of $180°$(trans). Then, the torsional kinetic energy gets transfered back to the C_1-C_2 bond and the system becomes confined at the potential well of $\theta_{12}=270°$ and $\theta_{34}=-180°$. If the system decays from this triplet energy minimum to the $(\theta_{12},\theta_{34} = 180°, -180°)$ ground state, the overall trajectory path results in the double torsion from the trans-trans to the cis-cis conformation. We may call this the 'dynamical double torsion'. Such a dynamical double torsion might play a important role in the vision process and other isomerization processes of polyenes.[2],[3]

References

1) IMS Ann. Rev., 11 (1978).

2) A. Warshel, *Nature* 260, 679 (1976).

3) J. Santiel, J. D'Agostino, E. D. Meganity, L. Metts, K. R. Neuserger, M. Wrighton and O. Zafirou, *Org. Photochemistry* 3, 1 (1973).

I-C-3 Potential Energy Surface Characteristics of Unimolecular Dissociation of Fluoroformaldehyde

Keiji MOROKUMA, Shigeki KATO and Kimihiko HIRAO *(Shiga Univ. of Medical Science)*

The mechanism of photodissociation of formaldehyde, having been extensively studied experimentally and theoretically, still remains unresolved. An experiment[1] for the molecular dissociation process $H_2CO \xrightarrow{h\nu} H_2 + CO$ has found that there is a time lag between the disappearance of H_2CO and the appearance of the product. The reaction must proceed via an unknown intermediate. A recent molecular orbital study[2] puts the barrier for the isomerization to hydroxycarbene HCOH nearly equal to the barrier for the direct dissociation and suggests the hydroxycarbene as an intermediate.[3]

In order to shed light on the problem, we have calculated the ground state potential energy surface for fluoroformaldehyde HFCO. The geometries of the reactant, dissociation product HF+CO and hydroxyfluorocarbene FCOH as well as the geometries of the transition states connecting them have been determined with the ab initio SCF method with the 4-31G basis set. The energy gradient technique has been used for geometry optimization. The obtained geometries, shown in Figure 1, resemble those of formaldehyde. The normal coordinates at both transition states show that the magnitudes of the imaginary frequencies are large: $1640i\ cm^{-1}$ for the HFCO $\rightarrow$ HF+CO transition state and $2320i\ cm^{-1}$ for the
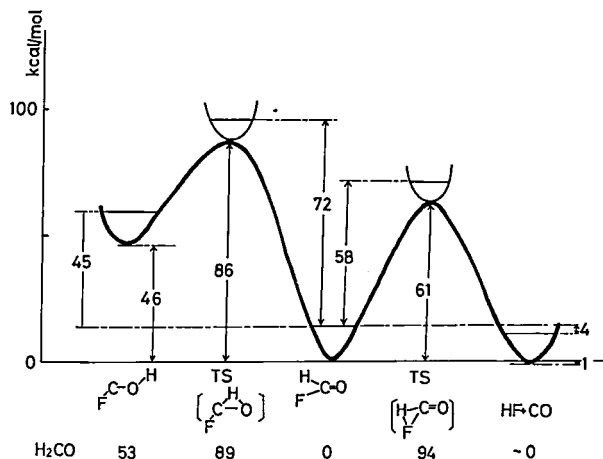
Figure 2. Relative energies of the HFCO system with and without zero point correction. Corresponding values[2] (without correction) of H_2CO system are also shown.

HFCO $\rightarrow$ FCOH transition state, and we expect a substantial tunneling effect near the threshold.

At these optimized geometries we performed SCF-CI calculations with the 6-31G** (split valence + polarization) basis set. CI was carried out with a direct CI program written by one of the authors (K. H.) and includes all the singly and doubly excited configurations (about 47000), in addition to the closed-shell SCF configuration. The calculated relative energies for HFCO with and without zero point energy correction are shown in Figure 2, where corresponding values[2] for H_2CO are also listed for comparison.

The most distinguished difference between the
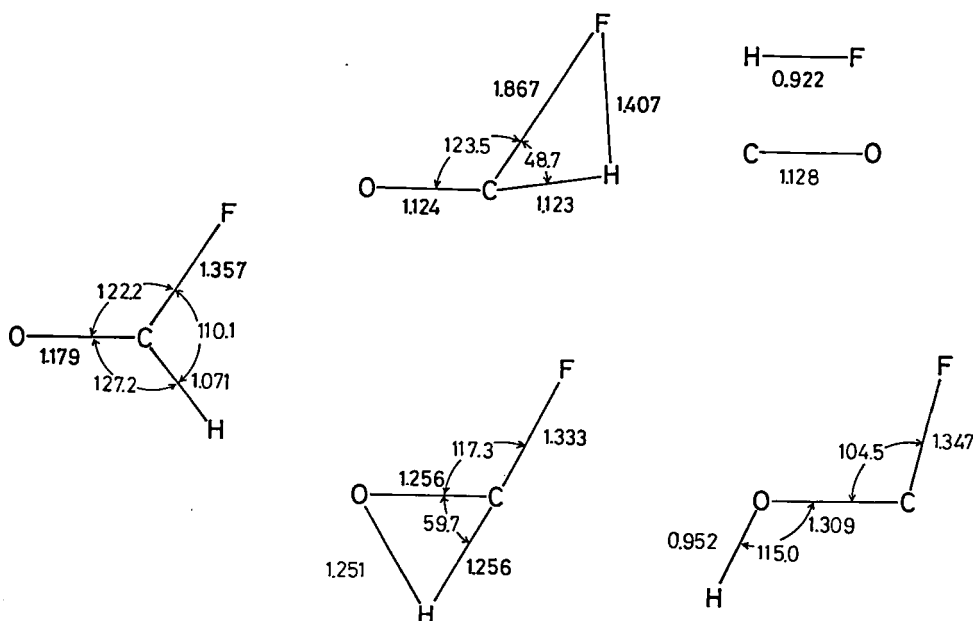
Figure 1. Optimized equilibrium and transition state geometries of species in the HFCO dissociation system.

HFCO and the H_2CO surface is the height of the direct dissociation barrier. In H_2CO the dissociation barrier and the isomerization barrier are of nearly the same height. In HFCO the dissociation barrier is substantially lower than the isomerization barrier. Therefore, if one can run a careful experiment at an energy between the two barriers (60 — 80 kcal/mol), one cannot use fluorohydroxycarbene as an intermediate. Since the UV absorption starts only at above 110 kcal/mol, this energy would have to be provided by some other means such as laser multi-

photon excitation. An observation whether the unimolecular dissociation reaction takes place at all and whether the time delay occurs if the reaction actually takes place would provide a key information for understanding the reaction mechanism.

References
1) P. L. Houston and C. B. Moore, *J. Chem. Phys.* 65, 757 (1976).
2) J. D. Goddard and H. F. Schaefer, *J. Chem. Phys.* 70, 5117 (1979).
3) J. R. Sodeau and E. K. C. Lee, *Chem. Phys. Lett.* 57, 71 (1978).

I—D Structure and Bonding in Metal Complexes

Complexes of metal and metal ions often play an essential role in homogeneous catalysis. The role of metal ions in biological catalytic reactions has also been emphasized. The last few years we have been interested in and done some preliminary studies on the -structure, bonding and reactions of transition metal complexes. Actual large scale MO calculations, however, became real only after IMS obtained its own computer in January 1979. This year we have concentrated our effort in understanding the nature of bonding of ligands in some complexes.

We also collaborated with Professor Saito's crystallography group in Tokyo in comparing directly X-ray determined electron density maps of transition metal complexes with MO-calcualted maps. On biological problems involving metal ions, we have learned a lot from collaboration with two quantum biology groups: Prof. Umeyama's group at Kitasato and Dr. Nagata-Prof. Kusunoki team.

I-D-1 Ab Initio SCF-MO Study on Ligand Distorsion and Bonding in $Ni(PH_3)_2L$ (L = C_2H_4 and C_2H_2) Complexes

Kazuo KITAURA, Shigeyoshi SAKAKI *(Kumamoto Univ.)* and Keiji MOROKUMA

The bonding in metal-olefin complexes has been qualitatively understood in terms of the Dewar-Chatt-Duncanson model. The present study is intended to elucidate the origin of binding semi-quantitatively in the metal-olefin and the metal alkyne complexes.

Ligand distorsion and bonding in $Ni(PH_3)_2L(L= C_2H_4$ and $C_2H_2)$ were investigated by ab initio SCF-

MO calculations. The basis sets used are for Ni the [4s3p2d] set which is contracted from the Roos-Veillard's [12s6p4d] sets[1] after a slight modification and for ligand atoms the 4-31G set with standard scale factors.

The geometry of $Ni(PH_3)_2$ fragment was constructed referring to the experimental structure of $Ni[P(C_6H_5)_3]_2C_2H_4$ and PH_3. Three geometrical parameters, R_{cc}, the bending angle and R_{NiC} were optimized. The results (Figure 1) agree well with the known structures of similar Ni-olefin and Ni-alkyne complexes. An increased C-C bond distance (1.42Å) and a substantial back bending (26°) indicate that the coordinated olefin has lost about half of its double-bond character. The coordinated alkyne is also considered to have a bonding character between a triple and a double bond.

The calculated binding energy (BE) is shown in Table I, along with its components, the deformation energy (DEF) and the interaction energy (INT=ES+ EX+CT+PL+MIX), obtained using the method of energy decomposition analysis for intermolecular interaction.[2] The forward- and the back-charge transfer energies are found to be larger in the alkyne complex than in the olefin complex, as is expected from the HOMO and LUMO energies of the ligands. The larger distortion destabilization of acetylene than that of ethylene cancels the charge transfer effect
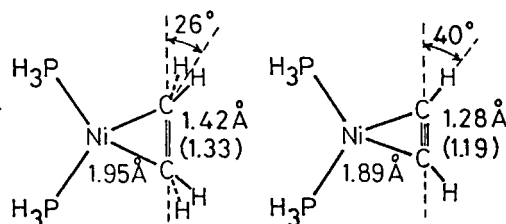
Figure 1. Distortion of coordinated ethylene and acetylene in $Ni(PH_3)_2C_2H_4$ and $Ni(PH_3)_2C_2H_2$. In the parenthesis are given the optimized C-C distances for free ligands.

19

Table I. Binding Energy and Its Component Analysis of the Interaction between the Ni(PH$_3$)$_2$ Fragment and Ligands[a]

	Ni(PH$_3$)$_2$C$_2$H$_4$	Ni(PH$_3$)$_2$C$_2$H$_2$
BE	−36	−37
DEF[b]	9	40
INT	−45	−77
ES	−132	−148
EX	168	189
CT	−86	−126
FCT	−41	−60
BCT	−44	−62
PL+MIX	−14	−8

[a] Energies in kcal/mol. The minus sign designates stabilization. BE=DEF+INT=DEF+(ES+EX+CT+PL+MIX). BE: binding energy, INT: interaction energy, ES: electrostatic energy, EX: exchange repulsion energy, CT: charge transfer energy, FCT: forward-charge transfer energy, BCT: back-charge transfer energy, PL: polarization energy and MIX: coupling term.
[b] The energy difference between the coordinated deformed ligand and the free ligand.

and results in the similar binding energy for both complexes. It is also found for both complexes that, as the bending angle increases, the back-charge transfer energy becomes larger more rapidly than any other energy component.

References

1) B. Roos, A. Veillard and G. Vinot, *Theo. Chim. Acta (Berl.)* **20**, 1 (1971).
2) K. Morokuma, *Acc. Chem. Res.*, **10**, 294 (1977).

I-D-2 Bonding of CO$_2$ in Transition Metal Complexes

Shigeyoshi SAKAKI *(Kumamoto Univ.)*, Kazuo KITAURA and Keiji MOROKUMA

CO$_2$ complexes of transition metals are candidates for fixing CO$_2$ molecules in the air. A few theoretical studies on the structure and binding in the complexes have been published so far.

There have been proposed two possible CO$_2$ coordination forms in a transition metal complex, namely, the side-on and the C-coordinated forms as shown in Figure 1. We have searched the favorable structure of Ni(CO$_2$)(PH$_3$)$_2$ using the ab initio SCF-MO method. The basis sets used were the [4s3p2d] set for Ni and the 4-31G set for other ligand atoms. The bending angle of CO$_2$ was optimized for both side-on and C-coordinated structures. The side-on structure with the optimized O-C-O angle of 139° was found to be more stable than the C-coordinated with the optimized angle of 170° (Figure 1). This is in accordance with the experimentally determined struc-

BE	−27 kcal/mol	6 kcal/mol
DEF	34	2
INT	−61	4
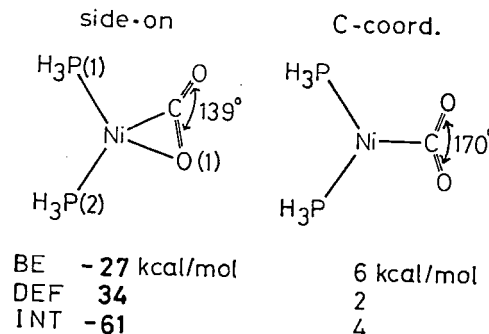
Figure 1. Comparison between side-on and C-coordinated complexes. The O-C-O angles are the optimized values. BE: binding energy, DEF: deformation energy, and INT: interaction energy. A minus sign means stabilization.
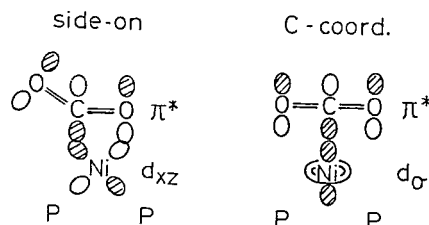
Figure 2. Orbital interactions in the side-on and the C-coordinated complexes.

ture of Ni(CO$_2$)(PCy$_3$)$_2$ where the side-on CO$_2$ has the O-C-O angle of 133°.

Mulliken populations are given in Table I. The 3d orbital population on Ni is larger and the population on CO$_2$ is smaller in the C-coordinated form than in the side-on form. It indicates that the back-charge transfer is more favored in the side-on structure. This is illustrated in Figure 2 from the orbital interaction point of view. In the side-on form the π^* orbital of CO$_2$ interacts mainly with the metal d$_{xz}$ orbital, while in the C-coordinated form the π^* orbital interacts with the dσ orbital which is more stable (therefore less interactive) than d$_{xz}$. The larger over-

Table I. Mulliken Populations of Ni(CO$_2$)(PH$_3$)$_2$

	Side-on	C-coord.
Ni	27.47	27.73
3d	9.14	9.63
PH$_3$(1)	17.93	18.07
PH$_3$(2)	17.96	18.07
CO$_2$	22.65	22.13
Ni-P$_1$	0.005	−0.109
Ni-P$_2$	−0.030	−0.109
Ni-C	0.109	0.043
Ni-O$_1$	0.055	−0.040

lap between the π^* and the d orbitals also favors the side-on form. Therefore, one can expect that the back-charge transfer interaction preferentially stabilizes the side-on structure in the Ni-CO_2.

In addition to the Ni-CO_2 complex, we have examined a possibility of CO_2 binding in Cu complexes. The end-on complex of a linear CO_2 was found to be the most stable among the three coordination forms (the side-on, the C-coord. and the end-on) of the $Cu(CO_2)(PH_3)_2$ complex, though the binding is weak (14 kcal/mol). The optimized Cu-C distance was 2.06Å.

I-D-3 Direct Comparison of Experimental and Theoretical Electron Density Distributions in CO (III) Complexes

Shigeru OHBA *(Univ. of Tokyo)*, Kazuo KITAURA, Keiji MOROKUMA and Yoshihiko SAITO *(Univ. of Tokyo and IMS)*

The electron density distribution in $K_2Na[Co(NO_2)_6]$ have been determined from the single-crystal X-ray diffraction method.[1] The result shows an aspherical electron density distribution around the Co atom and a substantial neutralization of Co positive charge. An ab initio SCF-MO calculation was performed for $[Co(NO_2)_6]^{3-}$, $[Co(CN)_6]^{3-}$ and $[Co(NH_3)_6]^{3+}$, and the electron density distribution was directly compared with the experiment. The basis sets used for the MO calculation are [4s3p2d] contracted from a modified Ross-Veillard's set[2] for Co and STO-3G for other ligand atoms.

Figure 1 shows experimental and theoretical difference electron density maps for $[Co(NO_2)_6]^{3-}$. Both are obtained by subtracting the sum of the spherically averaged ground state neutral atomic densities from the total electron density of the complex. The MO calculation reproduces the asphericity of density distribution around Co due to the nonbonding 3d electrons as well as the accumulation of electrons near the N atom along the Co-N bond due

(a)

(b)
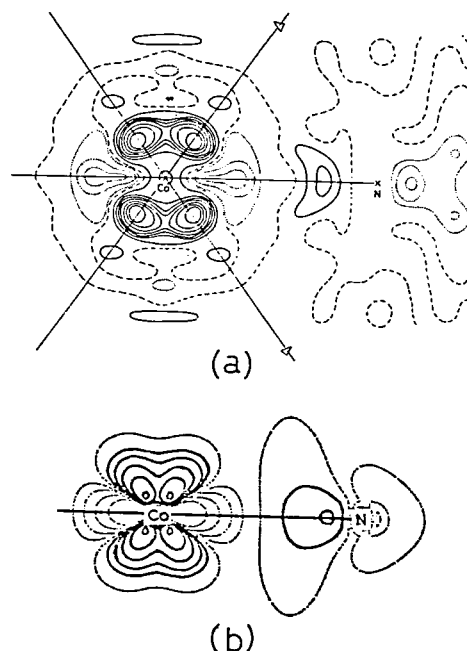
Figure 1. Section of the difference electron density through a Co-N bond and two threefold axis. Negative contours are dotted. 1-a is the experimental map and contour is at the interval of 0.2 $e \cdot Å^{-3}$. 1-b is the theoretical map and contours are ± 5.4, ± 2.7, ± 1.4, ± 0.7 and ± 0.3 $e \cdot Å^{-3}$

to the coordination bond formation.

The number of electrons in the sphere of radius 1.22Å (octahedral covalent radius of Co) centered on the cobalt atom for $[Co(NO_2)_6]^{3-}$ has been experimentally determined to be 26.3. (Table I) The corresponding theoretical value is 26.2, obtained by counting the number of electrons directly using a three-dimensional numerical integration method. The agreement between theoretical and experimental results is very satisfactory. The Mulliken population on the Co atom is found to be 26.4.

However, a care has to be paid in discussing the atomic charge based on Mulliken population, known to be strongly basis set dependent. Actually the Mulliken population on Co in $[Co(NH_3)_6]^{3+}$ is 26.3 and 25.3 with the [4s3p2d] and STO-3G basis set

Table I. Number of Electrons on Co and Mulliken's Population

	$[Co(NO_2)_6]^{3-}$		$[Co(CN)_6]^{3-}$		$[Co(NH_3)_6]^{3+}$	
Number of basis AO's	115		85		73 (126)[a]	
Internuclear distance (Å)	Co-N	1.952	Co-C	1.894	Co-N	1.979
Number of electrons in the sphere of radius 1.22Å centered on Co	calc.	26.2		26.7		26.0 (26.0)
	obs.	26.3		26.8		26.3
Mulliken Population	Co	26.4	Co	26.9	Co	26.3 (25.3)
	N	6.9	C	6.0	N	7.5 (8.1)
	O	8.3	N	7.5	N	0.7 (0.6)

[a] Numbers in parentheses are for a larger basis set. (See text.)

and the [5s4p3d] and 4-31G basis set, respectively, whereas the both basis sets give 26.0 as the number of electrons in the covalent radius.

References

1) S. Ohba, K. Toriumi, S. Sato and Y. Saito, *Acta Cryst.* B34, 3535 (1978).
2) B. Roos, A. Veillard and G. Vinot, *Theo. Chim. Acta (Berl.)* 20, 1 (1971).

I-D-4 Molecular Orbital Study on the Roles of Zinc Ion in Carboxypeptidase A

Setsuko NAKAGAWA *(Kitasato Univ. and IMS)*[1], Hideaki UMEYAMA *(Kitasato Univ.)*, Kazuo KITA-URA and Keiji MOROKUMA

Carboxypeptidase A(CPA) is a zinc-containing proteolytic enzyme. The X-ray crystallographic analyses of CPA showed that zinc, Glu 270 and Tyr 248 were important in catalysis for peptide substrate.[2] In order to elucidate the initial reaction step of CPA, the electronic structure of the active site of native CPA was studied.

A zinc ion, a Zn-coordinated water molecule and five amino acid residues (His 69, Glu 72, Asp 142, His 196 and Glu 270) in the active site of native CPA are considered in the ab initio SCF-LCAO-MO calculation. The basis set for Zn is a [11s7p5d] set contracted to [4s3p2d], and the basis set for other atoms is an STO-3G set. Figure 1 showed the assumed structure of the complex. Imidazole molecules are placed at the positions of His 69 and His 196 of the crystallographic data. Formic acides are placed at the position of Glu 72, Asp 142 and Glu 270. The distance between Zn and the oxygen of water molecule was chosen to be 2.0Å. Imidazole of His 196 is included in the SCF calculation only as fractional point charges.

The proton transfer from His 69 to Asp 142 is called the α proton transfer and that from the Zn-
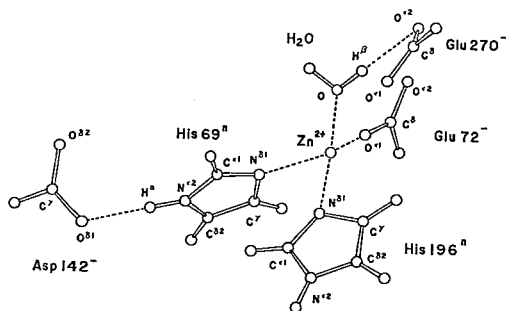
Figure 1. Assumed structure composed of Zn^{2+}, H_2O, His 69^n, Glu 72^-, Asp 142^n, His 196^n and Glu 270^n.
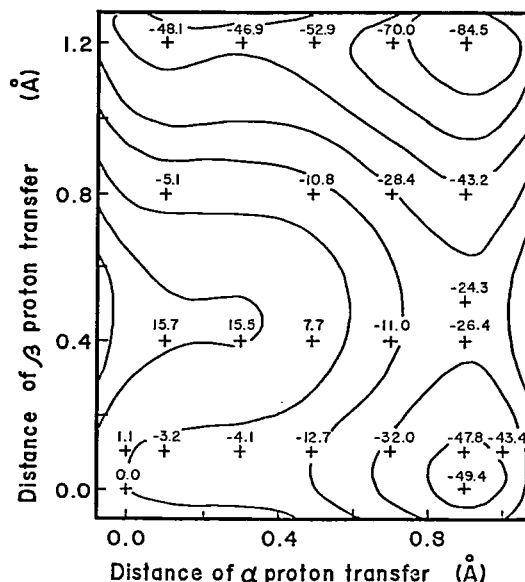
Figure 2. Potential energy surface for α and β proton transfers. The sign of + means calculated points. The unit is kcal/mol.

coordinated water molecule to Glu 270 is called the β proton transfer. The α proton was assumed to move along a line between $H(N^{\epsilon 2})$ of His 69 and $O^{\delta 1}$ of Asp 142 in Figure 1. The β proton was assumed to move along a line connecting O of the water molecule and $O^{\epsilon 2}$ of Glu 270. Calculation of the total energy was carried out for these two proton transfers. The results are shown in Figure 2. We can find two stable structures in the energy map. One is where α and β protons are moved from the original position by 0.9 and 0.0Å, respectively. This structure is more stable than the original structure by 49 kcal/mol. The other structure 85 kcal/mol more stable than the original, has α and β protons moved by 0.9 and 1.2Å, respectively. The α proton easily transfers from His 69 to Asp 142 without a potential barrier, and the β proton transfer has a potential barrier of about 20 kcal/mol. Thus, the structure in which the three anions (OH^-, His 69^- and Glu 72^-) surround Zn^{2+} is the most stable. The result implies that a hydroxyl ion is formed on Zn in an initial reaction step of CPA.

References

1) Visting Scholar, 1978–9.
2) W. N. Lipscomb, J. A. Hartsuck, G. N. Reeke, Jr., F. A. Quiocho, P. H. Bethge, M. L. Ludwig, T. A. Steits, H. Muirhead and J. C. Coppola, Brookhaven *Symp. Biol.*, 21, 24 (1968). F. A. Quiocho and W. N. Lipscomb, *Adv. Protein Chem.*, 25, 1 (1971).
3) S. Nakagawa and H. Umeyama, *J. Am. Chem. Soc.*, 100, 7716 (1978).

I-D-5 MO Studies of Molecular Mechanism and Role of Mn in Photosynthetic Water Decomposition

Masami KUSUNOKI *(Meiji Univ. and IMS[1])*, Kazuo KITAURA, Keiji MOROKUMA and Chikayoshi NAGATA *(National Cancer Center Research Inst.)*

Despite its importance in photosynthesis the molecular mechanism of water splitting reaction (WSR):

(1) $2H_2O \rightarrow O_2 + 4H^+ + 4e^-$ remains to be little understood.[1] Manganese ion has long been implicated to play an important role in the water splitting enzyme (WSE) system Y. It is considered to be probable that in the dark adapted chloroplast Mn is in the stable oxidation state of +2, and that the principal role of Mn in the process of accumulation of positive charges to the system Y involves a direct electron transfer from the internal aqueous phase of thyracoids. However, it is rather difficult to determine experimentally the actual environment of Mn.

Therefore, it would be worthwhile to infer the possible molecular mechanism from ab initio MO computations for some model MN (II, III, and IV) complex systems. In the present calculations, we have adopted the method of ab initio LCAO-MO-UHF (unrestricted Hartree-Fock) with a triple or double zeta Gaussian basis set for Mn and with a 4-31G or STO-3G set for other atoms.

In our model system, depicted in Figure 1, the WSE is replaced by an H_2O molecule and the ligands by fractional charges ($-0.3e$) placed at the corner of a square. The relative energies for this system with Mn(II) and Mn(III) and without Mn are plotted in Figure 1 as the function of the WSR coordinated, the distance between O and the separating proton H'. As seen in Table I, appreciable charge transfer occurs from H_2O to Mn(III), and the barrier for the dissociation is lowered substantially. The model thus suggests that Mn(III) can act as an activator of WSR. In fact, it is known that at low acidity hydrolysis occurs with Mn(III): Mn(III) + H_2O = Mn(II)OH + H^+, $K \sim 1$.

In photosynthesis the Kok mechanism states that the system Y including H_2O to be oxidized is charged up sequentially by photo-oxidized Chl a_{II}^+ via univalent electron transfer reactions, until a molecular
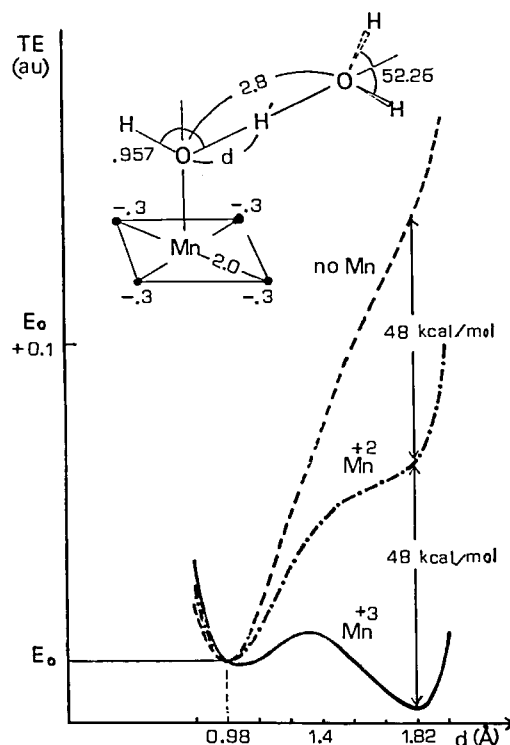
Figure 1. The ab initio relative energies as functions of the distance d. The Mn(II) and Mn(III) to O distances are assumed to be 2.07Å and 1.95Å, respectively, the optimum distances for Mn-OH$_2$ complex.

oxygen and four protons can be evolved. In this scheme, the pattern of oxygen release in a group of four short flashes has to be (0:0:0:1). While various patterns of four proton release have been proposed: (0:0:0:4) by Calvin *et al.*, (1:0:1:2) by Fowler and Crofts *et al.*, and (0:1:1:2) by Junge *et al.* and Renger. Our calculation shows that the ionization potential of the complex [Mn(II) (H$_2$O)$_4$ $\cdots$ OH$_2$] is substantially larger than that of the complex [Mn(III) (H$_2$O)$_4$ $\cdots$ OH$^-$]. The (1:0:1:2) model assumes that this is the case, whereas the (0:1:1:2) model assumes the opposite. Therefore, we consider the former more probable than the latter.

References

1) Visiting Scholar 1979–80.
2) *Photosynthetic Oxygen Evolution*, ed. H. Metzner, Academic Press, 1978.

Table I. Atomic Electron Population on Mn and H Which is Being Separated

d(O--H)	Å	0.84	0.98	1.12	1.40	1.68	1.82	1.96
no Mn	H'	0.58	0.53	0.54	0.54	0.52	0.53	0.58
Mn (II) Complex	H'	0.51	0.44	0.42	0.41	0.39	0.42	0.49
	Mn	23.08	23.09	23.09	23.12	23.16	23.17	23.19
Mn (III) Complex	H'	0.48	0.40	0.37	0.36	0.36	0.39	0.47
	Mn	22.24	22.25	22.28	22.34	22.42	22.48	22.64

23

I—E   Problems in Molecular Structures

Professor Harry King from SUNY Buffalo spent the winter in our Division as an Invited Foreign Scholar. Inspired by Dr. Herzberg's lecture in an IMS symposium, he has worked out the theory of Rydberg transitions in H_3.

We have had a close collaboration with Professor Tsuboi's IR group in Tokyo. We have used the energy gradient method, discussed in detail in I-B, to determine vibrational frequencies and intensities of rather large molecules of biological interest. It is our great pleasure to help experimentalists to resolve their problems and we plan to continue this collaboration.

A theoretical study on the structure of the free radical FSO has been carried out in conjunction with the microwave study of this free radical under way in the Division of Molecular Structure. The work on thiapentalens has been inspired by a talk at an IMS organic chemistry symposium.

I-E-1   Theory of the Rydberg Spectrum of Triatomic Hydrogen

Harry F. KING[1] and Keiji MOROKUMA

Herzberg has recently reported the observation of emission lines which he attributes to the Rydberg spectrum of triatomic hydrogen.[2] This is remarkable in being the first observation of a discrete Rydberg spectrum of a plyatomic molecule unstable in its ground electronic state. Motivated by this development we have carried out ab initio quantum calculations of Rydberg states of H_3 using a simple but realistic frozen core approximation. Here we report computed term values, transition probabilities, and related spectroscopic parameters which, hopefully, will assist spectroscopists in their analysis of the observed band structure.

Energies and properties of the fifteen lowest Rydberg states, shown in Table I, are computed using Koopmans' theorem with a large Gaussian basis set

Table I. Orbital Energies, Quantum Defects, and Expectation Values of Electronic Angular Momentum for the Fifteen Lowest Virtual Levels of Equilateral $H_3{}^+$ at R = 1.633324 Bohr; and Estimated Equilibrium Bond Lengths and Ionization Energies

k	State	$-\epsilon_k$ cm^{-1}	δ_k	$\langle L_z \rangle/\hbar$	R_k Bohr	ΔE_k cm^{-1}
1	(2p) 1E$'$	43235	0.4068	0.9711	1.86	—
2	(2s) 1A$'_1$	29880	0.0836	—	1.589	29977
3	(2p) 1A$''_2$	27892	0.0165	—	1.626	27893
4	(3p) 2E$'$	15615	0.3490	0.9775	1.659	15649
5	(3s) 2A$'_1$	12788	0.0706	—	1.617	12789
6	(3p) 2A$''_2$	12381	0.0229	—	1.636	12379
7	(3d) 3E$'$	12371	0.0216	−1.9807	1.642	12373
8	(3d) 1E$''$	12141	−0.0064	1.0000	1.640	12141
9	(3d) 3A$'_1$	12071	−0.0151	—	1.639	12070
10	(4p) 4E$'$	8183	0.3380	0.9725	1.647	8190
11	(4s) 4A$'_1$	7092	0.0663	—	1.634	7090
12	(4p) 3A$''_2$	6943	0.0244	—	1.638	6942
13	(4d) 5E$'$	6940	0.0236	−1.9735	1.641	6941
14	(4d) 2E$''$	6843	−0.0047	1.0000	1.640	6843
15	(4d) 5A$'_1$	6813	−0.0134	—	1.640	6813

Table II. Rydberg Vibronic Transitions for the D_3 Molecule Predicted by the Frozen-Core Model

Band	Upper state		Lower state		f^a	Type	Wavelength (Å)	ΔR_e (Bohr)
1	(3p)	$2^2E'$ (0,0)	(2s)	$1^2A'_1$ (0,0)	0.34	$\perp$	6980	0.070
2	(3p)	$2^2E'$ (0,0)	(2s)	$1^2A'_1$ (1,0)	0.29	$\perp$	8280	0.070
3	(3p)	$2^2A''_2$ (0,0)	(2s)	$1^2A'_1$ (0,0)	0.11	$\parallel$	5680	0.047
4	(3d)	$3^2A''_1$ (0,0)	(2p)	$1^2A''_2$ (0,0)	0.26	$\parallel$	6320	0.013
5	(3d)	$1^2E''$ (0,0)	(2p)	$1^2A''_2$ (0,0)	0.19	$\perp$	6350	0.014
6	(3s)	$2^2A'_1$ (0,0)	(2p)	$1^2A''_2$ (0,0)	0.03	$\parallel$	6620	0.009

^{a} Oscillator strength without Franck-Condon factor.

constructed to represent both core and Rydberg orbitals. Tests indicate that computed virtual orbital energies have converged to within a few wavenumbers of the spd SCF limit. All excited electronic states are computed to have geometries and vibrational force constants close to those of H_3^+. Jahn-Teller effects are weak. Small quantum defects and nearly integer values of electronic angular momenta indicate atomic-like character for the Rydberg states. Predicted vibronic transitions, shown in Table II, for D_3 are in remarkably close agreement with rotational band spectra recently observed by Herzberg. Results using our model are in complete accord with Herzberg's assignment of the strong emission bands observed near 5600 and 7100 Å, and offer a reasonable interpretation of the previously unassigned, weak emission bands observed near 6200 and 8500 Å.

References

1) IMS Invited Foreign Scholar 1978–9.
2) G. Herzberg, *J. Chem. Phys.*, 70, 4808 (1979).

Figure 1. Calculated excitation energies of FSO.

I-E-2 The Electronic Structure of the Ground ($^2A''$) and the First Excited ($^2A'$) State of the FSO Radical

Shogo SAKAI *(Kansai Univ.)*, Shigeki KATO and Keiji MOROKUMA

Very recently Endo, Saito and Hirota have carried out a microwave study on the FSO radical, and have determined its geometry and vibrational frequencies in the ground state.[1] However, other physicochemical properties of interest such as the dipole moment and the vibrational frequencies in excited states as well as the transition energies are still unknown.

We have calculated the electronic structure of the FSO radical in the ground ($^2A''$, π radical) and the first excited ($^2A'$, σ radical) states with the ab initio UHF and SCF-CI methods. The basis set chosen is the 4-31G set, augmented with a set of s and p type Gaussian bond functions on both O-S and S-F bonds. The equilibrium geometrical parameters were calculated by the use of the UHF energy gradient method and are listed in Table I. The calculated $^2A''$ state geometry is in excellent agreement with the experiment.

The corrected geometry for $^2A'$, obtained by adding to the calculated geometrical parameters the difference between the observed and calculated values for $^2A''$, constitutes a theoretical prediction. The

Table I. Summary of SCF Results for FSO

	$^2A''$ State		$^2A'$ State	
	cal.	obs.	cal.	corrected
r_{OS}, Å	1.44_3	1.457	1.68_3	1.69_7
r_{SF}, Å	1.56_0	1.596	1.56_7	1.60_3
$\angle OSF$,	$107._9^\circ$	108.4°	$95._1^\circ$	$95._6^\circ$
ν_1 (OS), cm^{-1}	1170	1010–982	780	670 (0.85)[a]
ν_2 (SF), cm^{-1}	885	872–867	910	890 (0.98)
ν_3 ($\angle OSF$), cm^{-1}	445	393–392	330	290 (0.78)
dipole moment[b]				
$|\mu|$, D	2.3		1.9	
θ	36°		46°	

[a] The scaling factor obtained from the calculated and average experimental values in $^2A''$ state and used to calculate the corrected value for $^2A'$.

[b] The dipole moment points to the direction bisecting the OSF angle. θ is the angle between the dipole moment and the S-O axis.

calculated fundamental vibrational frequencies in the $^2A''$ ground state also compare well with the corresponding experimental data. We determined the diagonal force constant scale factors by matching the calculated and experimental frequencies for $^2A''$ and used them to scale the calculated frequencies for $^2A'$. The corrected frequencies thus obtained constitute our prediction. We expect that our basis set estimates the absolute value of the dipole moment, but that its change upon excitation is reasonably predicted.

The calculated excitation energies, shown schematically in Figure 1, are obtained by CI calculations at the UHF optimized geometries. CI includes up to 3100 configurations with a perturbation correction for 25000 more doubly excited configurations. We expect that errors are about 0.1 eV.

Reference

1) Y. Endo, S. Saito, and E. Hirota, *IMS Rev. Ann.*, 42 (1979).

I-E-3 The Geometry and Electronic Structure of Thiapentalens

Keiji MOROKUMA and Mitsuyasu HANAMURA[1]

6a-Thia(6a-S^{IV})pentalens such as 1,6,6a-trithiapentalen 1 have been receiving much attention because of their unique S-X distances and pseudo-aromaticity. We have investigated the geometry and electronic

1 X = S
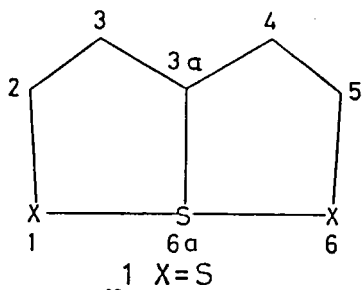
structure of 1 and its analogues using the ab initio SCF MO method. The geometries of 1,5-(iminomethyl-amino)-thiaziazole 2 and 1,3,4,6-tetraza-6a-thia(6a-S^{IV})-pentalenium cation 3 were fully optimized with the split-valence 4-31G basis set by the use of the technique of analytically calculating the energy gradient. As shown in Figure 1, the optimized geometry of 1 has a C_{2v} symmetry, in agreement with experiment, but has S(6a)-C and S(6a)-S bond lengths too long by 0.1Å. The same trends are seen in the calculated S(6a)-N bond lengths of 2 and 3. In order to analyze this discrepancy, we have calculated total energies at the experimental and the 4-31G optimized geometries with the 4-31G basis set augmented with bond functions. The bond functions
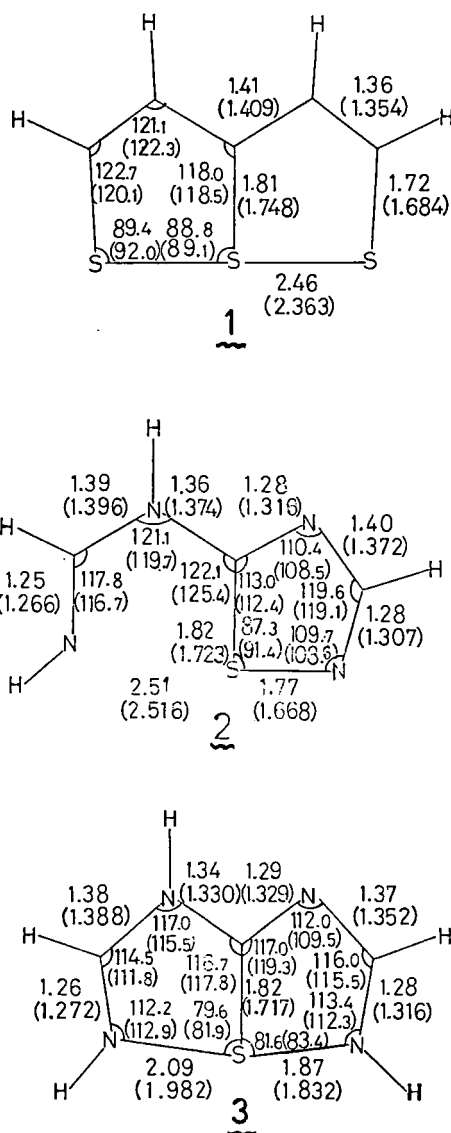
Figure 1. The calculated and experimental (in parentheses) geometries of 1, 2 and 3.

consist of a single set of Gaussian s- and p-functions centered at the midpoint of each bond around S(6a). The energy difference ΔE between the two geometries is shown in Table I. ΔE is of course positive for 4-31G. With the bond functions ΔE becomes negative for 1 and 2 and nearly so for 3. This suggests that the geometry optimization with the bond functions, which we have not done, would give optimized geometries which closely resemble the experimental geometries.

Table I. The Energy Difference ΔE between the Experimental and the 4-31G Optimized Geometries (in kcal/mol)

Basis	1	2	3
4-31G	10.0	10.6	12.0
4-31G + BF	−1.0	−1.0	2.9

Thus the discrepancy between the 4-31G optimized and the experimental geometries can be attributed to the effect of electronic polarization around S(6a). An examination of electron distribution in the S(6a) region reveals that the S(6a)-S bond in 1 is a weak σ bonding, while the both S(6a)-N bonds of 3 and the longer S(6a)-N bond of 2 are principally electrostatic in nature.

Note

1) IMS Graduate Student 1979– from Tohoku Univ.

I-E-4 Force Constants and Dipole Derivatives for Formamide from Ab Initio MO Calculation

Yoko SUGAWARA*, Yoshiaki HAMADA*, Akiko Y. HIRAKAWA*, Masamichi TSUBOI*, (*Univ. of Tokyo), Shigeki KATO and Keiji MOROKUMA

Determination of a force field for a large molecule is not a easy task. Especially interaction terms leave ambiguities even with additional pieces of information such as isotope shifts and centrifugal distortion constants. In such a case an ab initio MO calculation is expected to provide a helpful guide. In an attempt to establish a proper starting force constant set and to reexamine the force field of amide compounds, we have carried out the ab initio SCF MO calculation of formamide compounds. The energy gradient method was used to determine the equilibrium geometry and force constants. The basis set used is the 4-31G.

The calculated equilibrium geometry is planar, and agrees well with the structure determined by the microwave spectroscopy.[1] For in-plane vibrational modes, we have found the following. (see Table I and Figure 1)

1) Calculated frequencies were generally $10 \sim 20\%$ greater than the observed fundamental frequencies.
2) Isotope shifts ($-d_0$, $-d_1$, $-d_2$ and $-d_3$ species)
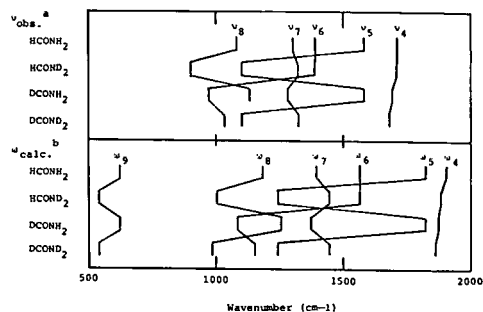
Figure 1. Isotope shifts for in-plane modes. ([a]CHCl$_3$ soln. Ref. 2. [b]This work.)

were well reproduced.
3) The calculated dipole moment derivatives showed a good correspondence with the infrared intensity pattern.
4) The general feature of the calculated force field showed a good correspondence with the modified Urey-Bradley force field which Tanaka et al. obtained based on the observed frequencies.[2]
5) The NH$_2$ rock-OCN bend cross term, which is zero in the Urey-Bradley force field, should be as large as -1.8mdyne/Å. For out-of plane modes, a good reproduction of experimental data was obtained by the calculation including polarization functions.

References

1) E. Hirota, R. Sugisaki, C. J. Nielsen and G. O. Sørensen, J. Mol. Spectrosc., 49, 251 (1974).
2) Y. Tanaka, K. Machida, J. Mol. Spectrosc., 63, 306 (1976).
3) J. C. Evans, J. Chem. Phys., 22, 1228 (1954).
4) S. T. King, J. Phys. Chem., 75, 405 (1971).

Table I. Observed and Calculated Vibrational Frequencies and Dipole Derivatives for In-Plane Mode

No.	ν obs.[a] (cm^{-1})	ω calc. (cm^{-1})	$(\partial\mu/\partial Q_j)^2$ ((D/Q unit)^2)	Assignment	
1	3545 ms	3964	0.42	NH$_2$	asym. stretching
2	3451 ms	3826	0.37	NH$_2$	sym. stretching
3	2852 ms	3249	0.50	CH	stretching
4	1734 vs	1898	2.99	CO	stretching
5	1572 mw	1822	0.39	NH$_2$	scissoring
6	1378 vw	1561	0.18	CH	bending
7	1255 s	1391	1.10	CN	stretching
8	(1084)	1178	0.06	NH$_2$	rocking
9	565	623	0.12	NCO	bending

[a] Gaseous state. Ref. 3 and Ref. 4.

I-E-5 Vibrational Modes of Uracil from Ab Initio MO Calculation

Yoshifumi NISHIMURA *(Univ. of Tokyo)*, Masamichi TSUBOI *(Univ. of Tokyo and IMS)*, Shigeki KATO and Keiji MOROKUMA

Resonance Raman spectroscopy of various biological chromophores should lead us to a useful piece of information on the vibronic levels and geometrical structures in their excited electronic states, if the vibrational modes are properly assigned to the observed Raman lines. In general, however, it is not easy to obtain unambiguously the force constants, especially coupling force constants, for such biological chromophores. Ab initio MO calculation should be able to provide a good starting point for force constant evaluation.

In this work we have calculated force constants of uracil with the ab initio SCF method with the STO-3G basis set. The energy gradient technique has been used to obtain the equilibrium geometry and diagonal and offdiagonal force constants. The calculated and experimental equilibrium geometries agree each other within 0.05Å of C-C and C-N bond lengths.

In Table I, are given the vibrational frequencies and the vibrational modes calculated on the basis of the ab initio MO set of the force constants. Calculated frequencies are higher than the corresponding observed frequencies by $10 \sim 30\%$. However, the agreement between the calculated and the observed pattern of spectra is satisfactory. Thus the six vibrational frequencies and vibrational modes, which have been previously assigned on the experimental and empirical basis to the six Raman lines (Ur I $\sim$ Ur VI, at 1680, 1630, 1475, 1397, 1231, and 783 cm^{-1}) of uridine in resonance with the 260 mm band,[1,2] well reproduced in the present calculation.

We find a discrepancy between the calculated and experimental frequencies as well as modes for vibrations coupling a ring motion and an N_3-H and/or a C-H inplane deformation motion. In an attempt to resolve this discrepancy, we have made a calculation for acrolein, which is considered to be a proper fragment of uracil, by the use of two basis sets, STO-3G and 4-31G. The results are given in Table II. Two sets lead to nearly equal vibrational modes, with 4-31G showing a slightly better agreement with the experiment.

References

1) Y. Nishimura, A. Y. Hirakawa and M. Tsuboi, *"Advances in Infrared and Raman Spectroscopy,"* ed. by R. J. H. Clark and R. E. Hester, Heyden, London (1978), Vol 5, Chap. 4.
2) Y. Nishimura, H. Haruyama, K. Nomura, A. Y. Hirakawa and M. Tsuboi, *Bull. Chem. Soc. Jpn.* **52**, 1340 (1979).
3) J. C. D. Brand and D. G. Williamson, *Disc. Faraday Soc.* **35**, 184 (1963).
4) R. K. Harris, *Spectrochim. Acta* **20**, 1129 (1964).

Table I. Vibrational Frequencies and Assignments of Uracil

STO-3G		Experimental	
Frequency (cm^{-1})	Assignment[a]	Frequency (cm^{-1})	Assignment[a]
4145	ν N_1-H	3160	ν N-H
4116	ν N_3-H	3160	ν N-H
3768	ν C-H in phase	3100	ν C-H in phase
3717	ν C-H out of phase	3080	ν C-H out of phase
2110	ν C_2=O	1716	ν C_2=O
2094	ν C_4=O, ν C=C in phase	1680	ν C_4=O, ν C=C in phase
2009	ν C_4=O, ν C=C out of phase	1630	ν C_4=O, ν C=C out of phase
1712	δ N_1-H	1508	δ N_1-H
1627	δ N_3-H	1453	ν ring + δ C_5-H
1613	δ C-H in phase	1423	δ N_3-ring
1549	ν ring	1397	ν ring
1426	ν ring (Kekulé type)	1231	ν ring (Kekulé type)
1358	δ C-H out of phase	1201	δ C_6-H
1231	ν ring	1099	δ C_5-H + ν ring
1065	ν ring, δ ring	1003	ν ring
1054	δ ring, ν ring	993	δ ring
839	ν ring (breathing)	781	ν ring (breathing)
601	δ ring	585	δ ring
578	δ C=O in phase	565	δ C=O
541	δ ring	550	δ ring
406	δ C=O out of phase	398	δ C=O

[a] ν, streching and δ bending

STO-3G	4-31G		Experimental[3],[4]	
Frequency (cm^{-1})	Frequency (cm^{-1})	Assignment[a]	Frequency (cm^{-1})	Assignment[a]
3811	3418	ν CH_2 antisymmetric	3103	ν CH_2 antisymmetric
3723	3371	ν C-H (β)	3028	ν C-H (β)
3652	3324	ν CH_2 symmetric	3000	ν CH_2 symmetric
3545	3184	ν C-H (α)	2800	ν C-H (α)
2094	1925	ν C=O, ν C=C in phase	1724	ν C=O
2018	1846	ν C=O, ν C=C out of phase	1625	ν C=C
1701	1613	CH_2 scis.	1420	CH_2 scis.
1601	1543	δ C-H (α)	1360	δ C-H (α)
1511	1443	δ C-H (β)	1275	δ C-H (β)
1315	1292	ν C-C, C-H rock	1158	ν C-C
1050	1022	C-H rock, ν C-C	912	CH_2 rock
616	627	C-C-O def. δ C-C-C	564	C-C-O def.
352	364	δ C-C-C, C-C-O def.	327	δ C-C-C

[a] $C\alpha$ is the carbonyl carbon and $C\beta$ is the central carbon atom.

I—E Surface Electronic Structure of Metal Oxides and Chemisorption Mechanisms

Metal oxides provide us inexpensive and practical catalysts with a great variety of properties. They are also important as electrode materials on which many interesting electrode and photo-electrode processes take place. Though any of real reactions on surfaces include many intricate processes, fundamental physical and chemical investigations are now becoming increasingly important.

We have begun theoretical studies of the electronic structure of ideal and real surface of metal oxides and their interactions with simple adsorbates, aiming to be the first step towards the elucidation of molecular processes on solid surfaces. Investigation of the localized electronic states induced by surface defects and their role on surface molecular processes are among the major interests of the project. Through the studies of several prototype oxides, ranging from simple metal to transition metal oxides, or from ionic to metallic oxides, the differences among each prototype in the characteristics of the surface electronic structure and their physical origins have been clarified.

I-F-1 Theory of the Surface Electronic Structure and Defect States of Rutile by the DV-Xα Cluster Calculation

Masaru TSUKADA, Chikatoshi SATOKO, and Hirohiko ADACHI (Osaka Univ.)

By the recent experiments of UPS and ELS, it has been verified that occupied defect states appear slightly below the Ti d conduction band, when the TiO_2 rutile crystal is bombarded by the Ar beam. Since the photo-electrochemical activities of the reduced TiO_2 surface is much stronger than that of the stoichiometric surface, the defect state induced by the oxygen removal seems closely related with the surface chemical activities.

We investigate the stable (110) rutile surface on which many experiments in ultra-high vacuum have

been worked out.[1,2] The DV-Xα calculation[3] is made for the surface cluster $(Ti_4O_{16})^{16-}$ which is shown in Figure 1a, and the surface defect cluster which is derived from Ti_4O_{16} cluster by the removal of the outermost oxygen ion, O(9). Our calculation revealed the oxygen ion is removed with the neutral
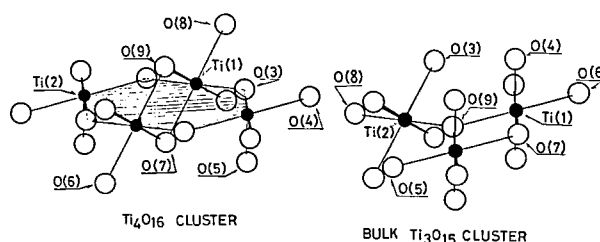
Figure 1. a) Structure of Ti_4O_{16} cluster for the ideal (110) rutile surface. White and black circles represent respectively the oxygen and titanium ion. The shadowed plane shows the (110) surface. b) The structure of the bulk Ti_3O_{15} cluster.

state leaving two electrons in the defect state and in the d states of nearby Ti ions. The state density of the clusters is depicted in Figure 2a. It is remarkable that with the O ion removal, the peaks A′, C′ of the cluster $(Ti_4O_{16})^{16-}$ representing the intrinsic surface state disappear and partly occupied defect level appears at about 1.8 eV below the lowest Ti d band.

To look for the change of the electronic structure as going from the bulk to the surface, the electronic structure of the bulk $(Ti_3O_{15})^{18-}$ cluster (see Figure 1b) is calculated. The state density is drawn in Figure 2b by the dashed line. It can be seen that the broadening of d levels due to the interaction among those on different Ti ions is relatively small compared with the crystal field splitting 10 D_q between A and B band. The local electronic structure associated with the bulk oxygen vacancy is investigated by the cluster Ti_3O_{14} obtained from Ti_3O_{15} cluster by the removal of the central O ion (Figure 1b). As seen by the full line in Figure 2b, the defect level is induced near the gap center and occupied by two electrons.

As seen in Figure 2 both the defect clusters in the bulk and on the top layer have the localised defect state, which explains the UPS structure in the gap region of the bombarded surface.[1,2] The ELS peak at 1.6 eV for the bombarded (110) surface corresponds to the transition from the defect level to the peak A of the top layer. The ELS peak[1] at 2.4 eV for the ordered (110) surface is assigned to the transition from the oxygen intrinsic surface state to the

titanium intrinsic surface state (C′ → A′ in Figure 2a). The UPS spectra[1,2] in the valence band region can be well explained by the state densities of the bulk cluster, which indicates that the emitted electrons in this energy region carry information within a few layers below the surface.

References

1) Y. W. Chung, W. J. Lo and G. A. Somorjai, *Surface Sci.*, **64**, 588 (1977). W. J. Lo, Y. W. Chung and G. A. Somorjai, *Surface Sci.*, **71**, 199 (1978).
2) V. E. Henrich, G. Dresselhaus and H. J. Zeiger, *Phys. Rev. Lett.*, **36**, 1335 (1976), Solid State Commun., **24**, 623 (1977).
3) M. Tsukada, C. Satoko and H. Adachi, *J. Phys. Soc. Japan*, **44**, 1043 (1978).

I-F-2 Surface Electronic Structure of $SrTiO_3$ by the DV-Xα Cluster Method

Masaru TSUKADA, Chikatoshi SATOKO and Hirohiko ADACHI *(Osaka Univ.)*

Transition metal oxides with the cubic perovskite structure have recently attracted much attention because of its catalytic and photocatalytic activities. A wide range of properties are expected to be obtained by the cation substitution. Among others strontium titanate is appropriate to initiate a theoretical study of the surface electronic states and their role on the catalytic reactions, since the electronic structure is relatively simple and the reliable experimental data in ultra-high vacuum are accumulated.[1]

To investigate the electronic structure of bulk and (100) surface, the molecular orbitals of the two bulk clusters, $(TiO_6)^{8-}$, $(Ti_2O_{11})^{14-}$ and the three surface clusters, $(TiO_5)^{6-}$, $(Ti_2O_9)^{10-}$, $(Ti_2O_{10})^{12-}$ are calculated by the DV-Xα cluster method. The structure of these clusters are shown in Figure 1. The localized
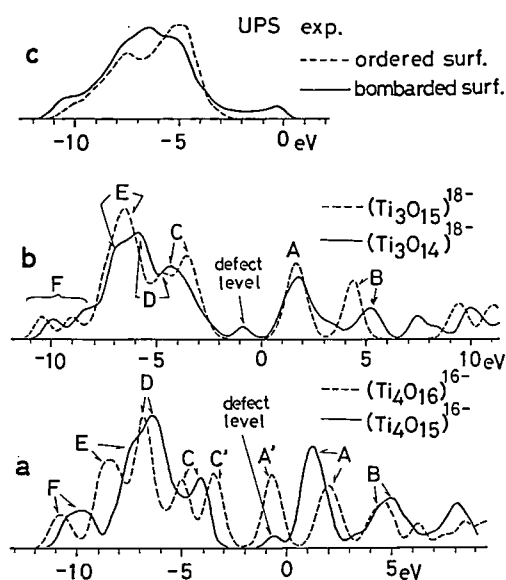
Figure 2. a) The state densities of the surface clusters, $(Ti_4O_{15})^{16-}$ (full line) and $(Ti_4O_{16})^{16-}$ (dashed line).
b) The state densities of the bulk cluster, $(Ti_3O_{14})^{18-}$ (full line) and $(Ti_3O_{15})^{18-}$ (dashed line).
c) The UPS spectra for the bombarded (full line) and the ordered (dashed line) (110) rutile surface.
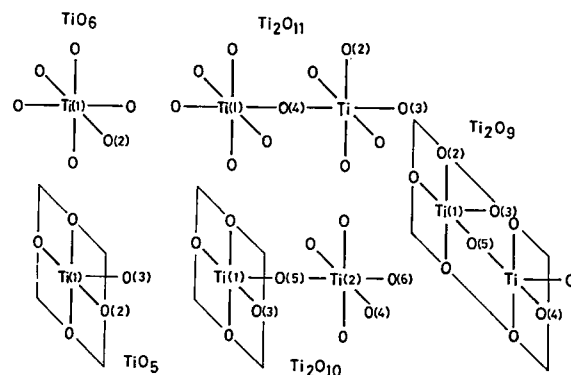
Figure 1. Structure of various clusters calculated in the present work.

defect states induced by the O vacancy are also investigated by the cluster Ti_2O_{10} (Ti_2O_{11} with O(4) missing), Ti_2O_8 (Ti_2O_9 with O(5) missing) and the surface TiO_3 cluster. The calculated shape and width of the bulk state density correspond well with the UPS and XPS experiments[1,2] and the APW[3] band calculation.

In the ideal (100) surface exposing Ti and O ions, the Ti $3z^2$-r^2 state is considerably admixed with the Ti 4s, $4p_z$ orbitals due to the strong surface field.[4] This polarization effect, together with the effect of the surface enhanced covalent mixing on the other d states, pushes down the energy of the $3z^2$-r^2 level ($25a_1$ level in Ti_2O_{10} cluster) relative to other levels to make it a shallow surface state. The xz, yz like d states on the top layer (17e in Ti_2O_{10} cluster) also form the shallow surface state, while xy and x^2-y^2 like d states can not be the surface state as seen in Figure 2. Our calculation demonstrates that the deep intrinsic surface states do not exist in the (100) surface in accordance with experiments. It is found that the reduction in the Madelung potential is largely cancelled out by the surface enhanced covalency and the charge redistribution effect. An interesting finding obtained by the calculations of various bulk and surface clusters is that the local electronic structure, e.g. the local state density or the metal d level structure is almost determined by the smallest cluster unit including the single metal ion and its nearest neighbor ligands. Especially the local electronic structure at the third atomic layer is scarcely changed from that of the bulk.

It was verified that the oxygen vacancy introduces deep gap states which are mainly derived by the adjacent metal orbitals. The defect level position differs remarkably whether it is associated to a single O vacancy or two vacancies sandwitching the Ti ion. In the former case the strong electric field on the metal site admixes Ti 4p, 4s, 3d states to form a base of the defect wave function extending towards the vacancy. The level position of this type of defect

states is generally very deep. The midgap extrinsic states found on vacuum fractured (100) surface is probably corresponding to such defect states associated with the O vacancy on the top layer. On the other hand another kind of gap states formed by Ar bombardment are assigend to the defect level associated with O vacancies within several layers from the surface. The energy loss peak at 2.2 eV for the bombarded surface is explained by the transition from the ground state to the excited state of the defect level.

References

1) V. E. Henrich, G. Dresselhaus and H. J. Zeiger, *Phys. Rev.*, B 17, 4908 (1978), R. A. Powell and W. E. Spicer, *Phys. Rev.*, B 13, 2601 (1976).
2) F. L. Battye, H. Hochst and A. Goldman, *Solid State Commun.*, 19, 269 (1976).
3) L. F. Mattheiss, *Phys. Rev.*, B 6, (1972).
4) C. Satoko, M. Tsukada and H. Adachi, *J. Phys. Soc. Japan*, 45, 1333 (1978).

I-F-3 Theory of Chemisorption of O, H and OH Group onto the SrTiO₃ (100) Surface

Masaru TSUKADA and Chikatoshi SATOKO

Photo-assisted decomposition of water over the surface of TiO_2 and $SrTiO_3$ has been current topics actively persued by electrochemists and surface scientists.[1] Towards the elucidation of the photo-dissociation mechanism, a lot of investigations should be worked out for the fundamental problems including the interaction of water molecule or their fragments with the semiconductor surfaces. The purpose of the present work is to study the electronic structures of the chemisorption systems of O, H, and OH group onto the $SrTiO_3$ (100) surface by means of several model clusters. The cluster levels of O-TiO_5, HO-TiO_5, O-TiO_3 and H-Ti_2O_9 are calculated by the DV-Xα method. Figure 1 shows the structure of the clusters and obtained Mulliken charge for the respective ions. The distance between the oxygen adatom and the surface Ti atom in the clusters is chosen as 3.69 au, which is equal to the Ti-O distance in the $SrTiO_3$ crystal. The distance between the hydrogen atom and the nearest oxygen atom in the clusters HO-TiO_5, H-Ti_2O_9 is assumed as 1.92 au, which is equal to the atomic distance of the isolated OH^- ion. The number attached to the chemisorption bonds represents overlap population calculated, which is a measure of the strength of the covalent bonding. The net charge of the clusters, OH-TiO_5, O-TiO_3, O-TiO_5 are assumed as 6−, 5.4−, 6− so that the Fermi energies are not contradict with that of the cluster $(TiO_5)^{6-}$ of the ideal surface.

The net charge (−0.77) and the overlap popula-
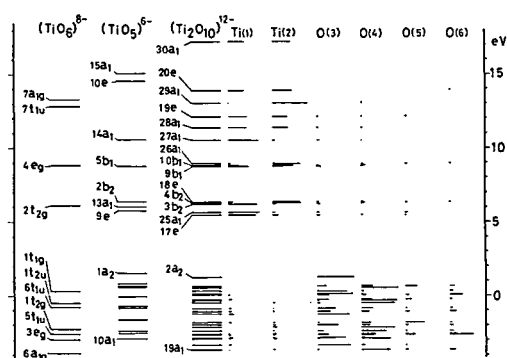
Figure 2. Level structures of $(TiO_6)^{8-}$, $(TiO_5)^{6-}$ and $(Ti_2O_{10})^{12-}$. Orbital components for the levels of $(Ti_2O_{10})^{12-}$ are also shown.
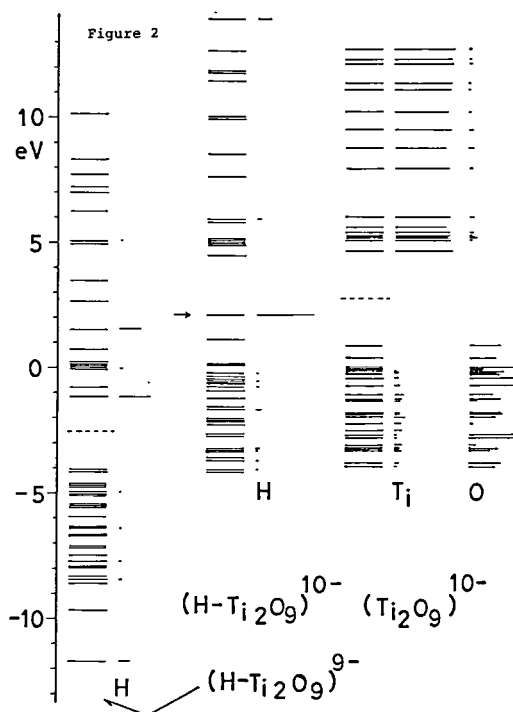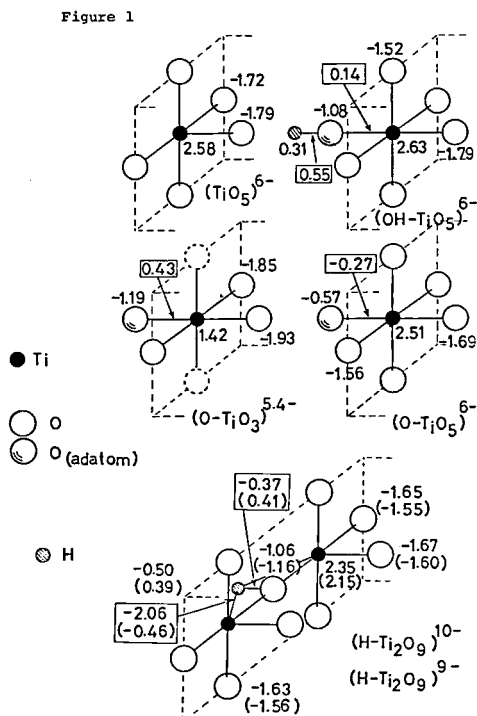
Figure 1

Figure 1. Structures of the clusters representing several chemisorption systems on $SrTiO_3$ (100) surface.

Figure 2. Level structure of $(Ti_2O_9)^{10-}$ and $(H-Ti_2O_9)^{10-,9-}$ clusters. Arrow and the dashed line indicate Fermi level.

tion (0.55) of the hydroxyl group chemisorbed on top of the Ti atom are close to those of isolated OH^- ion. The covalency of the O-Ti chemisorption bond (0.14) is much weaker than the O-H bond, though it has a bonding character. For the chemisorption of oxygen atom on top of the surface Ti atom modelled by the cluster, $(O-TiO_5)^{6-}$, the Ti-O chemisorption bond has an antibonding character (-0.27) and the ionicity of the oxygen adatom is very small (-0.57). This suggests that the chemisorption of oxygen atom on the ideal $SrTiO_3$ surface is much weaker than that of OH group, if it is chemisorbed. On the other hand, the result of the cluster $(O-TiO_3)^{5.4-}$, which is modelled on the oxygen chemisorption on top of the Ti atom sandwitched by the two oxygen vacancies, shows a strong bonding character of the chemisorption bond. This, together with the large ionicity of the adatom, indicates a strong binding of the oxygen adatom on the Ti sites of a reduced $SrTiO_3$ surface.

The level structures of the cluster $(H-Ti_2O_9)^{10-,9-}$ are shown in Figure 2 for the two charge states 9—, 10— with that of the cluster $(Ti_2O_9)^{10-}$ without the chemisorption. The former and the latter charge state correspond to the chemisorption of proton and hydrogen atom, respectively. Calculation for (H-$Ti_2O_9)^{10-}$ revealed a consistent level structure with that of $(Ti_2O_9)^{10-}$, whereas the energy levels of (H-$Ti_2O_9)^{9-}$ is not consistent with $(Ti_2O_9)^{10-}$. The resulted overlap populations for the H-O and H-Ti

bond are negative for the cluster $(H-Ti_2O_9)^{10-}$. The charge of hydrogen atom is also negative, indicating electrostatic repulsion by the nearest lattice oxygen ions. One may conclude, therefore, that the hydrogen atom is not chemisorbed on the oxygen site of the ideal $SrTiO_3$ surface. It should be remarked, that a weak chemisorption could take place, if the charge state $(H-Ti_2O_9)^{9-}$ were possible. The raising of the cluster potential due to the approach of OH^- ion, for example, would realize the charge state (H-$Ti_2O_9)^{9-}$ and therefore the weak hydrogen chemisorption.

Reference

1) T. Watanabe, A. Fujishima and K. Honda, *Bull. Chem. Soc. Jpn.* **49**, 335 (1976), J. G. Mavroides, J. A. Kaflas and D. F. Kolesar, *Appl. Phys. Lett.*, **28**, 241 (1976).

I-F-4 Surface Electronic Structure of Transition Metal Oxides

Chikatoshi SATOKO and Masaru TSUKADA

Transition metal oxides are interesting for their wide variety of electronic, magnetic and catalytic properties. This may be because they have partially filled d-orbitals which are in itinerant or not. Bulk electronic structures of the 3d-transition metal oxides

have been calculated by the augmented-plane-wave (APW) method[1] and others. However, the nature of their surface electronic structure has not been previously reported as far as we know. This may be an important factor in accounting for catalytic properties of transition metal oxides.[2] If the surface electronic structure has quite different character from the bulk, surface behaves quite differently in electronic and magnetic properties. It is interesting to know what mechanism is important to catalytic process in transition metal oxides. In order to pursue the behavior of catalytic process, more detailed knowledge about the surface electronic structure is needed.

Nondissociative ortho-para hydrogen conversion on transition metal oxides[3] has been studied for many years. The conversion rate has been said to be related with the surface magnetic properties. Experimentally, surface magnetism has been observed by the analysis of the extra diffraction spot intensities of the low energy electron diffraction.[4] Usually the exchange-interaction near the surface has been assumed to be equal to that of the bulk. However, theoretical understanding about the mechanism of the surface magnetic interaction is not sufficient.

We have calculated their surface electronic structure using the self-consistent cluster DV-Xα method. We include the electro-static potential of ions outside the cluster by Madelung potential. We have started to compare the electronic structure of the cluster model with the band structure of the bulk. The similar results are obtained by the cluster calculations as those by the band theory.[1] The d-levels shift downwards from TiO to NiO with the metal atomic number, and the Me 3d-O 2p gap energy becomes
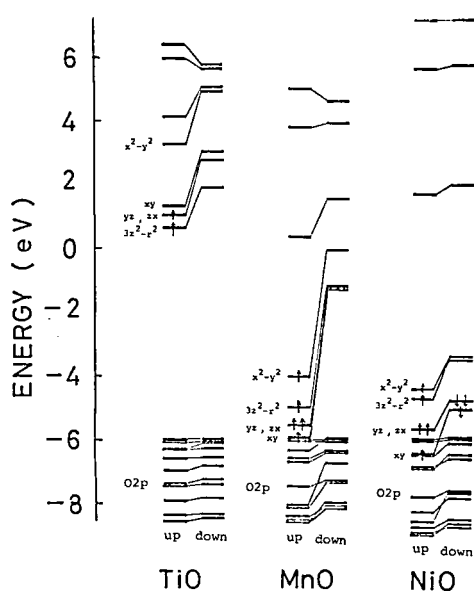
Table I. Matrix Elements of Surface Gradient Potential Between Metal Orbitals

	$<s\|V_s\|p_z>$	$<3z^2\text{-}r^2\|V_s\|p_z>$
NiO	0.11 ^{Ry}	0.02 ^{Ry}
MgO	0.14	–
TiO	0.21	0.11

smaller. The position of the metal 4s level is nearly constant for all metal oxides. This means that the cluster model for these covalent materials is a good approximation. We choose the model cluster of the surface as $(MO_5)^{8-}$. The energy structures in Figure 1 show the surface electronic structures of TiO, MnO and NiO. The energy scale is shifted so that the top of the majority valence band coincides with each other.

The high electric field is applied at the metal site on the surface. The matrix elements of dipole moments between the nickel, magnesium and titanium orbitals are given in Table I. The matrix element of TiO is not so small, and besides the 4s level of TiO is located near the 3d orbital. Therefore, the order of the polarization of the d-orbital is much larger than others. The surface electronic configuration is different from the bulk one. In the latter $3z^2\text{-}r^2$ orbital is unoccupied, while in the former the high polarized orbital is occupied. The surface electronic properties of TiO may be quite different from the bulk properties.

The surface atoms are more neutral than the bulk atoms. At the surface the mixing of the metal d-orbital and oxygen p orbital in the antibonding state is stronger than that in the bulk, because the energy gap of the former between the d- and p-orbitals is smaller than that of the latter. As the antibonding level have partially unfilled d-electron, the back-donation from the metal to the oxygen is partially missing.

References

1) L. F. Mattheiss, *Phys. Rev.*, B5, 290 (1972), L. F. Mattheiss, *Phys. Rev.*, B5, 306 (1972).
2) P. C. Gravelle and S. J. Teichner, *Adv. Catal.*, 20, 167 (1969).
3) C. F. Ng, *Chem. Phys. Lett.*, 62, 187 (1979), K. G. Petzinger and D. J. Scalapino, *Phys. Rev.*, B8, 266 (1973).
4) T. Wolfram et al., *Sur. Science*, 28, 45 (1971), K. Namikawa, *J. Phys. Soc. Japan*, 44, 165 (1978).

Figure 1. Surface electronic structure of metal oxides TiO, MnO and NiO. In the figure are shown orbital character and electron occupations of the d-orbitals.

I-F-5 The Bulk and the Surface Electronic Structures of ReO₃ by the Cluster Calculations

Masaru TSUKADA, Chikatoshi SATOKO, Fujio MI-NAMI* and Nobuo TSUDA* (*National Inst. for Researches in Inorg. Materials)

The compound ReO_3 exhibits a high conductivity in spite of its partially ionic character. The crystal structure of ReO_3 is similar to the perovskites ABX_3; B and X are respectively replaced by Re and O ions, while no ions are located on the A site. Therefore, a close relation is expected between the electronic structure of ReO_3 and various perovskites including $SrTiO_3$ and $KMeF_3$. The surface of ReO_3 is important because of its catalytic activities in disproportionation and dimerization reaction of olefins. Tsuda, Fujimori and Sekita[1] found that the disproportionation reaction of propylene occurs at the surface oxygen point vacancy, whereas the dimerization takes place on the oxygen layer defects. However, there have been no detailed theory of such surface systems to explain the experimental result.

The purpose of the present work is to study theoretically the surface electronic structure of ReO_3 including the O vacancies and their interaction with olefins. As the first step of the study, we apply the DV-Xα method to the electronic states of the bulk ReO_3 and its (100) surface with and without the O vacancy. Calculated level structures are shown in Figure 1 for the bulk $(ReO_6)^{6-}$ cluster, the surface $(ReO_5)^{4-}$, $(Re_2O_9)^{6-}$ clusters without the defect, the surface Re_2O_8 cluster with single O vacancy. The structures of the clusters are the same as the corresponding ones in $SrTiO_3$ (Figure 1 in section I-F-2). The energy scale is shifted in the Figure so that the Fermi level coincides with each other. The level structure of the bulk $(ReO_6)^{6-}$ cluster corresponds fairly well with Mattheiss's APW band calculation.[2] Partial density of state of Re 5d components reveals similar shape as the XPS spectrum.[3] The lowest Re 5d level $4t_{2g}$ is partially occupied by one electron. The upper three levels of the oxygen 2p states $1t_{1g}$, $2t_{2u}$, $9t_{1u}$ are not admixed with the Re 5d components, while the admixture amounts to as large as 26% in the $3t_{2g}$ and $5e_g$ states. This large mixing of the Re 5d and O 2p states causes the much wider width of the O 2p band as compared with that in $SrTiO_3$; the admixture of Ti 3d components in the O 2p states are about 12% in $SrTiO_3$ crystal. A
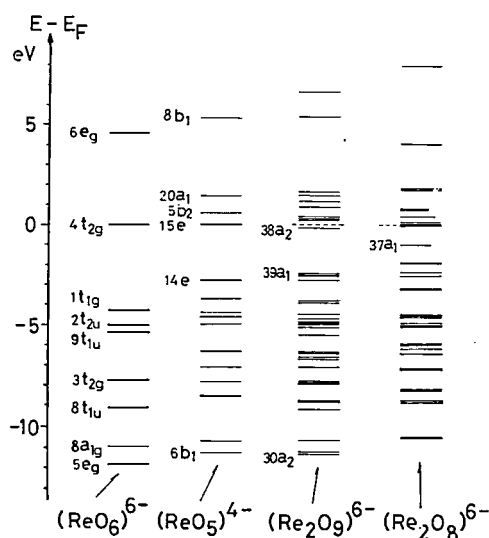
Figure 1. Level structures of the clusters, $(ReO_6)^{6-}$, $(ReO_5)^{4-}$, $(Re_2O_9)^{6-}$, $(Re_2O_8)^{6-}$. The dashed line indicates the Fermi level.

considerable narrowing of the Re 5d- O 2p gap is observed for the case of the surface $(ReO_5)^{4-}$ cluster. This is mainly caused by the surface enhanced covalency effect, as also verified by the reduction of the Re net charge from +3.84 in $(ReO_6)^{6-}$ to +3.35 in $(ReO_5)^{4-}$. The 6 e_g level in ReO_6 cluster splits into 20 a_1 ($3z^2$-r^2 like) level and 8 b_1 (x^2-y^2 like) level in the surface ReO_5 cluster and 20 a_1 level shifts considerably downwards due to the surface field on the Re site. The level structure of the larger surface cluster $(Re_2O_9)^{6-}$ is similar to that of $(ReO_5)^{4-}$. For the assumed formal net charge of the clusters, the lowest Re 5d level 38 a_2 is occupied by two electrons whereas that in $(ReO_5)^{4-}$, 15 e accomodates one electron. For the case of the defect cluster $(Re_2O_8)^{6-}$, a deep defect level 37 a_1 appears at the middle of the gap between the Re 5d and O 2p band. The defect wave function is composed mostly of Re 5d, 6s, 6p orbital adjacent to the vacancy. Calculations of ethylene chemisorption systems, $(C_2H_4)_2$-Re_2O_8 are in progress to elucidate the mechanism of olefin metathesis reaction.

References

1) N. Tsuda, A. Fujimori and M. Sekita, submitted to J. Chem. Soc., Faraday Trans., I.
2) L. F. Mattheiss, Phys. Rev., 181, 987 (1969), ibid., B2, 3918 (1970).
3) G. K. Wertheim, L. F. Mattheiss and M. Campagna, Phys. Rev. Lett., 32, 977 (1974).

I—G Electronic and Magnetic Properties of transition Metal Compounds by the DV-Xα Calculations

Transition metal compounds exhibit a wide variety of structural, electrical and magnetic properties depending on their composition. Up to now continual efforts are directed toward the search of new compounds which have the characteristics more suitable for various applications.

To perform reliable band calculations for the electronic structure is not straightforward for these compounds, because of the partial charge transfer, spin polarization, large anisotropy and so on. We apply the first principle DV-Xα calculations for the electronic structure of these compounds to contribute to the full understanding of their physical and chemical properties.

I-G-1 Discrete Variational Xα Cluster Calculations-Application to Transition Metal Complexes

Hirohiko ADACHI *(Osaka Univ.)*, Syoji SHIOKAWA *(Osaka Univ.)*, Masaru TSUKADA, Chikatoshi SATOKO and Satoru SUGANO *(Tokyo Univ.)*

Recently, the multiple scattering(MS) Xα method has been applied to many transition metal complexes, demonstrating that the Xα molecular cluster approach is excellent in describing their electronic structures.[1] However, the muffin-tin potential approximation used in the MS-Xα method is sometimes inadequate for quantitative description of detailed electronic states mainly because of the use of a constant potential in the intersphere region. On the other hand, the DV-Xα method[2] need not use the muffin-tin approximation but generally uses more accurate SCF potential, and is superior to the MS-Xα.

In the present work, the DV-Xα cluster method is applied to study some properties of the level structure, spin polarization effects and covalency for MeX_6^{4-} clusters (Me=Cr, Mn, Fe, Co, Ni and Cu, X=F, Cl, and Br) in perovskite type and rutile, $CdCl_2$, CdI_2 type compounds. The variation of the level structure for perovskite compounds, $KMeF_3$ are summarized in Figure 1. The splitting ΔE_1 ($=10D_q$) between $2t_{2g\uparrow}$ and $4e_{g\uparrow}$ slowly falls with metal atomic number from 7400 cm^{-1} for $KCrF_3$ to 6000 cm^{-1} for $KCuF_3$. The splitting of the d levels due to the spin polarization ($\Delta E_2 = \epsilon(t_{2g\downarrow}) - \epsilon(t_{2g\uparrow})$) is proportional to the magnetic moment. The energy gap between the fluorine p band and the Me 3d (ΔE_3) is greatly reduced, when the interactions between Me 3d and F 2p orbitals become stronger with the increasing atomic number. The p band width ΔE_4 is somewhat broadened when the metal atomic number increases. The calculated value of ΔE_1, $\Delta E_1' = \epsilon(4e_{g\downarrow}) - \epsilon(2t_{2g\downarrow})$, $\Delta E_2'/\mu_d$, $\Delta E_2/\mu_d$ ($\Delta E_2' = \epsilon(4e_{g\downarrow}) - \epsilon(4e_{g\uparrow})$, $\mu_d = |n_{d\uparrow} - n_{d\downarrow}|$) are listed in Table I. According to Hyper-Hartree-Fock model, ΔE_1 and $\Delta E_1'$ should agree with $10D_q$, and $\Delta E_2/\mu_d$ and $\Delta E_2'/\mu_d$ should be equal to 3.5B+1.4C. The calculated values of ΔE_1 or $\Delta E_1'$ are fairly in good agreement with experimental value of $10D_q$. The values $\Delta E_2/\mu_d$, $\Delta E_2'/\mu_d$ agree well with those estimated from the experimental Racah parameters. The values of ΔE_1, however, are systematically larger than $\Delta E_1'$ and ΔE_2 larger than $\Delta E_2'$. The reason is that the e_g state interacts most strongly with ligand p states, then is pushed up largely by the interaction because the σ type interaction of the e_g is stronger

Table I. Level splittings by ligand field and spin polarization for various compounds

| | μ_d | $10D_q$ | | | Spin polarization | | |
		ΔE_1	$\Delta E_1'$	exp.	$\Delta E_2/\mu_d$	$\Delta E_2'/\mu_d$	exp. 3.5B+1.4C
$KCrF_3$	4	0.91	0.83		0.97	0.95	
$KMnF_3$	5	0.83	0.72		1.00	0.98	
$KFeF_3$	4	0.83	0.73		1.00	0.97	
$KCoF_3$	3	0.80	0.71		0.99	0.96	
$KNiF_3$	2	0.80	0.73	0.90	0.97	0.93	1.15
$KCuF_3$	1	0.73	0.69		0.88	0.83	
MnF_2	5	1.11	1.09	0.97	0.99	0.98	1.00
$MnCl_2$	5	1.08	0.73	1.03 (0.93)	1.00	0.93	0.90 (0.98)
$MnBr_2$	5	1.41	0.95	1.17 (0.87)	0.81	0.74	0.90 (0.98)
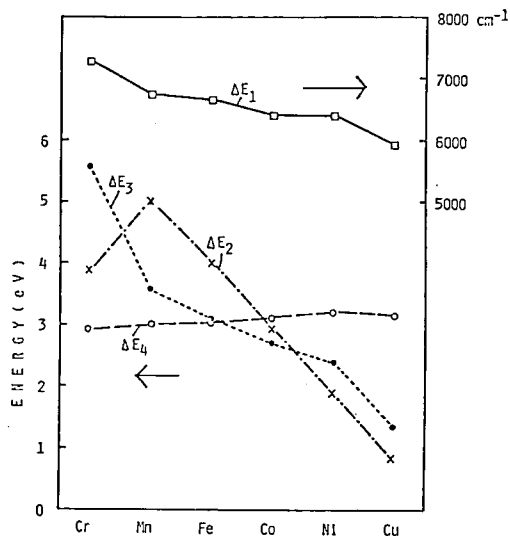
Figure 1. Variation of level structure of clusters for $KMeF_3$ type compounds.

Figure 2. Valence leves of MnF_6^{4-} clusters in MnX_2. (a) For MnF_2, (b) for $MnCl_2$ and (c) for $MnBr_2$.

than π type of the t_{2g} and the $e_{g\uparrow}$ level lies nearer the ligand p levels than the $e_{g\downarrow}$.

The level structure of MnX_6^{4-} (X=F,Cl,Br) clusters in the manganese dihalide crystals is shown in Figure 2. As can be seen in the figure, the Mn 3d, 4s, 4p levels and empty ligand levels are systematically shifted towards the ligand valence band with the atomic number of halogen. The trend agrees with the observed optical absorption spectra. The levels derived from Cl 3d or Br 4d orbitals are densely distributed over the energy region $9 \sim 18$ eV for $MnCl_6^{4-}$ and $MnBr_6^{4-}$. From the state density curve an intense and broad spectrum with a peak around $14 \sim 16$ eV is expected due to the intra-halogen p $\to$ d transition. In fact such a structure is observed in the UV absorption spectra by Sakisaka et al.[3]

References

1) S. Larsson and J. W. D. Connolly, *J. Chem. Phys.*, **60**, 1514 (1974).
2) F. W. Averill and D. E. Ellis, *J. Chem. Phys.*, **59**, 6413 (1974).
3) Y. Sakisaka, T. Ishii and T. Sagawa, *J. Phys. Soc. Japan*, **36**, 1365 (1974).

I-G-2 Electronic Structure of Transition Metal Disulphides by the DV-Xα Cluster Method

Hirohiko ADACHI *(Osaka Univ.)* and Masaru TSU-KADA

Layer compounds of transition-metal dicalcoge-nides[1] show a great variety of electronic properties ranging from insulating HfS_2 to superconducting $NbSe_2$. Intercalation of these compounds with alkali metals or organic molecules is quite important from the view point of the development of new super-conducting materials, batteries, photo-voltaic cells. Surface properties of these materials are also interesting because of their catalytic properties.

Although there have been many band theories applied on the electronic structure of such layer compounds, reliable first principle band calculations[2] are difficult due to their anisotropic and partially ionic characters. In the present work we apply the DV-Xα cluster calculation for several transition-metal disulphides including TiS_2, ZrS_2, HfS_2, MoS_2, WS_2. One of the aims of the present work is to elucidate the origin of the change of covalent vs ionic character and that of the lattice structure, when the metal changes from IVa group to VIa group.[3] For the disulphides of IVa elements, the coordination of the metal ion is octahedral, while it is trigonal prismatic for VIa elements.

Level structures calculated for the clusters $(TiS_6)^{8-}$, $(ZrS_6)^{8-}$, $(HfS_6)^{8-}$, $(MoS_6)^{8-}$, $(WS_6)^{8-}$ in the corresponding disulphides crystal are shown in Figure 1. In this figure the absolute energy scale is shifted so that the top of the Sulphur 3p band coincides. By comparing the level structure of $(ZrS_6)^{8-}$ to that of $(MoS_6)^{8-}$ and that of $(HfS_6)^{8-}$ to $(WS_6)^{8-}$, one notices that the gap between the metal d state and the sulphur 3p state is considerably smaller in VIa metal disulphides than in IVa metal disulphides. On the other hand, the sulphur 3p band width is

much broader for the former than the latter. This indicates that the covalent bond character is predominant in VIa metal disulphides, whereas ionic picture is plausible in the disulphides of Zr, Hf. This fact is also verified by the reduced ionic charge of group VIa element as compared with group IVa element as listed in Table I. That the covalent character of VIa metal disulphides is closely related with their trigonal prismatic structure is verified by the calculations of the hypothetical model cluster $(MoS_6)^{8-}$ of O_h symmetry with the same Me-S distance as $(MoS_6)^{8-}$ D_{3h} cluster. As seen in Figure 2, the level structure of $(MoS_6)^{8-}$ O_h cluster indicates much more ionic character of the hypothetical lattice with the octahedral coordination than the actual lattice with the trigonal prismatic coordination. Moreover, the Me-S bond overlap population for the O_h and D_{3h} clusters are respectively calculated to be 0.163, 0.176 for $(MoS_6)^{8-}$ clusters, while they are respectively 0.264 and 0.257, for $(TiS_6)^{8-}$ clusters. The reason of the stability of the trigonal prismatic lattice for VIa metal disulphides is the splitting off and the downward shift of the $3z^2-r^2$ level, which accomodates two electrons. The state densities obtained from the level structures of the various transition metal disulphides explain fairly well XPS and UPS experiments.[4]

References

1) J. A. Wilson and A. D. Yoffe, *Adv. in Phys.*, 18, 193 (1969).
2) L. F. Mattheiss, *Phys. Rev.* B8, 3720 (1973).
3) R. M. White and G. Lucovsky, *Solid State Commun.*, 11, (1972).
4) P. M. Williams and F. R. Shepherd, *J. Phys.* C6, L36 (1973).
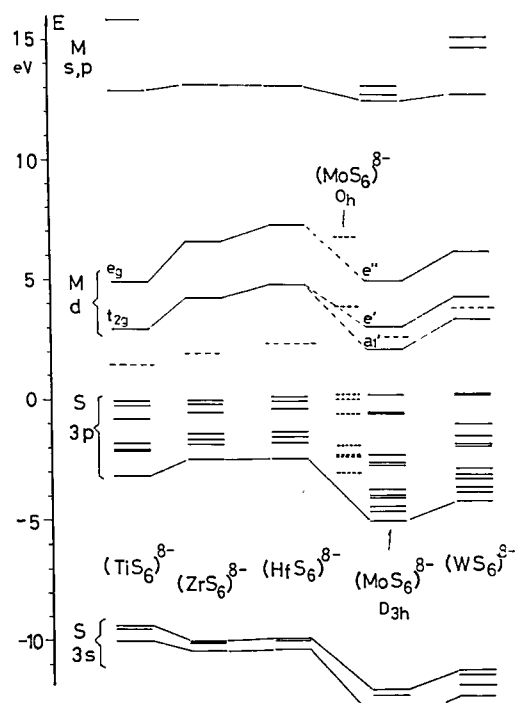
Figure 1. Level structures of several clusters

Table I. Net Charges for Several Clusters

Cluster	Coordination symmetry	Metal net charge	Sulphur net charge
$(TiS_6)^{8-}$	O_h	+1.89	−1.65
$(TiS_6)^{8-}$	D_{3h}[a]	+1.82	−1.64
$(ZrS_6)^{8-}$	O_h	+2.10	−1.68
$(MoS_6)^{8-}$	D_{3h}	+1.89	−1.65
$(MoS_6)^{8-}$	O_h[a]	+2.01	−1.67

[a] This structure is hypothetical.

I—H Development of the New Discrete-Variational Method for the Electronic Band Structure of Surfaces and Low Dimensional Crystals

Reliable valence electronic structures of solids can be obtained by the DV-Xα cluster method as verified by numerous calculations by us and other groups. Especially this method is quite practical for the large systems with low symmetry such as solid surfaces and amorphous materials. Nonetheless several shortcomings of the cluster approximation have been recognized, e.g. the artificial accumulation of cluster charges or inaccuracy in the treatment of delocalized wave functions.

To get rid of the problems, it seems necessary to start from the other limit, i.e. to calculate band structure of the periodic system, if necessary using the extended unit cell. For this purpose we develop a new Discrete-Variational-Numerical-Basis-LCAO band method, which is specially suited for the first principle calculations of low dimensional compounds or surface systems.

I-H-1 Applications of the Discrete Variational Calculation to Clusters, One-, Two- and Three-dimensional Lattices and Surfaces

Chikatoshi SATOKO and Masaru TSUKADA

Recently there have been much efforts devoted toward developing theoretical computational procedures for the surface and bulk electronic structure. One of the methods is the local cluster approach[1] in which the crystal is treated as the small cluster embedded in the remaining atoms of the crystal. The dominant contribution of the remaining atoms to the cluster are considered by Madelung potential.[2] In this approximation the electronic structure, the density of states, chemical bonding character are easily treated and solved. However, there remain many problems unsolved. The net charge of the cluster is assumed to be equal to the formal one. Though the effect of the excess charge is partly recovered by the static Coulomb potential of the remaining atoms of the crystal, the charges of the ions are often different from the formal one as generally assumed. Moreover, the surrounding atoms of the cluster have the missing bond, which induces the inequality of equivalent atoms. On the other hand there are also researches of the electronic structure using band methods for the periodic unit cell. The translational symmetry reduces the infinite problem to the finite problem. A Korringa-Kohn-Rostoker (KKR) calculation or scattering wave (SW) calculation in the muffin-tin approximation[3] is appropriate to the bulk electronic structure. However, in one- and two-dimensional crystal or surfaces all non-muffin-tin corrections to the potential must be considered. To get over the difficulties in the muffin-tin approximation, we develop a new calculational method for the electronic structure of low dimensional materials and surfaces using discrete variational numerical-basis-set LCAO band method.

A Bloch basis function with a wave vector k is expressed in the LCAO approximation as

$$\phi_{km} = \frac{1}{\sqrt{N}} \sum_i e^{-ik \cdot R_i} \phi_{im},$$

where N is the number of unit cell in the crystal, R_i the position of the j-th unit cell, and ϕ_{im} an atomic orbital centered on the m-th atom in the i-th unit cell. Matrix elements of the seqular equation are yielded by the numerical integration over a single unit cell:

$$<\phi_{km} |F| \phi_{kn}> = \sum_{ij} e^{-ik(R_j - R_i)} \int d\tau \, \phi_{im}^* F \, \phi_{jn}.$$
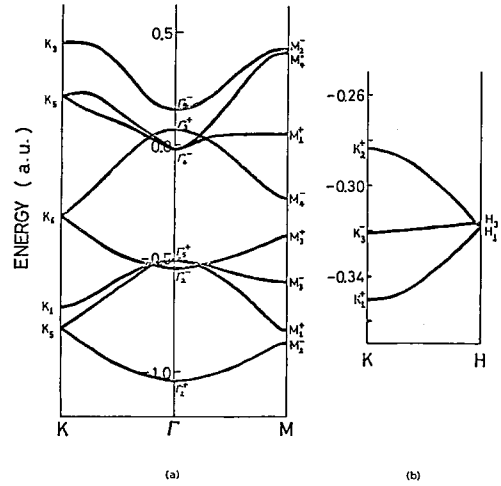
Figure 1. (a) Energy band of single-layer graphite.
(b) Energy band dependence upon k_z along K-H[4] of multi-layer grpahite.

Random sampling points for the numerical integration are distributed as the muffin-tin type. A proper sphere around each atom is taken. In the exterior region outside the sphere random sampling points are uniformally distributed. In the atomic sphere random sampling points are distributed in the total symmetric form. This distribution have the several characteristics as follows; Firstly, charge of the atom can be easily calculated in the Mulliken form and/or in the atomic sphere. Secondly we can efficiently calculate electronic states without the symmetrized orbitals. In the non-symmetric distribution of random sampling points matrix elements between s-type and p-type orbitals of the same atom is not always equal to zero, while in our symmetric distribution these matrix elements are equal to zero. This is an important property for our calculation of system with low symmetries. Thirdly, this muffin-tin type distribution can be related with the SW calculation. We can use the SW eigen-function for the basis function. Fourthly, it is convenient to calculate the change of the atomic configuration. The relative positions of random sampling points within the atomic sphere are fixed with the change of the atomic configuration. This property is important for the calculation of chemisorption systems to save a computing time.

We calculate the electronic structure of graphite using our method. The energy band of a single-layer graphite is presented in Figure 1 (a). The behavior of this band seems to be similar with the result of Painter and Ellis.[4] The Fermi-level passes through the states K_6 at the point K in the Brillouin zone. However, the result of multi-layer structure in Figure 1 (b) is different from that of them. The states K_6 are split into the states K_2, K_3 and K_1. In our result the dispersion from the states K_3 to the states H_3 in the Brillouin zone is positive ($\gamma_2 =$

−0.05 eV),[5] while in their result it is negative. Our calculation predicts the hole occupancy around H point, which is in agreement with experimental results.

References

1) H. Adachi, M. Tsudaka and C. Satoko, *J. Phys. Soc. Japan*, 45, 974 (1978).

2) C. Satoko, M. Tsukada and H. Adachi, *J. Phys. Soc. Japan*, 45, 1333 (1978).

3) J. C. Slater and K. H. Johnson, *Phys. Rev.*, B5, 844 (1972), K. H. Johnson and F. C. Smith, Jr., *Phys. Rev.*, B5, 831 (1972).

4) G. S. Painter and D. E. Ellis, *Phys. Rev.*, B1, 4747 (1970).

5) J. C. Slonczewski and P. R. Weiss, *Phys. Rev.*, 109, 272 (1958).

I—I Energy Band Calculations of Low Dimensional Materials

Recently a great deal of attention is concentrated on the developments of new low-dimensional compounds with the practical importance. Typical examples may be the search of one-dimensional metals or superconductors. Intercalated compounds of graphite or other layer crystals have attracting much interests from the view points of superconductivities, catalyses, batteries and photo-voltaic cells.

We started the project of the first principle band calculation of low-dimensional compounds. Though in the present stage only the energy band of simple systems, such as polyethylene, polyacethylene and graphite are completed, we intend to study the electronic structure of more complicated complexes by the method described in the last section.

I-I-1 Electronic Band Structure of Polyacethylene and Polyethylene

Chikatoshi SATOKO and Masaru TSUKADA

During the last decade the electronic and optical properties of quasi one-dimensional crystals have been clarified on the basis of the energy band theory. In one-dimensional metals, the Fermi surface is given by points and there are the divergences in the density of states with the exponent of a minus half. For this characters one-dimensional metals[1] have the properties full of variety such as charge density wave, Peierls transition and high-temperature superconductor.

Band calculations for the one-dimensional crystal[2] have been made by empirical methods (EH, CNDO, INDO) and ab-initio methods using a linear-combination of Gaussian-type orbitals in the HF- and HFS-potential approximation. Results of the semi-empirical methods depend on the parameters arbitrarily chosen. Ab-initio methods require an excessive computing time. So we develop the DV-LCAO method for the one-dimensional crystal, a brief summary of which is presented in the previous section. We apply this method to the band calculation of polyacethylene which is one of the simplest conjugate organic polymers. We also calculate the energy band of polyethylene which has been given by various methods.

The molecular potential for the LCAO method is calculated as the sum of Coulomb and exchange contributions. The Coulomb contribution is obtained from the sum of various free-atom Coulomb potential centered on the atomic sites. The exchange contribution is given by statistical local expression and is written as

$$V_{xc}(r) = -3\alpha \, [3/8\pi \, \rho(r)]^{1/3},$$

where α is chosen as 0.7 in our calculation and $\rho(r)$ is obtained from spherically symmetric superposition of the free atom charge densities.

Our preliminary results which are obtained without iterations are presented in Figure 1 (a) and (b) for cis-polyacethylene and polyethylene, respectively. Chain symmetries are $(ml)_t$ for both materials.[3] Symmetry labels at Γ-point in the Brillouin zone follow Bethe's notations for the irreducible representation of the site group C_{2v}, though Tobin's notation in linear group[4] was based in the isomorphic group D_{2h}.

Figure 1. (a) Energy band of cis-polyacethylene.
(b) Energy band of polyethylene.

The energy band of cis-polyacethylene shows a energy gap 1.6 eV between the highest occupied state Γ_{3g} and the lowest unoccupied state Γ_{2u} which are made up of C $2p\pi$ character. Observed measurements show a steep absorption edge at the energy 1.2 ± 0.1 eV.[5] The observed absorption edge cannot directly correspond to the transition from the valence to the conduction band in one-dimensional chain. If we consider the effect of the chain-chain interaction and the electron-hole interaction, our results will agree well with the observed value. This one-dimensional transition is allowed for the optical polarization along the chain axis, and is not allowed for the other polarizations. The chain-chain interaction will relax this polarization selection rules. The dependence of the absorption on the optical polarization will be useful for the estimation of the energy gap. The second absorption maximum will occure due to the transition from the state Γ_{4g} to the state Γ_{2u}. The state Γ_{4g} is made up of the C $2pz$ and H ls character. This transition is allowed by the optical polarization perpendicular to the C-H plane. The width of the conduction band $(\Gamma_{2g}-\Gamma_{2u})$ and the valence band $(\Gamma_{3g}-\Gamma_{3u})$ are of order 3.7 eV and 6.3 eV, respectively. We are carrying out further studies of the effect on the electronic structure by the chain-chain interaction and chemical doping.

In polyethylene the calculated valence-conduction gap between the Γ_{4g} and Γ_{1u} states is 8.9 eV which is consistent with the observed value.[6] The photoelectron peak positions of Wood et al.[7] may be assigned to the transition from the states Γ_{1g}, Γ_{1u} and Γ_{3g}. To make a more reliable comparison between the calculated valence band and the photoelectron spectra, theoretical calculation of the photoelectron intensity is necessary.

References

1) H. J. Keller, Low dimensional cooperative phenomena, Plenum Press, New York (1975).
2) W. L. McCubbin, Chem. Phys. Lett. 8, 507 (1971), K. Morokuma, J. Chem. Phys. 54, 962 (1971), E. Clementi, J. Chem. Phys. 54, 2492 (1971), J. E. Falk and R. J. Flaming, J. Phys. C6, 2954 (1973).
3) R. H. Baughmon et al., J. Chem. Phys. 68, 5405 (1978).
4) M. C. Tobin, J. Molec. Spectrosc. 4, 349 (1960).
5) W. Bludau et al., Bull. Am. Phys. Soc. 23, 304 (1978).
6) R. H. Partridge, J. Chem. Phys. 49, 3656 (1968).
7) K. Seki et al., J. Chem. Phys. 66, 3644 (1977), M. H. Wood et al., J. Chem. Phys. 56, 1788 (1972).

I—J Theoretical Study of Molecular Photoionization and Molecular Inner Shell Excitation

Because of the recent development of the synchrotron radiation source and of the electron energy loss technique, the dependence of the total and differential photoionization cross section on the excitation energy even at the inner shell region has been studied experimentally for atoms and some simple molecules. From the theoretical point of view, however, especially for molecules, the continuum wavefunction of the ejected electron is difficult to be calculated. In order to circumvent the difficulty, the methods are developed, in which the discrete (square integrable) basis functions are used to describe the continuum part of the wavefunction. The Stieltyes-Tchebycheff procedure developed by Langhoff has successfully been applied to several molecular total photoionization cross section both for the inner shell and for the valence region. In the present project, using the quantum chemical method, the observed spectra of the inner shell excitation for series of molecules are analyzed. In addition, a new basis function suitable for the molecular photoionization calculation is proposed.

I-J-1 The Gaussian-Plane Wave Function for Calculation of Molecular Photoionization Cross Section

Suehiro IWATA[1] (Inst. Phys. Chem. Res. and IMS)

The Stieltyes-Tchebycheff procedure by Langhoff[2] for calculating the molecular photoionization cross section is particularly attractive since the well-developed quantum chemical techniques and computer programs can be applied. One of the difficulties in the Stieltyes imaging, in our own experience,[3] is choice of the basis functions to be used. There seems to be no systematic ways to augment the basis functions for an ionization cross section.

In the present work, a new type of square integrable function is proposed. Most of recent molecular quantum chemical calculations are based on the gaussian type function (GTF):

$$G(l, m, n, \alpha; r) = x^l y^m z^n \exp(-\alpha r^2) \qquad (1)$$

The new function is a simple modification of it as

$$GP(\alpha, k; r) = \exp(-\alpha r^2 + ikr) \qquad (2)$$

The exponent α should be chosen such that the size of the molecule or the atom is smaller than $1/\sqrt{\alpha}$. The function (2) may be called the gaussian-plane wave function (GPF). Because of the gaussian part, the function is confined within the molecular region, but it oscillates dependent on $|k|$. GPF is practically discrete on "energy $k^2/2$", because two GPF's, $GP(\alpha,k)$ and $GP(\alpha,k')$, become nearly overcomplete if $(k-k')^2/2 \lesssim 2\alpha$. In addition, the direction of the wave vector k has to be discrete as well as on "energy $k^2/2$". In the present approximation, only a limited number of directions is chosen in the basis such as $n_i = k_i/|k| = (0,0,1), \ldots, (1/\sqrt{2}, 1/\sqrt{2}, 0), \ldots, (1/\sqrt{3}, 1/\sqrt{3}, 1/\sqrt{3}), \ldots$ In practice, the real representation of (2),

$$CGP\ (\alpha, k; r) = \exp(-\alpha r^2) \cos(k r), \text{ and}$$

$$SGP\ (\alpha, k; r) = \exp(-\alpha r^2) \sin(k r), \quad (3)$$

is convenient. The continuum wavefunction of the ejected electron near the molecule may be approximated as

$$\psi(\epsilon, r) = \sum a_{i\epsilon}\, G(l_i m_i n_i \alpha_i ; r) +$$

$$\sum\sum w_l\, [b_{j1\epsilon}\, CGP\ (\alpha_j k_j; r)$$

$$+ c_{j1\epsilon}\, SGP\ (\alpha_j k_j; r)], \quad (4)$$

where the weight w_1 is required because of the discreteness of the direction n.[4]

The advantage of the present GP basis functions is that any types of many-center molecular integrals between GP functions and between GP and GT functions can be given in closed forms as in the case of GTF. All the necessary matrix element of the one-electron operators except the core attraction operator can be written in terms of Hermite polynominals $H_n(z)$ as $S(n,k,\alpha) = \int_{-\infty}^{\infty} dx\ x^n \exp(-\alpha x^2 + ikx) = (-i)^n\ (\pi/\alpha)^{1/2} \exp(-k^2/4\alpha)\, H_n\ (-k/2\sqrt{\alpha})$. To obtain the matrix elements of the core attraction and the electron repulsion, the Laplace transformation,

$$1/r = \int_{-\infty}^{\infty} du \exp\left\{-u^2(x^2 + y^2 + z^2)\right\},$$

and the transformation of the variable, $u^2 + \alpha = \alpha/(1-t^2)$, are required. After some manipulation, the final expressions are given in terms of the auxiliary function:

$$ES(m,\beta,\gamma) = \int_0^1 dt\ (1-t^2)^m \exp\{-\beta(1-t^2)\}$$
$$\times \cos\{\gamma(1-t^2)\}$$

$$EC(m,\beta,\gamma) = \int_0^1 dt\ (1-t^2)^m \exp\{-\beta(1-t^2)\}$$
$$\times \sin\{\gamma(1-t^2)\}$$

For the atomic (one-center) problem, where γ is zero, the auxiliary function ES becomes the confluent hypergeometric function.

To determine the wavefunction (4), the static exchange approximation (equivalent to the Improved Vertual Orbital (IVO), or Hole Potential method in quantum chemistry) is used. The configuration interaction may also be applied. In both methods, the traditional quantum chemical program packages can be used with a few changes. At present the method is being applied to the one-center problem.

References and Note

1) IMS Adjunct Associate Professor for 1979—
2) G. R. J. Williams and P. W. Langhoff, *Chem. Phys. Letteres*, **60**, 201 (1979) and references therein.
3) S. Iwata, N. Kosugi, and O. Nomura, *Jpn. J. Appl. Phys.*, **17S**, 109 (1978) and *Chem. Phys.*, to be published.
4) M. Abramowitz and I. Stegun, *'Handbook of Mathematical Functions'*, Dover Publish. Inc., New York (1972).
5) J. C. Browne and R. D. Rochusta, *J. Chem. Phys.*, **36**, 1933 (1962).

RESEARCH ACTIVITIES II

Division of Molecular Structure

The most fundamental problem the Division is interested in is the precise determination of molecular structures by spectroscopic methods with high resolution and high sensitivity. A special emphasis is placed on the detection and identification of transient molecular species such as free radicals and molecular ions. One of the main tools is a microwave spectrometer, which covers the frequency region up to 180 GHz with a phase-lock system. A CO_2, N_2O, or CO laser source is used with an intracavity cell as a laser magnetic resonance (LMR) spectrometer. Tunable lasers, dye lasers in the visible region and diode lasers in the infrared region, which have been installed as main facilities of the Large Scale Research Equipments, are also used as sources for spectroscopy of unstable molecular species. Fluorescence excited by the dye lasers provides a very sensitive method of detecting new free radicals. Diode laser spectroscopy with Zeeman modulation is also useful for free radical studies. Double resonance spectroscopy, microwave-optical (MODR) and microwave-infrared (MIDR), provides a new spectroscopic method. For an investigation of unstable species from a more dynamical point of view, highly-excited atoms are produced by electron bombardment and their reactions with other atoms or molecules are analyzed in detail. In addition to transient species a few non-polar molecules of fundamental importance are being investigated by microwave spectroscopy, and also molecules with large-amplitude internal motions by diode laser spectroscopy.

II—A   High Resolution Spectroscopy of Transient Molecular Species

Transient species which appears as intermediates in chemical reactions supply important information on reaction mechanisms; without knowledge of such species it is not easy to understand chemical reactions properly. At present we know only a small fraction of such species, because most of them are of short life. We need spectroscopic and other methods which are sensitive enough to detect these species. High resolution spectroscopy not only provides molecular constants at a very high precision, but also allows us to sort out the spectra of unstable species among those of others and thus to unambiguously identify chemical species present in our reaction system. The open-shell electronic structure characterizes many of the unstable species and causes additional complexities in their spectra due to fine structure and hyperfine structure interactions. Analyses of these structures in the spectra provide us with information on the electronic properties of open-shell molecules which would not be obtained for molecules without unpaired electrons. Besides these fundamental implications in the field of molecular science and chemical reaction, the present project will be of some significance in related fields such as astrophysics and environmental researches.

II-A-1   Microwave Spectroscopy of the FSO Radical : Molecular Structure, Force Constants, and Dipole Moment

Yasuki ENDO, Shuji SAITO, and Eizi HIROTA

We have observed microwave spectra of a new free radical FSO, which was generated by a reaction of carbonyl sulfide with products of a microwave discharge in an oxygen and carbon tetrafluoride mixture. In order to determine the molecular structure, spectra of the $F^{34}SO$ species in natural abundance (about 4 %) were observed and analyzed. Because the number of the observed lines is smaller, cen-

Table I.   Molecular Constants of $F^{34}SO$ (MHz)[a]

Rotational constants	A	37 536.604	(63)
	B	9 334.694	(7)
	C	7 456.138	(6)
Spin-rotation constants	ϵ_{aa}	−333.48	(66)
	ϵ_{bb}	35.89	(16)
	ϵ_{cc}	1.82	(15)
	$|\epsilon_{ab}+\epsilon_{ba}|/2$	214.2	(22)
Hyperfine constants	a_F	66.82	(53)
	T_{aa}	−115.7	(20)
	T_{bb}	−117.7	(9)

[a] Values in parentheses denote 2.5 times standard errors and apply to the last digits of the constants.

42

Table II. Quadratic Force Constants, Vibrational Frequencies, and Inertia Defects of FSO

Force constant[a]	Value	Error 1[b]	Error 2[c]
F_{11}	9.2^d	—	0.5
F_{22}	4.08	0.13	0.07
F_{33}	0.5382	0.0036	0.0002
F_{12}	0.140	0.083	0.018
F_{23}	0.050	0.011	0.006
F_{13}	0.0^d	—	—

Vibrational frequency[e]	Value	Error 1[b]	Error 2[c]
ω_1	1215	2	33
ω_2	763	12	6
ω_3	396.2	1.3	0.1

Inertia defect[f]	Δ_0	$\Delta_3 - \Delta_0$
obs.	0.17449 (5)	0.33978 (8)
calc.	0.1764 (7)	0.33978

[a] Internal coordinates chosen are $R_1 = \delta r(\text{S-O})$, $R_2 = \delta r(\text{S-F})$, and $R_3 = r\delta\theta(\text{F-S-O})$, where $r = [r(\text{S-O})$ $r(\text{S-F})]^{1/2}$. The unit for F_{ij} is md/Å.
[b] 2.5 times standard errors in the least-squares fitting.
[c] Due to uncertainty of ± 0.5 md/Å in F_{11}.
[d] Fixed.
[e] In cm^{-1}.
[f] In amu Å^2.

trifugal distortion constants for both overall rotation and spin-rotation interaction and an off-diagonal hyperfine constant were fixed to the values of $F^{32}SO$. Talbe I lists molecular constants which were derived. Structure parameters calculated from the rotational constants of the two isotopic species are $r(\text{S-F}) = 1.602$ Å, $r(\text{S-O}) = 1.452$ Å, and $\theta(\text{F-S-O}) = 108.32°$.

Because no spectroscopic data had been reported on vibrational frequencies, harmonic force constants were estimated by analyzing the centrifugal distortion constants and inertia defects obtained for $F^{32}SO$. We have made an additional measurement on satellite spectra due to the first excited F-S-O bending (ν_3) state. It is well-known that vibrational changes of the inertia defect are more useful than the ground-state inertia defect for force constant determination. We found, however, that our data are still not sufficient to determine all six harmonic force constants. We thus assumed $F_{13} = 0$ and $F_{11} = 9.2 \pm 0.5$ md/Å. The former assumption does not affect the calculated vibrational frequencies, because its contributions are very small. The latter was estimated by Badger's rule with the reported force constants of SO, SO_2, and F_2SO. Table II summarizes the quadratic force constants thus derived. Error 1 denotes fitting errors (2.5 times standard deviations) and error 2 those due to the estimated uncertainty in F_{11} (± 0.5 md/Å). Vibrational frequencies calculated from the force constants are also listed in Table II with uncertainties arising from two sources of errors. They will be of some use for future spectroscopic investigations of FSO.

Stark effects of five transitions of $F^{32}SO$ were measured to determine dipole moment components.

The $J = 2 \leftarrow 1$ transition of carbonyl sulfide was used as a reference. A Hamiltonian including Stark effects was used to set up an energy matrix. Because only Stark components with $F \leq 2$ and $M_F \leq 2$ were observed, the matrix was truncated at $F = 3$. The dipole moments thus derived are $\mu_a = 0.373$ (11) D, $\mu_b = 1.620$ (13) D, and $\mu_{total} = 1.662$ (17) D, with 2.5 times standard errors in parentheses. A small μ_a value is consistent with the fact that only b-type transitions have been observed. Dipole moments of other molecules involving S-O and/or S-F show that the S-O bond moment (1.5 - 1.6 D) is larger than the S-F bond moment (0.7 - 1.0 D). Therefore, of the two possible orientations one in which the total moment makes an angle of 34.9° with S-O is preferred.

An assumption that noise level of the spectrum corresponds to an absorption coefficient of 1×10^{-9} cm^{-1} (at 40 GHz) leads to the abundance of FSO in the sample to be 1.5 - 2.0%.

II-A-2 Dipole Moment of the HO_2 Radical from its Microwave Spectrum

Shuji SAITO and Chi MATSUMURA *(National Chemical Laboratory for Industry)*

The HO_2 radical had been assumed to be an important intermediate in reactions involving hydrogen and oxygen. Its existence has only recently been verified by high-resolution spectroscopic methods such as far-infrared LMR[1], microwave[2], and elec-

tron paramagnetic resonance spectroscopy[3], all in the gas phase. Most of its molecular constants have thus been evaluated[4] very precisely except for the dipole moment, which is indispensable to determine the concentration of HO_2 in various systems from observed spectral intensities. In the present work we analyzed the Stark effects of microwave transitions of HO_2 to determine its dipole moment.

The HO_2 radical was produced by the reaction of microwave-discharged oxygen with allyl alcohol or with propene. A 100 kHz sine-wave Stark modulated microwave spectrometer at Sagami Chemical Research Center[5] was used. Transitions for which Stark effects were measured are $1_{01} \leftarrow 0_{00}$, $J = 3/2 \leftarrow 1/2$, $F = 2 \leftarrow 1$ and $1 \leftarrow 0$; $7_{17} \leftarrow 8_{08}$, $J = 15/2 \leftarrow 17/2$, $F = 8 \leftarrow 9$ and $7 \leftarrow 8$ and $J = 13/2 \leftarrow 15/2$, $F = 7 \leftarrow 8$ and $6 \leftarrow 7$; $9_{09} \leftarrow 8_{18}$, $J = 17/2 \leftarrow 15/2$, $F = 9 \leftarrow 8$ and $8 \leftarrow 7$.

An energy matrix was set up using a coupling scheme of the following form: $N + S = J$, $J + I = F$. Fortunately, for HO_2 Stark matrix elements are much smaller than differences between pair levels which they connect, so that the Stark coefficients can be calculated by a second-order perturbation theory, where spin-rotation interaction energies are added to rotational energies in the denominators.

Resolved Stark components of $1_{01} \leftarrow 0_{00}$ in fact showed quadratic Stark effect up to a field of 1 kV/cm. Unfortunately, two b-type transitions exhibited only unresolved Stark patterns, so that their Stark effects were analyzed by a simulation method.

The dipole moments thus determined are μ_a = 1.412 (33) D, μ_b = 1.541 (16) D, and μ_{total} = 2.090 (34) D, with three times standard errors in parentheses. It is reasonable to assume that the total dipole moment makes an angle of 25.0°, rather than 60.0°, with the O-H bond. If it is the case, the O-H and O-O bond moments are 1.65 D and 0.91 D, respectively. The former value is close to the O-H bond moments in H_2O (1.54 D)[6] and in H_2O_2 (1.60 D).[7]

References

1) J. T. Hougen, H. E. Radford, K. M. Evenson, and C. J. Howard, *J. Mol. Spectrosc.*, **56**, 210 (1975).
2) S. Saito, *J. Mol. Spectrosc.*, **65**, 229 (1977).
3) C. E. Barnes, J. M. Brown, A. Carrington, J. Pinkstone, T. J. Sears, and P. J. Thistlethwaite, *J. Mol. Spectrosc.*, **72**, 86 (1978).
4) J. M. Brown and T. J. Sears, *J. Mol. Spectrosc.*, **75**, 111 (1979).
5) S. Saito, *J. Mol. Spectrosc.*, **48**, 530 (1973).
6) M. Lichtenstein, V. E. Derr, and J. J. Gallagher, *J. Mol. Spectrosc.*, **20**, 391 (1966).
7) J. T. Massey and R. W. Hart, *J. Chem. Phys.*, **23**, 942 (1955).

II-A-3 Laser Magnetic Resonance Spectroscopy of SO in the $X^3\Sigma^-$ State with a CO_2 Laser as a Source

Kentarou KAWAGUCHI, Chikashi YAMADA, and Eizi HIROTA

The ground vibronic state of SO is known to be $^3\Sigma^-$ and is thus expected to demonstrate typical LMR spectra characteristic of a triplet molecule.

Because the origin of the fundamental band of $^{32}S^{16}O$ is located at 30 cm^{-1} or more above the upper limit of the region covered by a $C^{18}O_2$ laser, transitions which were observed involve high-N levels (N = 17 - 29). For such large N values *transitions with $\Delta J = \Delta N = -1$, which are referred to as "main" transitions, are difficult to magnetically tune, and in fact only a few main transitions were observed. In contrast transitions of $\Delta J = 0$, $\Delta N = -1$, called "satellite" transitions, show large Zeeman effects, and most observed transitions are of this type, although their intensities are a few thousandths of those of main transitions. As Figure 1 shows for the case of N = 21, Zeeman components of $J = N - 1$ and $J = N + 1$ (except two largest M_J components of the latter and $M_J < 0$ components) show avoided crossings at some magnetic fields, which induce additional transitions (referred to as magnetic-field-induced transitions, MFIT). They may be characterized as
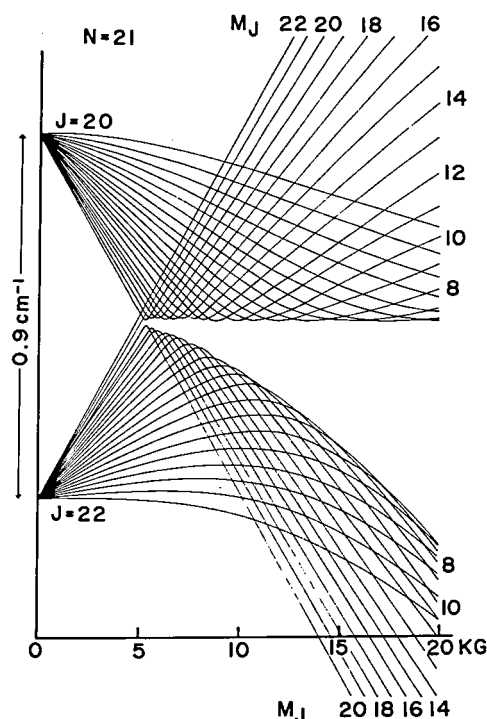
Figure 1. Zeeman effects of the v = 1, N = 21, J = 20 and 22 levels. Zeeman components with $M_J \leq 20$ show avoided corssing due to mutual interaction via an intermediate J = 21 level.

Table I. Vibrational Frequencies of $X^3\Sigma^-$ SO[a]

Species	Band	Origin	Obs.-Calc. I[b]	Obs.-Calc. II[c]
$^{32}S^{16}O$	$v = 1 \leftarrow 0$	1138.0089 (4)	−0.0003	−0.0018
	$v = 2 \leftarrow 1$	1125.3085 (28)	+0.0004	+0.0042
$^{34}S^{16}O$	$v = 1 \leftarrow 0$	1126.9295 (30)	−0.0002	+0.0012
$^{32}S^{18}O$	$v = 1 \leftarrow 0$	1095.4265 (8)	+0.0013	+0.0102
$^{32}S^{16}O$	ω_e[d]		1150.710 (11)	1150.717 (80)
	$\omega_e x_e$[d]		6.3505 (51)	6.353 (39)

[a] In cm^{-1}.
[b] Using atomic masses.
[c] Using nuclear masses.
[d] Values in parentheses denote three standard errors.

either $\Delta J = +1$ or -3, using J values in the limit of zero magnetic field. Their intensities depend critically upon the field strength at which avoided crossing occurs; they range from 0.5 % to 25 % of the zero-field intensity of the main transition. Figure 2 shows an example of MFIT, N, $J = 27, 28 \leftarrow 28, 27$, which appears at around 5 kG along with a series of Lamb dips of a main transition, N, $J = 27, 28 \leftarrow 28, 29$. A characteristic feature of MFIT is, as seen from Figure 2, that lines with positive and negative Zeeman coefficients appear alternately and series of lines are suddenly terminated at some magnetic field. When a main transition occurs in a region near avoided crossing, spectral patterns similar to MFIT are observed, but in this case series of lines continue without any abrupt termination. A few sharp, but weak resonances were also observed which cannot be explained by any of the above mechanisms. They are assigned to $\Delta N = -3$ transitions which are made allowed by the $\Delta N = \pm 2$ matrix elements of the spin-spin interaction.

The $v = 1 \leftarrow 0$ and $v = 2 \leftarrow 1$ bands of $^{32}S^{16}O$ and the fundamental band of $^{34}S^{16}O$ were thus ob-

served and analyzed to determine band origins, g factors, and, in some cases, spin-spin and spin-rotation interaction constants. For $^{32}S^{18}O$ the band origin is low enough to observe low-N transition.

Four values of band origins listed in Table I were used to estimate the harmonic frequency ω_e and the anharmonicity constant $\omega_e x_e$, where the reduced mass dependences, $\omega_e \propto 1/\sqrt{\mu}$ and $\omega_e x_e \propto 1/\mu$, were assumed. As Table I shows, use of atomic masses rather than nuclear masses reproduces the observed values more closely. The electron cloud thus seems to follow the nuclei when the latter vibrate.

II-A-4 Laser Excitation Spectroscopy of HSO and DSO : Molecular Structure of HSO

Masao KAKIMOTO, Nobukimi OHASHI[1] *(Kanazawa Univ. and IMS)*, Shuji SAITO, and Eizi HIROTA

Schurath *et al.*[2] established the existence of the HSO radical by observing chemiluminescence spectra emitted from an O, H_2S, and O_3 three-components system. Resolution of their monochromator is, however, insufficient to completely resolve rotational structures, and thus makes their assignments somewhat ambiguous. We have achieved much higher resolution by observing laser excitation spectra on a two-components reaction system, either CH_3SH or H_2S and discharge products in oxygen gas. For observation of DSO spectra we replaced H_2S with D_2S, which was synthesized from DCl and FeS. Appropriate choice of reactant pressures eliminated chemiluminescence almost completely.

We have improved our spectrometer by introducing a new system for laser wavelength measurements, as shown in Figure 1. A part of the dye laser output was divided into three parts; the first part was used to monitor the dye laser mode by an etalon (ET. 1), the second part to generate frequency markers by a second etalon (ET. 2, FSR 1.5 GHz), and the last
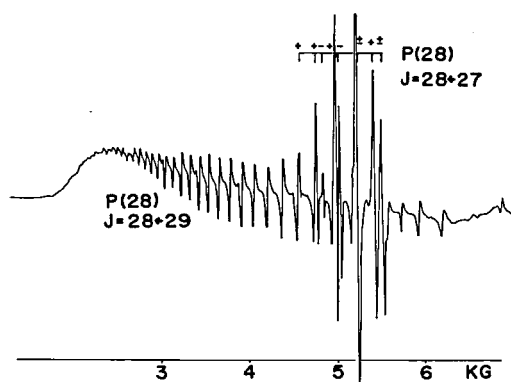
Figure 2. Lamb dips of a main transition, N, $J = 27,28 \leftarrow 28,29$ recorded with the R(14) line of a 9 μm $C^{18}O_2$ laser as a source. The laser polarization chosen corresponds to $\Delta M_J = \pm 1$ selection rules. Eight lines near 5 kG are assigned to MFIT with $N, J = 27,28 \leftarrow 28,27$.

45

Table I. Molecular Constants of HSO and DSO[a]

Species	Constant	$\widetilde{A}^2A'(003)$	$\widetilde{X}^2A''(000)$
HSO	A	291 862 (16)	299 478 (20)
	B	16 934.7 (17)	20 504.4 (17)
	C	15 802.1 (17)	19 135.6 (17)
	Δ_N	0.0483 (22)	0.0318 (25)
	Δ_{NK}	3.318 (38)	0.857 (58)
	Δ_K	39.9 (18)	27.2 (20)
	δ_N	0.00506 (58)	0.00202 (56)
	δ_K	4.01	0.45 (38)
	ϵ_{aa}	17 854 (165)	−10 292 (64)
	ϵ_{bb}	87 (32)	−433 (32)
	ϵ_{cc}	−352 (32)	−5 (32)
	ν_0	16 483.0252 (13)	
DSO	A	151 710 (14)	158 750 (18)
	B	16 748.4 (25)	19 836.2 (28)
	C	14 910.8 (25)	17 573.6 (26)
	Δ_N	0.0354 (38)	0.0281 (41)
	Δ_{NK}	0.889 (52)	0.847 (55)
	Δ_K	6.94 (59)	8.9 (10)
	δ_N	0.0032 (12)	0.00192 (84)
	δ_K	0.52 (24)	−0.15 (20)
	ϵ_{aa}	8 688 (175)	−5 668 (101)
	ϵ_{bb}	136 (36)	−347 (38)
	ϵ_{cc}	−285 (38)	51 (36)
	ν_0	16 413.8740 (20)	

[a] In MHz, except for ν_0, which is given in cm^{-1}. Numbers in parentheses denote 2.5 times standard deviations and apply to the last digits.

part to excite iodine fluorescence. The wavenumbers of I_2 lines measured by Gerstenkorn and Luc[3] with a precision of 10^{-3} to $10^{-4} cm^{-1}$ were used as the standards.

The band we observed corresponds to the $\widetilde{A}^2 A'$ (003) ← $\widetilde{X}^2 A''(000)$, if we adopt the vibronic assignment of Schurath et al.[2] We assigned 646 lines to $K' ← K'' = 2 ← 3, \cdots, 3 ← 2$ subbands for HSO

Figure 1. Block diagram of the spectrometer. Following notations are used:

BS1, BS2, BS3 : Pyrex glass beam splitters,
M1, M2, M3 : 100% reflection mirrors,
F : optical filter, L : lens system,
PM1, PM2 : photo multipliers,
ET.1 ET.2 : etalons (FSR = 2 GHz for ET.1 and 1.5 GHz for ET.2),
PD1, PD2 : silicon photodiodes.

and 637 lines to $K' ← K''$, $3 ← 4, \cdots, 6 ← 5; 0 ← 0, \cdots, 4 ← 4; 1 ← 3, \cdots, 3 ← 1$ subbands for DSO. Least-squares analyses of the observed spectra gave molecular constants listed in Table I. Six observed rotational constants are used to calculate the r_0 structures for both the excited and ground state, which are shown in Table II. It is seen that the S-O bond length changes by as much as +0.17 Å and the H-S-O angle by −10.9°, whereas the H-S length is little affected, upon excitation. The large change in S-O is consistent with Schurath's observation of strong progression in the ν_3 or S-O stretching mode. The ratio of ϵ_{aa}'s of HSO and DSO is found very close to that of the A rotational constants, as expected from a theory.[4]

One interesting feature of the DSO spectra is that forbidden transitions ($\Delta K = 0, \pm 2$) appear due to axis switching. A theory by Hougen and Watson[5] was combined with the structure parameters of Table II to estimate an axis-switching angle to be 3.2°, which accounts for the observed intensities of forbidden transitions. Because the corresponding angle of HSO

Table II. Molecular Structure of HSO

	$\widetilde{A}^2A'$ (003)	$\widetilde{X}^2A''$ (000)
r (S-O) (Å)	1.661	1.494
r (H-S) (Å)	1.342	1.389
θ (H-S-O)	95.7°	106.6°

Table I. Molecular Constants of HSO in $\tilde{X}^2 A''$ (000) (in MHz)[a]

Constant	Value	Constant	Value
A	299 485.13 (43)	Δ_N^S	0.0003 (33)
B	20 503.665 (10)	$(\Delta_{NK}^S + \Delta_{KN}^S)/2$	−0.230 (90)
C	19 134.836 (20)	Δ_K^S	2.05 (12)
		δ_N^S	0.0077 (83)
Δ_N	0.03020 (33)	δ_K^S	0.6 (12)
Δ_{NK}	0.8997 (16)		
δ_N	0.00179 (19)	a_F	−36.3 (12)
		T_{aa}	−12.11 (30)
ϵ_{aa}	−10 366.43 (98)	T_{bb}	10.77 (28)
ϵ_{bb}	−426.64 (18)		
ϵ_{cc}	0.23 (14)		
$|\epsilon_{ab} + \epsilon_{ba}|/2$	386.2 (33)		

[a] Values in parentheses denote 2.5 times standard errors and apply to the last digits of constants. Δ_K and δ_K are fixed to the values obtained by dye laser spectroscopy.

is 1.65°, axis-switching transitions will be about one fourth as intense as those of DSO. We have not attempted to observe such transitions for HSO.

References and Note
1) IMS Visiting Scientist for 1978–79.
2) U. Schurath, M. Weber, and K. H. Becker, *J. Chem. Phys.*, 67, 110 (1977).
3) S. Gerstenkorn and P. Luc, "*Atlas du Spectre d'Absorption de la Molécule d'Iode*", Ed. du CNRS, Paris, 1978.
4) R. F. Curl, *J. Chem. Phys.*, 37, 779 (1962).
5) J. T. Hougen and J. K. G. Watson, *Canad. J. Phys.*, 43, 298 (1965).

II-A-5 Microwave Spectroscopy of HSO and DSO

Yasuki ENDO, Shuji SAITO, and Eizi HIROTA

As described in II-A-4 we have observed and analyzed dye laser excitation spectra of HSO and DSO. Because this is a new method, we thought it would be nice to confirm the derived results by other methods. Microwave spectroscopy is particularly suitable for this purpose, because it is of much higher resolution. Furthermore, it will provide us with hyperfine coupling constants, which make it possible to discuss electron spin densities in the molecule.

Early attempts to observe the microwave spectra using a Stark modulation spectrometer failed probably because the lifetime of the radical is too short. However, a source modulation spectrometer, which is described in detail in II-C-1, gives us much higher sensitivity. A glow discharge cell attached to the spectrometer permits us to generate unstable species *in situ*. In addition, recent improvements of molecular constants as listed in II-A-4 had limited frequency regions to be searched to very narrow ranges. We thus were able to observe microwave spectra of both HSO and DSO in the ground vibronic states.

We generated HSO(DSO) by exciting DC discharge in a mixture of O_2(16 mTorr) and H_2S(D_2S) (10 mTorr) contained in the cell. For HSO 12 a-type and 2 b-type rotational transitions were observed, each split by the spin-rotation and hyperfine interactions. A least-squares analysis of the observed spectra leads to molecular constants listed in Table I. We had to fix two centrifugal distortion constants. The present results, which are at least an order of magnitude more accurate, agree remarkably well with those obtained by dye laser spectroscopy. A work on DSO is still under way, but has so far substantiated the validity of the analyses of dye laser spectra described in II-A-4.

II-A-6 Diode Laser Spectroscopy of the NS Radical

Keiji MATSUMURA,[1] Kentarou KAWAGUCHI, Keiichi NAGAI, Chikashi YAMADA, and Eizi HIROTA

The NS radical is similar in electronic structure to a more well-known molecule NO. Its electronic spectra have been extensively studied as summarized by Jenouvrier and Pascat.[2] Carrington and his coworkers[3] and Uehara and Morino[4] observed gas-phase electron paramagnetic resonance spectra of NS in the ground vibronic $^2\Pi$ state. Amano *et al.*[5] have characterized the ground-state NS molecule much more in detail by observing microwave spectra in both $^2\Pi_{1/2}$ and $^2\Pi_{3/2}$. Although some information on vibrational spectra has been provided from analyses of electronic spectra, no direct observation of vibrational spectra of NS has been made. In the present work we observed the fundamental band of NS by infrared diode laser spectroscopy and determined the band origin and the molecular constants in the $v = 1$ state from analyses of the observed

spectra.

The spectrometer used is a Laser Analytics LS-3. We modulated a laser diode by 5 kHz sine wave and demodulated the absorption signal by a phase sensitive detector operated at 10 kHz. This source modulation technique makes the baseline flat and gives sensitivity an order of magnitude better than a simple video detection scheme. The wavelength of the laser light was calibrated by using ν_1 and $2\nu_2$ bands of N_2O as references. Fortunately Olson et al.[6] have recently made a comprehensive survey on the N_2O spectra and listed accurate wavenumbers for lines of the two bands. We generated NS by passing a mixture of nitrogen (190 mTorr) and sulfur monochloride (20 mTorr) through a microwave discharge.

We observed 12 and 11 vibration-rotation transitions, respectively, for $^2\Pi_{1/2}$ and $^2\Pi_{3/2}$; each of the $^2\Pi_{1/2}$ lines was split into two by Λ-type doubling. Analyses of the observed spectra were carried out separately for $^2\Pi_{1/2}$ and $^2\Pi_{3/2}$, where the following expressions were used for rotational levels:

$$E_R(^2\Pi_{1/2}, v) = B_{v1} \ (J + 1/2)^2 - D_{v1} \ (J + 1/2)^4$$

$$\pm (1/2)p_v (J + 1/2),$$

$$E_R(^2\Pi_{3/2}, v) = B_{v2} \ (J + 1/2)^2 - D_{v2} \ (J + 1/2)^4.$$

The ground-state rotational and the Λ-doubling constants were fixed to the microwave values reported in Ref. 5. Table I lists molecular constants which are thus derived.

The difference between two effective band origins is ascribed to the vibrational change of the spin-orbit interaction constant: $\nu_0(^2\Pi_{3/2}) - \nu_0(^2\Pi_{1/2}) = A_{v=1} - A_{v=0}$, which is 0.1736 (22) cm^{-1}. Eqs. (12) and (13) of Ref. 5, when two effective B con-

stants of Table I, $B_{v=1,i}$ (i = 1, 2), are substituted, give the rotational constant in v = 1, B_1, to be 0.766 105 (16) cm^{-1}, and thus lead to the equilibrium rotational constant B_e and the vibration-rotation constant α_e, as shown in Table I. The equilibrium bond length is calculated to be 1.49402 (4) Å. The effective centrifugal distortion constant remains the same within experimental errors upon vibrational excitation, but differs slightly for the two spin sub-levels. A straightforward extension of the perturbation treatment of Ref. 5) gives expressions for D_{v1} and D_{v2} as follows;

$$D_{v1} = D_v - B_v^4/A^3,$$

$$D_{v2} = D_v + B_v^4/A^3.$$

Averages of D_{v1} and D_{v2} thus give the equilibrium centrifugal distortion constant D_e to be 0.000 00129 (33) cm^{-1}, which is in excellent agreement with the value 0.000 001287 cm^{-1} calculated using an equation $D_e = 4B_e^3/\omega_e^2$. The Λ-doubling constant was found to be the same for $v = 1$ and $v = 0$ within experimental errors.

References and Notes

1) IMS Graduate Student for 1978–79.
2) A. Jenouvrier and B. Pascat, Can. J. Phys., 51, 2413 (1973). See also N. A. Narasimham and T. K. Balasubramanian, J. Mol. Spectrosc., 40, 511 (1971); T. K. Balasubramanian and N. A. Narasimham, J. Mol. Spectrosc., 53, 128 (1974).
3) A. Carrington and D. H. Levy, J. Phys. Chem., 71, 2 (1967); A. Carrington, B. J. Howard, D. H. Levy, and J. C. Robertson, Mol. Phys., 15, 187 (1968).
4) H. Uehara and Y. Morino, Mol. Phys., 17, 239 (1969).
5) T. Amano, S. Saito, E. Hirota, and Y. Morino, J. Mol. Spectrosc., 32, 97 (1969).
6) W. B. Olson, A. G. Maki, and W. J. Lafferty, The 34th Symposium on Molecular Spectroscopy, Columbus, Ohio, 1979, paper TE14, and private communication. The authors are grateful to Dr. Maki for sending us a list of N_2O spectral line wavenumbers prior to publications.

Table I. Molecular Constants of $^{14}N^{32}S$ in $X^2\Pi_r$ (in cm^{-1})^a

Constant	$^2\Pi_{1/2}$ (i=1)	$^2\Pi_{3/2}$ (i=2)
$B_{v=1,i}$	0.763 351 (17)	0.768 816 (26)
$D_{v=1,i}$	0.000 001 19 (21)	0.000 001 40 (30)
$p_{v=1}$	0.013 26 (13)	——
$B_{v=0,i}$	[0.769 602 (4)]^b	[0.775 157 (6)]^b
$D_{v=0,i}$	0.000 001 19 (24)	0.000 001 40 (35)
$p_{v=0}$	[0.013 253 (13)]^b	——
ν_0	1204.275 5 (12)	1204.101 9 (19)
B_1	0.766 105 (16)	
B_0	[0.772 401 (5)]^b	
α_e	0.006 296 (16)	
B_e	0.775 549 (10)	
D_e	0.000 001 29 (33)	
r_e(Å)	1.494 02 (4)	

^{a} Values in parentheses denote three times standard errors and apply to the last digits of the constants.
^{b} Ref. 5) fixed.

II-A-7 Diode Laser Spectroscopy of the CF Radical

Kentarou KAWAGUCHI, Chikashi YAMADA, Yoshiaki HAMADA (Univ. of Tokyo), and Eizi HIROTA

Porter et al.[1] and Carroll and Grennan[2] observed and analyzed electronic spectra of CF, emitted, respectively, from discharges in perfluorocyclobutane diluted with argon and in a mixture of carbon tetrafluoride and helium. Carrington and Howard[3] observed EPR spectra of CF in J = 3/2 and 5/2 of $^2\Pi_{3/2}$, generated by reactions of discharge products of CF_4 with a few organic molecules such as ketene and acetaldehyde. However, no gas-phase vibrational

Table I. Molecular Constants of CF (in cm^{-1})^a

Constant	Present	Ref. 1)	Ref. 2)
$B_{v=1}$	1.387 723 (70)	1.3896 (3)	1.388$_2$
$B_{v=0}$	1.406 058 (57)	1.4080 (3)	1.406$_2$
α_B	0.018 335	0.0184	0.018$_0$
ν_0	1286.1193 (9)	1285.9 (1)	1286.3$_0$
$A_{v=1} - A_{v=0}$	−0.6483 (6)	−0.6493	
$p_{v=1}$	0.008 08		
$p_{v=0}$	0.008 15		

^{a} Values in parentheses denote standard errors and apply to the last digits of the constants.

spectra have been reported. In the present work we observed and analyzed the fundamental band of CF.

A diode laser spectrometer Laser Analytics LS-3 was incorporated with a White-type multi-reflection cell of about 50 cm length; laser light traverses ten times through the cell so that the total path length is about 10 m. The cell is equipped with two electrodes, to which we apply 60 Hz high voltage to induce discharges in the cell. We have tested both carbon tetrafluoride and tetrafluoroethylene to generate CF, and found the latter to give spectra about five times stronger. The optimum pressure is 40-50 mTorr. We also introduced nitrogen gas of about 800 mTorr in front of mirrors to prevent solid reaction products from being deposited on surfaces of mirrors.

Zeeman modulation, which is described in detail in II-A-10, was used. For a linear molecule belonging to Hund's case (a) the $^2\Pi_{1/2}$ state normally shows very small Zeeman effects. However, in the case of CF, mixing of $^2\Pi_{1/2}$ and $^2\Pi_{3/2}$ is so large that even the $^2\Pi_{1/2}$ spectra were observed by Zeeman modulation. The observed transitions are three P branches and five R branches for $^2\Pi_{3/2}$ and three P branches and three R branches for $^2\Pi_{1/2}$. All $^2\Pi_{1/2}$ lines are split by Λ-type doubling.

A preliminary analysis was carried out using formulas given by Hill and Van Vleck[4] (the spin-rotation interaction was neglected). Table I lists the derived constants, which are compared with those of Refs. 1) and 2).

The concentration of the CF radical in the cell is estimated from observed intensities to be about 0.045%, or 6×10^{11} molecules/cm^3, when the pressure of C_2F_4 is 40-50 mTorr.

References

1) T. L. Porter, D. E. Mann, and N. Aquista, *J. Mol. Spectrosc.*, **16**, 228 (1965).
2) P. K. Carroll and T. P. Grennan, *J. Phys.*, **B3**, 865 (1970).
3) A. Carrington and B. J. Howard, *Mol. Phys.*, **18**, 225 (1970).
4) E. Hill and J. H. Van Vleck, *Phys. Rev.*, **32**, 250 (1928).

II-A-8 Diode Laser Spectroscopy of the CCl Radical

Chikashi YAMADA, Keiichi NAGAI, and Eizi HIROTA

Verma and Mulliken[1] and Gordon and King[2] independently observed spectra of CCl emitted from a discharge in carbon tetrachloride. Although they determined molecular constants of the ground vibronic state fairly accurately, the present work was started to provide more precise information on vibration-rotation energy levels of CCl in the ground electronic state. No spectroscopic measurements in the gas phase have been carried out in infrared and microwave regions.

We generated CCl in a discharge cell from a mixture of 100 mTorr of carbon tetrachloride and 1 Torr of argon; discharge was excited by applying 60 Hz high voltage to the electrodes. The spectrum increases in intensity with discharge current. Absorption lines originating from the $^2\Pi_{3/2}$ state were first detected by Zeeman modulation; six Q branch and eight R branch lines were observed. Later six R branch lines of $^2\Pi_{1/2}$ were detected by source modulation. Furthermore, $v = 2 \leftarrow 1$ hot-band transitions, four and one R branches respectively for $^2\Pi_{3/2}$ and $^2\Pi_{1/2}$, were also seen. For $C^{37}Cl$ seven R branch and five R branch transitions were measured respectively for $^2\Pi_{3/2}$ and $^2\Pi_{1/2}$. All $^2\Pi_{1/2}$ transitions were found to be split by Λ-type doubling.

Laser wavelengths were measured by using OCS ν_1 band transitions as references, the wavenumbers of which were in turn calibrated by using a gain cell containing $^{13}CO_2$ or directly measured by a high-precision wavelength meter described in II-C-2. An air-spaced confocal etalon of 30 cm length produces fringe patterns to interpolate between two reference lines, and fringes were recorded simultaneously with observed spectra on a strip-chart recorder. For this purpose laser diodes were modulated at a frequency different from the Zeeman modulation frequency.

Analyses of the observed spectra were carried out using an expression for rotational energy levels

Constant	Value	Constant	Value
$A_{v=0}$	$[134.96]^b$	$p_{v=0}$	$[0.013\ 8]^b$
$A_{v=1}$	133.714 90 (10)	$p_{v=1}$	0.013 694 (82)
B_e	0.697 069 (92)	$D_{A,\ v=0}$	$[-0.000\ 216\ 4]^b$
α_e^B	0.006 794 (22)	$D_{A,\ v=1}$	$-0.000\ 238$ (12)
D_e	$[0.000\ 001\ 763]^b$	ω_e	877.47 (26)
β_e	0.000 000 021 (57)	$\omega_e x_e$	5.89 (21)
r_e	1.645 25 (11) Å	$\omega_e y_e$	0.126 (46)

[a] Values in parentheses denote 2.5 times standard errors and apply to the last digits of the constants.
[b] Fixed.

presented by Mizushima.[3] Amano et al.[4] have also given a similar formula which they derived by a second-order perturbation treatment of vibrational effects. Mizushima's equation corresponds to an extension of Amano's result, and notations used by the two groups may be referred to each other as follows:

Mizushima	Amano	Present
$D_{\phi\Pi vA}$	$\epsilon^2 A'$	D_A
$D_{\phi\Pi v}$	D_e	D_v

where $\epsilon = B_e/\omega_e$ and $A' = (\partial A/\partial\xi)_e$ with $\xi = (r-r_e)/r_e$. Amano neglected the vibrational change of the centrifugal distortion constant. We have simplified Mizushima's notations as shown above. Data on both $C^{35}Cl$ and $C^{37}Cl$ were simultaneously subjected to the least-squares analysis, where isotope mass dependences of constants were assumed. Table I lists molecular constants which were thus derived. Although a direct comparison with the results of Refs. 1) and 2) is not possible, the present results are at least an order of magnitude more precise.

References

1) R. D. Verma and R. S. Mulliken, J. Mol. Spectrosc., 6, 419 (1961).

2) R. D. Gordon and G. W. King, Canad. J. Phys., 39, 252 (1961).

3) M. Mizushima, "The Theory of Rotating Diatomic Molecules", John Wiley & Sons, New York, 1975.

4) T. Amano, S. Saito, E. Hirota, Y. Morino, D. R. Johnson, and F. X. Powell, J. Mol. Spectrosc., 30, 275 (1969).

II-A-9 Diode Laser Spectroscopy of the BO_2 Radical: Renner Effect in Excited Bending States and Anharmonicity of the ν_3 Vibration

Kentarou KAWAGUCHI, Eizi HIROTA, and Chikashi YAMADA

Boron dioxide has attracted much attention because it exhibits Renner effects in its excited bending states, and has thus been investigated in detail by electronic,[1] laser-excited fluorescence,[2] optically detected magnetic resonance,[3] and intermodulated fluorescence spectroscopy.[4] Pople[5] and Hougen[6] have developed theories of the Renner effect and applied them to triatomics including BO_2 and CO_2^+. However, no high-resolution infrared spectroscopy has been reported on BO_2. In the present work we observed the ν_3 band by using a diode laser spectrometer. Fortunately, the ν_3 band of BO_2 is very strong as in the case of CO_2, which has permitted us to observe hot band spectra arising from ν_2, $2\nu_2$, and ν_3. The ν_3 mode of BO_2 is anomalously low in frequency, i.e. 1322 cm^{-1} to be compared with 2349 cm^{-1} of CO_2. Johns[1] assigned weak fluorescence among the $\tilde{A}^2\Pi_u \rightarrow \tilde{X}^2\Pi_g$ system to the (000) → (002) band and suspected that this band could only be seen because of large anharmonicity of the ν_3

Table I. Molecular Constants Associated with the ν_3 Fundamental Band of $^{11}BO_2$ in $\tilde{X}^2\Pi_g$[a]

Constant	$^2\Pi_{3/2}$	$^2\Pi_{1/2}$
B'	9743.4 (17)	9786.4 (11)
B''	9852.0 (17)	9896.9 (12)
D'	0.0030 (12)	0.00406 (90)
D''	0.0033 (12)	0.0043 (11)
p_Λ'		167 (14)
p_Λ''		151 (15)
ν_0	1279.0332 (12)	1277.4920 (12)

[a] In MHz except ν_0, which is given in cm^{-1}. Values in parentheses denote three standard errors and apply to the last digits of the constants.

Constant	$^2\Delta_{5/2}$	$^2\Delta_{3/2}$	$^2\Sigma^+$	$^2\Sigma^-$
B'	9780.6 (6)	9825.4 (14)	9803.54 (96)	9797.7 (31)
B''	9889.2 (6)	9936.9 (16)	9914.00 (95)	9905.2 (32)
D'	0.00340 (48)	0.0046 (11)	0.00434 (54)	0.0051 (48)
D''	0.00368 (54)	0.0048 (13)	0.00450 (54)	0.0052 (54)
γ'			5063 (48)	4947 (94)
γ''			4560 (47)	4531 (96)
$\gamma_D{}'$			−0.073 (27)	−0.14 (13)
$\gamma_D{}''$			−0.071 (27)	−0.12 (14)
ν_0	1276.5426 (6)	1275.5181 (15)	1281.0668 (9)	1268.0180 (18)

^{a} See Footnote a of Table I.

vibration in the ground electronic state.

The spectrometer used is a Laser Analytics LS-3. As in II-A-6 N_2O lines were used as wavelength standards, and a confocal, air-spaced Ge etalon of 30 cm length, which was newly constructed, was used to measure the frequency difference between BO_2 lines and N_2O reference lines. This etalon is found much better in reproducibility of fringes than an etalon made of pure Ge, which is commercially available.

Boron dioxide was first generated by a reaction of microwave discharge products of oxygen with BCl_3. However, stronger spectra were observed using a discharge cell containing a mixture of O_2 and BCl_3 (with pressures of 500 mTorr and 15 mTorr respectively), excited by 60 Hz high voltage. We introduced nitrogen gas in front of mirrors for multiple reflection, which stabilized the discharge in the mixture and prevents solid reaction products from being deposited on mirror surfaces. Laser light traverses 4 to 12 times through the cell; the effective path length is thus 6 to 19 m, but in the case of Zeeman modulation about 60% of the optical path is in the magnetic field.

BO$_2$ ν_3 Band

Q-Branch of $^2\Pi_{3/2}$

1279.1   1278.8 cm^{-1}
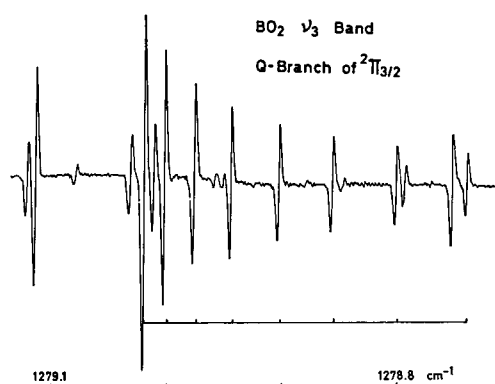
Figure 1. Q branch transitions of the ν_3 band of $^{11}BO_2$ in $^2\Pi_{3/2}$.

First, a few low-J transitions in $^2\Pi_{3/2}$ were detected by Zeeman modulation. Figure 1 shows Q branch lines of $^{11}BO_2$ in $^2\Pi_{3/2}$. Higher J transitions in $^2\Pi_{3/2}$ and also transitions in $^2\Pi_{1/2}$ were observed by source modulation. It is interesting to note that Λ doubling does not cause any splittings in the spectra of $B^{16}O_2$, but leads to staggering in successive rotational transitions, because every other rotational levels are missing due to zero nuclear spin of $^2\Pi_{1/2}$, but is barely visible for $^2\Pi_{3/2}$.

A preliminary analysis was carried out using a formula analogous to the Hill-Van Vleck equation:

$$E = B \left[(J + 1/2)^2 - K^2 \right] \pm (1/2) \left[4B^2 (J + 1/2)^2 + A (A - 4BK) \right]^{1/2}. \tag{1}$$

For BO_2 $A = -148.6$ cm^{-1} [1] is much larger in magnitude than BJ, so that the square root in Eq. (1) is expanded to introduce effective B constant $B_{eff} = B[1 \pm B/|A|]$. The observed lines, 31 for $^2\Pi_{3/2}$ and 20 for $^2\Pi_{1/2}$, lead to molecular constants of $^{11}BO_2$ listed in Table I. It is interesting to note that the band origin, 1279.03 cm^{-1} ($^2\Pi_{3/2}$) and 1277.49 cm^{-1} ($^2\Pi_{1/2}$), is much lower than that obtained from electronic spectroscopy; Johns[1] determined $(2\nu_3)$ to be 2644 cm^{-1}. To confirm Johns' data the $2\nu_2 \leftarrow \nu_3$ hot band is being measured.

Hot bands originating from the first excited bending states, i.e. $\nu_2 + \nu_3 - \nu_2$, were also observed. The ν_2 state is split by spin-orbit interaction and Renner effect into four sublevels, Σ_u^+, $\Delta_{3/2,u}$, $\Delta_{5/2,u}$, and Σ_u^-. For the Σ states the expressions for rotational energy given by Hougen[6] were used with addition of a centrifugal distortion term γ_D for the spin-rotation interaction. Table II summarizes preliminary values of molecular constants.

References

1) J. W. C. Johns, Canad. J. Phys., 39, 1738 (1961).
2) D. K. Russell, M. Kroll, and R. A. Beaudet, J. Chem. Phys., 66, 1999 (1977).

3) M. S. Kim, R. E. Smalley, and D. H. Levy, *J. Mol. Spectrosc.*, **71**, 458 (1978).
4) R. S. Lowe, H. Gerhardt, W. Dillenschneider, R. F. Curl, Jr., and F. K. Tittel, *J. Chem. Phys.*, **70**, 42 (1979).
5) J. A. Pople, *Mol. Phys.* **3**, 16 (1960).
6) J. T. Hougen, *J. Chem. Phys.*, **36**, 519 (1962).

II-A-10 The ν_2 Band of the Methyl Radical Investigated by Diode Laser Spectroscopy with Zeeman Modulation

Chikashi YAMADA, Kentarou KAWAGUCHI, Keiji MATSUMURA,[1] and Eizi HIROTA

The methyl radical is one of the most important free radicals. However, few high resolution spectroscopic investigations on it have been reported in the gas phase. Herzberg[2] observed a few bands for CH_3 and CD_3 in the 130 - 220 nm region, but he could resolve rotational structure only for the 214 nm band of CD_3. From the B constant thus obtained he calculated r_0(C-H) to be 1.079 Å on an assumption of the planarity of the molecule. He also estimated ν_2, the out-of-plane bending frequency, to be 580 cm^{-1}. On the other hand, Jacox[3] observed the ν_2 band at 603 cm^{-1} for CH_3 trapped in an argon matrix. Tan et al.[4] identified the Q-branch absorption of the CH_3 ν_2 band at 607 cm^{-1} by a gas-phase flash photolysis study with a rapid scan infrared spectrometer. We started the present work to obtain more precise information on the molecular structure of CH_3.

Because the CH_3 radical is paramagnetic, we have developed Zeeman modulation for diode laser spectroscopy. This technique will allow us to pick up lines due to paramagnetic species among those of other stable molecules with diamagnetism. We had also anticipated to eliminate fringe patterns that arise from reflection of laser light by optical elements and limit the sensitivity of source modulation; if fringes were suppressed, we could make the path length longer to increase the sensitivity.

In order to modulate Doppler-broadened infrared lines (the linewidth ranges from several tens to over one hundred MHz), we need Zeeman fields as high as 1 kG, because Zeeman coefficients of vibration-rotation transitions of paramagnetic molecules are of the order of 0.1-1 MHz/G. We have wound coils in three layers on a Pyrex glass tube of 80 mm diameter using "formal" wires of 2.3 mm diameter. The total length of the coil is 500 mm. Addition of a coil 46 mm long at each end improves homogeneity of the magnetic field to better than 1%. Inductance and resistance of the Zeeman coil thus made are 4.7 mH and 1 Ω. Maximum current which can be fed is 50 A for DC and 56 A for AC (1 kHz peak to peak); both correspond to a magnetic field of 800 G. AC current

is decoupled from DC by a choke coil of L = 69 mH and R = 0.8 Ω immersed in an oil tank. The Zeeman coil is covered by another Pyrex glass tube to circulate oil of low viscosity for cooling. Figure 1 shows the Zeeman coil.

The methyl radical is generated by pyrolyzing *tert*-butyl peroxide, $(CH_3)_3COOC(CH_3)_3$ [hereafter abbreviated as TBP]. A cell with heating coil wound on it was inserted in the Zeeman coil; TBP of about 2 Torr was decomposed in the cell at 370 - 400°C and decomposition products, which mainly consist of acetone and ethane, were continuously pumped out. We observed about 90 lines in the regions of 860-888 and 910-968 cm^{-1}, using a diode laser spectrometer. Wavelengths of absorption lines were measured as described in II-A-9. We believe almost all observed lines are due to the CH_3 radical, because of the following reasons.
(1) The lines were detected by Zeeman modulation.
(2) We observed identical spectra by passing CH_3I or acetone through a 60 Hz discharge. (In this case we used a multi-reflection cell mentioned in II-A-9.)
(3) Some of the observed lines are doublets; although we could not measure splittings, they are of the order of $10^{-3} - 10^{-2}\,cm^{-1}$. These splittings will be ascribed to spin-rotation interaction. The ϵ_{bb} component of the coupling constant may be estimated by

$$\epsilon_{bb} \sim -4A^{SO} \sum_n | <0|L_b|n><n|BL_b|0> |$$
$$/[E(n) - E(0)], \qquad (1)$$

where A^{SO} denotes the spin-orbit coupling constant of carbon ($\sim 20\,cm^{-1}$). When we include in the summation only one excited state of $^2E'$ symmetry located at about $11 \times 10^4\,cm^{-1}$ above the ground state, ϵ_{bb} is calculated to be about 0.007 cm^{-1}. A formula for ϵ_{cc} similar to Eq. (1) predicts ϵ_{cc} to be very small, because there are no excited states known which belong to $^2A_1''$. For an R branch transition, $N + 1 \leftarrow N$, spin splitting is given by
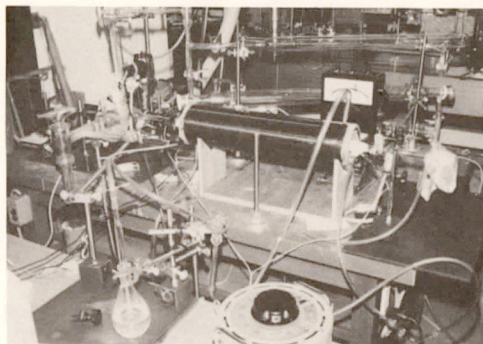

Figure 1. The Zeeman coil.

$$\Delta \nu = \epsilon_{bb} + (\epsilon_{bb} - \epsilon_{cc})K^2/[N(N+2)], \qquad (2)$$

which, when $\epsilon_{bb} = 0.007 \text{ cm}^{-1}$ and $\epsilon_{cc} = 0$ are substituted, ranges from 0.007 cm^{-1} for $K = 0$ to 0.014 cm^{-1} for $K = N \gg 1$, in qualitative agreement with the observed splittings.

(4) We applied CO_2 LMR spectroscopy to a few observed lines in higher frequency region, and found that two lines at 884.1924 cm^{-1} and 887.9178 cm^{-1} show respectively four and two Lamb dips, due to hyperfine interactions.

Unfortunately, the frequency region we covered by laser diodes presently available is 300 cm^{-1} or more apart from the band origin. Therefore N values of the observed transitions are too large to make a definite assignment.

References and Note

1) IMS Graduate Student for 1978–79.
2) G. Herzberg, *Proc. Roy. Soc. London*, A262, 291 (1961).
3) M. E. Jacox, *J. Mol. Spectrosc.*, 66, 272 (1977).
4) L. Y. Tan, A. M. Winer, and G. C. Pimentel, *J. Chem. Phys.*, 57, 4028 (1972).

II-A-11 Laser Excitation Spectroscopy of Carbenes: The HCF Molecule

Masao KAKIMOTO, Shuji SAITO, and Eizi HIROTA

Carbenes play important roles in reactions of organic molecules, and their existence postulated for long time has recently been verified in part by spectroscopic methods. Special attention has been given to the two lowest electronic states; questions that have often been asked are which is lower, singlet or triplet, and how much the energy difference between them is. Obviously a triplet molecule will behave quite differently from the same species in a singlet state, in chemical reactions in which it participates. We have thus started systematic studies on carbenes with hope to clarify their molecular properties in a few lowest electronic states. In the present work we investigated the $\tilde{A}^1 A''(000) \leftarrow \tilde{X}^1 A'$ (000) band of HCF by dye laser excitation spectroscopy. Merer and Travis[1] have observed the $\tilde{A} \leftarrow \tilde{X}$ band by using a 35-ft grating spectrometer and have found anomalies which they ascribed to interactions between the $\tilde{A}$ state and higher vibrational levels of the $\tilde{X}$ state. Because our resolution is an order of magnitude or more higher than theirs, we will be able to improve the precisions of molecular constants and also to provide more detailed information on anomalies.

We generated HCF by the reaction of microwave discharge products of CF_4 with CH_3F. A typical

Table I. Molecular Constants of HCF in $\tilde{A}^1 A''$ (000) and $\tilde{X}^1 A'$ (000) (in MHz)^a

Constant	$\tilde{X}^1 A'(000)$	$\tilde{A}^1 A''(000)$
A	466 574 (17)	770 200 (72)
B	36 664.8 (17)	34 823 (19)
C	33 867.8 (17)	33 192 (19)
Δ_J	0.119 5 (81)	0.086 7 (42)
Δ_{JK}	2.44 (11)	−0.04 (51)
Δ_K	75.9 (27)	1417 (23)
δ_J	0.009 56 (63)	0.005 (9)
δ_K	1.48 (33)	−13.0 (42)
H_J	−0.000 014 (13)	−0.000 022 0 (54)
H_{JK}	0.000 01 (20)	−0.000 7 (11)
H_{KJ}	0.002 6 (78)	−0.192 (57)
H_K	−0.02 (11)	8.6 (17)
h_J		0.000 009 4 (66)
h_{JK}		−0.006 2 (93)
h_K		7.0 (57)
$\nu_0(\text{cm}^{-1})$		17 277.4790 (19)

^{a} Values in parentheses denote three standard errors and apply to the last digits of the constants.

partial pressure of CH_3F was 3 mTorr, and the total pressure was about 80 mTorr. We saw fluorescence for a length of 15-20 cm in a cell, when the linear flow velocity of the sample was about 20 m/sec. Therefore, the lifetime is of the order of 10 msec, which contrasts with that ($< 20 \mu$sec) estimated by Merer and Travis. We also observed identical spectra when we replaced CH_3F by ketene or CH_3Cl, and also by CH_3CHO, C_3H_6 or CH_4 but with intensities much reduced. We detected 853 lines in the region of 17 188 to 17 391 cm^{-1}, which we assigned to 560 transitions, but there remain many weak lines unassigned. Figure 1 shows a part of excitation spectra. Subbands we analyzed include $K_a' \leftarrow K_a'' = 3 \leftarrow 4$, $\cdots\cdots, 2 \leftarrow 1$, and also $0 \leftarrow 0, 1 \leftarrow 1, 2 \leftarrow 2, 3 \leftarrow 3$, $2 \leftarrow 0$, and $0 \leftarrow 2$, which are made allowed by axis switching.

First a least-squares analysis was carried out using molecular constants of both the upper and the lower states and the band origin as parameters. However, even for this (000) - (000) band some parts of the spectra are obviously subjected to local perturbation. So a different approach was taken which consists of two steps: determination of ground-state parameters from ground-state combination differences, followed by evaluation of upper-state constants from the observed transition frequencies with ground-state constants fixed to the values already obtained in a previous step. This procedure has an advantage that perturbations do not affect ground-state constants. Table I lists molecular constants thus obtained. It is to be noted that we need to include additional centrifugal distortion terms for the upper state. We have established that the $J_{1,J}$ levels with $J = 5, 6$ and $J = 10, 11$ are perturbed. The $J_{2,J-1}$ levels with $J = 15, 16$ are also affected, but to much less degree.
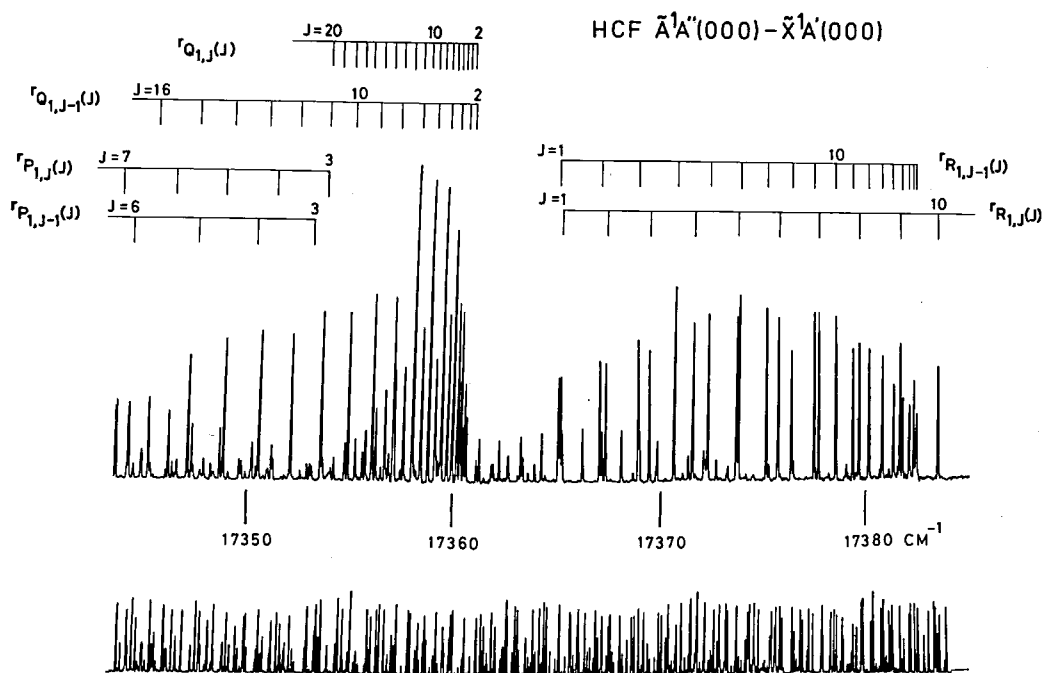
Figure 1. A part of dye laser excitation spectra of HCF. The lower trace shows iodine excitation spectra used as wavelength standards.

Because the upper state we are looking at is the ground vibrational level of the $\tilde{A}$ state, perturbing states must belong to lower electronic states, either the ground state or the lowest triplet state. Zeeman effects of the observed lines are being examined to discriminate contributions of the latter against the former ones.

Reference

1) A. J. Merer and D. N. Travis, *Canad. J. Phys.*, **44**, 1541 (1966).

II-A-12 Laser Excitation Spectroscopy of Carbenes: The HCCl and CCl$_2$ Molecules

Masao KAKIMOTO, Shuji SAITO, and Eizi HIROTA

As a further extension of II-A-11 we have tried to detect other carbenes such as HCCl and CCl$_2$. The HCCl molecule was previously investigated by Merer and Travis,[1] who observed absorption spectra of HCCl and DCCl in the region 550-820 nm in the flash photolysis of dibromochloromethane. On the other hand no high-resolution spectroscopic works have been reported on CCl$_2$. Shirk[2] and Huie et al.[3] observed fluorescence induced by an Ar ion and a dye laser, respectively. Andrews,[4] Jacox and Milligan,[5] Tevault and Andrews,[6] and Bondybey[7] detected CCl$_2$ in Ar matrices by observing its infrared and/or visible spectra.

We generated HCCl by a reaction of microwave discharge products of CF$_4$ with CH$_3$Cl. This system produces much stronger spectra of HCF, as mentioned in II-A-11, but could be used to observe laser-excited fluorescence of HCCl as well. We have concentrated ourselves on the $\tilde{A}^1A''$ (050) $\leftarrow \tilde{X}^1A'$ (000) band and observed 662 lines in the regions of 16539 - 16656 cm^{-1}. As Merer and Travis[1] showed, the HCCl spectra are more severely perturbed than the HCF spectra. We have examined $^PQ_1(J)$ and $^PP_1(J)$ with $J = 1$ - 15 in some detail, which clearly show irregularities around $J' = 8$ - 11. When perturbed lines are observed under a magnetic field of 10 kG, they decrease in intensity and increase in width, whereas other lines are not affected. Some weaker lines which do not seem to belong to the two branches show even larger Zeeman effects (see Figure 1). Therefore, the perturbation we looked at is probably due to a highly excited vibrational state associated with the lowest triplet state. More detailed analyses of the observed spectra are under way.

Huie et al.[3] passed a mixture of CF$_2$ = CCl$_2$ and O$_2$ through a discharge to obtain CCl$_2$. This system was, however, found to emit too strong chemiluminescence to observe laser excitation spectra. We thus used a reaction of discharge products of CF$_4$ with CH$_2$Cl$_2$. Because the CCl$_2$ molecule is heavy, laser excitation spectra we observed are very dense.

References

1) A. J. Merer and D. N. Travis, *Canad. J. Phys.*, **44**, 525 (1966).

2) J. S. Shirk, *J. Chem. Phys.*, **55**, 3608 (1971).
3) R. E. Huie, N. J. T. Long, and B. A. Thrush, *Chem. Phys. Lett.*, **51**, 197 (1977).
4) L. Andrews, *J. Chem. Phys.*, **48**, 979 (1968).

5) M. E. Jacox and D. E. Milligan, *J. Chem. Phys.*, **53**, 2688 (1970).
6) D. E. Tevault and L. Andrews, *J. Mol. Spectrosc.*, **54**, 110 (1975).
7) V. E. Bondybey, *J. Mol. Spectrosc.*, **64**, 180 (1977).
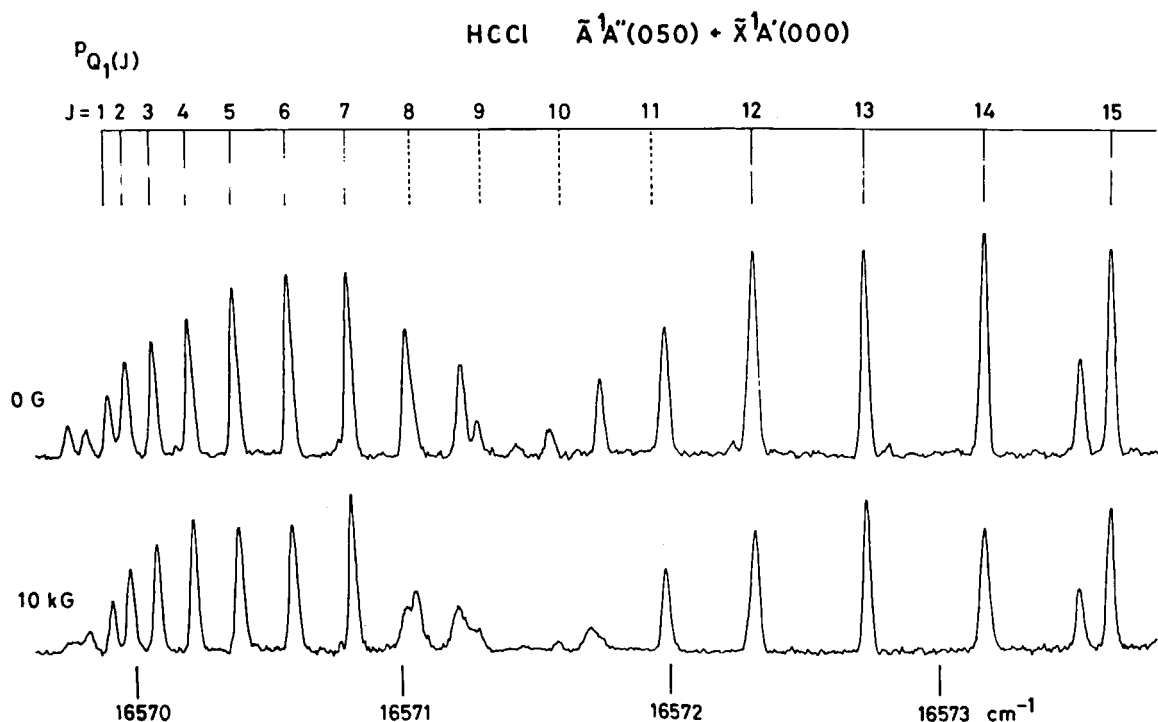
Figure 1. The $^{P}Q_1$ (*J*) branch of HCCl. Some zero-field spectral lines in the upper trace clearly exhibit Zeeman effects, when observed under a magnetic field of 10 kG, as shown in the lower trace.

II—B   Microwave Spectroscopy of Non-polar Molecules

Most non-polar molecules are of high symmetry and thus play important roles in the theory of molecular structure. It is therefore very unfortunate that we can not apply microwave spectroscopy to them, which is known to provide most accurate data on molecular structure. However, recent advances in theory and experiment of molecular spectroscopy have made it possible to observe weak rotational transitions in molecules which are normally classified as non-polar molecules. The observation is based upon small dipole moments which are induced by one of three following mechanisms: (1) degenerate vibration, (2) centrifugal distortion, and (3) isotopic substitution. The present project is concerned with the last mechanism. Among pioneer works, CH_3D by Klemperer and his coworkers (molecular beam electric resonance) and by Ozier and his coworkers (far-infrared) and HC $\equiv$ CD by Muenter and Laurie and by McKnight and Gordy should be mentioned. We also have reported microwave spectra of ethane (CH_3CD_3, $^{13}CH_3CD_3$, $CH_3{}^{13}CD_3$), allene ($CH_2{=}C{=}CD_2$), and methane (CH_2D_2). At present we know little about the origin of induced dipole moments, but in polyatomic molecules they seem to be amplified by intramolecular vibrations.

II-B-1   Microwave Spectrum of Ethylene-cis-1, 2-d_2

Kazuhiko YOSHIDA[1] *(Sophia Univ.)*, Yasuki ENDO, Shuji SAITO, and Eizi HIROTA

The C = C bond length in ethylene has been

chosen as a standard in the discussion of molecular structure. It is therefore desirable to determine structural parameters of ethylene as precisely as possible. Although only three parameters are needed to completely specify the structure of this molecule, the ground-state rotational constants, which are most precise among those available from spectroscopic experiments, are not readily used for structure deter-

Table I. Rotational and Centrifugal Distortion Constants of Deuterated Ethylenes (MHz)[a]

Constant	$CH_2 = CHD$	$CH_2 = CD_2$	cis-CHD = CHD
A	120 091.396 (62)	97 507.7 (52)	99 667.256 (42)
B	27 470.252 (28)	25 674.948 (99)	25 417.206 (19)
C	22 298.221 (18)	20 269.110 (68)	20 199.074 (11)
Δ_J	0.036 48 (99)	0.031 2 (16)	0.035 88 (52)
Δ_{JK}	0.196 4 (30)	0.200 3 (50)	0.115 9 (52)
Δ_K	$(0.0)^b$	$(0.0)^b$	1.459 3 (29)
δ_J	0.008 28 (14)	0.010 7 (24)	0.008 649 (43)
δ_K	$(0.0)^b$	$(0.0)^b$	0.196 2 (30)

[a] Values in parentheses denote standard errors and apply to the last digits of the constants.
[b] Assumed.

mination because of contamination from zero-point vibrations. The ground-state rotational constant, e.g. B_0, is related to that in the equilibrium, B_e, by

$$B_e = B_0 + \sum_s \alpha_s^B / 2 \qquad (1)$$

where the second term in the right-hand side containing the vibration-rotation constant α_s^B denotes the contribution of the zero-point vibration. Because α_s^B is mass-dependent, B_0 cannot be interpreted purely geometrically. Evaluation of α_s^B is normally impossible, because it involves cubic potential constants that are difficult to estimate. On the contrary, when we have more than three rotational constants, we will get some information on cubic constants. For ethylene, which is a planar molecule, two rotational constants for each isotopic species may be used to evaluate or estimate structural parameters as well as cubic constants. The third rotational constant combined with two others gives the inertia defect, which may be used to calculate quadratic force constants. There are four deuterated species which may have dipole moments sufficiently large to make microwave measurements feasible, that is, $CH_2 = CHD$, $CH_2 = CD_2$, cis-CHD = CHD, and CHD = CD_2. We have already analyzed microwave spectra of the first two species. In the present work we will report the data on the third one, whereas the last one still remains to be studied.

Rotational spectra of cis-CHD = CHD will follow the b-type selection rule, and will thus show very small Stark effects. Therefore, a source-modulation microwave spectrometer described in II-C-1 was used. We have observed 15 transitions to determine rotational constants and centrifugal distortion constants, as listed in Table I, where the data on the first two species are also included for comparison. There have been reported no high-resolution infrared data on cis-CHD = CHD to be compared with the present results.

We have now six ground-state rotational constants in addition to three inertia defects. Therefore, three pieces of information may be used to improve cubic

anharmonic constants. Machida and his coworkers[2] have calculated anharmonic force field mainly using vibrational data. He is refining his harmonic as well as anharmonic potential constants by adding our data to those already reported.

References and Notes
1) IMS Graduate Student for 1977–79.
2) See K. Machida and Y. Tanaka, J. Chem. Phys., 61, 5040 (1974).

II-B-2 Dipole Moments of Acetylene-d in Excited Bending States

Keiji MATSUMURA[1] (Kyushu Univ.), Takehiko TANAKA (Kyushu Univ.), Yasuki ENDO, Shuji SAITO, and Eizi HIROTA

It has been known that the dipole moment changes its value upon vibrational excitation. Although the absolute magnitudes of changes are small, fractional changes may become large for molecules which are made slightly polar by isotopic substitution. As we have recently shown, this is particularly the case for acetylene-d in the excited bending states, $v_4 = 1$ and $v_5 = 1$; the dipole moments in these states are 0.0236 D and 0.0560 D, respectively. These two values are much larger than those normally expected for isotope-induced dipole moments, which range from 10^{-3} to 10^{-2} D. However, the ground-state dipole moment of acetylene-d has not been measured, and thus we have not been able to assess how much moments are induced by the two bending modes. A second-order perturbation treatment gives an expression for the dipole moment in a vibrational state:

$$\mu_v = \mu_e + \sum_s \delta\mu_s (v_s + d_s/2). \qquad (1)$$

The dipole moments in the v_4 and v_5 states, which we determined, thus correspond to

$$\mu_4 = \mu_0 + \delta\mu_4, \tag{2}$$

$$\mu_5 = \mu_0 + \delta\mu_5, \tag{3}$$

where μ_0 denotes the ground-state moment tiven by

$$\mu_0 = \mu_e + \sum_s \delta\mu_s d_s/2. \tag{4}$$

Therefore, it is not possible to separately determine μ_0, $\delta\mu_4$, and $\delta\mu_5$ from the observed μ_4 and μ_5. We have thus decided to challenge observations of microwave spectra in $3\nu_4$ and $3\nu_5$. This is certainly a formidable experiment, becuase $3\nu_5$ is located more than 2000 cm^{-1} above the ground state. We will, however, gain intensities from the fact that dipole moments may increase with excitation of two more vibrational quanta.

A K-band Stark cell 50 cm long was used, which was heated up to $100°C$. We observed spectra only in Π sublevels of $3\nu_4$ and $3\nu_5$. The dipole moments obtained from the Stark effects are listed in Table I along with those in ν_4 and ν_5 obtained previously. Four observed moments are analyzed using Eq. (1) to determine μ_0, $\delta\mu_4$, and $\delta\mu_5$. Only the choice of signs shown in Table I reproduces the observed data and leads to reasonable constants. The minus signs for the ν_4 and $3\nu_4$ moments mean that they are opposite in sign to the ground-state moment. It should be noted that the CCH or CCD bending mode decreases the dipole moment of HCCF[2] or DCCF.[3] Therefore, the CD moiety of acetylene-d is more positive than the CH moiety. We wish also to stress that we are able to determine μ_0, which is almost impossible to obtain from the ground-state spectra with very small Stark effects.

Because the equilibrium dipole moment is probably of the order of 10^{-4} D, substitution of the observed μ_0, $\delta\mu_4$, and $\delta\mu_5$ allows us to estimate the sum of the three stretching modes contributions to the dipole moment, $\delta\mu_1 + \delta\mu_2 + \delta\mu_3$, to be -0.00478 (53) D. Therefore, the major term of μ_0 is zero-point contributions of the two bending modes, a negative one from ν_4 and a larger positive one from ν_5.

Table I. Dipole Moments of C_2HD (in D)

State	obs.[a]	(o-c) $\times 10^5$
ν_4	$(-) 0.02359$ (5)	0
ν_5	0.05601 (9)	0
$3\nu_4(\Pi)$	$(-) 0.09077$ (26)	2
$3\nu_5(\Pi)$	0.1472 (21)	-85
μ_0	0.01001 (15)	
$\delta\mu_4$	-0.03360 (13)	
$\delta\mu_5$	0.04600 (17)	
$\delta\mu_1 + \delta\mu_2 + \delta\mu_3$	-0.00478 (53)[b]	

[a] Values in parentheses denote 2.5 times standard errors.
[b] Obtained assuming $\mu_e = 0$.

Table II. Rotational Constants and ℓ-Type Doubling Constants of C_2HD in $3\nu_4(\Pi)$ and $3\nu_5(\Pi)$ (MHz)[a]

Constant	$3\nu_4$	$3\nu_5$
B_V	29 969.052 (44)	29 861.189 (27)
q_V	135.529 (25)	108.642 (27)

[a] Values in parentheses denote 2.5 times standard errors.

The vibrational contribution consists of two terms:

$$\delta\mu_s = \delta\mu_s{}^{anh} + \delta\mu_s{}^{2nd}, \tag{5}$$

where the anharmonic term:

$$\delta\mu_s{}^{anh} = -\sum_{s' \subset \Sigma^+} (1/4\pi\omega_{s'})(h/c\omega_{s'})^{\frac{1}{2}} \times (\partial\mu/\partial Q_{s'}) \phi^{sss'} \tag{6}$$

involves the cubic anharmonic potential constant $\phi^{sss'}$ and the first derivative $(\partial\mu/\partial Q_{s'})$, and the second-order term:

$$\delta\mu_s{}^{2nd} = (h/8\pi^2 c\omega_s)(\partial^2\mu/\partial Q_s{}^2) \tag{7}$$

the second derivative $(\partial^2\mu/\partial Q_s{}^2)$. Infrared intensities measured by Eggers et al.[4] and anharmonic potential constants estimated by Strey and Mills[5] allow us to further analyze the observed $\delta\mu_s$. We conclude that $\delta\mu_s{}^{anh}$ plays a dominant role for $\delta\mu_1$, $\delta\mu_2$, and $\delta\mu_3$, i.e., for stretching mode contributions, whereas $\delta\mu^{2nd}$ is more important for bending contributions.

Table II summarizes molecular constants of acetylene-d in $3\nu_4(\Pi)$ and $3\nu_5(\Pi)$.

References and Note

1) IMS Graduate Student for 1978–79.
2) T. Tanaka, C. Yamada, and E. Hirota, *J. Mol. Spectrosc.*, 63, 142 (1976).
3) K. Matsumura, K. Tanaka, C. Yamada, and T. Tanaka, *J. Mol. Spectrosc.*, to be published.
4) D. F. Eggers, Jr., I. C. Hisatsune, and L. V. Alten, *J. Phys. Chem.*, 59, 1124 (1955).
5) G. Strey and I. M. Mills, *J. Mol. Spectrosc.*, 59, 103 (1976).

II-B-3 Barrier to Internal Rotation in Ethane from the Microwave Spectrum of CH_3CHD_2

Eizi HIROTA, Shuji SAITO, and Yasuki ENDO

Ethane is one of the simplest molecules of high symmetry that have a freedom of internal rotation. This high symmetry, however, makes it difficult to investigate internal rotation in C_2H_6 by spectroscopic methods; the torsional mode ν_4, which belongs to the A_{1u} species under the assumption of D_{3d} overall symmetry, is inactive both in the infrared and Raman

Table I. Molecular Constants of Ethane-1,1-d_2

Constant	Value[a]	Uncertainty		
		I[b]	II[c]	III[d]
A	60 809.592	0.059	±1.289	∓0.001
B	17 770.87	0.16	±0.00	∓0.06
C	17 084.84	0.16	∓1.29	±0.06
D	[−566.319][e]		[±50.][e]	
Δ_J	0.02333	0.00045	∓0.000 00	∓0.000 00
Δ_{JK}	0.0602	0.0020	±0.000 0	±0.000 0
Δ_K	0.177	0.015	∓0.000	∓0.000
δ_J	0.00079	0.00016	±0.000 00	∓0.000 00
δ_K	0.050	0.081	∓0.001	∓0.000
F	257.70	0.35	±0.07	±0.00
V_3	2.8783	0.0028	±0.000 9	∓0.048 9
V_6	[0][e]			[±0.0576][e]

[a] In MHz, except for F (in GHz) and V_3 and V_6 (in kacl/mole).
[b] 2.5 times standard errors in a least-squares analysis.
[c] Due to the uncertainty in D of ±50 MHz. The signs should be taken in the same order.
[d] Due to the uncertainty in V_6 of ±0.0576 kcal/mole (2% of V_3). The signs should be taken in the same order.
[e] Assumed.

spectrum, and the absence of a dipole moment excludes possible studies by microwave spectroscopy. Therefore, reasonable estimates of the barrier have been made either by thermodynamic measurements or by observations of infrared combination bands. Weiss and Leroi[1] were, however, able to directly observe the torsional bands for three isotopic species, C_2H_6, CH_3CD_3, and C_2D_6, by using sample pressures of a few atm. They could explain the observed data in terms of a single cos 3α potential function with a coefficient of V_3 = 2.928 ± 0.025 kcal/mole. However, there are ambiguities as to mechanisms for observation of these forbidden bands. We have thus thought it would be worthwhile to determine the barrier more unambiguously by applying microwave spectroscopy to deuterated ethanes. This method will also provide information on the reduced moment of inertia. In the present work we investigated CH_3CHD_2; when V_3, the barrier, is lower than 3-5 kcal/mole, we will be able to observe splittings for rotational transitions of this species.

The spectrometer used is described in detail in II-C-1. The cell was cooled down to about 150 K. A sample of ethane-1,1-d_2 was obtained from Merck, Sharp & Dohme, Canada and was used without further purification. An assumption that the dipole moment is located along the C-D bonds led to a ratio of 0.75/1.0 for a-type/c-type transition intensities. However, we found a-type transitions to be stronger than c-type ones, and thus concluded that a simple bond-moment picture failed for deuterated ethanes. We observed 16 a-type R-branch transitions, of which 6 showed splittings due to internal rotation. An example $2_{11} \leftarrow 1_{10}$, shown in Figure 1, exhibits the smallest splitting of 0.252 MHz among the observed ones. We also observed two R branches and eight Q
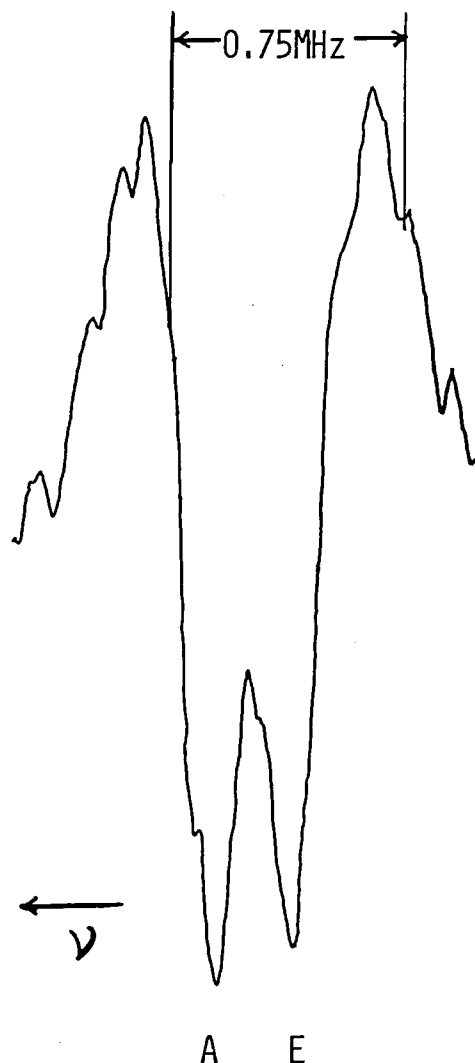

Figure 1. The $2_{11} \leftarrow 1_{10}$ transition of CH_3CHD_2. The integration time is 100 sec. The sample pressure is reduced to about 10 mTorr to resolve small splitting.

branches of c-type, all of which showed much larger splittings ranging from 11 to 48 MHz.

Although the barrier is as high as 3 kcal/mole, the framework CHD_2 is not much heavier than the top CH_3. We have therefore applied the Internal Axis Method (IAM) to analyze the observed spectra. The Hamiltonian used is given by

$$H = AJ_a{}^2 + BJ_b{}^2 + CJ_c{}^2 + D(J_cJ_a + J_aJ_c)$$

$$+ Fp'^2 + V(\alpha) + H_{CENT'} \quad (1)$$

where H_{CENT} denotes centrifugal distortion effects on the overall rotation, but we have neglected those on the torsion. An energy matrix was set up using products of the symmetric-top wavefunction and the torsional eigenfunction. The latter is obtained by solving an eigenvalue problem of the following torsional operator:

$$H_{TORS} = F[-i(d/d\alpha) - \rho k]^2$$

$$+ (V_3/2)(1 - \cos 3\alpha). \quad (2)$$

Table I lists the molecular constants obtained from a least-squares analysis. The standard deviation is 0.033 MHz, which is only slightly larger than the experimental errors of 0.01-0.02 MHz. We could not determine D, a term associated with an off-diagonal component of the inertia tensor, and thus fixed it to a calculated value. Fortunately, the uncertainty in D does not affect V_3, as shown in Table I.

A much more disturbing effect is due to intramolecular vibrations. As Lees and Baker[2] have shown, centrifugal distortion effects on the torsion affect the barrier not separably from those of the V_6 term. We have assumed the uncertainty in V_6 to be 2% of V_3, which includes those due to neglect of centrifugal effects on the torsion (see the uncertainty III of Table I). Kirtman et al.[3] estimated the decrease in barrier from C_2H_6 to C_2D_6 to be 0.102 kcal/mole. Therefore, the barrier in C_2H_6 will be very close to 2.90 kcal/mole, probably within ±0.03 kcal/mole of this value.

References

1) S. Weiss and G. E. Leroi, J. Chem. Phys., 48, 962 (1968).
2) R. M. Lees and J. G. Baker, J. Chem. Phys., 48, 5299 (1968).
3) B. Kirtman, W. E. Palke, and C. S. Ewig, J. Chem. Phys., 64, 1883 (1976).

II-B-4 Microwave Spectrum of Carbon Dioxide-^{18}O

Yasuki ENDO and Eizi HIROTA

Because of its great importance in various fields carbon dioxide has been investigated in detail by spectroscopic methods. Unfortunately the normal isotopic species $^{12}C^{16}O_2$ lacks a dipole moment to be studied by microwave spectroscopy, although laser transition frequencies $(00^01) \to (10^00)$ and $(00^01) \to (02^00)$ have been very precisely measured by observing beat notes between laser lines and harmonics of microwaves. We have attempted in the present work to observe pure rotational transitions of $^{12}C^{16}O^{18}O$ in the ground vibronic state, and we succeeded, for the first time, in observing microwave spectra of a non-polar molecule which is made polar by substitution of an isotope other than deuterium, namely ^{18}O. Gangemi[1] estimated the electric dipole moment of $^{12}C^{16}O^{18}O$ by taking into account only the first derivative of the moment with respect to the internuclear distance. Our experience on acetylene-d (II-B-2) indicates that stretching modes contribute to the dipole moment mainly through first derivatives. Therefore, Gangemi's estimate, 1.15×10^{-3} D, for the isotope-induced dipole moment of $^{12}C^{16}O^{18}O$ may be of correct order of magnitude. Oberly et al.[2] have analyzed the $(10^01, 02^01) \leftarrow (00^00)$ bands of this molecule to determine the rotational and the centrifugal distortion constants in the ground state. When the abundance of the isotopic molecule is 39.5%, a rotational line at 110 GHz (J = 5 ← 4) has an absorption coefficient of $1 \times 10^{-8} cm^{-1}$ at 180 K (the pressure broadening parameter of 7.3 MHz/Torr is assumed), which is large enough to be detected by our source-modulation spectrometer.

The microwave spectrometer used is described in II-C-1. A sample of carbon dioxide obtained from British Oxygen Company is used, which contains ^{18}O of 26.6 atom %. When a statistical distribution is assumed, the abundance of $^{12}C^{16}O^{18}O$ in the sample is

Table I. Observed Transition Frequencies and Molecular Constants of Carbon Dioxide-^{18}O (MHz)

$J' \leftarrow J''$	ν_{obs}	Error(σ)	o-c
3 ← 2	66 227.013	0.070	0.042
5 ← 4	110 377.190	0.041	0.032
6 ← 5	132 451.645	0.057	−0.015
7 ← 6	154 525.605	0.035	−0.051
8 ← 7	176 599.082	0.030	0.022

Constant[a]	Present	Ref. 2)
B_0	11 037.8918 (57)	11 037.8 (15)
D_0	0.003 520 (53)	0.003 5 (15)

[a] Values in parentheses denote standard errors and apply to the last digits of the constants.

calculated to be 39.5%, in agreement with our result using a mass spectrometer. The cell was cooled down to about 170 K, and the typical sample pressure was 20 mTorr. Table I lists the observed transition frequencies. Because the lines are weak, the precisions of the measured frequencies are lower than those (0.01-0.02 MHz) achieved for other molecules which exhibit much stronger absorption signals. Table I also shows the rotational and the centrifugal distortion constants obtained by a least-squares analysis, which are to be compared with the IR values of Ref. 2).

To estimate the dipole moment, the intensity of the $J = 5 \leftarrow 4$ transition was compared with that of a near-by OCS line. The result is 0.7×10^{-3} D with an error of $0.10 - 0.15 \times 10^{-3}$ D, in fair agreement with Gangemi's value.

The present results will be of some use to search carbon dioxide molecules in interstellar space by radiotelescope; this molecule prevails in the interstellar medium, but no reliable means are available at present to estimate its abundance.

References

1) F. A. Gangemi, J. Chem. Phys., 39, 3490 (1963).
2) R. Oberly, K. N. Rao, L. H. Jones, and M. Goldblatt, J. Mol. Spectrosc., 40, 356 (1971).

II—C   Development of New Instruments

The scope of researches is limited by capabilities of instruments. This is particularly the case for spectroscopic investigations of simple molecules, one of the main problems the Division is interested in. When we repeat investigations using spectrometers of similar performance, we will obtain almost identical results. It is therefore very urgent for us to always maintain our research facilities at levels of performance as high as possible. High precisions with which we determine molecular parameters often unravel new aspects of molecular properties that have not been known before. Needless to say, high sensitivity will supply us with fundamentally new information on molecular systems we are investigating. Along with these efforts to improve our facilities and with their applications to more interesting problems, we should also try to develope methods that are based upon something new. This project obviously premises not only detailed knowledge on molecules under investigation, but also that concerning with related fields. Various kinds of technical problems are to be solved. In this sense joint researches including collaboration with Development Workshop are indispensable. Developments of instruments that are thus brought about will open new research areas in the field of molecular science.

II-C-1   A Source-Modulation Microwave Spectrometer with a Free-Space Cell

Yasuki ENDO, Tetsuo SUZUKI[1] (Tokyo Metropolitan Univ.), Shuji SAITO, and Eizi HIROTA

Source modulation is an old technique in microwave spectroscopy; in 1945-46 when microwave spectroscopy started, most people used this method. However, once Hughes and Wilson[2] invented Stark modulation, source modulation has rarely been used. One of the most serious disadvantages of source modulation is that it cannot discriminate absorption signals from much larger baseline distortions due to reflections of microwaves by microwave components. Therefore, the sensitivity achieved with source modulation is much lower than that by Stark modulation. However, when we work in shorter wavelength regions (e.g. above 100 GHz), the transmission of microwaves through a Stark cell becomes worse. Recent advances in computer technology have remedied difficulties arising from baseline distortions to some extent; we can easily correct for distortions by fitting the base-line to a polynomial. A work on non-polar molecules[3] (cf. II-B) motivated us to revive source modulation. The Stark effects usually get smaller for higher-J transitions. This is another reason for difficulties we face at in using Stark modulation in mm- and submm-wave regions.

Woods[4] also set up a source-modulation spectrometer, and has applied it successfully to spectroscopy of unstable species including a few molecular ions. He has shown that, with a glass pipe of sufficiently large diameter, we can eliminate disturbance of microwave transmission by plasma caused by glow discharges in the cell. We have followed him to construct a free-space glow-discharge cell, which is shown in Figure 1. It is made of a Pyrex glass tube 350 cm long and 15 cm in diameter, sealed with a Teflon lens at each end. It is equipped with a cylindrical electrode made of either copper or stainless steel near at each end, to which we can apply a DC voltage of up to 4 kV and 500 mA. The cell can be kept at any temperature between $-100°C$ and liquid nitrogen temperature, by adjusting the amount of liquid nitrogen flowing through copper tubes surrounding the cell. We found microwave transmission is better for this cell than for a K-band Stark cell of 50 cm length,
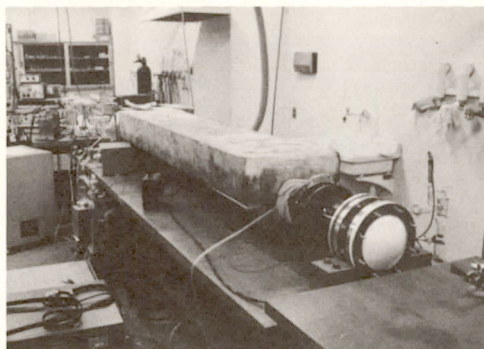
60

Figure 1. Free-space glow-discharge cell.

Figure 2. Block diagram of a computer-control system for a source-modulation microwave spectrometer.

at 120 GHz or higher. We have wound a coil on the cell, which was found to be useful to discriminate lines due to paramagnetic species from others.

The modulation waveform we used consists of two identical square waves of 50 kHz with a phase difference of $\pi/2$, and the absorption signal is demodulated by a phase sensitive detector (PSD) operated at 100 kHz. A source klystron, which is free-running, is repetitively swept by applying a saw-tooth of a few Hz to the reflector. We superimpose a small DC voltage to compensate for frequency drift of the source klystron. A YHP 2113 minicomputer with peripherals shown in Figure 2 controls the spectrometer and processes the observed signals. A start pulse, which is delayed from the start of the saw-tooth signal by a short time, opens a gate to receive signals both from the PSD and a receiver; 1024 data points are allocated to the two signal channels alternately. An interpolation receiver receives beat notes between the source klystron and an X-13, which is phase-locked to a temperature-stabilized crystal oscillator by a Microwave Systems MOS 5. The frequency of the X-13 is continuously monitored by a microwave counter YHP 5340A. The receiver dial is normally set to 0.5-2.0 MHz, which means that absorption signals are recorded in a region of ±0.5 to ±2.0 MHz about a center frequency. This technique is based upon the assumption that the source klystron changes its frequency linearly for the frequency interval swept. A few test runs indicate that this requirement is well satisfied. Because the beat notes are split by modulation into sidebands, a peripheral unit we made shapes them into square waves and computes their centers. The minicomputer corrects baseline distortions, if any, by fitting them to a polynomial. The error of a measured line frequency is typically 0.01-0.02 MHz.

We have tested the sensitivity of the spectrometer by using the $J = 11 \leftarrow 10$ transition of $^{18}O^{13}C^{34}S$ at 122 GHz. We found that the minimum absorption coefficient is 7×10^{-10}cm^{-1}, which is an order of magnitude smaller than that by Stark modulation using a 50 cm long Stark cell. The good sensitivity
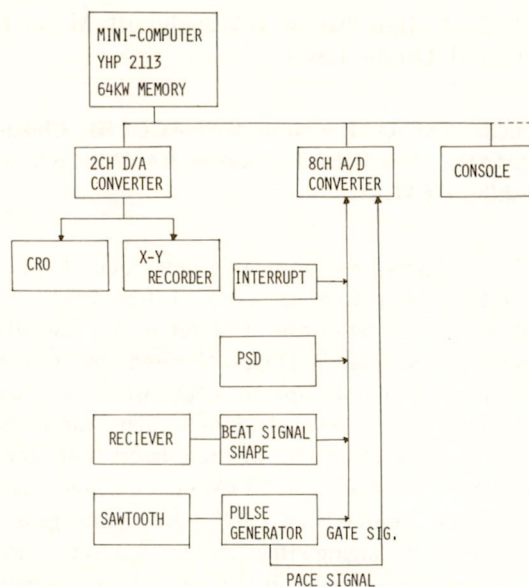
we can achieve may be ascribed to the following reasons:

(1) Good microwave transmission characteristics of the cell allows us to make the path length as long as 350 cm.
(2) Because both the source klystron and the detector are not fixed to the cell, we can adjust their positions so as to minimize microwave reflection.
(3) The computer averages and smoothes noises, whereas the signals are accumulated on its memory. It also corrects for baseline distortions.

We may mention two other aspects which make the spectrometer more suitable for investigating unstable molecules.

(4) We can choose an optimum temperature between 77 and 170 K.
(5) We can generate unstable species *in situ* in the cell.

Applications of this spectrometer are found in II-A-5, II-B-1, II-B-3, and II-B-4.

References and Note

1) IMS Graduate Student for 1977–78.
2) R. H. Hughes and E. B. Wilson, Jr., *Phys. Rev.,* **71,** 562 (1947); K. B. McAfee, Jr., R. H. Hughes, and E. B. Wilson, Jr., *Rev. Sci. Instrum.,* **20,** 821 (1949).
3) E. Hirota and M. Imachi, *Canad. J. Phys.,* **53,** 2023 (1975).
4) R. C. Woods, *Rev. Sci. Instrum.,* **44,** 282 (1973).

II-C-2 A High-Precision Wavelength Meter for Infrared Diode Laser

Keiichi NAGAI, Kentarou KAWAGUCHI, Chikashi YAMADA, Eizi HIROTA, Kazuo HAYAKAWA, and Yoshihiro TAKAGI

Diode lasers have brought a new epoch for high-resolution infrared spectroscopy. Infrared light they emit has a spectral purity of better than a few MHz, which makes possible Doppler-limited spectroscopy and even sub-Doppler spectroscopy, when combined with some techniques such as molecular beams. One of the greatest advantages of these lasers is obviously tunability; one diode can be swept for a few tens or even a few hundreds of cm^{-1} (with many gaps in between) by changing either current fed to the diode or temperature at which it is kept. The potentiality of this light source has been demonstrated by examples mentioned in II-A-6 through II-A-10.

One problem with tunable lasers is how to determine the wavelength of the laser light. Hall and Lee[1] have developed a wavelength meter for cw dye lasers which allows us to determine the wavelength with a precision of 0.01 cm^{-1}. In the present work we have set up a similar λ meter for infrared lasers. It is a Michelson interferometer with motor-driven corner cube reflectors. Fiugre 1 shows a blockdiagram of our λ meter, and Fiugre 2 its picture. A diode laser beam is made colinear with a He-Ne laser beam by using a ZnSe beam splitter, and the two beams, after divided into two by a second ZnSe beam splitter, enter into a vacuum box containing moving corner cubes. They are reflected back to the second ZnSe, where the divided beams are combined and proceed to a Ge plate. The He-Ne laser beam is reflected by this Ge plate and focused onto a PIN photodiode, while the infrared beam passes through the Ge plate to an infrared detector. The corner cubes move with a velocity of about 10 cm/sec and traverse over a distance of up to 1 m. This velocity produces about 4×10^4 fringe counts/sec for infrared light of about 1000 cm^{-1}. To improve the precision the signal frequency of infrared is multiplied by 100 by a phase

Figure 2. Wavelength meter constructed by K. Nagai (standing nearby the equipment) and others. Housing of a vacuum box has been removed to show corner reflectors on a carriage.

Table I. Measurements of CO_2 Laser Wavelengths

CO_2 Line	$\omega_{meas.}$ (cm^{-1})	(σ)	$\omega_{ref.}$ (cm^{-1})	Δ ($10^{-4} cm^{-1}$)
10.4 μm band				
P (30)	934.8940	(3)	934.8945	−5
P (24)	940.5481	(4)	940.5481	0
P (22)	942.3822	(4)	942.3833	−1
P (20)	944.1934		944.1940	−6
	~944.1940			~0
P (18)	945.9800	(3)	945.9802	−2
P (16)	947.7423	(3)	947.7420	+3
R (16)	973.2886	(4)	973.2885	+1
	973.2884	(2)		−1
R (20)	975.9300	(3)	975.9304	−4
	975.9295	(3)		−9
9.4 μm band				
P (20)	1046.8532	(2)	1046.8542	−10
	1046.8533	(1)		−9
P (16)	1050.4405	(4)	1050.4413	−8
	1050.4410	(3)		−3

Table II. Measurements of N_2O ν_1 Band Wavelengths

N_2O 10^00-00^0 band Line	$\omega_{meas.}$ (cm^{-1})	(σ)	$\omega_{ref.}^{a}$ (cm^{-1})	Δ ($10^{-4} cm^{-1}$)
R (12)	1295.4762	(4)	1295.4763	−1
R (17)	1299.3826	(8)	1299.3832	−6
R (30)	1309.1222	(4)	1309.1224	−2
R (33)	1311.2840	(5)	1311.2837	+3

[a] Ref. 2).

lock device (PLL, phase lock loop, of Figure 1), and is compared with that of He-Ne laser light ($\lambda = 632.991399$ nm) used as a reference. When the He-Ne laser fringe counts reach a pre-set value (10^6), the infrared fringe numbers counted are shown on a display.

There are two main sources of errors to be considered. The first, diffraction error is estimated to be

Figure 1. Block diagram of the wavelength meter.

about 10^{-7}, when the diameter of the infrared beam is 10 mm. The second, alignment errors are more serious; if optical axes of infrared and reference beams differ by 1 mrad, the error amounts to 5×10^{-7}. To minimize this error, we have inserted two slits of 7 mmϕ at distance of 4 m, as shown in Figure 1, which limit deviations of optical axes to less than 1.7 mrad.

We have tested performance of the λ meter on CO_2 laser lines, for which very accurate wavelengths or frequencies are available. Table I lists the results. Several measurements were carried out on the 10.4 μm P(20) line under different conditions; the results fall in a region indicated in Table I. Two values shown for each of 10.4 μm R(16) and R(20) and and 9.4 μm P(20) and P(16) were obtained using two different arrangements of optical elements. The

alignment error is thus of the order of $5 \times 10^{-4} cm^{-1}$, in good agreement with the expectation. The deviations from the reference values do not overpass the limit of $10^{-3} cm^{-1}$, and are thus tolerable for Doppler-limited spectroscopy. Recently Olson et al.[2] calibrated N_2O ν_1 and $2\nu_2$ bands by using spectroscopic results already reported; the precisions they obtained are $10^{-3} cm^{-1}$ or better. We have measured the wavenumbers of four lines of N_2O ν_1 band with our λ meter, which agree well with Olson's values as shown in Table II.

References

1) J. L. Hall and S. A. Lee, *Appl. Phys. Lett.*, **29**, 367 (1976).
2) W. B. Olson, A. G. Maki, and W. J. Lafferty, 34th Symposium on Molecular Spectroscopy, Columbus, Ohio, June, 1979, Paper TE 14.

II—D   Double Resonance Spectroscopy Using a Tunable Diode Laser

Lasers provide us with a variety of nonlinear spectroscopic techniques for gas phase molecular spectroscopy with ultra-high resolution and ultra-high sensitivity. One of such techniques, laser-microwave double resonance, is a useful method for, a) assignments of complicated absorption spectra, b) microwave spectroscopy of excited molecules, c) observation of nearly forbidden microwave transitions such as pure rotational transitions of nonpolar molecules, and d) investigation of state-to-state relaxation processes. In the infrared region, this technique has been applied to many molecular systems using fixed frequency lasers or semitunable lasers. However, in order to apply the technique, in general, to molecular systems of interest in spectroscopy, it is highly desirable to use a tunable laser in double resonance. The purpose of this project is to establish the experimental technique of infrared- microwave double resonance using a tunable diode laser, and to apply it to actual molecular systems in the whole infrared region.

II-D-1   Infrared-Microwave Double Resonance of NH_3 Using a Tunable Diode Laser

Michio TAKAMI *(Inst. Phys. Chem. Res. and IMS)*

[*Appl. Phys. Lett.* 34, 684 (1979)]

The purpose of this work is to investigate the feasibility and characteristics of infrared-microwave (IR-MW) double resonance using a tunable diode laser (TDL). For microwave spectroscopy of excited molecules by double resonance, the laser should satisfy the following two conditions. First, the laser power should be strong enough to saturate a vibration-rotation of molecules.[1] Second, the amplitude and frequency noise of the laser should be small so that it does not cause too much noise and excess broadening of the double resonance signal. By focusing the output of a TDL, Jennings[2] was recently able to observe an inverted Lamb dip in the ν_2 sP(4,3) line of NH_3. His experiment shows that the first condition can be satisfied by a TDL in spite of its large

frequency fluctuation. Our interest in the present work is to find if a TDL can satisfy the second condition.

A block diagram of the experiment is shown in Fiugre 1. The double resonance effect was observed as a variation of infrared absorption caused by microwave pumping. The double resonance cell was a 30-cm-long section of WRJ-140 waveguide (15.8×7.9 mm) with NaCl windows. The laser beam was focused into the cell with a spherical mirror of r = 50cm or 100 cm. The beam waist at the focus was less than 1 mm. A PbSnTe photodiode was used to detect the laser radiation. The J = K = 3 inversion line of NH_3 in the ground vibrational state was pumped by an OKI 24V11 klystron. The microwave radiation was square wave frequency modulated at 100 kHz and scanned. The output of the photodiode was lock-in amplified.

The TDL used was a Laser Analytics Inc. Model LS-3. The laser output showed large frequency fluctuation of more than 20 MHz, arising probably from current fluctuation of the laser power supply. This fluctuation caused a large amplitude noise at the
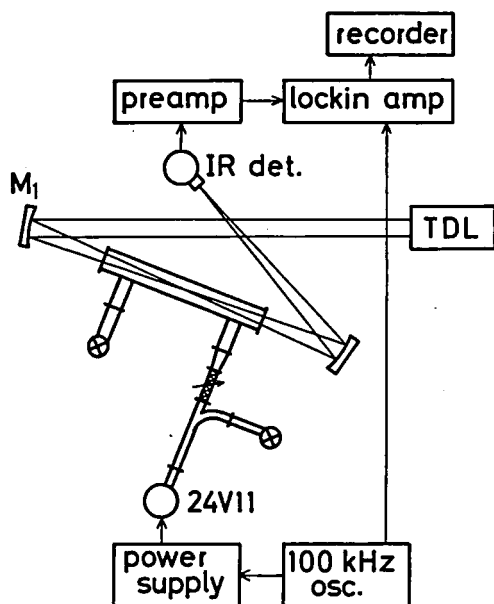
Figure 1. A block diagram of IR-MW double resonance experiment using a TDL. The laser beam is focused into the cell with a spherical mirror M_1 of $r = 50$ or 100 cm.

shoulders of the infrared absorption lines.

The double resonance effect was observed in several three-level systems of NH_3. Pressure dependence of the signal was observed in the three-level system in which the lowest energy state is the common level of double resonance as shown in Figure 2. When the transition 3-1 is not saturated by the laser, microwave pumping of the transition 2-1 decreases the infrared absorption (the lowest order effect). When the infrared transition 3-1 is well saturated, on the contrary, the microwave pumping increases the infrared absorption because of the population inversion between the levels 1 and 2 at the laser frequency (a higher-order effect). Therefore, saturation of the infrared transition can be observed as the reversed sign of the signal at low pressure.[3]
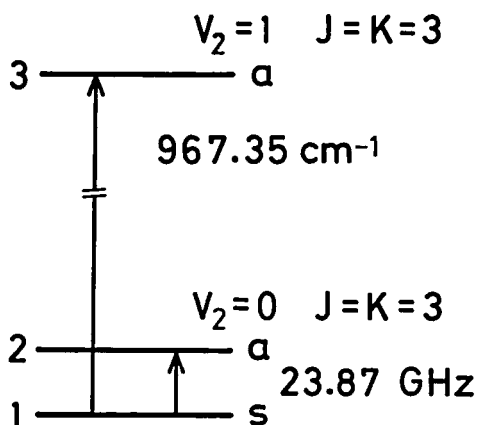
Figure 2. A three-level system of NH_3.

A preliminary double resonance experiment on the $\nu_4 sQ(5,5)$ line of NH_3 showed that the infrared transition could not be saturated by unfocused laser beam. In a second experiment, the double resonance effect was observed on the $\nu_2 sQ(3,3)$ line of NH_3 with a focused laser beam (Figure 1). Figure e shows typical traces of the signal. The line shape is the derivative of a Lorentzian because of phase sensitive detection. Fiugre 3(a) is the trace at 17 mTorr of NH_3 and shows the lowest-order signal. Fiugre 3(b) is the signal at about 1 mTorr observed with four times greater gain, where the sign of the signal reversed by saturation of the infrared transition. The HWHM of the signal is slightly less than 4 MHz. Note that Figure 3(b) shows a greater S/N ratio in spite of the four times greater gain. This is because the frequency fluctuation of the laser gives rise to greater amplitude noise for stronger infrared absorption.

In conclusion, feasibility of IR-MW double resonance using a TDL was demonstrated on NH_3. The infrared absorption line of NH_3 was found to be well saturated by the TDL at low pressure.

References

1) M. Takami and K. Shimoda, *Jpn. J. Appl. Phys.* 12, 603 (1973).
2) D. E. Jennings, *Appl. Phys. Lett.* 33, 493 (1978).
3) M. Takami and K. Shimoda, *Jpn. J. Appl. Phys.* 11, 1648 (1972); M. Takami, *Jpn. J. Appl. Phys.*, 15, 1889 (1976).

(a)   (b)
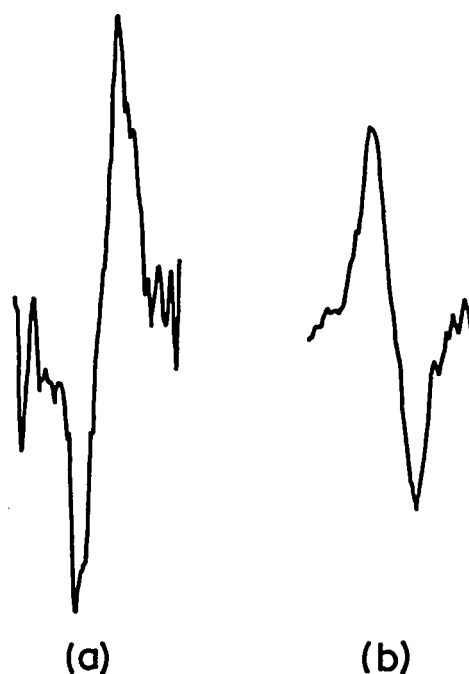
Figure 3. Typical traces of the double resonance signal. Microwave frequency was scanned over the J = K = 3 inversion line of NH_3. Time constant was 0.3s and the scan width about 40 MHz. (a) Signal at 17 mTorr of NH_3. (b) Reversed signal at about 1 mTorr of NH_3. Gain is four times greater than (a).

II-D-2 Dipole Moment and Infrared-Radio-frequency Double Resonance Spectroscopy of CF_4 in the $v_3 = 1$ State

Michio TAKAMI *(Inst. Phys. Chem. Res. and IMS)*

Molecules with tetrahedral symmetry have vibrationally induced dipole moment in their triply degenerate vibrational states. This effect was predicted first by Mizushima and Venkateswarlu,[1] and confirmed experimentally in the $v_3 = 1$ state of $CH_4$ using the 3.39 μm He-Ne laser.[2,3] Subsequently, two pure rotational transitions allowed by the vibrationally induced dipole moment were observed in the same excited state of CH_4 by infrared-microwave double resonance.[4,5] Similar dipole moments have also been observed in GeH_4 $(v_2 = 1)$[6] and CH_4 $(v_4 = 1)$.[7] In the present work, the existence of vibrationally induced dipole moment in the $v_3 = 1$ state of CF_4 was confirmed using a tunable diode laser. Six pure rotational transitions among the fine structure splitting of the $v_3 10_{11} (J=10, R=11)$, 11_{12}, 14_{15}, and 22_{23} states were also observed by infrared-radiofrequency double resonance.

A polar behavior of CF_4 in the $v_3 = 1$ state has been reported by Muenter *et al.* using the technique of molecular beam electric deflection.[8] From the intensity of the $2v_3$ band of CF_4, the vibrationally induced dipole moment in the $v_3 = 1$ state was estimated to be well over 0.01 debye.[1,9] Recently, Suzuki *et al.* investigated the v_3 band of CF_4 using a tunable diode laser.[10] The existence of the dipole moment was confirmed by observing Stark effect on the infrared absorption lines assigned in the above work. The laser beam was focused into a 20 cm long Stark cell of 1 mm electrode spacing. The Stark signal was observed by applying 0 to 4 kV/cm sinusoidal or square wave field at 100 kHz. Figure 1a and b shows the observed infrared and Stark spectrum when the laser was scanned over the P(23) lines. The absorption spectrum is shown as the second derivatives of the lines. A typical first order Stark effect was observed in the $E^{(4)}$ and $E^{(3)}$ lines. From the observed Stark effect on the $12_{13}E^{(2)}$ and the $13_{14}E^{(3)}$ lines, the dipole moment was determined tentatively as 0.036 ± 0.004 debye neglecting higher order corrections.

The experimental procedure of infrared-radiofrequency double resonance was the same as the previous work on NH_3[11] except that a 30 cm long coaxial cell was used instead of the waveguide cell. The pressure of CF_4 was kept at about 1 mTorr by flowing the gas through the cell. The laser beam was focused into the cell with an r = 1 m spherical mirror. The infrared signal was detected with a PbSnTe photo-diode. The rf field of the order of 10 V/cm was applied with 35 kHz amplitude modulation.

Table I. Radiofrequency transitions of CF_4 in the $v_3 = 1$ state

Transition			v_{obs}(MHz)	v_{calc}(MHz)[b]
10_{11}	$F_1^{(3)}$ -	$F_2^{(3)}$	53.578 ± 0.020^a	58.456
11_{12}	$F_1^{(3)}$ -	$F_2^{(3)}$	22.306	24.089
14_{15}	$F_1^{(4)}$ -	$F_2^{(4)}$	17.631	18.734
22_{23}	$F_1^{(4)}$ -	$F_2^{(4)}$	55.886	56.788
	$F_1^{(5)}$ -	$F_2^{(5)}$	83.969	87.055
	$F_1^{(6)}$ -	$F_2^{(6)}$	12.359	12.983

^{a} The largest standard deviation among the six measurements.
^{b} Calculated from the constant in Ref. 10.

1281.45   .50   CM^{-1}
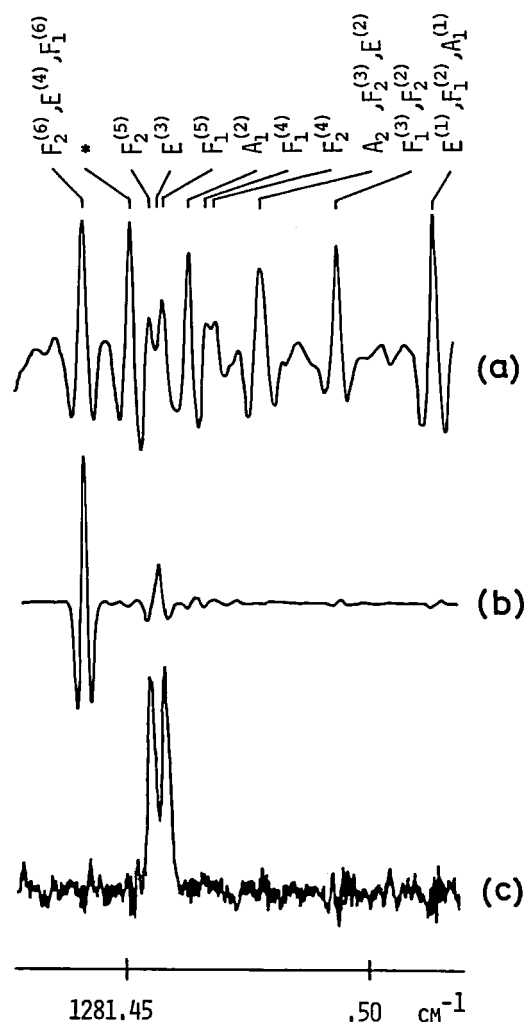
Figure 1. Infrared absorption, Stark, and double resonance spectrum of CF_4 when the laser is scanned over the v_3P(23) lines. a) Infrared absorption spectrum. The trace shows the second derivatives of the lines. The assignments are shown by the symmetry of the upper states. The peak with asterisk belongs to P(24). b) Infrared Stark spectrum. The Stark field is 0 to 3 kV/cm sinusoidal field at 100 kHz. c) Double resonance signal when the rf frequency is fixed at 83.97 MHz with 35 kHz amplitude modulation. The time constant is 1 sec.

Double resonance signals were observed as the increase of infrared absorption when the pure rotational transitions were saturated in the excited state. The observed frequencies are shown in Table I. The line width of the rf transitions was about 100 kHz (HWHM). Figure 1c shows the double resonance signal when the rf frequency was fixed at 83.97 MHz, which corresponded to the $22_{23}F_1{}^{(5)} - F_2{}^{(5)}$ transition, while the laser frequency was scanned. The two peaks correspond to the signals arising from the two infrared lines, $F_1{}^{(5)}$ and $F_2{}^{(5)}$, of P(23). Note that the signal is observed only when the infrared transitions are saturated by the laser.[12] Further studies including accurate determination of the dipole moment are in progress.

References

1) M. Mizushima and P. Venkateswarly, *J. Chem. Phys.* **21**, 705 (1953).
2) K. Uehara, K. Sakurai, and K. Shimoda, *J. Phys. Soc. Japan* **26**, 1018 (1969).
3) A. C. Luntz and R. G. Brewer, *J. Chem. Phys.* **54**, 3641 (1971).
4) R. F. Curl, Jr. and T. Oka, *J. Chem. Phys.* **58**, 4908 (1973).
5) M. Takami, K. Uehara, and K. Shimoda, *Jpn. J. Appl. Phys.* **12**, 924 (1973).
6) W. A. Kreiner, B. T. Orr, U. Andresen, and T. Oka, *Phys. Rev.* **A15**, 2298 (1977).
7) I. Ozier and A. Rosenberg, *J. Chem. Phys.* **69**, 5203 (1978).
8) A. A. Muenter, T. R. Dyke, W. E. Falconer, and W. Klemperer, *J. Chem. Phys.* **63**, 1231 (1975).
9) P. N. Schatz and D. F. Hornig, *J. Chem. Phys.* **21**, 1516 (1953).
10) T. Suzuki, H. Okada, and T. Fujiyama, *Bull. Chem. Soc. Japan*, in press.
11) M. Takami, *Appl. Phys. Lett.* **34**, 684 (1979).
12) M. Takami and K. Shimoda, *Jpn. J. Appl. Phys.* **12**, 603 (1973).

II-D-3 Tunable Diode Laser Spectroscopy of HN_3

Koichi YAMADA *(Inst. Phys. Chem. Res.)* and Michio TAKAMI *(Inst. Phys. Chem. Res. and ImS)*

The molecules such as HNCS, HNCO, or HN_3 are called sometimes as "quasi-linear molecules" which are characterised by their very small moment of inertia along the a-axis.[1] Because the moment of inertia critically depends upon the relative position of the hydrogen atom, there exists a strong coupling of rotational and vibrational motion, which sometimes causes breakdown of the Born-Oppenheimer approximation to separate them. Consequently, the vibration-rotation spectra of HN_3 often show complicated band structures caused by large frequency anomaly.[2-5]

In order to investigate the effect of vibrational excitation on the quasilinearity, we studied the high resolution infrared spectrum of the ν_2 and ν_3 bands of HN_3 using a tunable diode laser. In the ν_3 band, many lines with $K_a \geq 2$ were assigned based upon their Stark behavior. For the $K_a = 0$ or 1 lines, however, there still is ambiguity in their assignments. The infrared-microwave double resonance technique will provide with a method to confirm the assignments unambigously by saturating the microwave transitions in the ground vibrational state, whose transition frequencies have been measured accurately.[6,7]

References

1) K. Yamada and M. Winnewisser, *Z. Naturforsch.* **31a**, 139 (1976).
2) D. A. Daws and G. C. Pimetel, *J. Chem. Phys.* **23**, 1258 (1955).
3) C. B. Moore and K. Rosengren, *J. Chem. Phys.* **44**, 4108 (1966).
4) D. M. Levine and D. A. Dows, *J. Chem. Phys.* **46**, 1168 (1967).
5) M. Carlotti, G. Dilonardo, G. Galloni, and A. Trombetti, *Trans. Faraday Soc.* **67**, 2852 (1971).
6) R. Kewley, K. V. L. N. Sastry, and M. Winnewisser, *J. Mol. Spectrosco.* **12**, 387 (1964).
7) M. Winnewisser and R. L. Cook, *J. Chem. Phys.* **41**, 999 (1964).

II—E Large Amplitude Intra-Molecular Motions

The subject of this study is a molecular distortion, whose amplitude is much greater than that of the usual molecular vibration, but which does not yet cause a decomposition of the molecule. Such a distortion takes place in the course of an internal rotation, inversion, and isomerization reaction of a molecule. High resolution infrared spectroscopy provides useful pieces of information on the detailed itinerary of a travel of a molecule from one equilibrium conformation to another and the amount of energy required in such a travel. For example, every vibrational level (v) of the hydrazine molecule splits into three sublevels because of the inversion motions of the two amino groups. The wavefunction $\psi_{vj}(\eta)$ associated to each of these sublevels represents a unique

distribution of the probability with which any given η (inversion) coordinate occurs. An effective rotational constant A_{vj} derived from an infrared analysis is taken as the rotational constant $A(\eta)$ of the distorted molecule averaged over the all possible η values with the weight given by $|\psi_{vj}(\eta)|^2$. A number of A_{vj} values should, therefore, form a set of data for obtaining $A(\eta)$, and this is considered to be a valuable piece of information of the geometry of the molecule distorted along η.

II-E-1 Diode Laser Spectroscopy of NH_2NH_2

Yoshiaki HAMADA *(Univ. of Tokyo)*, Masamichi TSUBOI *(Univ. of Tokyo)*, Kentarou KAWAGUCHI, Chikashi YAMADA, Keiichi NAGAI, and Eizi HIROTA

Infrared absorption spectrum of NH_2NH_2 has been observed with the resolution of 0.02 cm^{-1} by the use of a Laser Analytics Model LS-3 Diode Laser Spectro-meter in the spectral regions 1310-1240 and 880-860 cm^{-1}. The pressure of NH_2NH_2 was kept at about 5 torr in a cell with optical path length 150 cm. Frequencies of the observed absorption lines were determined with standard lines of N_2O or OCS and with an etalon fringe pattern overlapped on the sample spectrum. The standard lines were identified by the use of a wavelength meter constructed in this laboratory (see II-C-2). 18 Q branch clusters have been found with proper K-structures, and each of them was assigned to a particular transition involving the inversion levels.

II—F Production of Highly Excited Atoms from Molecules

Atoms with very high principal quantum numbers (say $n \lesssim 50$) can be produced in the gas phase by impact of low-energy electrons on atoms or simple molecules. Such "highly excited Rydberg atoms" have long natural radiative lifetimes (from microseconds to milliseconds depending on their quantum numbers). Therefore, these atoms are metastable species of high electronic energy, i.e., potential sources of novel chemical reactions. The main purpose of the present project is to investigate mechanisms of formation of Rydberg atoms from molecules and their reactions with other neutral atoms or molecules. Since one of the electrons in such an atom is bound to the nucleus only very loosely, their reactions are expected to be a hybrid of an ion-molecule reaction and a free electron-molecule reaction. An apparatus has been designed and constructed to produce Rydberg atoms from molecules by electron impact and to measure the following properties: (a) distribution of their principal quantum numbers, (b) distribution of their kinetic energies, and (c) relative cross sections of ionization by collision with target molecules and, if possible, angular distributions of the resulting ions. Our study is being extended to similar measurements on highly excited hydrogen/deuterium molecules.

II-F-1 Construction and Testing of an Apparatus for Production of Highly Excited Atoms and for Measurement of Their Properties

Tamotsu KONDOW *(Univ. of Tokyo)*, Tsutomu FUKUYAMA *(National Institute for Environmental Studies)*, and Kozo KUCHITSU *(Univ. of Tokyo and IMS)*

The three main parts of the apparatus, (i) the electron source, (ii) the molecular beam source, and (iii) the field-ionizer and the mass spectrometer unit, were installed in the vacuum chamber (Figure 1). Various adjustments and testings were made searching for their optimal operating conditions. The overall setup of the parts is shown in Figure 2.

1) *Electron source:* The filament is a tungsten hair-pin, on which lanthanum boride fused on a tantalum piece is spot-welded; the tantalum sheet protects the filament from corrosion by the lanthanum boride. The electron beam emitted from the cathode is focused with a Wehnelt cone, accelerated to 500 eV, decelerated with retarding lenses to 50-25 eV, and is allowed to pass through a field-free collision chamber. The molecular beam passes perpendicularly through the center of the collision chamber, where the electron beam is focused. The final energy of the electrons can be varied from 5 to 500 eV. The size and the spatial position of the electron beam is monitored by measuring electric currents collected on an aperture and a Faraday cup mounted behind the collision chamber. Ions formed in the collision chamber as byproducts of the electron impact are removed from the molecular beam by applying 100 V to a pair of electrostatic deflectors. A typical electron current obtained is 45 μA at 30 eV with a fila-

ment current of 2.5 A.

2) *Molecular beam source:* Tests were made using nitrogen gas. With a nozzle of 90 μm diameter and a nozzle to skimmer distance varied from 2 to 17 mm and with a stagnation pressure of about 100 Torr, a beam intensity of the order of 10^8 particles/cm^3 was obtained at 80cm from the nozzle. The angular spread of the beam was estimated to be less than 3° from the cutoff of the beam signal measured by shifting a mass spectrometer off the beam axis. A further test is being made using a nozzle of 45 μm.

3) *Mass spectrometer:* The ionizer of the spectrometer has four symmetrical filaments supported in a square shape with a cylindrical grid placed in the center. The electron energy can be adjusted from the threshold to 100 eV. The energy and the focusing of the ions adjusted by use of five lenses. The quadrupole mass filter is made by Extranuclear Labs (EFLS-4-162-5). The ion energy is varied from 4 to 20 eV depending on the mass of the ion being analyzed. A small ceramagnetic electrode minimizes the distortion of the field caused by the quadrupole fringe field so as to keep the ion energy as low as possible. The maximum resolution obtained is 20 mu at 28 u. The sensitivity is such that at 10^{-9} Torr the H_2^+ signal of 3000 cps is obtained at an ion energy of 10 eV and a bombarding electron current of 90 μA.

Field ionization of highly excited atoms is used for two purposes: for controlling their principal quantum numbers and for detecting the highly excited atoms as ions. Adjustments of the electrodes used for these purposes are being made.
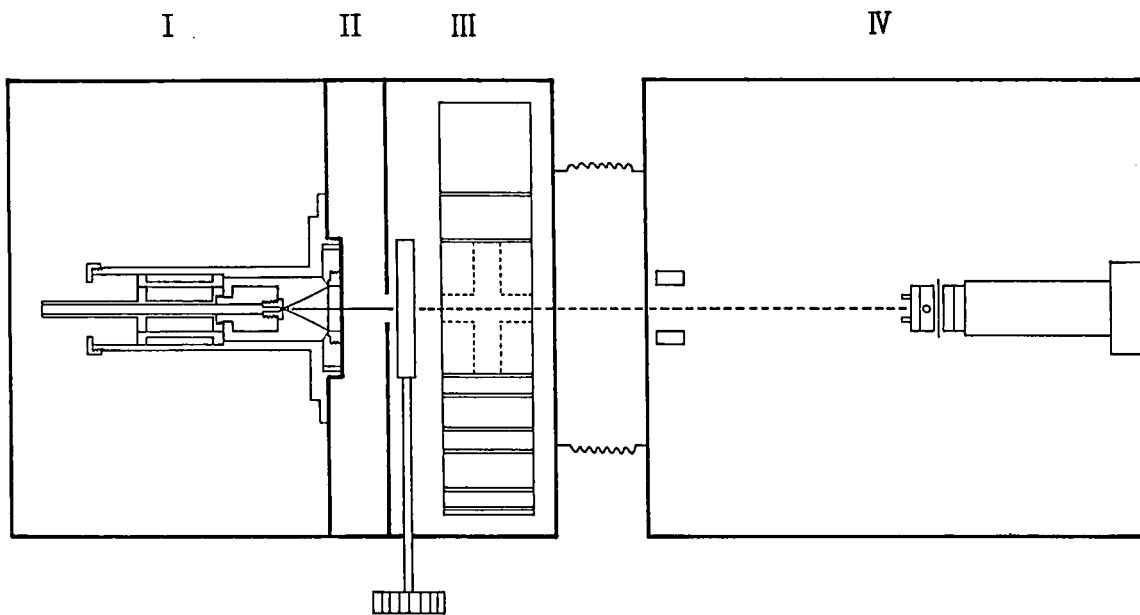

Figure 1.

I   II   III   IV
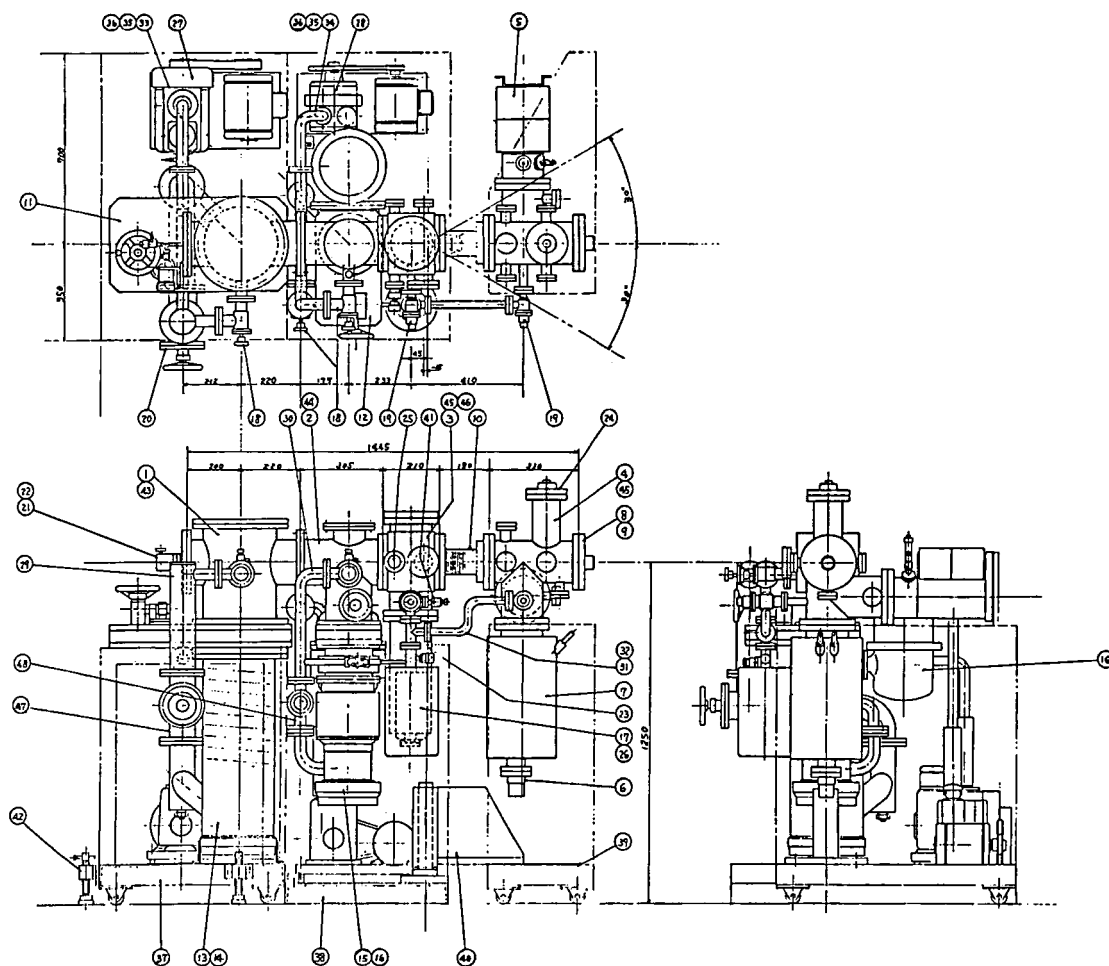
Figure 2.

RESEARCH ACTIVITIES III

Division of Electronic Structure

The goal of the Division is a development of novel functions of molecules through studies of the electronic structure. To fulfill this goal basic characters of electronic spectra should be investigated. The emphasis is made on the research of electronically excited states of molecules. The dynamic behavior of fluorescence under various conditions, reactivities of excited molecules, and characteristics of the electron transfer in excited states are the important features of molecules. The investigation of the local dynamic structure of biomolecules is an important application of fluorescence dynamic studies.

Unique properties of the solid-molecule interface are also studied with the emphasis of deveioping a novel method for solar energy conversion. The fundamental and dynamical processes of photoelectrode and photo-catalysis are investigated by measuring transient photocurrents, luminescence of molecules adsorbed on solid surfaces and the photochemical products by a pulsed laser excitation in ultrahigh vacuum. Together with the investigation on the molecular processes of solar energy conversion nto electricity and chemical energy, new materials for this purpose are being searched.

III—A   Primary Photochemical Reactions of Organic Compounds

The photochemical reactions such as photoisomerization, photosubstitution, photoelimination, photo-addition, and photoionization differ, in many cases, from thermal reactions and give unique products, since the reaction occurs from the completely different electronic states. The energy of light which is absorbed by molecules is as large as of that of ·a chemical bond, and therefore reactivities are greatly enhanced in excited states. Thus the utilization of photochemical reactions is important for synthetic chemistry and solar energy conversion. Mechanistic investigations are very important for better understanding of photobiology and the developments of novel chemical reactions and solar energy conversion.

The cis-trans geometrical isomerization is one of the simplest chemical reactions and has been an active research project for many decades. We have observed extremely intense and sharp $S_n \leftarrow S_1$ absorptions of cis- and trans-stilbene with a picosecond flash technique. The decay of the transient absorption of trans-stilbene is an exponential decay with single component, being same as the fluorescence decay at room temperature. A theoretical calculation indicated that the character of the transition is of a charge transfer within the molecule.

III-A-1   Picosecond flash photolysis of cis- and trans-stilbene. Observation of an intense intra-molecular charge-resonance transition.

Keitaro YOSHIHARA, Akira NAMIKI, Minoru SUMITANI, and Nobuaki NAKASHIMA

The photoisomerization process of stilbene has long attracted much interest, since the molecule has an absorption band in the near UV region and, having only two stable isomers, yields the relatively simple reactions. For this reason we can obtain a detailed information about the mechanism of the isomerization process. Two possible mechanisms of isomerization have been proposed; reaction occurs through the lowest triplet state, T_1 (the triplet mechanism), or through the excited singlet state, S_1 (the singlet mechanism).

In order to clarify the mechanism of the direct photoisomerization, it is necessary to study transient absorptions of the reaction intermediates. In the present work we report the flash photolysis of trans- and cis-stilbene at 77K and at the room temperature. Extremely strong $S_n \leftarrow S_1$ absorptions were found. The band width of the transoid was very sharp and showed a large temperature dependence. A theoretical interpretation for this strong feature of absorption is given by using a simple PPP type calculation, and a localized orbital analysis. An .attempt to observe a twisted singlet state was made.

The excitation source of the photolysis system is the 4th harmonic (266 nm) of a passively mode-locked Nd^{3+}:YAG laser. A single pulse was selected from pulse trains by a Pockels cell and amplified by two stages of amplifiers. The pulse width of the second harmonic (532 nm) was measured with a Hamamatsu streak camera (HTV C979) to be 15 ps. An analysing light is the picosecond continuum light from carbon tetrachloride excited by the residual 1.06 µm light from the original pulse and traversed a variable optical delay relative to the exciting source. The double beam technique was applied by splitting the picosecond continuum into two halves, one being

introduced into the sample and the other being used as a reference beam. Both beams were passed through a spectrograph and detected by an intensified silicon vidicon detector coupled to an optical multichannel analyzer OMA (PAR 1205A). The OMA was used with a two-dimensional mode in order to accepted the sample and reference beam separately. Collected data were transferred to the CPU memory of a mini-computer (NOVA 3) and accumulated in a disk. Data were handled with suitable programs in obtaining the spectrum in the absorbance scale for the present double beam experiment.

The transient absorption spectrum of trans-stilbene in 3-methylpentane at the room temperature is shown in Figure 1(a). The spectrum was taken immediately after the laser pulse had reached its maximum intensity. The absorption at 77K is shown in Figure 1(b). Attempts were made to observe a transient absorption of cis-stilbene both at the room temperature and 77K. We have succeeded in observing it only at 77K, as shown in Figure 1(c). The absorption intensities were estimated by a comparation with the $S_n \leftarrow S_1$ absorption of anthracene, coronene, pyrene, and benzene.

The decay of the transient absorption of trans-stilbene was exponential with a single component (110 ± 10 ps), being same as the fluorescence decay at room temperature, and thus assigned to the $S_n \leftarrow S_1$ absorption. The molar coefficient of the absorption was $\approx 7 \times 10^5 M^{-1}cm^{-1}$ with the full width at half maximum of $1 \times 10^3 cm^{-1}$. The band width had a strong temperature dependence and became only 500 cm^{-1} at 77K. A MO calculation, using a semi-empirical Hamiltonian of PPP-type, was made to analyse the nature of this observed intense absorption, and was found that the character of the transition
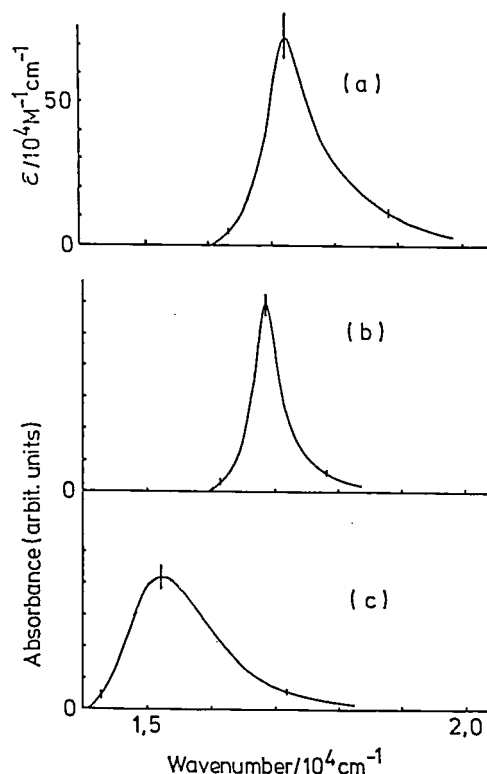

Figure 1. Transient absorption spectra of trans- and cis-stilbene. a) transient absorption of trans-stilbene at 297K and b) at 77K, and c) of cis-stilbene at 77K.

was of the charge-resonance among the ethylenic and the two phenyl moieties in stilbene.

III—B   Electronic Stuctures of Excited states

In order to explain the chemical reactivities of excited states, it is important to know both static and dynamic properties of excited states. Exploration of a hidden state, which is optically forbidden from the ground state, is an interesting subject, since a crossing of these state in the reaction coordinate may play an important role. Benzene is one of the most fundamental molecules in organic photochemistry and not much is known about such electronic excited states. Laser flash photolysis allows us to study one photon absorption from the lowest excited to higher excited states in a very wide wavelength region. The molecular orbital calculations give us an important key to assign the states.

Dynamic behaviour of the excited states of the donor-acceptor systems conjugated by methylene chains gives detailed informations on the electron transfer process. The picosecond fluorescence characteristics of these intramolecular exciplex were studied with special attentions on the rise and decay dynamics of fluorescence of a chromophor and of an exciplex.

Energy transfer processes among monolayer dyes on single crystals were studied with a picosecond laser and a streak camera. Analysis of the decay characteristics was made with Förster-type energy transfer in two dimension. Intersystem crossing which is enhanced by internal heavy atom effect was studied with halogenated naphthalenes. Fluorescence decays were measured with a picosecond laser and the decay channels to the individual triplet spin sublevels were determined.

Fluorescences from Cs_2 give one of the most fundamental knowledges on the potential surfaces of molecules. Various types of molecular and atomic emission was analyzed and a particular attention was paid on the effect of kinetic energy on fluorescence.

III-B-1 Nanosecond Laser Photolysis of Benzene Monomer and Excimer

Nobuaki NAKASHIMA, Minoru SUMITANI, Iwao OHMINE, and Keitaro YOSHIHARA

Photochemical processes of benzene have long been of interest because, upon excitation, the molecule undergoes a variety of chemical reactions which result in various isomers.[1] To understand these processes a detailed knowledge of excited state spectra is required. Several experimental techniques have been applied for the benzene spectra.[2] One photon absorption spectra from the ground state have been measured up to 115 nm in the liquid phase and a rigid matrix and up to 36.5 nm in the gas phase. Assignments of $^1B_{2u}$, $^1B_{1u}$, $^1E_{1u}$, $\sigma^* \leftarrow \sigma$, and Rydberg transitions have been made and these results were shown to be in reasonable agreement with the theoretical predictions.

Recently, the special attention has been paid to the existence of the optically forbidden $^1E_{2g}$ state. Theory predicts that the lowest $^1E_{2g}$ state, which corresponds to the ^1A state in linear polyens, is a covalent state and is located near the optically allowed $^1E_{1u}$ state. Multiphoton techniques and Raman spectroscopy have been employed to identify this state. However, a definite conclusion has not yet been obtained, since these experiments are restricted in the frequency range or indirectly measuring the state. The electron impact experiment were also applied and gave the reasonable assignments for the singlet and triplet states in the low energy region. This technique, however, does not have clear selection rule and shows too many levels in the high energy region.

Another method to search the forbidden state more directly in a wide frequency region is the one photon absorption spectroscopy from the lowest excited singlet or triplet state. Flash photolysis in the microsecond region were carried out for $T_n \leftarrow T_1$ absorptions. The $S_n \leftarrow S_1$ absorptions were also measured by ns laser or pulse radiolysis techniques.[3-6] In these experiments, however, the fourth harmonic (265 nm) of the Nd laser, where benzene has only a very weak absorption $\epsilon \sim 7.5 \, M^{-1}cm^{-1}$, has been applied. Other techniques used are two photon
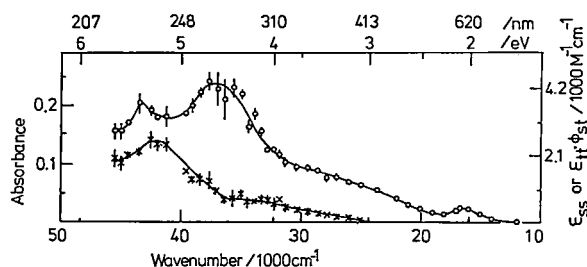

Figure 1. Time-resolved absorption spectra of benzene in cyclohexane (4.6×10^{-3}) vs. monitoring light energy. Upper spectrum (ϕ) taken immediately after excitation, corresponds to $S_n \leftarrow S_1$ transition. Lower spectrum (*) taken 160 ns after excitation, corresponds to $T_n \leftarrow T_1$ transition.
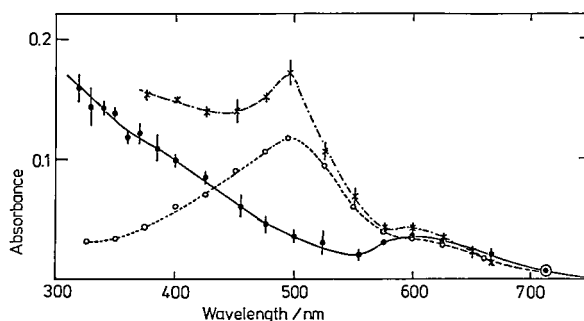

Figure 2. Concentration dependence of transient spectra; (ooo): 4.6×10^{-3} M, expanded that of Figure 1, (***): 1.1×10^{-1} M, (ooo): 3.4×10^{-1} M.

excitation by the second harmonic of a ruby laser at 347.2 nm and pulse radiolysis. A highly concentrated samples ($> 10^{-1}$ M) used in these experiments and thus sometimes the excimer absorption were measured. For example, the transient absorption of benzene 400–575 nm region was assigned to an $S_n \leftarrow S_1$ transition,[3-5] but later it was indicated to be benzene excimer absorption.[6]

In the present work we used a KrF excimer laser for the transient absorption of a dilute benzene soluton, and obtained spectra in a wide frequency region. The $S_n \leftarrow S_1$ and $T_n \leftarrow T_1$ absorption spectra are measured with the time resolved spectroscopy as shown in Figure 1. The transient absorption band at 500 nm, which was observed previously by several workers at high concentration, disappeared completely upon the dilution of the sample as shown in Figure 2. Thus this was assigned to be the excimer band. We made the P-P-P type calculation and assigned the other states as follows; 620 nm ($^1E_{1u}$, f=0.003), $540 \sim 325$ (1^1E_{2g}, f=0.04) and 270 (2^1E_{2g}, f=0.12). The $T_n \leftarrow T_1$ spectrum showed a single peak at 235 nm (f $\sim$ 0.35) and a shoulder around 310 nm (f=0.12).

References

1) D. Bryce-Smith and A. Gilbert, Tetrahedron, 32, 1309 (1976).
2) M. B. Robin, Higher Excited States of Polyatomic Molecules Vol. 1/2 (Academic Press New York 1974/75).
3) R. Bonneau, J. Joussot-Dubien, and R. Bensasson, Chem. Phys. Letters, 3, 353 (1969).
4) R. Cooper and J. K. Thomas J. Chem. Phys. 48, 5097 (1968); J. K. Thomas and I. Mani, J. Chem. Phys., 51, 1834 (1969).
5) J. T. Richards and J. K. Thomas, Chem. Phys. Letters, 5, 527 (1970).
6) R. Benssason, J. T. Richards, and J. K. Thomas, Chem. Phys. Letters, 9, 13 (1971).

III-B-2 Photoinduced Charge Transfer Processes in Intramolecular Heteroexcimer Systems — Time-Resolved Fluorescence Studies

Masahito MIGITA, Tadashi OKADA, Noboru MATAGA, Yoshiteru SAKATA, Soichi MISUMI *(Osaka Univ.)*, Nobuaki NAKASHIMA, and Keitaro YOSHIHARA

We are studying dynamical behavior and electronic structures in the excited state of the intramolecular heteroexcimer systems; (p-N, N-dimethylaniline) - $(CH_2)_n$-(1-pyrenyl) (n=1,2,3, abbreviated as P_n), (p-N, N-dimethylaniline)-$(CH_2)_n$-(9-anthryl) (n=0,1,2, 3, abbreviated as A_n). Fluorescence spectra of these compounds depend upon solvent polarity.[1,2] For example, P_2 and P_3 show the heteroexcimer fluorescence both in nonpolar and polar solvents, but P_1 shows the heteroexcimer fluorescence only in polar solvents. Thus, the heteroexcimer state seems to be stabilized considerably by the interaction with the surrounding polar solvent molecules in addition to the coulomb interaction between A^- and D^+ in the charge transfer state. Furthermore, we found that the formation of charge transfer state of P_3 in polar solvents is much faster compared with the case of nonpolar solvents.[3] This result suggests that orientational fluctuations of surrounding polar solvent molecules and an initial small approach of the donor and acceptor may induce the charge transfer in polar solvents.

In order to elucidate the details of these elementary processes of intramolecular heteroexcimer formation, the fluorescence rise and decay curves in polar and nonpolar solvents were measured in the picosecond time scale. The sample solution was excited by the third harmonic of psec pulse from a mode-locked Nd^{3+}:YAG laser and the fluorescence was detected by a Hamamatsu C-979 streak camera. The observed rise times of heteroexcimer fluorescence (τ_r) and decay times of locally excited state of pyrene or anthracene moieties (τ_d) are indicated in Table 1.

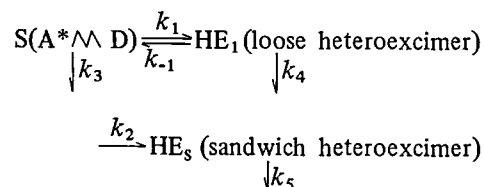The charge transfer process depends upon the number of methylene groups. It becomes slower with increase of methylene groups. The results can be well understood on the basis of the stabilization of the heteroexcimer state due to the solvation and the internal rotations around single bonds. The extent of such conformation change becomes smaller with an increase of solvent polarity.

From the studies of the transient absorption spectra of P_3 in polar solvents, the following reaction mechanism involving loose and sandwich heteroexcimers has been derived.[4]

$$S(A^* \wedge\wedge D) \underset{k_{-1}}{\overset{k_1}{\rightleftharpoons}} HE_l \text{ (loose heteroexcimer)}$$

with k_3, k_4 deactivation paths, and

$$\xrightarrow{k_2} HE_s \text{ (sandwich heteroexcimer)}$$

with k_5.

k_3, k_4 and k_5 are deactivation processes of each species. Time dependence of each species may be written as,

$$[S] = C_1 \exp(-\lambda_1 t) + (C_0 - C_1) \exp(-\lambda_2 t)$$

$$[HE_l] = C_2 [\exp(-\lambda_1 t) - \exp(-\lambda_2 t)]$$

$$[HE_s] = C_3 [(\lambda_1 - k_5) \exp(-\lambda_2 t) - (\lambda_2 - k_5) \exp(-\lambda_1 t) + (\lambda_2 - \lambda_1) \exp(-k_5 t)]$$

In view of the result, we have made a closer examination of fluorescence rise and decay curves of P_3 in 2-propanol at several different wavelengths. We have observed a double exponential decay when measured at a shorter wavelength region and a fluorescence rise and decay curve when measured at a longer wavelength region of heteroexcimer band. The time constants λ_1^{-1} and λ_2^{-1} were obtained to be 1.1 nsec and 350 psec, respectively. These λ values are in a satisfactory agreement with the values obtained by the analysis of the transient absorption measurements. Thus, it is confirmed also by means of time-resolved fluorescence measurements that in the case of P_3 in polar solvents a charge transfer state with loose structure is formed at first and more stable heteroexcimer state is formed from it.

References

1) T. Okada, T. Fujita, M. Kubota, S. Masaki R. Ide, Y. Sakata, and S. Misumi, Chem. Phys. Lett. **14**, 563 (1972); R. Ide, Y. Sakata, S. Misumi, T. Okada, and N. Mataga, J. C. S. Chem. Commun. 1009 (1972).
2) S. Masaki, T. Okada, N. Mataga Y. Sakata, and S. Misumi Bull. Chem. Soc. Jpn. **49**, 1277 (1976).
3) T. Okada, T. Saito, N. Mataga, Y. Sakata, and S. Misumi Bull. Chem. Soc. Jpn., **50**, 331 (1977).
4) T. Okada, M. Migita, N. Mataga, Y. Sakata, and S. Misumi, to be published.

Table I. The fluorescence decay time of locally excited state (τ_d) and the rise time of heteroexcimer fluorescence (τ_r) in hexane and 2-propanol

	Solvent	τ_d	τ_r
A_1	2-propanol	40 ± 9 psec	54 ± 9 psec
A_2	2-propanol	98 ± 5 psec	93 ± 23 psec
A_3	2-propanol	206 ± 27 psec	140 ± 31 psec
P_1	2-propanol	62 ± 6 psec	93 ± 21 psec
P_2	2-propanol	170 ± 31 psec	192 ± 39 psec
P_3	2-propanol	883 ± 183 psec	*ca.* 500 psec*
A_3	hexane	2.3 ± 0.1 nsec	2.6 ±0.4 nsec
P_3	hexane	4.6 ± 1.0 nsec	3.9 ± nsec

* see text

III-B-3 Fluorescence Dynamics of Monolayer Rhodamine B on Organic Single Crystals

Nobuaki NAKASHIMA, Keitaro YOSHIHARA, and Frank WILLIG *(Fritz-Haber Inst.)*

Fluorescence lifetimes of monolayer rhodamine B (surface coverage: ca. 0.4) on various organic single crystals were measured for the first time. It was found that they became much shorter (ca. 30 ~ 100 ps) than the lifetime in a dilute solution (1.5 ns). The shortening of the lifetime on an anthracene single crystal could be regarded as an electron-transfer quenching from anthracene to excited rhodamine B. However, such a process hardly occurs in case of phenanthrene, naphthalene, and other organic polymers since it requires more thermal energy. In the present work, it was pointed out that for the latter cases the fluorescences were quenched by energy transfer from the rhodamine B monomer to the dimer.

A new decay equation was derived in order to explain a nonexponential decay. When excited molecules on a surface were quenched by the Föster-type dipole-dipole interaction, the fluorescence decay is given as,

$$P(t) = \exp\left\{-\frac{1}{\tau_0} t - c(t/\tau_0)^{1/3}\right\}, \qquad (1)$$

where τ_0 is the lifetime of an excited molecule and c is $\Gamma(2/3)nR_0^2$. R_0 is a critical distance of energy transfer and n is the number of quencher molecules/cm^2. The orientational factor in R_0 is 0.88 and 0.84 depending on parallel and random orientation of dyes on the two-dimensional arrangement, respectively. It should be noted that the power of the second term in the exponential function in eq. 1 is 1/3 on surface and is different from 1/2 in solution. It is difficult to observe the absorption spectrum of dimer at the surface coverage of 0.4. However, the dimer absorption is clearly seen at higher concentrations. We assume the quenching site of fluorescence is at a dimer. In solution dimer is known to be non-fluorescent. If a monomer which contacts with adjacent monomer is a quencher site, the observed decays can be roughly explained by eq. 1. An apparent decay time at the surface coverage of 0.4 was observed to be about 100 ps. This decay can be reproduced with eq. 1 using critical distance of 47 Å.

In order to support the above quenching mechanism on a surface, the energy transfer in aqueous solution, in which monomer and dimer are in equilibrium, was examined. Figure 1 shows the results for various concentrations of dyes. Fluorescence decay curves were well approximated by the decay function of the Förster energy transfer. From the fitting curves critical distances were obtained as follows; $R_0 = 76$ Å at 2×10^{-3}M, $R_0 = 59$ Å at 10^{-2}M, $R_0 = 56$ Å at 2×10^{-2}M.

The calculated critical distance from the monomer to the dimer is 43 Å and between monomers 45 Å. Therefore the observed concentration dependence
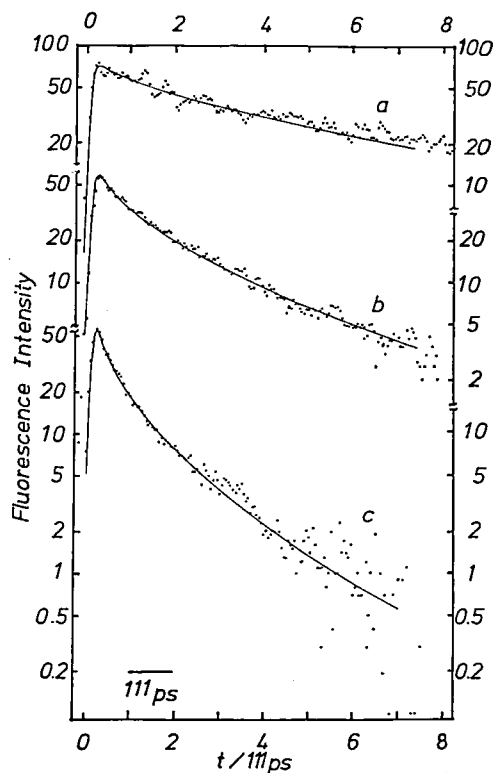

Figure 1. Observed (dots) and fitting decay curves (solid lines) by the Förster energy transfer including finite exciting pulse width of ca. 15 ps.
a; 2×10^{-3}M^{-1}, $R_0 = 59$ Å   b; 10^{-2}M^{-1}, $R_0 = 59$ Å
c; 2×10^{-2}M^{-1}, $R_0 = 56$ Å
for fitting the Förster decay function.

was explained by a contribution of energy transfer between monomers. The transient diffusion effect may aslo contribute to the larger value. One can expect that the equilibrium between monomer and dimer ($K = 1.5 \times 10^3$M^{-1}) shifts to the dimer side at higher concentrations and that an R_0 determined experimentally approches to the calculated monomer-dimer distance, 43 Å. Consequently, R_0 in water and on surface are in fairly good agreement.

The quenching mechanism by a contact dimer on the surface can explain the short lifetimes as well as a decrease of photocurrent upon increasing dye concentration on anthracene. A detailed analysis of observed decay with eq. 1 is in progress.

III-B-4 Internal heavy atom effect on the triplet spin sublevels of the lowest triplet state of naphthalene. II. Intersystem crossing processes from the singlet excited state to the individual spin sublevels of the lowest triplet state.

Hiroyuki SAIGUSA, Tohru AZUMI *(Tohoku Univ.)*, Minoru SUMITANI, and Keitaro YOSHIHARA *(IMS)*

Table I. The rate constants of the intersystem crossing from the singlet excited state to the individual triplet sublevels.

	k_F/s^{-1}	k_x^{isc}/s^{-1}	k_y^{isc}/s^{-1}	k_z^{isc}/s^{-1}
naphthalene [a]	1.0×10^7	5.1×10^6	2.0×10^6	8.6×10^5
FN	3.1×10^7	1.0×10^7	1.4×10^7	1.2×10^6
CℓN	5.9×10^8	2.1×10^8	3.7×10^8	6.7×10^6
BrN	1.5×10^{10}	6.8×10^9	7.8×10^9	9.8×10^7

a For naphthalene, the ratio of the ISC is taken from: M. A. El-Sayed, W. R. Moomaw, and J. B. Chodak, Chem. Phys. Lett., **20**, 11 (1973).

Despite of rather extensive studies on the heavy atom effect, those concerned with the ISC from the singlet excited state to the triplet state are only scarce. This is probably due to the difficulties associated with the measurements of the ISC rates, being of the order of picosecond in the heavy atom substituted compounds. Recent progress in the picosecond spectroscopy enables us to attempt this important subject.

In this study, we have evaluated the rates of ISC to individual sublevels from (i) fluorescence lifetimes (ii) fluorescence quantum yields, and (iii) spin sublevel properties obtained by the zero field ODMR experiments. As far as we are aware of, this is the first study which reports the rate constants of ISC to individual sublevels.

The molecules we have studied are a series of halonaphthalenes: 1-fluoronaphthalene (FN), 1-chloronaphthalene (ClN), and 1-bromonaphthalene (BrN). The fluorescence lifetimes were measured for ethanol solutions ($\sim10^{-4}$M) at the room temperature. The excitation source was the fourth harmonic (266 nm) of a passively mode-locked YAG laser. The pulse width of the second harmonic (532 nm) was 15 ps. The decays of the fluorescence of ClN and BrN were measured with a Hamamatsu TV streak camera. Distortions of the camera and streak speed were fully corrected. The decay of the fluorescence of FN was, on the other hand, measured with a photodiode. The fluorescence quantum yields were measured with reference to 1N H_2SO_4 solution of quinine sulfate ($\sim10^{-5}$M) .

Efforts to obtain the data for iodonaphthalene were unsuccessful because, first of all, the fluorescence decay time was shorter than the pulse width of the exciting light, and further, one of the MIDP signals was unobserved.

The observed fluorescence decay rate constants k_F are tabulated in Table I. These data, in combination with the quantum yield data, enable us to obtain the absolute values of the rate constants of ISC. In this calculation, we have assumed that the internal conversion process is negligible. (This assumption was found justified even for naphthalene and hence is regarded much more so in the halonaphthalenes.) We next assume that the ratios of the rate constants of ISC to individual sublevels observed at 1.4 K in tetramethylbenzene host are invariant at room temperature in ethanol solvent. Then, the

absolute values of the rate constants of ISC to the individual sublevels k_i^{isc} are obtained. The results are shown in Table I. If the temperature and solvent effects on k_i^{isc} are so large that their ratios k_i^{isc}/k_j^{isc} (i, j = x, y, z) are also dependent largely on temperature and solvent, the results should be modified. We believe, however, that the effect to the ratios is not so large and the results shown in Table I are qualitatively correct.

As is seen in Table I, the heavy atom enhancement of the ISC rate is observed for all the three sublevels. It is, however, noted that the enhancement is significant only in k_x^{isc} and k_y^{isc}. The enhancement in k_z^{isc} is not negligible but is only small.

The heavy atom enhancement is most significant for the rates to the in-plane sublevels and is less significant for the rate to the out-of plane sublevel. The experimental results are interpreted satisfactorily within the framework of current theories of radiationless transitions

III-B-5 Laser induced fluorescence, energy transfer, and dissociation of Cs₂

Hajime KATO *(Kobe Univ)* and Keitaro YOSHIHARA

Laser induced fluorescences of Cs_2 excited by the Ar^+ laser lines have been studied. A spectrum of the over-all fluorescence excited by the 4765 Å (20981.0 cm^{-1}) laser line is shown in Figure 1. Series of lines with vibrational progression were observed from about 21500 to 19100 cm^{-1}. The emission intensity drops to low intensity in the lower energy region than 19100 cm^{-1}. The spectrum gradually becomes diffuse and quasicontinuous, and the intensity decreases as it extends to about 18000 cm^{-1}. Again from about 17800 cm^{-1} the diffuse bands appear. The intensity increases toward low frequency and fluctuates. The fluctuation interval and the band width also increase. The most intense and broad band has a maximum of intensity at 16400 cm^{-1} and the band disappears completely at about 16200 cm^{-1}. This most intense band has a structure of fluctuation, which consists of several peaks at regular intervals of
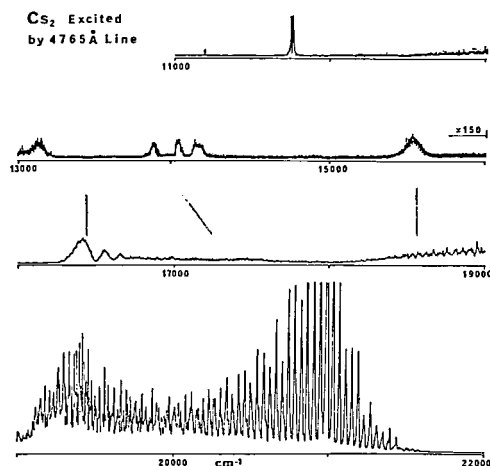
Figure 1. Fluorescence spectrum of Cs_2 excited by the 4765 Å Ar^+ laser line with out-put power 200 mW. The vapor pressure of Cs_2 and Cs were 1.8×10^{-4} and 1.1×10^{-1} torr respectively, and the cell temperature was 500 K. A spectral slitwidth was 5 cm^{-1}.
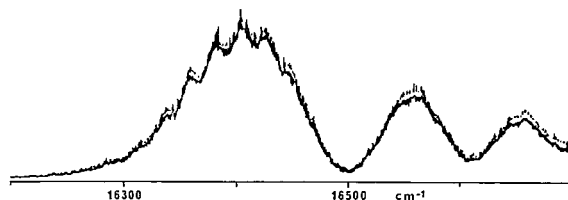

Figure 2. The diffuse fluctuation bands of Cs_2 excited by the 4765 Å line. The conditions for the measurement were the same as those shown in Figure 1.

25 cm^{-1} (See Figure 2). When the laser line of excitation was changed, neither the position of maximum intensity nor the pattern of bands showed any significant change.

Atomic fluorescences of Cs at 11732 cm^{-1} (6p $^2P_{3/2} \to$ 6s $^2S_{1/2}$) and 11178 cm^{-1} (6p $^2P_{1/2} \to$ 6s $^2S_{1/2}$) were observed. The spectrum of the lines shown in Figure 2 is self-reversed, which confirms that the lines are really those of an atom.

A series of lines with vibrational progression and the successive diffuse bands in the region down to 16200 cm^{-1} were found to be polarized and identified as the resonance fluorescence. The diffuse fluctuation band with a maximum of intensity at 16400 cm^{-1} consists of several bands at regular interval and is independent on the line of excitation. By applying the theory on the role of kinetic energy in the Franck-Condon principle proposed by Mulliken, the band was identified as a transition from the internuclear distance of maximum kinetic energy in the vibrational level of the excited state $E^1\pi_u$. All the other fluorescence bands of low frequency were observed to be depolarized completely, and the intensities increased when a foreign gas was added. These bands were identified as the fluorescence from the states which were populated by collision-induced transitions from the E state. Atomic fluorescence $6p^2P_{3/2} \to 6s^2S_{1/2}$ is interpreted as the production of the excited atom Cs $6p^2P_{3/2}$ by predissociation of Cs_2 E $^1\pi_u$ through interaction with, most probably, Cs_2 B $^1\pi_u$.

III—C   Studies on Transient Phenomena in Biology

Studies of fluorescence in biopolymers give important informations on their dynamic behaviour as well as their higher order structures. Fluorescence dynamics is related to the energy transfer, electron transfer, and hydrogen bonding between the fluorescent chromophore and residues. Their distance, mutual orientation, and flexibility are important factors which influence the fluorescence lifetimes, quantum yields, and the polarization.

Investigations of fluorescence dynamics of coenzyme were performed with a picosecond laser. It has been found that the fluorescence is quenched dynamically in the dimer as well as in the monomer. The picosecond fluorescence dynamics were studied for photosynthetic pigments. Fluorescence decays and the transient of a spinach chloroplast with a concentrated reaction center and chlorophyll a were measured.

III-C-1   Picosecond Fluorescence Lifetime of Coenzyme of D-amino Acid Oxidase

Nobuaki NAKASHIMA, Keitaro YOSHIHARA, Fumio TANAKA (Mie Nursing College) and Kunio YAGI (Nagoya Univ.)

The fluorescence lifetime of the coenzyme, FAD, of D-amino acid oxidase [D-amino acid: O_2 oxidoreductase (deaminating), EC 1.4.3.3.] was measured with a picosecond technique at various concentrations of the enzyme. The enzyme was excited by the 3rd harmonic (355 nm) of a mode-locked Nd:YAG laser. The fluorescence decays were measured with a Hamamatsu TV streak camera (HTV C979). Previously we obtained evidence for the difference in the lifetime between the monomer and the dimer. In this work, fluorescence lifetimes were measured in wide range concentrations and analysed in more detail.

In Figure 1, fluorescence decay curves of FAD in the enzyme at two extreme concentrations in our measurements. At both concentrations of the enzyme, the fluorescence decay curves were non-
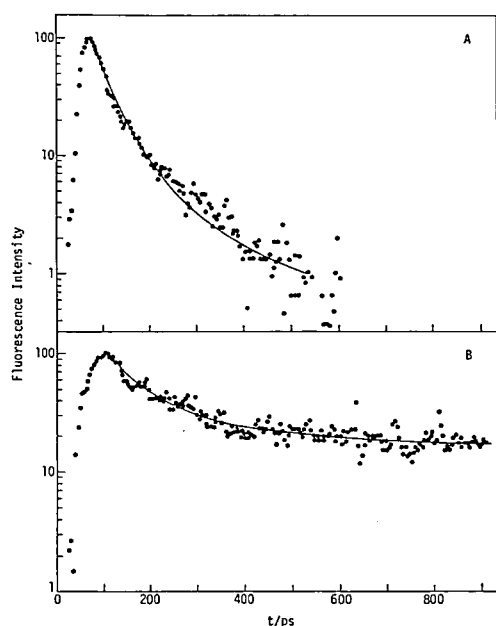
Figure 1. Fluorescence decay curves of FAD in D-amino acid oxidase. The enzyme concentration was 1×10^{-4}M in Figure 1(A) and 1×10^{-6}M in Figure 1(B). Solid curves indicate decay functions obtained by fitting them with three exponential terms. The parameters obtained are listed in Table I.

Table I. Decay parameters

	Dimer	Monomer	Free flavin adenine dinucleotide
Lifetime (ps)	τ_2	τ_1	τ_3
	40 ± 10	130 ± 20	2300 ± 700
Fractions	a_2	a_1	a_3
1×10^{-6}M	0.24	0.52	0.24
1×10^{-4}M	0.90	0.09	0.01

exponential.

In our previous work it was demonstrated that D-amino acid oxidase possesses three fluorescent species, FAD combined with a dimeric form of the protein, FAD combined with the monomeric form of the protein, and free FAD dissociated from the enzyme[1]. From these results, it is reasonably accepted that the fluorescence decay curves fit a function with three exponential components.

When the enzyme concentration was varied, the respective values at intermediate concentrations did not change appreciably within experimental uncertainty, whereas the component fraction did change remarkably. Average lifetimes from analysis at various concentrations and fractional component are shown in Table I.

The relative quantum yield of fluorescence of flavin adenine dinucleotide combined with protein moiety was evaluated at both concentrations from the dynamic studies (r_t) and from the measurements under steady state excitation (r_s) as shown in Table I. At the concentration of 1×10^{-6}M, where the fluorescent species is mostly the monomer of the holoenzyme, r_t was $0.25 \sim 0.28$. r_t was 0.11 at 1×10^{-4}M where the dimer is the dominant species. r_s was 0.27 at 1×10^{-6}M and 0.08 at 1×10^{-4}M. At the lower concentration r_t is in good agreement with r_s, while r_t is larger than r_s at the higher concentration. These results suggest that the fluorescence of flavin adenine dinucleotide in the monomer and dimer is mostly quenched by a dynamic process. These facts indicate that the local structure around FAD may be flexible.

The dynamic quenching processes both in the monomer and dimer show that FAD has an extended

form in the enzyme. In any case, rate constants of intermolecular interaction between the excited flavin and amino acid residue(s) in the protein moiety are different in the monomer and dimer. The difference indicates that the micro-environment of falvin adenine dinucleotide in the monomer is different from that in the dimer, and should be correlated with difference in property between the monomer and the dimer of D-amino acid exidase.

References

1) F. Tanaka and K. Yagi, Biochemistry 18, 1531 (1979)

III-C-2 Transient Behaviour of the P700 enriched Particles

Akira NAMIKI, Nobuaki NAKASHIMA, Keitaro YOSHIHARA, and Isamu IKEGAMI (Teikyo Univ.)

Using the highly enriched P700 particles, kinetics of the energy transfer in the antenna chlorophylls and the reaction center were studied with the method of the absorption and fluorescence spectroscopies in the picosecond time scale. It was found that the time profile after the laser excitation for the recovery of the ground state depletion and the excited state populations were composed from a fast (25 ps) and a slow (1.0 ns) components as shown in Figure 1. The slow component could be ascribed to the behaviour of the distant chlorophylls (chl-a-672) while the fast component was concerned to the nearest neighbour chlorophylls (chl-a-685) to the reaction center The variation in the yields of the fast components was recognized for the change of the redox state of the reaction centers. For the active reaction centers (reduced form), the efficient energy transfer from the chl a-685 to P700 occurs with a speed of about 25 ps.
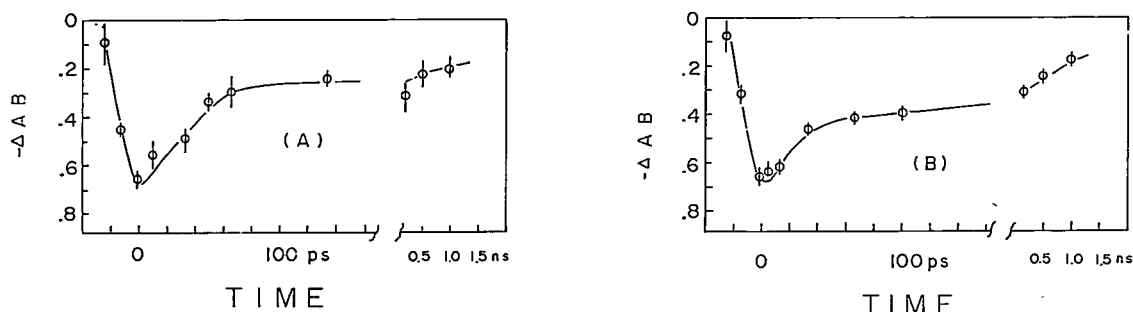
Figure 1. Plots of the recovery of the ground state depletions monitered at the peak of the chlorophyll absorption band. Each point was obtained by averaging the 2 or 3 data. (A): $P700.Z$, (B): $P700^+.Z$.

III—D Photoelectrochemical Energy Conversion

Photoelectrochemical cell is one of the devices for converting solar radiation directly into electrical and chemical energy. It is important to elucidate the processes of the energy conversion at semiconductor/electrolyte interface, not only from the view point of the application but from the pure scientific point of view.

III-D-1 Dynamical Behaviour of the Photo-current at MoSe₂ and TiO₂ Photoelectrodes Studied by a Pulsed Laser

Tomoji KAWAI and Tadayoshi SAKATA

[*Surface Sci.* 81 L640 (1979)]

[*Chem. Phys. Letters*, in Press]

Photoelectrode processes which play an important role in solar energy conversion at solid-liquid junctions are essentially dynamic ones. They include light absorption, relaxation, charge separation, recombination and electron transfer at the electrode surface. (see Figure 1) One attractive method to study these primary processes separately would be a

pulse technique which allows to obtain directly a time resolved spectra of photocurrent responses after pulsed illumination. We have come to the conclusion that the detection of fast time resolve photocurrent signals should be possible provided adequate photochemical systems are chosen. We have selected and TiO_2 layered n-type $MoSe_2$ photoelectrodes. These systems have been shown to provide a stable and efficient photoanode for solar energy conversion.

(a) $MoSe_2$ electrode

A time resolved transient photocurrent observed in the nanosecond region when illuminating on $MoSe_2$-I^- semiconductor-liquid junction with a pulsed laser, consists of the first rapid one which follows the incident light pulse and of a second one with a

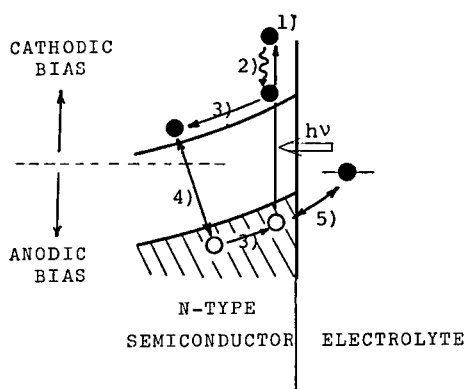Figure 1. Schematic diagram of photoelectrode processes at a n-type semiconductor: (1) light absorption, (2) relaxation, (3) charge separation, (4) recombination, (5) charge transfer reaction.
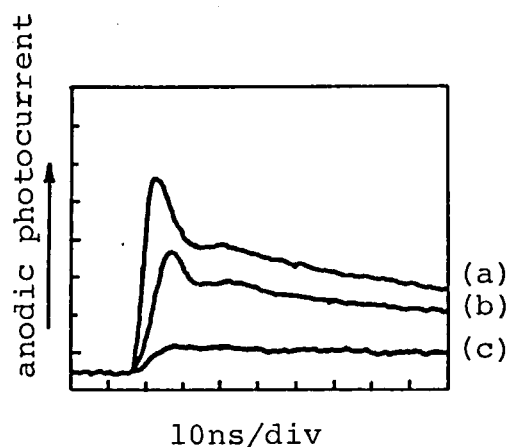

Figure 2. Time resolved curves of photocurrents obtained by the pulsed laser illumination of the $MoSe_2$-I^- system (1N KI). (a) no bias, without filter, (b) with filter of O.D.= 1.2, (c) with filter of O.D.=2.2.

slower decay (Figure 2). From the dependence of the photocurrent on light intensity, bias voltage and the effective concentration of the electrolyte, the observed two components in the spectrum were explained to originate from charge carrier generation in the solid and electron transfer acroses the electrode interface respectively. Since these processes could be detected independently, we will now be able to discuss which step is the rate determining and which process should be improved on each sample for the increase of the quantum efficiency of the solar energy conversion.

(b) TiO₂ electrode

Since the TiO_2 electrode is able to oxidize water, the observed photocurrent should be related with the O_2 evolution. Dynamical features of the photocurrent were found to depend greatly on the pH of aq. electrolyte solution. Figure 3 shows the time dependence of the photocurrent without bias voltage. In the basic solution the anodic photocurrent rises quite rapidiy with the maximum at 20 ns after a light pulse. On the other hand, in the acidic solution, a very fast cathodic current, being followed by a slow anodic one after about 10 ns, was observed. This remarkable difference is considered to come from the difference of the reaction: In the basic solution, oxygen is produced from oxidation of OH⁻, while in the acidic solution it is produced from the oxidation of H_2O molecule. The photocurrent depended greatly on the bias voltage in the acidic solution. When a cathodic bias (-1.5V) was applied, the fast cathodic current was increased. Under anodic bias (+1.5V), the cathodic one disappeared and the anodic one was enhanced. These transient behaviours were also changed by adding various redox reagents to the electrolyte solution, such as hydroquinoe and ascorbic acid.
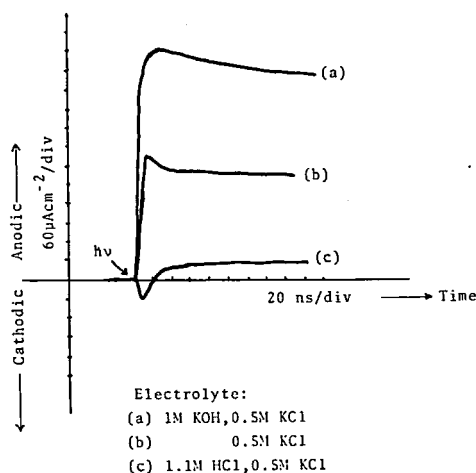
III-D-2 Photoinduced Layer Phenomenon Affecting Solar Energy Conversion—MoSe₂-I⁻ System—

H. TRIBUTSCH, T. KAWAI and T. SAKATA
[Electro. Chimica Acta, in Press]

Layered n-type $MoSe_2$ electrode in contact with an electrolyte containing KI solution has been shown to provide a stable and efficient photoanode for solar energy conversion. Without application of an external voltage, the energy conversion efficiency for red and near infrared light has been determined to be 8%, which correspond to a quantum efficiency for the photoinduced oxidation of I⁻ of 38%. The latter increases when an anodic potential is applied and, depending on the quality of crystals, reaches up to 70%.

We have tried to elucidate the reasons why this system shows an excellent performance, by using techniques of absorption spectroscopy, pulsed laser induced transient photocurrent and the analysis of photovoltage. The following results were obtained: When iodine is photooxidized at a n-type $MoSe_2$ electrode at a high rate, a dim film is observed to spread over the metalic bright electrode and the reflected light intensity drops by 70 to 80 percent throughout the visible and near infrared spectral region. The phenomenon can-in a reversible way-be controled by small potential variations (0 to + 0.5V vs SCE) and beyond +1.0V produces electrochemical oscillations, which are paralleled by an additional reflection change which can be seen to propagate across the electrode surface. Evidence is given that the spreading of the dim film is actually a phase transition from dispersed to crystalline iodine with an asymmetrical size distribution within the I⁻ depleted diffusion layer (Figure 1). The resulting gradient of the refraction index works like an anti-reflecting coating.

The time resolved transient photocurrent for MoSe₂-I⁻ photoelectrochemical cell was observed in

Figure 3. Time resolved photocurrents of TiO_2 in the solution of (a) 1M KOH, (b) 0.5M KCl, (c) 1.1M HCl.
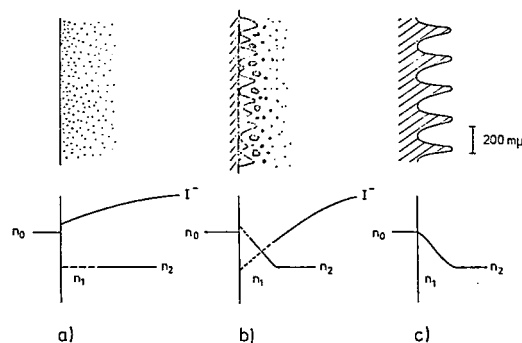

Figure 1. Model for optical situation at an electrode surface during the oxidation of iodine:
a) formation of dispersed iodine (below film formation potentials);
b) formation of an asymmetrically shaped iodine layer;
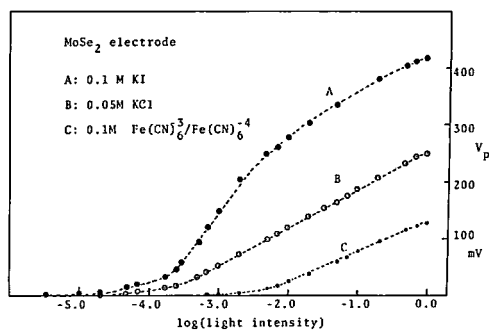c) reflection decreasing surface structure of a night moth cornea.

Figure 2. Dependence of photovoltage on light intensity in various kind of solution. I⁻ solution exhibited excelent performance for MoSe₂ photoelectrode.

a nanosecond region by using a pulsed laser. (see III-D-1)

A phenomenological theory of the photovoltage at a $MoSe_2$-I⁻, Fe^{2+} and Br⁻ is also proposed. This theory was found to explain well the dependence of the photovoltage on the light intensity. The validity of the theory was proved experimentally. The slope of the curve of the photovoltage plotted against the logarithmic light intensity was found to be inversely proportional to the sum of the transfer coefficient and the corresponding coefficient of the photocurrent, which can explain the dependence of the slope on the kind of electrode and redox system. (Figure 2) The high performance of the photosystem of $MoSe_2$-I⁻ was found to originate from the fact that the ratio of the photocurrent against the dark current was extremely large compared with that of the other system.

III-D-3 On the Mechanism of Photocatalytic Decomposition of Water on Semiconductor Electrodes— O_2 Evolution —

Tadayoshi SAKATA and Tomoji KAWAI

[*Berichte Bunsenges, Phys. Chem.* 83 486 (1979)]

The photoelectrocatalytic decomposition of water was discovered by Fujishima and Honda.[1] They succeeded in O_2 evolution from water by using TiO_2 as a photoanode. Independently of their discovery, Krasnovskii and Brin reported the O_2 evolution from a suspension of semiconductors such as WO_3, TiO_2 and ZnO in water.[2] Since the decomposition of water is considered to be a good way to produce hydrogen, an extremely important fuel, from an abundant raw material (water), the above discoveries are quite meaningful although the systems at present are inefficient, being far from practical use.

Since their discoveries, much work has been done on the photoelectrolysis of water and several semiconductors such as SnO_2, $SrTiO_3$, $KTaO_3$, WO_3 and Fe_2O_3 have been found to be stable photoanodes

for the O_2 evolution. However the mechanism of O_2 evolution on semiconductor surfaces is still not well understood. In many papers it is discussed on the basis of the redox potentials of water. Since a redox potential is defined for an oxidation-reduction system in the thermal equilibrium, it is not appropriate to discuss the charge transfer (CT) reaction in terms of the redox potential at the interface because it is essentially a vertical transition.

The reaction rate of electron transfer is expressed as,

$$k = \int \nu(E) \, W_{acc}(E) \, W_{don}(E) \, dE \qquad (1)$$

Here $\nu(E)$ is the electron exchange term, $W_{acc}(E)$ the state density of acceptors (holes) and $W_{don}(E)$ the state density of donors (electrons). In the present case, $W_{don}(E)$ is the distribution function of electron energy of the reactive species such as OH⁻, H_2O and ·OH.

Since the position of valence band has been determined for the various semiconductors by the electrochemical method, $W_{acc}(E)$'s are known. For $W_{don}(E)$'s of OH⁻, H_2O and ·OH, we estimate them under a simple approximation, since any experimental data are not available.

Estimation of electron energy in the highest occupied orbital of molecule M in water. For the following electron transfer reaction,

$$M \xrightarrow{\text{vertical transition}} M^+ + e_{vac} \qquad (2)$$
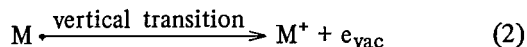
the vertical ionization energy in water, W^v, is expressed approximately by

$$W^v = IP^{gas}(M) - P^{elect}(M^+) + P^{st}(M) \qquad (3)$$

Here $IP^{gas}(M)$ is the vertical ionization potential of M in gas phase, $P^{elect}(M^+)$ is the electronic polarization energy of M^+ in water and $P^{st}(M)$ is the static polarization energy of M in water. For the evaluation of the electronic polarization, we used the Born's equation, that is $P(M^+) = Q^2/2r(1-1/n^2)$. Here Q is the charge of M^+ and r is the radius of the ion M^+. The value of W^v corresponds to the energy value where the distribution of $W_{don}(E)$ has the maximum value. In this way, the vertical ionization energy and the distribution function $W_{don}(E)$ were estimated for the reactive species OH⁻, H_2O and ·OH.

The result is shown in Figure 1. In the same figure energy levels of conduction band and valence band at the semiconductor electrolyte interface at pH 13 are shown on the left hand for various kind of semiconductors which are known as stable photoanodes for O_2 evolution.

A Probable Reaction Path for O_2 Evolution. From the above energetical consideration the following conclusions are obtained.

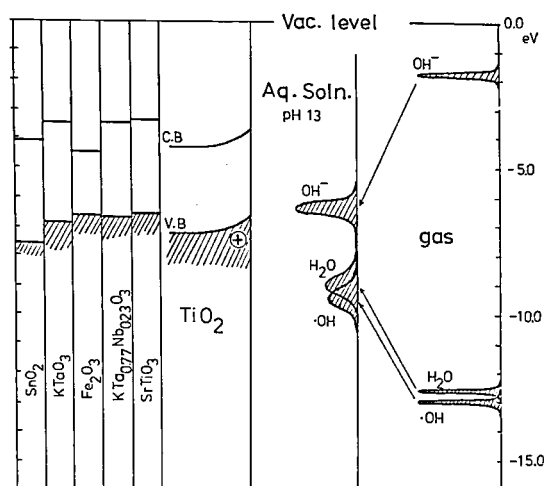1) The highest occupied levels of OH⁻, ·OH, and H_2O are located lower than the redox potential of O_2/OH⁻.

Figure 1. Evaluated distribution functions of electron energy in the basic aqueous solution (pH 13) and in the gas phase for reactive species, OH^-, H_2O, and $\cdot OH$ (right hand), and the band edges of various semiconductors at the interface to electrolyte solution (pH 13).

2) Among them the distribution function of OH^- is the highest and has the largest overlap with the top of valence band of the semiconductors which work as stable photoanodes for O_2 evolution as seen in Figure 1. Therefore the oxidation of OH^- would be the first step in the basic aq. solution. On the other hand, oxidation of H_2O molecule becomes possible in the acidic solution since the energy levels of the oxide semiconductors at the surface shift lower (-0.06 eV/pH) due to the acid-base equilibrium of the surface OH group. Therefore, $\cdot OH$ can be formed at the semiconductor surface both from oxidation of H_2O in the acidic aq. solution and from oxidation of OH^- in the basic aq. solution. As the second step, the oxidation of $\cdot OH$ may look like one of the possible reactions. However it seems difficult because the highest occupied level of $\cdot OH$ is located deeply as seen in Figure 1.

The path through the recombination of $\cdot OH$ is more probable because of the following reasons.
1) The formation of hydrogen peroxide is observed near the photoanode. It was made sure by iodine starch reaction. Wrighton et. al. already reported the formation of H_2O_2.
2) TiO_2 and $SrTiO_3$ are the good catalysts for the decomposition of H_2O_2. This fact was demonstrated by the vigorous evolution of O_2 from the surfaces of TiO_2 and $SrTiO_3$ when they are immersed in the solution of H_2O_2 (several %). Therefore semiconductors such as TiO_2 and $SrTiO_3$ act as good catalysts for the following reaction.

$$2H_2O_2 \xrightarrow{\text{TiO}_2, \text{ SrTiO}_3} O_2 + 2H_2O \qquad (4)$$
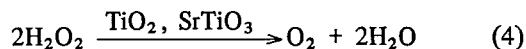
Furthermore this O_2 evolution from H_2O_2 was found to be accelerated 10 - 30 times when the catalysts were illuminated with 500 W Xenon lamp.
These results suggest that the formation of H_2O_2 and its catalytic decomposition on semiconductor surface
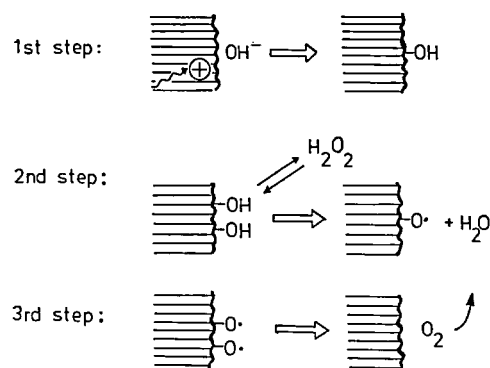

Figure 2. One of the most probable paths for O_2 evolution in basic aqueous solution.

are important paths.

By summarizing the above results, the most probable reaction path for O_2 evolut on on the oxide semiconductors is shown schematically in Figure 2.

References

1) A. Fujishima, K. Honda, Nature, 238, 37 (1972); Bull. Chem. Soc., 44, 1148 (1971).
2) A. A. Krasnovski, G. P. Brin, Dok. Akad. Nauk SSSR, 147, 656 (1962); 168, 1100 (1966).

III-D-4 Flourescence Quenching via Charge Injection at the Interface Between Tetra - phenylporphine and SnO_2

Katsumi TANIMURA, Tomoji KAWAI, and Tadayoshi SAKATA

Because of the enhanced reactivity, an organic dye absorbed on the solid surface has been one of the most attractive subjects in the current field of solar energy conversion. In order to clarify the primary process of the photosensitization, or the charge injection from excited molecules into the conduction band of solids, we have studied here photochemical behaviour of the porphyrin adsorbed on semiconducting SnO_2 surface.

Tetraphenylporphine (H_2TPP) was adsorbed on SnO_2 surface in vacuo ($\sim 1 \times 10^{-7}$ Torr) with a controlled deposition rate of 0.5 Å/s. The thickness of the film prepared was monitored and determined by a Sloan thickness meter (DTM200). The single-photon counting system (ORTEC SP-3X) was used for the measurements of emission and excitation spectra and of the decay curve of luminescence from the adsorbed molecules.

Optical absorption for the molecules adsorbed on SnO_2 with a coverage of 0.2 − 0.6 ($\sim 10^{13}/cm^2$) could not be detected by means of a commerical spectrophotometer. In order to know transition energies from ground to excited states in adsorbed molecules, we measured the excitation spectrum of fluorescence, which corresponds essentially to the absorption
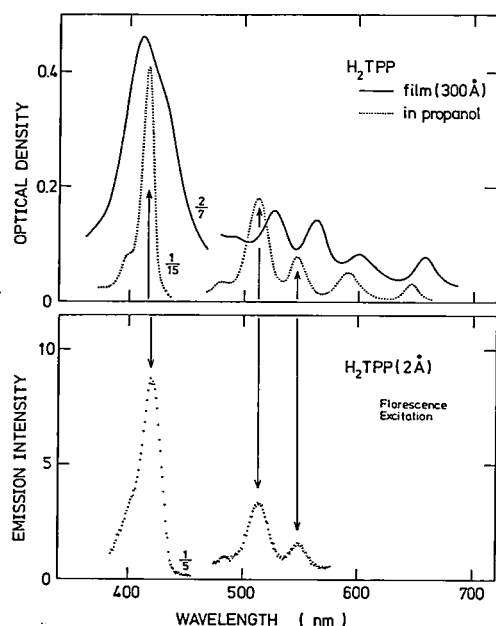
81

Figure 1. The fluorescence-excitation spectrum of an H_2TPP film (2 Å thickness) on quartz, and absorption spectra of the solid film on H_2TPP (300 Å thickness) and of the molecule in benzene (10^{-6} mol).

Figure 2. Relative yield of fluorescence of H_2TPP adosrbed on SnO_2 as a function of the distance from the SnO_2 surface. The solid curve represents the theoretical curve (see the text). Excitation was made at 525 nm, or at the $Q_y(1-0)$ absorption band.

spectrum for such a weak absorbance. The spectrum is shown in Figure 1, and is compared with the absorption spectra of the solid H_2TPP film and of the molecule in propanol. One can see that the excitation spectrum follows quite well the absorption spectrum of H_2TPP in solution, although a slight red shift of the Soret band peak is noticed for the former. It was also found that the emission spectrum of the adsorbed molecule is essentially the same as that of the molecule in benzene. These results show that the electronic structure of the H_2TPP adsorbed on SnO_2 is similar to that in solution.

The relative fluorescence yield of the H_2TPP on SnO_2, which is defined here as the intensity ratio of the fluorescence from molecules on SnO_2 to that from molecules on quartz, was measured as a function of the distance from the SnO_2 surface. The KCl film evaporated on SnO_2 was used as the spacer between SnO_2 and H_2TPP. The result is shown in Figure 2. Although fluctuation of data is not very small, one can easily see that the quenching is effective only at the distances below 20 Å. The yield of the H_2TPP in direct contact with SnO_2 is 0.32 ± 0.06. This value indicates that the rate constant of the additional radiationless deexcitation resulting in
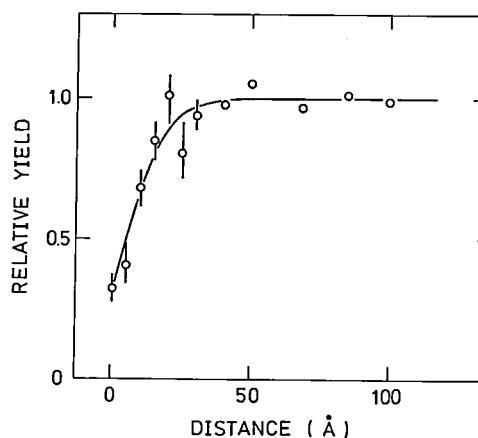
quenching is about two times greater than the reciprocal of the lifetime of the S_1 state of the H_2TPP adsorbed on quartz

The quenching effect can be attributed to the electron transfer from the S_1 state into the conduction band of SnO_2, based on following experimental results:

1) Anodic photocurrent was observed in the electrochemical cell having an working electrode of SnO_2 on which H_2TPP was adsorbed with a coverage less than unity, when the electrode was excited by light corresponding to the absorption band of the molecule. Thus, electron injection, in fact, takes place from the excited H_2TPP into the conduction band of SnO_2.

2) The relative fluorescence yield of H_2TPP is hardly affected by the adsorption on KI film (the atomic number of I is greater than that of Sn), but reduced by the contact with SnO_2. Then, it is deduced that the external heavy atom effect can be ignored in the present quenching effect.

We measured the decay time of fluorescence of the H_2TPP on quartz (and on SnO_2) by means of single photon counting technique using a nanosecond-light pulser. It was found, however, that the decay time is less than 2 ns, too fast to permit determination of a precise value. This result indicates that the electron-transfer rate concerned is faster than 1×10^9 s^{-1}.

III—E Photocatalytic Effects of Semiconductors

Essential roles are played by semiconductors in the photocatalytic effects to which a particular attention has been paid in connection to the solar energy conversion through such processes as photolysis of water and photoreduction of N_2. In order to elucidate the mechanism of these effects, we need detailed knowledges of the characteristics of adsorbed molecules on the surface as well as of the correlation between reactivities and structural and electronic conditions of the surface. Work on the following topics is in progress with the purpose of clarifying the photocatalytic effects of semiconductors from the view point of solar energy conversion.

III-E-1 Dynamics of Photocatalytic Reactions on Semiconductor Surface

Tadayoshi SAKATA and Tomoji KAWAI

The absorption of light by a semiconductor which is interacting with molecules on its surface causes various effects on adsorbed molecules. It affects the adsorption capacity of the semiconductor and surface reactions. Extensive studies have recently been made on these phenomena, the photocatalytic effects, on which a particular interest has been focussed in connection with the conversion of solar energy into chemical energy such as photolysis of water,[1] reduction of nitrogen and carbon dioxide,[2] and photosynthesis of aminoacids.[3]

In order to make clear the detailed mechanism of these photocatalytic reactions, we studied the dynamical behaviors of photoinduced reaction by using a quadrupole mass spectrometer (QMS) and a n-sec pulsed laser. Photochemical reactions of adsorbed molecules on the semiconductor which is located in a ultrahigh vacuum system are induced by exciting the semiconductor surface by the pulsed laser. The transient signals of photoproducts were selectively detected by QMS, the output signal of which was put into an oscilloscope and recorded as shown in Figure 1. This new technique can give us following informations:

1) *Photoproducts*: Photoproducts can be detected sensitively and identified from the analysis of QMS signals.
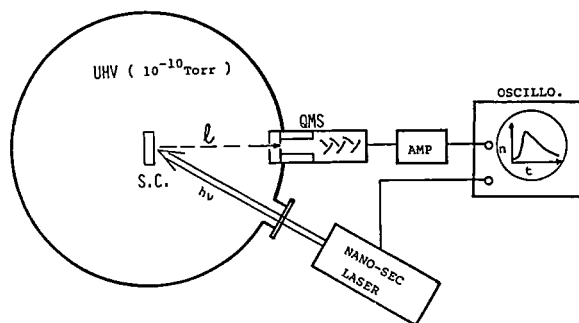
2) *Residence time on surface and the distribution of translational energy*: Their information can be obtained by analyzing the time response curve.

As an example, we would like to describe briefly the result of the photocatalytic reaction of CO_2 and H_2O on TiO_2. Table 1 shows photoproducts which were identified by examining m/e with photoresponse and their transient behavior. As seen in this table, some products have free energies higher than the initial molecules, CO_2 and H_2O. This demonstrates the CO_2 fixation by using water and light energy.

Figure 2 shows a photoresponse signal of H_2O (m/e=18) generated from surface OH group. A sharp rise with some delay time after laser pulse and a gradual decay, as seen in Figure 2, are found to be observed commonly for the other photoproducts, although the time scale is different depending on the kind of molecules. Most of these characteristic features could be explained by assuming Boltzmann distribution of translational energy and a very short residence time in the time scale of observation. The number of the observed molecules, $N_{obs}(t)$ with mass m, is expressed as,

$$N_{obs}(t) = 2N_0 \left(\frac{m}{2\pi kT}\right)^{3/2} \exp\left(-\frac{ml^2}{2kTt^2}\right)\frac{l^3}{t^4} dS.$$

Here, t is time after laser pulse, N_0 is the total number of molecule with m, l is the distance between the sample and the detector of QMS, and dS is the solid angle of the aperture of the detector viewed from the sample. In order to see how good the above assumption is, the logarithm of the product of the

Figure 1. UHV apparatus for the study of laser induced surface reaction.
S.C., semiconductor sample; QMS, quadrupole mass spectrometer; l, the distance between the surface of the sample and the entrance of the quadrupole (9 cm).
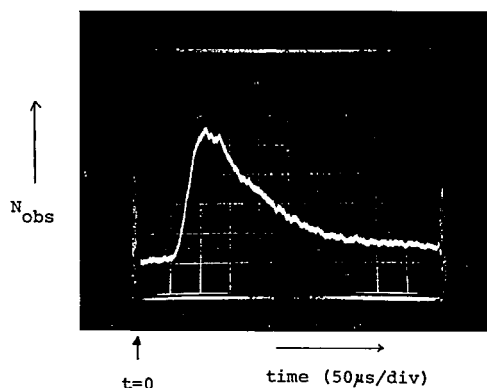

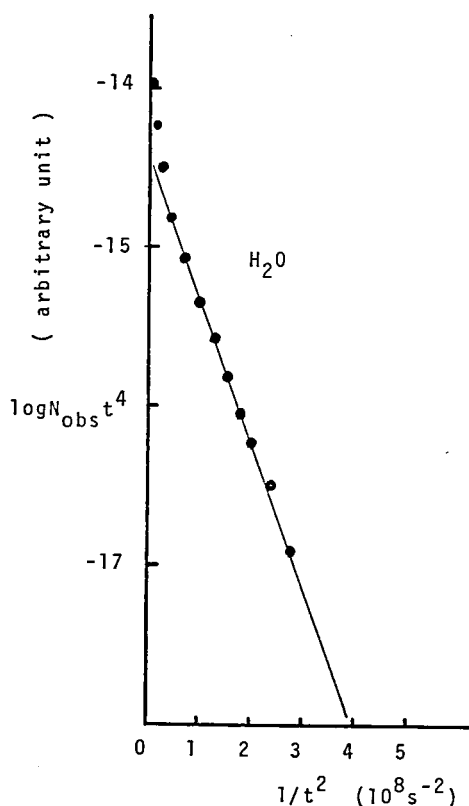Figure 2. A transient signal of H_2O (m/e=18) from TiO_2.

Figure 3. The plot of logarithmic N_{obs} t^4 against t^{-2} for H_2O from TiO_2

observed signal intensity N_{obs} and t^4 is plotted against t^{-2} in Figure 3. Since the linear relationship holds in a wide range of $1/t^2$, the equation (3) is found to be satisfied well. Photochemical reaction on the surface occurrs in a very short time and Boltzmann distribution is realized. By this method we could determine, the temperature for each molecular assembly. An interesting fact is that the temperature determined by this method depends greatly on the kind of molecule. From this result "local temperature" near each reaction site at the surface is assumed before the whole surface reaches a thermal equlibrium.

References

1) A. Fujishima and K. Honda, Nature, **238**, 37 (1972); Bull. Chem. Soc. Jpn., **44**, 1148 (1971).
2) G. N. Schrauzer and T. D. Guth, J. Am. Chem. Soc. **99**, 7189 (1977).
3) H. Reiche and A. J. Bard, J. Am. Chem. Soc., **101**, 3127 (1979).

III-E-2 Hydrogen Evolution from Water by Using Solid Carbon and Light Energy
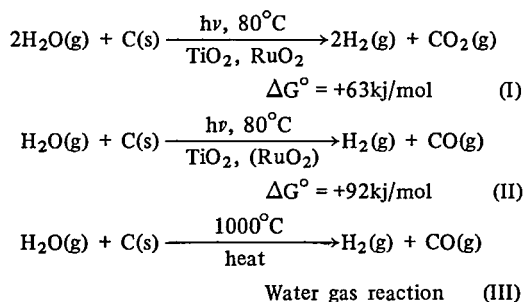
Tomoji KAWAI and Tadayoshi SAKATA

For the utilization of solar energy, decomposition

of water to produce hydrogen for the use in hydrogen energy system has attracted much attention of many scientists. Since some of the semiconductors (TiO_2, $SrTiO_3$ etc.) can decompose water to produce hydrogen and oxygen by using light energy, several reports appeared concerning the decomposition of water using powered semiconductors. One problem, arising when powered semiconductor is used for this purpose, is that the decomposition of H_2O into H_2 and O_2 in one cell makes an explosive gas. Furthermore, although Scrauzer and Guth reported that trace of H_2 and O_2 was detected by the decomposition of water gas on TiO_2,[1] reverse reaction to consume H_2 and O_2 will increase simultaneously when the amount of the product is increased. Accordingly, the produced hydrogen or oxygen should be changed to more stable gaseous chemical species. Since a lot of carbon exists in the form of coal on the earth, the use of solid carbon will be an interesting problem. From these points of view, we have examined the photocatalytic decomposition of water on TiO_2 with solid carbon. We found that the reactions (I) and (II) in Table I occur to produce hydrogen gas from water vapor and solid carbon when we illuminate mixed powders of TiO_2, RuO_2 and active carbon exposed to water vapor at 60 – 80°C. The free energies are increased by 63 and 92 kJ/mol respectively utilizing light energy. When D_2O was used instead of H_2O, D_2 was detected which demonstrates that the evolved hydrogen was really produced from the decomposition of water.(Figure 1) Direct reaction of carbon (cokes) with water using heat energy is known as the reaction (III) which takes place at more than 1000°C. In our photocatalytic reaction, however, the reaction with water proceeds at lower temperatures, using carbon as a raw material to decompose water producing hydrogen. This indicates that produced oxygen on the surface of photocatalyst has a strong oxidizing power for carbon oxidation.

We have examined the effect of several kinds of metals as catalyst (Ru, Ni and Pt) with TiO_2. Although the evolved hydrogen is increased to about 7 – 15 times in the first stage of the reaction, this would be due to the oxidation of metal itself by the oxygen produced from H_2O, assisting hydrogen evolution.

In the photodriven ammonia synthesis from N_2

Table 1. Photocatalytic and thermal reactions between H_2O and solid carbon. (g) gas, (s) solid.

$$2H_2O(g) + C(s) \xrightarrow[\text{TiO}_2, \text{RuO}_2]{h\nu, 80°C} 2H_2(g) + CO_2(g)$$

$$\Delta G° = +63\text{kj/mol} \qquad \text{(I)}$$

$$H_2O(g) + C(s) \xrightarrow[\text{TiO}_2, (\text{RuO}_2)]{h\nu, 80°C} H_2(g) + CO(g)$$

$$\Delta G° = +92\text{kj/mol} \qquad \text{(II)}$$

$$H_2O(g) + C(s) \xrightarrow[\text{heat}]{1000°C} H_2(g) + CO(g)$$

Water gas reaction   (III)
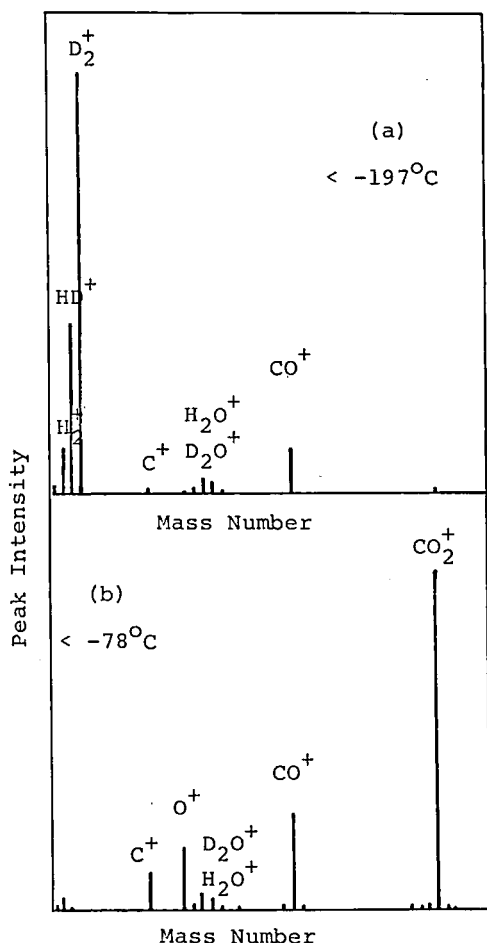
Figure 1. Mass spectra of the photo-produced gases on TiO_2-RuO_2-C-D_2O (90%). (a) a fraction not trapped at $-197°C$: D_2, H_2 and small amount of CO, and (b) a fraction not trapped at $-78°C$: mainly CO_2. C^+, O^+ and CO^+ in (b) are fragments of CO_2^+. H_2O^+ and D_2O^+ are due to background gas and incompleteness of the trapping of water. Pressure of the mass chamber during measurements are 2×10^{-7} Torr.

and H_2O[1] and CO_2 reduction by H_2O,[2] hydrogen produced from water was used, whereas the oxygen evolved changes its form by reacting with carbon, and gaseous hydrogen is produced in our system. Since a lot of carbon exists on the earth in the form of coal, this method may be interesting as one possible way for coal gasification and hydrogen evolution from water accompanied by the storage of solar energy.

References

1) G. N. Schrauzer and T. D. Guth, J. Am. Chem, Soc., 99, 7189 (1977).
2) J. C. Hemminger, R. Carr, and G. A. Somorjai, Chem. Phys. Lett., 57, 100 (1978).

III-E-3 Hydrogen Evolution through Photo-reduction of Methylviologen by Chlorophyll-a

Takashi KOISO *(Nagoya Inst. Tech.)*, Tadayoshi SAKATA, Tomoji KAWAI, and Masataka OKUYAMA *(Nagoya Inst. Tech.)*

In the photosynthesis in green plants redox reaction induced by photo-excitation of chlorophyll plays an important role. Through the cooperation by antenna chlorophyll (chl) and the reaction center in the photosystem I and II, photolysis of water followed by the charge separation is achieved. Much work has been done on the chlorophyll aggregate and the reaction center. On the other hand, the construction of an artificial system with a similar function has been pursued from the viewpoint of conversion of solar energy into chemical energy. We tried hydrogen evolution through photo-oxidation-

(A)

R=Phytyl chain

(B)
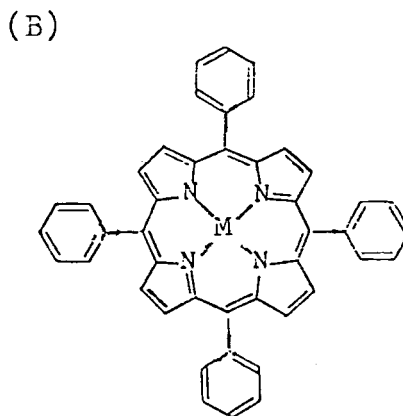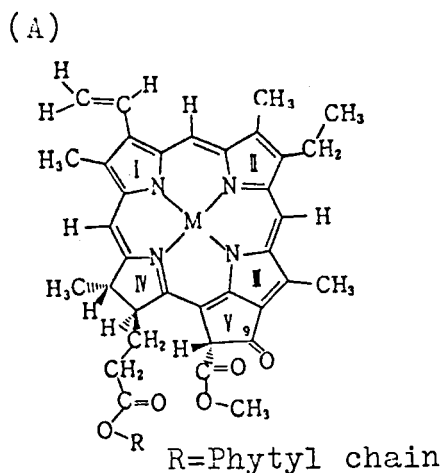
(A) Chlorophyll-a

(B) Tetraphenylporphyrin

M: Mg, Zn, Cu.

Figure 1. Molecular structure of chlorophyll-a (M=Mg) and tetraphenylporphines.

Figure 2. Spectral changes of the solution (photocatalyst, chl-a; electron donor, EDTA; electron acceptor, MV^{2+}) due to the reduction of MV^{2+} during illumination by a monochromatic light at 665 nm.

Table I.

		Quantum efficiency
a	Mg Chl-a	28%
	Zn Chl-a	40%
	Cu Chl-a	13%
b	Mg TPP	10%
	Zn TPP	40%
	Cu TPP	1%

$(MV = 2 \times 10^{-3}$ M. $EDTA = 10^{-2}$ M.$)$

reduction by using chlorophyll-a, its derivatives and tetraphenylporphines (TPP's) as photocalyst.

[A] *Photoreduction of Methylviologen*
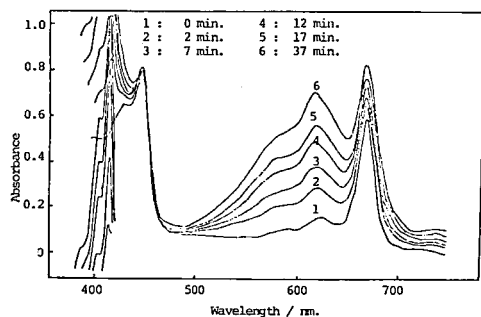
When chlorophyll-a is excited by visible light it turned out to oxidize EDTA and reduce methylviologen. Due to the formation of reduced methylviologen the deaerated solution colored blue by illumination. Besides chl-a, its derivatives such as Zn-chl and Cu-chl work well as a photocatalyst for the reduction of methylviologen (MV^{2+}). Figure 2 shows the spectral change of the solution (photocatalysts: chl-a, electron donor: EDTA, electron acceptor: MV^{2+}) during illumination with a monochromatic light at 665 nm. The introduction of air into the solution after illumination extinguished the blue color of the reduced methylviologen ($MV^{+\cdot}$), but did not cause any change of the absorption intensity of photocatalysts such as chl-a and its derivatives. This indicates that they work effectively as photocatalysts. The quantum yield depended on the kind of the central metal and was comparatively high. For comparison, tetraphenylporphines (TPP) which have similar electronic and molecular structures with chlorophyll were used for the photoreduction of MV^{2+}. The quantum yield shown in Table 1 (b) depends on the kind of central metal ions, indicating similar tendency with chl's. Since the fluorescence intensity of chl-a and Zn-TPP is hardly nfluenced by adding EDTA or MV^{2+}, the triplet state is considered to be responsible for the above reaction. For the

triplet lifetime, Mg-TPP has the longest lifetime, Zn TPP the next one, and Cu-TPP the shortest one. It seems due to the shortest lifetime that the quantum yield for Cu-TPP is the lowest However it can not be explained in terms of the triplet lifetime that the quantum yield for Mg-TPP is smaller than that for Zn-TPP. Another factor to be taking into consideration would be the rate of triplet populat on. For Zn-TPP the triplet population is greater than that for Mg-TPP. This seems to be one of reasonable factors which contribute to the quantum yield. Another important factor would be the relative position of electron energy levels between TPP, EDTA, and MV^{2+}, because the electron transfer rate is deter mined mainly by the overlap between their distribution functions.

[B] *Hydrogen Evolution through* $MV^{+\cdot}$

Since the redox potential of $MV^{2+}/MV^{+\cdot}$ is -0.44V vs NHE, the hydrogen evolution from $MV^{+\cdot}$ is thermodynamically possible:

$$MV^{+} + H^{+} \longrightarrow MV^{2+} + 1/2\ H_2$$

$$\Delta G^{\circ} = -0.44\ eV$$
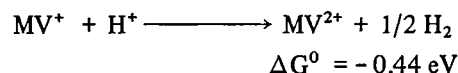
however, this reaction hardly proceed due to the small reaction rate. A catalyst such as Pt and Pd can accelerate the rate.[1] We tried hydrogen evolution by making use of the above reaction. When Pt catalyst was added to the solution of EDTA, MV^{2+} and chl-a (or Zn-TPP), a strong signal at m/e = 2 of a quadrupole mass spectrometer was observed, which indicates the hydrogen evolution.

Reference

1) T. Kawai, K. Tanimura and T. Sakata, Chem. Lett. 137 (1979).

The projects of "Molecular Approaches to Solar Energy Conversion' (III D — III E) are summarized schematically in the following figure.

Nanosec. Laser
N₂, Dye Laser

Photoelectrochemical System

Ultra-high Vacuum System for Surface Analysis and Photo-catalysis

Photon Counting System for Surface Analysis and Measurement of Life Time

PHOTOELECTRODE PROCESS

PHOTOCATALYSIS

Photoinduced surface reaction on semiconductor; Pulsed laser dynamics, Energy partitioning, Production of energy rich materials, UHV condition.

Evolution of hydrogen from water by solar energy. Carbon and water, Chlorophyll, Porphyrine, Inorganic semiconductors.

Photocurrent dynamics, Laser pulse illumination, $MoSe_2$, TiO_2, $SrTiO_3$ etc.

Layer compound photoelectrode, $MoSe_2$, MoS_2, TaS_2. Intercalation, Battery effect, High energy effeciency.

Theory on photolysis of water, Electron energy level in gas and solution.

Reduction of N_2, CO_2 by photocatalytic process.

Theory of photovoltaic effect, Dye, Layer compound.

Luminscence of adsorbed molecule on the surface.

III—F   Elementary Processes in Chemical Reactions of Vibrationally and/or Electronically Excited Molecules

The purpose of the project is to perform a detailed study on the reactivity of molecules in vibrationally and/or electronically excited states and on the distribution of energy among the internal states of reaction products. The multiphoton excitation to higher vibrational excited states and the tunable laser excitation to particular vibrational and vibronic excited states will clarify the reactivity of excited molecules. We are constructing a crossed molecular beam apparatus for the purpose of studying the effect of laser irradiation and product internal energy distribution under the collision free condition. With the quadrupole mass spectrometer and the laser induced fluorescence technique, the molecular beam apparatus will be a powerful tool in clarifying the elementary chemical reaction mechanism. Although this project has just started, we give below some preliminary results and research plans.

III-F-1 Infrared Multiphoton Process in Vapor Phase Molecules

Ichiro HANAZAKI, Susumu KUWABARA, and Iwao NISHIYAMA

Infrared multiphoton dissociation of ammonia and ethylene was studied by observing emissions from the reaction products (NH_2, NH, and C_2). The dependences of the emission intensity on the CO_2

TEA laser intensity and on the sample pressure were studied in detail. The optoacoustic measurement was also applied to this system and the number of photons absorbed in the focal region was correlated to the emission intensity.

III-F-2 Tunable Infrared Laser and Its Application to the Production of Vibrationally Excited Molecules

Ichiro HANAZAKI and Iwano NISHIYAMA

It is important to have a tunable intense infrared laser source in order to excite each vibrational mode selectively and to detect reaction products with a good signal-to-noise ratio. We have already constructed a optical parametric oscillator (OPO) pumped with a Nd:YAG laser. In addition to the OPO, which is still being improved to get a higher infrared energy useful for our purpose, we are planning to obtain a strong infrared light by taking the difference of frequencies of the second harmonics of the YAG laser and the YAG-pumped dye laser in a non-linear crystal.

III-F-3 The Laser Induced Fluorescence Study of Chemical Reduction

The laser induced fluorescence technique of a highly sensitive mean to detect the small number of molecules being produced in the vapor phase chemical reaction. A tunable ultraviolet laser source is being constructed by making use of the second harmonics of the YAG-pumped dye laser. This technique can be used with the molecular beam apparatus described below either to observe the internal state distribution of the reaction products or to detect time-resolvedly the species being produced.

III-F-4 Crossed Molecular Beam Study of the Reaction of Vibrationally and/or Electronically Exited Molecules

Ichiro HANAZAKI and Iwao NISHIYAMA

A crossed molecular beam apparatus is being constructed with a quadrupole mass spectrometer and fascilities for irradiating the beam with lasers and for observing the laser induced fluorescence. It will be a powerful tool for observing the effect of internally excited molecule with the mass analyzer and also for observing the product internal state distribution with the optical means such as the light emission or the laser induced fluorescence.

III-G Experimental Study on Photochemical Processes of Chemical Evolution in Condensed Phase.

Nobuyuki NISHI and Ichiro HANAZAKI

According to Whipple's model,[1] comets are composed of frozen gas mixtures of water, ammonia and methane. Comets are subject to strong irradiations of ultraviolet light, electrons, and protons from the sun around their lower apsides. "What happens on comets under such extreme conditions?" Lederberg[2] has suggested that the synthesis of organic molecules occurs. In order to solve this question, we are now constructing an instrument which consists of a vacuum ultraviolet excimer laser, an electron source, and a low temperature gas target in high vacuum. The strong laser light of 157 nm can directly dissociate the O-H bond of water and the N-H bond of ammonia. The transient phenomena of the reactions are followed by using an optical spectrometer and a mass spectrometer for the purpose of getting precise informations about reaction mechanisms and the role of excited electronic states. This subject is also related to laser synthesis of organic molecules.

References
1) F. L. Whipple, Astrophys. J., 111, No. 2 (1950).
2) J. Lederberg, in "Science in Space", McGraw-Hill Book Co., New York (1961), chap. 9.

III-H Multiphoton Molecular Spectroscopy

Interaction between molecule and light is the fundamental basis of molecular spectroscopy, by which we can obtain various kinds of molecular information. Usual molecular spectroscopy which is widely used now is based on interaction involving one photon. However, when very intense light like laser is used, higher order interactions involving multiphotons become important, opening new fields of molecular spectroscopy. The purpose of the project is to obtain new molecular information which is not accessible in usual methods, by employing multiphoton molecular spectroscopy.

III-H-1 Multiphoton Ionization Spectra of Benzene Vapor

Junichi Murakami, Koji Kaya *(Tohoku Univ.)*, and Mitsuo Ito *(Tohoku Univ. and IMS)*

When a molecule is irradiated by intense laser light, it simultaneously absorbs n photons and reaches to continuous ionized state. Ionization occurs when the energy of discrete molecular level coincides with m ($<$ n) times the incident photon energy. Therefore, by scanning the laser light frequency and detecting the ions produced, we can obtain m-photon absorption spectrum of the molecule. This method has a great advantage that the spectral region of very high energy can be studied by using photon of much less energy. Another advantage is that detection of ions can be made with great sensitivity and in good S/N ratio. By using this method, many investigations have been carried out for the vapor of many organic compounds. However, all the electronic states so far detected by this method are restricted to Rydberg states and the spectra of valence states have never been reported.

We have constructed an apparatus of multiphoton ionization which can be applied for low temperature molecular beam produced by jet nozzle. With this apparatus, we could observe for the first time the two-photon resonant four-photon ionization spectrum of S_1 valence state of molecular beam of benzene. A dye laser of visible region excited by a nitrogen laser was used as the exciting light. The spectrum obtained exhibits vibrational fine structure as shown in Figure 1. It agrees with the two-photon excitation spectrum of benzene vapor measured by using the fluorescence as a probe. However, the relative intensities of the vibronic bands were found to be quite different between the two spectra, indicating fundamental differences in their molecular processes and in nature of the interactions with light. Further studies are now in progress for low temperature benzene vapor and for various benzene derivatives.
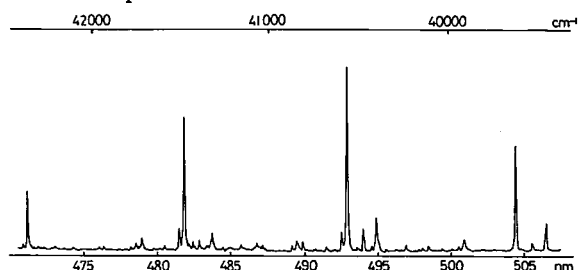

Figure 1. Two-photon resonant four-photon ionization spectrum of $^1B_{2u} \leftarrow {}^1A_{1g}$ transition of benzene vapor. Lower scale is the wavelengths of dye laser and upper scale the corresponding two-photon frequency. During the scanning of the spectrum, the power of the dye laser was kept constant.

Figure 2. Hyper Raman spectrum of liquid cyclohexane excited by the frequency doubled YAG laser at 532 nm. The spectral slitwidth is about 40 cm^{-1} and the wavelength interval of successive data point is 0.25 A or about 3 cm^{-1}. The presentation is five-point running average of the virgin data, which is the accumulation of four independent measurements.

III-H-2 Hyper Raman Spectroscopy

Atsunari HIRAYA, Yasuo UDAGAWA *(Tohoku Univ.)*, and Mitsuo ITO *(Tohoku Univ and IMS)*.

Raman scattering is a two-photon process in which one photon is absorbed and another photon is emitted. However, when the incident light is strong, we can observe very weak phenomenon in which two photons are simultaneously absorbed and another one photon is emitted. This is a three-photon process and called as hyper Raman. Selection rule of hyper Raman is different from Raman and also different from IR. Therefore, by using hyper Raman spectroscopy, we can detect the molecular states which cannot be reached by usual Raman and IR.

Cyclohexane gives a nice opportunity for the application of hyper Raman spectroscopy, because it has three a_{1u} vibrational modes active only in hyper Raman under D_{3d} point group. A frequency doubled Nd-YAG laser (532 nm) of 10 pulses per second of about 20 mJ was used as the exciting source. Hyper Raman scattering from liquid cyclohexane was detected by a photomultiplier and a gated photon counter. After every 400 laser shots the signal count rate was recorded and stored in a microcomputer for storage and further processing, and then the monochromator was step scanned by 0.25 Å. It takes about 4 hours to scan 360 data points which corresponds to about 1000 cm^{-1}, and the process was repeated and the data were averaged.

The hyper Raman spectrum of liquid cyclohexane thus obtained is shown in Figure 2. It is very similar to the IR spectrum. However, in addition to the counterparts of IR absorption bands, a strong band was observed at 1107 cm^{-1} and assigned to an a_{1u} vibrations, which is forbidden both in IR and Raman and allowed only in hyper Raman. A fact worthwhile to note is the presence of second harmonics seen in the figure, because a centrosymmetric molecule like cyclohexane should show no hyper Rayleigh line. This suggests the effect of intermolecular interaction in liquid. Hyper Raman spectroscopy now attained the stage of practical use by employing a high repetition pulsed laser. Various kinds of new information will be obtained in near future from this new spectroscopy.
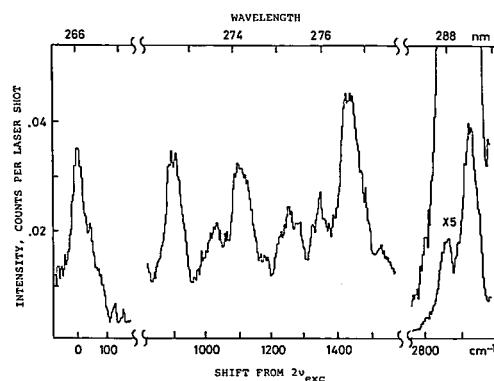

Figure 2.

III-I Picosecond-Backward Echo and FID in Molecular Systems

Masahiro MATSUOKA *(Kyoto Univ. and IMS)*

We have considered a new method to measure picosecond relaxation times of molecular systems. It is based on a backward-wave-generating three-pulse echo [1, 2], and a similar backward two-pulse free induction decay (FID) [2]. The use of the backward-wave and proper selections of input-pulse polarizations allow us to detect the signals in the picosecond time domain without any optical shutters. Both the population and the phase relaxation times of the electronic transitions as well as the vibrational transitions within an electronic level are expected to be measured by the backward echo. The backward FID is useful in homogeneously broadened systems where the echoes are not possibie.

Three pulses all of the same frequency but with the wavevectors k_1, k_2 and k_3 are applied at the times τ_1, τ_2, and τ_3 respectively. Here, τ's are the arrival times of the pulses at the sample origin. In a gaseous sample, the backward echo will be generated at the time $\tau_e = \tau_3 \cos\theta + \tau_2 - \tau_1 \cos\theta$ into the direction $k_e = k_3 - k_2 + k_1$, backward to the second pulse, for the configuration shown in the Figure 1, where θ is a small angle.

In this three-pulse echo process, off diagonal density matrix elements are responsible to the echo magnitude during the period between τ_1 and τ_2, so that a phase memory time of the superposition state of the ground and the electronically excited states can be measured by this echo. On the other hand, between τ_2 and τ_3 the diagonal matrix elements are responsible, so that the population lifetime and the velocity distribution of each vibrational level can be measured.

If two different frequencies are used for the input pulses instead, and the difference frequency between them is resonant to a vibrational transition of electronic states, the previous diagonal matrix elements are replaced by off-diagonal elements between the corresponding vibrational levels. The phase memory time of the vibrational transitions can then be measured.

In the case of FID, the first pulse of the wavevector k_1, and the second counter propagating pulses with k_2 and $-k_2$ are applied at τ_1 and τ_2, respectively. In the gaseous sample, the FID signal will be generated into the direction $k_f = -k_1$, backward to the first pulse, as in the Figure 2, where θ is arbitrary but neither equal to $0°$ nor $180°$. The signal will appear continuously starting from τ_2, and decays due to dephasing. The backward FID becomes important for direct observation of the picosecond relaxation times in homogeneously broadend systems.

References

1) M. Fujita, H. Nakatsuka, H. Nakanishi, and M. Matsuoka, Phys. Rev. Lett., 42, 974 (1979).
2) M. Matsuoka, H. Nakatsuka, and M. Fujita, "Laser Spectroscopy IV, Proc. 4th International Conference, Rottach-Egern (1979)" Springer Series in Optical Sciences, H. Walther and K. W. Rothe Ed. Springer-Verlag (to be published)
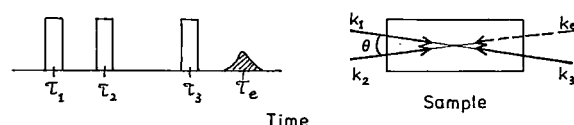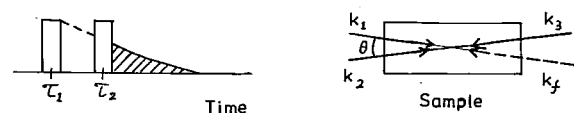
Figure 1.

Figure 2.

RESEARCH ACTIVITIES IV

Division of Molecular Assemblies

This Division conducts a wide scope of experimental studies in solid state chemistry, photochemistry and chemical kinetics. At present three laboratories, Solid State Chemistry, Photochemistry and Molecular Assemblies, have been established.

The research in Solid State Chemistry Laboratory covers the following projects: Studies on electronic structures and electrical properties of aromatic solids are being carried out using as a probe their photoelectric phenomena such as photoconduction and photoemission. A photoelectron spectrometer which can control a wide range of the specimen temperature, was assembled. We are also carrying out an experimental research on physicochemical and also electrochemical properties of hydrogenase and its electron carrier, cytochrome c_3; these properties might be related to its enzymatic activities.

The photoionization processes of simple molecules, such as diatomics and triatomics, are being studied by using both mass spectrometric and photoelectron spectroscopic techniques. In particular, the threshold electron spectra have been measured with our apparatus which is equipped with a helium Hopfield continuum light source.

As an application of the photoionization technique, the internal energy dependence of ion-molecule reactions is being studied intensively. A technique which utilizes the threshold electron-secondary ion coincidence has been developed for this purpose.

The emphasis of the Photochemistry Laboratory, established in 1978, is placed on the deeper understanding of the photon-molecule interaction which may lead to photochemical reactions and photoionizations. We also pursue new types of interactions between photons and molecules, involving multiphoton excitation and ionization of molecules using high power pulsed lasers. For the present objectives two new molecular beam apparatus are to be constructed; one for photoelectron and photoionization spectroscopy to follow the ionization channels upon irradiation of a pulsed laser, and the other for photofragment spectroscopy to detect neutral phot fragments.

In Molecular Assemblies Laboratory, the intercalation compounds of graphite with alkali metals and also ferric chloride are being investigated.

IV—A Photoelectric and Optical Properties of Organic Solids in Vacuum Ultraviolet Region

Two new machines, a high-vacuum photoelectron spectrometer equipped with temperature controlled system and a double quantum electron spectrometer, were constructed. We have started to use the synchrotron radiation machine, University of Tokyo, as an extreme vacuum ultraviolet light source for studying optical properties of polymers. The analysis of photoelectron spectra gives a reliable information about the electronic properties of the organic semiconductors and their related compounds.

IV-A-1 Anisotropic Carbon 1s XUV Absorption Spectra of Oriented st-1,2-Polybutadiene

Kazuhiko SEKI, Shimpei HASHIMOTO *(Japan Synthetic Rubber Co.)*, Koichi INOUE*, Kazumichi NAKAGAWA, Naoki SATO, Kiyoshi TAKAGI *(Nagoya Univ.)*, Shigemasa SUGA*, Hiroshi KANZAKI*, and Hiroo INOKUCHI *(*Univ. of Tokyo)*

Recently much attention has been paid to the electronic excitation from the C_{1s} orbital of organic compounds with the advent of the synchrotron radiation light source and the development of electron energy-loss spectroscopy. In the case of polymers with unsaturated functional groups, fine structures at the lower energy side of the "$C_{1s} \rightarrow$ continuum" excitation were ascribed to $C_{1s} \rightarrow \pi^*$ excitation by the comparison with molecular orbital calculations.[1] Similar fine structures have been also reported for unsaturated compounds in gas phase.[2] With this interpretation, we expect to observe an anisotropic C_{1s} absorption if we can orient π^* orbitals by controlling the orientation of unsaturated groups. As a part of our study of the electronic structure of polymers using polymer films oriented by uniaxial elongation,[3] we observed such an anisotropy for the first time, using highly polarized synchrotron radiation light from the 1.3 GeV Electron Synchrotron at the University of Tokyo and thin elongated films of syndiotactic (st)-1,2-polybutadiene (PB)

$$-(-CH_2-CH-)- , \quad \text{which is one of the simplest}$$
$$\underset{|}{CH=CH_2}$$

polymers containing π bond. The observed anisotropy

wavelength/nm
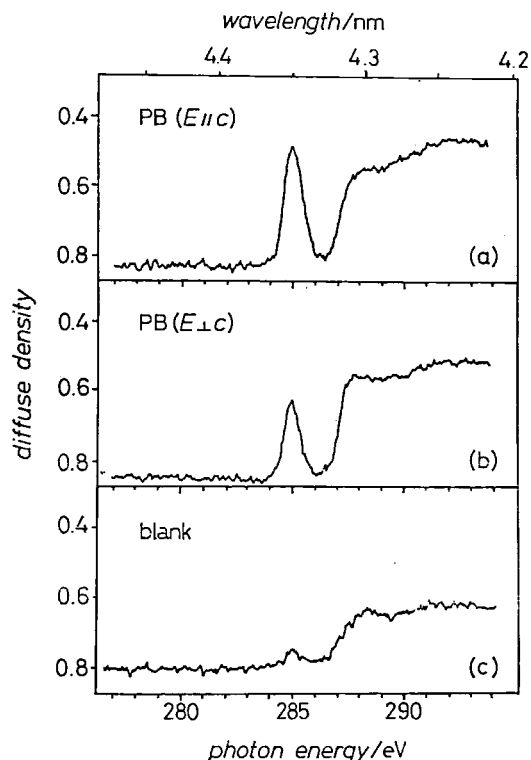
Figure 1. Anisotropic C_{1s} absorption spectra of elongated st-1,2-polybutadiene film.

Figure 2. Crystal sturcture of st-1,2-polybutadiene (Ref. 4).

gives another independent confirmation for the assignment as the $C_{1s} \rightarrow \pi^*$ excitation.

The spectra were measured with a JASCO EX-2000 2 m grazing incidence vacuum spectrograph with Kodak SWR photographic plates. Figure 1 (a) and (b) show the anisotropic absorption spectra of a 5 times elongated st-1,2-PB film of about 0.2 μm thickness (after elongation) with the direction of elongation c parallel and perpendicular, respectively, to the direction of the electric vector E of the incident light. Since the contamination on the grating caused a rather strong absorption above 286 eV (Figure 1 (c): the spectrum without sample), we will not discuss the spectra in this region in detail, but will concentrate our attention on the sharp peak at 284.9 ± 0.2 eV, whose intensity is clearly anisotropic. As our preliminary result for polyethylene —(—CH₂ —CH₂—)— showed no such a peak, this peak is ascribed to the transition from the C_{1s} to the π^* orbital of the vinyl group. Similar peaks have also been reported in other unsaturated polymers and were assigned as the $C_{1s} \rightarrow \pi^*$ excitation by the comparison with MO calculations.[1] Using this assignment, we can theoretically interpret the anisotropy as follows.

Figure 2 shows the structure of the crystalline part of elongated st-1,2-PB film analyzed by X-ray diffraction.[4] The principal chain and the plane including the vinyl group is parallel and perpendicular to the c-axis, respectively, and the c-axis is oriented parallel to the direction of elongation. Although we must consider the contribution of the amorphous part of the polymer as well, the polarized IR absorp-
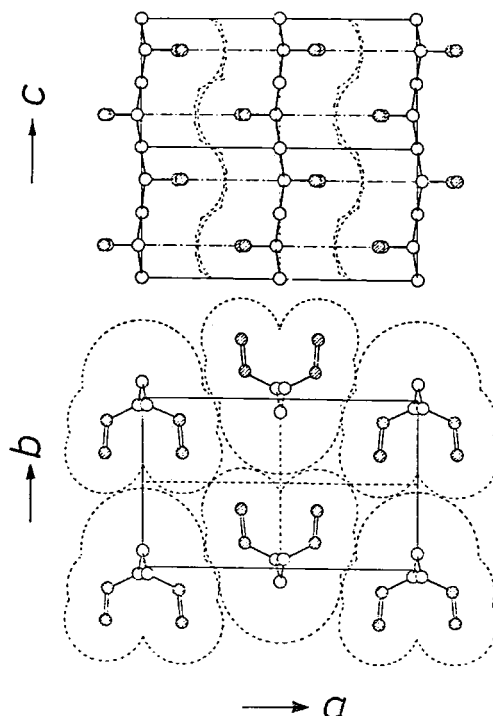
tion spectra of the elongated film showed that the principal chain and the vinyl group are highly oriented to the direction stated above.

It is expected that the C_{1s} excitation occurs only from the C_{1s} orbitals of the vinyl group, since only they have considerable overlap with the π^* orbital. These C_{1s} orbitals are symmetric with respect to the plane including the vinyl group, while the π^* orbital is antisymmetric. Therefore, the dipole transition will be allowed only for the incident light with the electric vector E perpendicular to this plane, that is, $E//c$. This expected anisotropy agrees with the experimental results shown in Figure 1. This consistency offers another independent confirmation for the assignment of this peak as the $C_{1s} \rightarrow \pi^*$ excitation.

These findings suggest that such anisotropic absorption measurements with the polarized light will be a useful tool for the interpretation of core excitation spectra of organic compounds.

References

1) J. J. Ritsko, L. J. Brillson, R. W. Bigelow, and T. J. Fabish, J. Chem. Phys., 69, 3931 (1978); J. J. Ritsko and R. W. Bigelow, ibid., 69, 4162 (1978).
2) W. Eberhardt, R. -P. Haelbich, M. Iwan, E. E. Koch, and C. Kunz, Chem. Phys. Lett., 40, 180 (1976).
3) S. Hashimoto and H. Inokuchi, Polymer J., 8, 631 (1976); S. Hashimoto, S. Hino, K. Seki, and H. Inokuchi, Chem. Phys. Lett., 40, 279 (1976): S. Hashimoto, K. Seki, N. Sato, and H. Inokuchi, IMS Ann. Rev., 67 (1978).
4) C. Natta and P. Corradini, J. Polym. Sci., 20, 251 (1956).

IV-A-2 On the Origin of Photo-Electron-Microscope-Pictures of Organic Samples

F. WILLIG *(Fritz-Haber Inst. and IMS)*, G. FRAHM *(F. -H. Inst.)*, W. ENGEL *(F. -H. Inst.)*, N. SATO, K. SEKI, and H. INOKUCHI

The first report on photo-electron-microscope (PEM) pictures were made on biological samples deposited on metal substrates by Griffith *et al.*[1] As they used a light source of the photon energy higher than the ionization threshold of the samples, the contrast in those PEM pictures was explained by the different photoemission cross sections of different molecules in the uppermost surface layer of the samples. Engel and Grund also presented PEM pictures of biological materials with the maximum resolution of about 20 nm.[2] However, as their light source supplied photon energies lower than the ionization threshold, the origin of the contrast in their PEM pictures might be different from that of Griffith *et al.* In this report we present an experimental evidence that a PEM picture of organic materials is due to the electrons photoinjected from the metal substrate into organics without direct photoionization of any molecule in the organic layer.

On the surface of copper or gold disks placed were organic materials which were several tens nanometer thick films of hexatriacontane, polyethylene, and Epon and Methacrylat with or without enclosures of biological materials. Experiments were carried out on two different apparatus. One of them was a photoelectron spectrometer described previously. The photoemission measurement revealed us the ionization threshold energy of organic materials and also the surface coverage of the metal substrate by the deposited organic layer. The other was a PEM.[2] Under the light beam of the high pressure mercury arc focussed onto the cathode of the PEM, the integrated and spatially resolved photocurrent was obtained. The latter was illustrated as pictures. The applied field strength in the organic layer was about 3×10^6 V m^{-1}.

From the photoemission spectra we determined the ionization energy at 8.4 ± 0.3 eV for hexatriacontane and at about the same for polyethylene, in good agreement with previous result.[3] These energies are higher by more than 2 eV than the maximum of the photon energy in our PEM. The photoemission spectra also showed mostly saturated coverage on the metal substrate with hexatriacontane or polyethylene.

By the illumination of the light ($h\nu \lesssim 5.5$ eV) on the organic materials on the gold substrates a photocurrent was obtained in our PEM. The photocurrent showed a remarkable time dependence and the same threshold as a bare gold disk. The integrated photocurrent showed in all cases a linear dependence on the incident light intensity. The brightness of the PEM pictures changed with the integrated photocurrent. In some cases the brighter spots in the pictures increased in size and became more diffuse. The decrease in brightness with increasing thickness of the organic layer was observed.

As the high pressure mercury arc can cause no direct photoemission from the organic samples, it is shown that the PEM pictures of them can be obtained via photoinjection of electrons from the metal substrate. The photoinjected electrons by illumination of the low-energy photons are transported along the conduction bands of organic materials which is bent by the applied electric field. In this process some portion of the electrons are scattered or trapped to lose their energy. Other electrons can reach at the surface of organic materials and a part of them are emitted into the vacuum. One origin of contrast in the PEM pictures is a spatial variation in the electron current density effected by the electron escape depths and the effective trapping sites.[4] Another origin is a strong local variation in the thickness of the organic layer.

References

1) O. H. Griffith *et al.*, *Proc. Natl. Acad. Sci. U. S. A.*, 69, 561 (1972).
2) W. Engel and S. Grund, *Proc. 8th Int. Congr. Electron Microscopy*, Canberra, Vol. II, p. 656, 1974.
3) M. Fujihira and H. Inokuchi, *Chem. Phys. Lett.*, 17, 554 (1972).
4) K. -P. Charle and F. Willig, *Chem. Phys. Lett.*, 57, 253 (1978).

IV-A-3 Photoelectron Spectra of *l*-Tryptophan in Gas and Solid Phases

Kazuhiko SEKI and Hiroo INOKUCHI

Besides the importance in biological investigation, the measurement of the gas phase ionization potential of tryptophan is interesting from the following physico-chemical viewpoint. Recently there has been some attempt to determine the energy of excess electrons in solid media by the comparison of the ionization potentials of tryptophan in the media and in vacuum.[1] However, no experimental value of the gas phase ionization potential for tryptophan has been available. Further, it is known that amino acids tend to change their state of protonation, and it will be interesting to know its effect on the electronic structure of tryptophan.

To clarify these points, we measured the gas and solid phase photoelectron spectra of *l*-tryptophan.[2] The gas phase photoelectron spectrum was measured with a Perkin-Elmer PS-18 photoelectron spectrometer with He I resonance line ($h\nu = 21.22$ eV). Since tryptophan is reported to decompose upon vaporization,[3] we examined the IR spectra of films formed by the condensation of some portion of the sample vapor on a NaCl plate. It showed no decomposition.

Figure 1 shows the gas phase photoelectron spectrum of *l*-tryptophan sublimed at $180 - 200$°C. We examined the correlation of the photoelectron
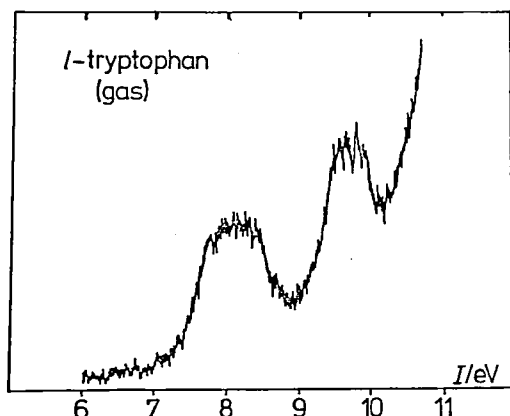
Figure 1. Photoelectron spectrum of *l*-tryptophan in the gas phase with He I resonance line (21.22eV).

Table I. Ionization Potentials of *l*-tryptophan in Gas and Solid Phases.

	E^a_{th}/eV	I^b/eV			
Gas	7.3$_5$	8.1,	9.7		
Solid	6.1	7.2,	9.1,	11.1,	13.4, 14.7
Shift^c	1.2	0.9,	0.6		

a Photoelectron emission threshold energy
b ionization potentials of peaks and shoulders
c difference between the gas nad solid state values

spectrum of tryptophan with reported those of indole and alanine, the constituent parts of tryptophan. The correlation among their MO's (by INDO method) was also examined. In the MO calculation, MO's for both the neutral (-COOH, -NH₂) and zwitterion (-COO⁻, -NH₃⁺) forms of tryptophan were calculated. These correlations showed that gas phase tryptophan is in the neutral form, as other amino acids are. The first peak at 8.1 eV is assigned as the two π ionizations from the indole ring, and the second at 9.7 eV as the combined contribution of the third π ionization of indole and the ionization of the N lone pair of the amine part. As for the ionization threshold, a value of 7.3 eV was obtained in the present study.

However, the possibility of the change of protonation makes it difficult to compare directly the ionization potentials of gas phase and in solid solution. To understand such an effect, we measured the photoelectron spectra of solid tryptophan, which is in the zwitterion form. The used instrument is reported previously.[4] Figure 2 shows the obtained spectra. It is known that the peak intervals of photoelectron spectra do not change much between gas and solid phases for molecules with the same structure in the both phases. However, as seen in Table I, no good correspondence was found for *l*-tryptophan.
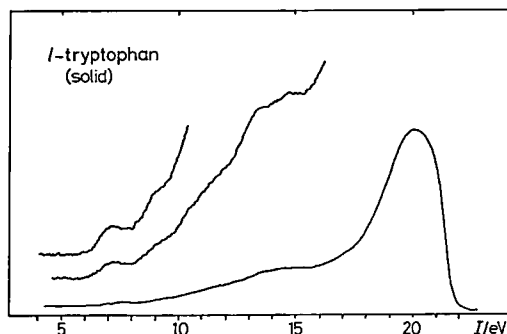
This should be due to the neutral (gas) ⇄ zwitterion (solid) change. The MO calculation suggests that the ionization threshold of zwitterion is 1.5 eV smaller than that of the neutral form. Considering the gas-to-solid change of the threshold for usual molecules (e. g. 1.7 eV for aromatic hydrocarbons), the solid ionization threshole of tryptophan is expected to be 3.2 eV smaller than that for gas phase. However, the observed value is only 1.2 eV. This may suggest that the large change of the ionization threshold by the neutral ⇄ zwitterion change is cancelled by the Madelung energy by the surrounding molecules, which tends to increase the solid state photoemission threshold. Such findings show that the effect of the change of the state of protonation is a rather complex one, and more effort has to be done for better understanding of the ionization of such kind of molecules in solid media.

References

1a) A. Bernas, M. Gauthier, D. Grand, and D. Parlant, *Chem. Phys. Lett.*, **17**, 439 (1972).
1b) J. Moan, *Chem. Phys. Lett.*, **18**, 446 (1973).
2) After the competion of the present work, an independent measurement for gas phase was published: P. H. Cannington, and N. S. Ham, *J. Electron Spectrosc.*, **15**, 79 (1979).
3) K. Seki, N. Sato, and H. Inokuchi, *IMS Ann. Rev.*, **65** (1978).

IV-A-4 Photoelectron Spectroscopy of Naphthalene Evaporated Films Irradiated by Electron-Beam

Kazumichi NAKAGAWA, Kazuhiko SEKI, Naoki SATO, and Hiroo INOKUCHI

Several radical species produced in naphthalene crystals irradiated with ionizing radiation have been assigned:[1,2] among them, 1- and 2-hydronaphthyl radicals (see Figure 1) show the charge-transfer transitions between the radicals and neighbouring molecules.[3,4] Although the values of ionization potentials as well as electron affinities of 1- and 2-hydronaphthyl radicals are essential to study the mechanism of the charge-transfer transitions, no experimental data have been obtained. It is also of interest to study the ionization potentials of other unstable radical species in irradiated naphthalene solids using the ultraviolet photoelectron spectroscopy (UPS).

Figure 2. Photoelectron spectrum of *l*-tryptophan in the solid phase with He I resonance line (21.22 eV).
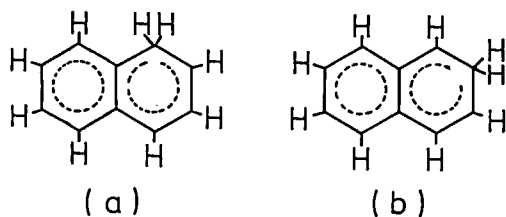
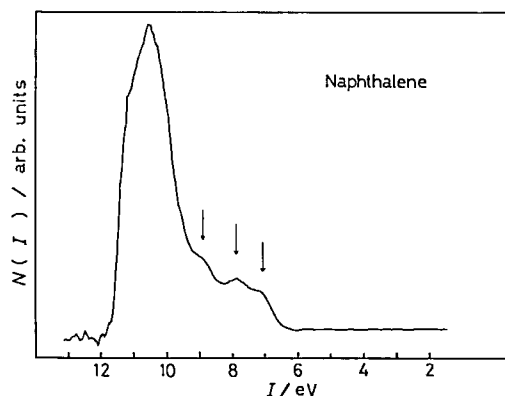Figure 1. 1-hydronaphthyl radical (a) and 2-hydronaphthyl radical (b).

Figure 2. Photoelectron spectrum of naphthalene evaporated film at 77 K. The 11.7 eV resonance line of argon discharged light source was used. I and $N(I)$ are ionization potential and the number of photoelectrons of which ionization potential is I, respectively.

Inthis work, we improved the apparatus so as to measure photoelectron spectra of organic substances having high vapour pressure, and studied the photoelectron spectra of evaporated naphthalene films irradiated by an electron-beam.

Naphthalene films were made by evaporation of naphthalene on a copper substrate cooled at 77 K in a vacuum chamber. The pressure of the chamber was 8×10^{-7} Pa. The photoelectron spectra were measured using the argon resonance line ($h\nu \sim 11.7$ eV). The kinetic energies of the photoelectron were analyzed by a spherical retarding-type analyzer. Figure 2 shows the photoelectron spectrum of the naphthalene evaporated film kept at 77 K. Three small peaks were observed at 7.1, 7.9, and 8.8 eV. The ionization threshold energy was obtained to be 6.4 eV. The energy values of the three peaks agree well with those of naphthalene solid obtained by Grobman and Koch.[5]

The naphthalene evaporated films were irradiated at 77 K with an electron beam generated from a hand-made electron gun. The electron beam energy was from 20 eV to 2×10^3 eV and the beam current was 1 to 500 μA. Figure 3 shows the spectrum measured at 77 K after irradiation with a 200 eV electron beam. The beam current and the irradiation time were 30 μA and 8 min, respectively. Three
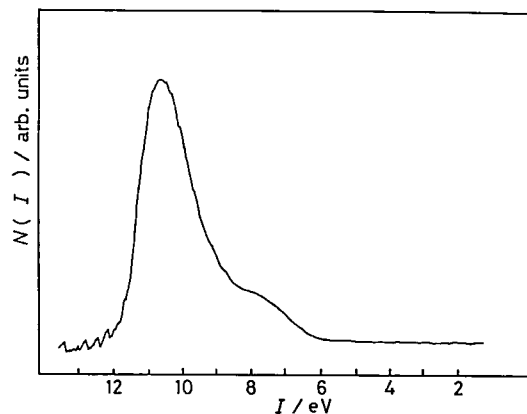

Figure 3. Photoelectron spectrum of naphthalene evaporated films irradiated with 200 eV electron beam.

peaks in Figure 2 disappeared and only a structureless broad shoulder was observed around 7.5 eV. No distinct peak could be found below 6.4 eV; the the values of the first ionization potentials of the radicals should be smaller than the ionization threshold energy of naphthalene. The broad shoulder around 7.5 eV in Figure 3 was still observable after raising the temperature up to 370 K.

It is clear that the spectral change from Figure 2 to Figure 3 was caused by electron irradiation. The remaining broad shoulder in Figure 3 up to 370 K shows that the naphthalene molecules were converted into other chemical species having a low vapour pressure. By the low energy electron diffraction, Firment and Somorjai[6] found that the electron irradiation on naphthalene evaporated films produced the chemical species having a vapour pressure lower than naphthalene. They suggested that these chemical species were polymer-like. The spectral change caused by electron irradiation observed in the present work may be explained with the formation of polymer-like species. However, this interpretation has some ambiguity, because the effect of contamination by remaining gases cannot be neglected; in fact, a slow change of the spectrum in Figure 2 was found.

The spectral change which gives a positive proof on the formation of radical species is yet to be found. Further efforts are being made to study the photoelectron spectra of the radical species.

References

1) N. Itoh and T. Chong, *Radiation Chemistry* (in Japanese) 12, 2 (1977).
2) K. Nakagawa and N. Itoh, *Chem. Phys.*, 40, 69 (1979).
3) K. Nakagawa and N. Itoh, *Chem. Phys.*, 16, 461 (1976).
4) K. Nakagawa and N. Itoh, *Chem. Phys. Lett.*, 47, 367 (1977).
5) W. D. Grobman and E. E. Koch, "Photoemission in Solids II", eds. L. Ley and M. Cardona, Springer-Verlag, New York, 1979, pp. 261–298.
6) L. E. Firment and G. A. Somorjai, *Surf. Sci.*, 55, 413 (1976).

IV—B Photoconduction in Organic Solids

Photoconduction in molecular solids has been shown to be a phenomenon which involves the generation of highly excited states of molecules, their conversion to ionized states and the migration of these states. This phenomenon depends strongly on the purity, crystallinity, and surface states of solid specimen: An ultra-high vacuum apparatus for the photoconduction measurement was constructed. Further, a workshop for the purification and crystal-growth of organic substances was arranged in cooperation with Chemical Materials Center.

IV-B-1 Ultra-high Vacuum Apparatus for Measurements of Photoconduction of Organic Films

Naoki SATO, Hiroo INOKUCHI, and Kikujiro ISHII
(Gakushuin Univ.)

One of us (H. I.) and his co-workers have investigated the photoconduction properties (internal photoelectric effects) of several condensed aromatic hydrocarbons.[1] The electrical conductivity of them has been found to have dependence on ambient oxygen pressure.[2] As oxygen molecules may affect to the electrical conduction on the process of the charge carrier transport in the organic solids, the photoconductivities of them should be also dependent on ambient oxygen. In order to clarify the oxygen effects on electron transport and also to obtain the intrinsic values of photoconductivies we have constructed an ultra-high vacuum photoconductivity apparatus (UHV-PCA). In this report we introduce the characteristics of the UHV-PCA machine.

For the precise investigation of electrical conduction mechanisms of organic solids it is most preferable to perform the measurements on their single crystals. In the case of a large molecule of the condensed aromatics, however, it is hard to make the available size of the single crystal for optical measurements.

We dare to work on their evaporated films which are polycrystals in most cases. The UHV-PCA is designed to be fitted to this purpose.

Figure 1 depicts the UHV-PCA. The machine is consisted of a measurement chamber, main pumps with a gate valve, and rough evacuation systems. Two sorption pumps or a turbomolecular pump is available as the roughing pump. The main pump is an ion-sputtering pump with a subsidary titanium getter pump, by which we can reach the vacuum near 10^{-8} Pa. There are eight radial ports on the side of the chamber and also eight vertical ports on the lid of the chamber. One of the vertical ports is located in the centre of the chamber and is for the cryostat on which the sample specimen is mounted. This cryostat is rotatable over 270° and is controlled temperature from 90 K to 600 K. The sample specimen is prepared by vacuum evaporation of the organic compounds on a quartz plate with some evaporated metal electrodes. On both evaporation processes the mask-manipulators are useful. As the sample evaporator can be cooled at near liquid nitrogen temperature during the system bakeout, it is possible to prepare the solid samples of high vapour pressure at room temperature.

A LEED/Auger electron optics is attached to one of the side ports. This may enable to monitor the film structure of the sample. As two optical ports face each other along a central line, it is possible to measure the action spectrum of photoconduction as well as the optical absorption spectrum simultaneously. For the irradiation of light to the sample we can use the constant-photon-number monochromator with two types of light source.[3]

Kamura et al.[4] found a high photoconductivity of tetrabenzoperylene (TBP) and its similar molecule in films. But the purity of TBP used at that time was not sufficiently good. Now we obtain the high purity compounds,[5] we are going to do over again to obtain the intrinsic photoconductivity by the use of this machine UHV-PCA. As TBP has the characteristic structure in the crystal,[6] there may be some phase transition in the region of temperature which can be covered by the UHV-PCA, then we can find the relation between the crystal structure and the electrical properties.
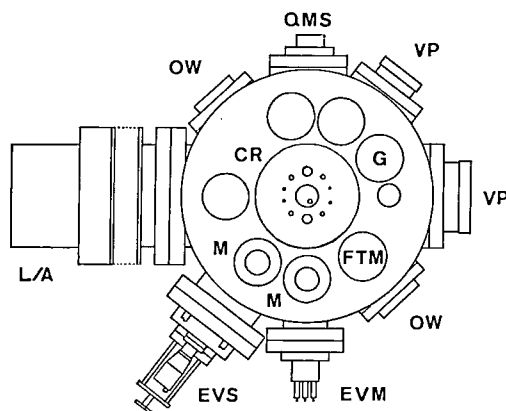

Figure 1. The chamber of the UHV-PCA. CR, flange of liquid nitrogen cryostat; G, ionization gauge; FTM, sensor of film thickness monitor; M, manipulator of masking plate; EVM, evaporator of metals; EVS, evaporator of samples; L/A, LEED/Auger electron optics; OW, optical window; QMS, quadrupole mass spectrometer; VP, viewing port.

References

1) For example, H. Inokuchi, N. Matsubara, Y. Maruyama, and E. Clar, Nature, 205, 64 (1965).
2) Y. Maruyama and H. Inokuchi, Bull. Chem. Soc. Jpn.,

39, 1418 (1966); H. Inokuchi, Y. Hori, and Y. Maruyama, 2nd Int. Conf. on Conduction in Low-Mobility Materials, p. 375, Taylor & Francis Ltd., 1971; Y. Hori, S. Iwashima, and H. Inokuchi, *Bull. Chem. Soc. Jpn.*, 43, 3249 (1970).
3) K. Ishii, unpublished.
4) Y. Kamura, H. Inokuchi, J. Aoki, and S. Fujisawa, *Chem. Phys. Lett.*, 46, 356 (1977).
5) S. Iwashima, H. Honda, J. Aoki, and M. Takekawa, *Nippon Kagaku Kaishi*, 1979, 443 (in Japanese).
6) Y. Kohno, M. Konno, Y. Saito, and H. Inokuchi, *Acta Cryst.*, B31, 2076 (1975).

IV-B-2 Time Dependence of Crystallization of Tetrabenzo[a, cd, i, lm]perylene (TBP) Amorphous Film as a Function of Purity

Satoshi IWASHIMA *(Meisei Univ.)*, Junji AOKI *(Toho Univ.)*, Naoki SATO, and Hiroo INOKUCHI

As purification methods for condensed polycyclic aromatic hydrocarbons, we are using several chemical and physical processes. As chemical processes, the raw material is boiled with maleic anhydride and chloranil, neutralized by aqueous solution of sodium hydroxide, and extracted with toluene: The extracted compound is treated with metallic sodium in 2,2'-dioxydiethyl ether. As physical processes, the column chromatography and the recrystallization method are useful. Four high-purity aromatic hydrocarbons, their impurity contents being kept to be less than 10^{-6} mole/mole, were prepared by the above processes: they are violanthrene A, violanthrene B, isoviolanthrene A and TBP.

From the investigation of absorption and fluorescence spectra of TBP thin film, we found that the rate of crystallization from the amorphous thin film depends on the purity of specimen. The spectra of TBP, containing 10^{-6} mole/mole impurity, showed amorphous ones and changed to those of crystalline states at room temperature in several hours. The amorphous spectral patterns of very high-purity TBP film, its impurity content being less than 10^{-8} mole/mole, changed to the crystalline ones immediately after film preparation. These findings suggest that the crystallization speed of amorphous film of organic compounds apply to the determination of purity.

The single crystal preparation of TBP for photoconduction measurements is still in due course.

IV-B-3 Purification and Crystal Growth of Organic Substances

Kazumichi NAKAGAWA, Kikujiro ISHII *(Gakushuin Univ.)*, and Hiroo INOKUCHI

A workshop for purification and crystal growth of organic substances, especially of aromatic hydrocarbons, was arranged in cooperation with Chemical Materials Center of IMS. In the workshop, we prepare oxygen-free substances by means of vacuum treatment and also apply molten-zone-refining furnaces for purification. Bridgeman furnaces are prepared for crystal growth. Using non-mixing two kinds of heat-transfer materials, silicone oil and ethylene glycol, the sharp and large temperature gradient in Bridgeman furnace was produced.

Five grams of naphthalene and anthracene single crystals were obtained using appropriate ampules. For the naphthalene crystal, the lifetime of triplet excitons was easily reached to 100 ms. Preparation of benzene crystal is also planned.

IV—C Reaction Mechanism of Hydrogenase and Electron Transport Behaviour of Cytochrome c_3

Hydrogenase, a bacterial enzyme, catalyses three types of reaction, *i.e.*, (1) conversion between hydrogen modifications, para-H_2 and ortho-H_2, (2) exchange reaction between hydrogen isotopes, and (3) reversible oxidoreduction of an electron carrier with H_2 and protons.

These enzyme in the dry state catalyses not only the conversion and exchange reactions, but also the reversible oxidoreduction of the electron carrier, cytochrome c_3, with H_2. These reversible reaction applies to obtain ferricytochrome c_3 and ferrocytochrome c_3 in solid states as a same specimen. The unusual electrochemical behaviour of ferricytochrome c_3 being studied extensively (See section VII-A and VII-B).

IV-C-1 Ionization Potentials of C-type Cytochromes*

Naoki SATO, Keisaku KIMURA, Shojun HINO *(Chiba Univ.)*, Tatsuhiko YAGI *(Shizuoka Univ.)*, and Hiroo INOKUCHI

Cytochromes, kinds of hemoprotein, play important roles in biological redox processes. Cytochrome c and c_3 having one and four hemes in a molecule, respectively, operate as the electron carriers in life. The redox potentials of the two cytochromes[1,2] are considerably different, which is due to the chemical environment of a heme. Though the electronic structures of porphyrins and phthalocyanines as the model compounds of hemes have been investigated,[3] the dependence of ionization potential on their metal oxidation state is not known well. We have determined the ionization potentials of ferricytochrome

97

c (c(O)), ferrocytochrome c (c(R)), ferricytochrome c_3 (c_3(O)), and also ferrocytochrome c_3 (c_3(R)) in their solid films by vacuum-ultraviolet photoemission spectroscopy.

The description of sample preparation was previously given.[4] c_3(R) was prepared under ambient hydrogen. Each sample was deposited into ca. 100 nm-thick film on a small copper disk from aqueous solution. The photoemission measurements were carried out as described previously.[5] In the case of c_3(R) of a small ionization potential we tried to obtain the preciser threshold energy by the use of a low energy light source with an ultraviolet monochromator, which covered the wavelength region between 200 nm (6.20 eV) and 260 nm (4.77 eV). In experiments the photoelectron energy distribution curves (EDCs)[6] for a certain monochromatic light and the spectral dependence of the quantum yield (SDQY)[7],[8] were obtained. Analyzing the results, we determined the ionization potentials.

After evaluating the values determined by several methods, most probable values of the ionization potentials of cytochromes are summarized in Table I. It is found that the ionization potential of the ferri-form is larger than that of the ferro-form for both cytochromes and the ionization potential of cytochrome c_3 is smaller than that of cytochrome c in the same oxidation state. Threshold electrons are thought to be emitted from porphyrin π orbitals of the hemes, not from localized d orbitals of the central iron atoms. The decrease of ionization potential from the ferri-form to the ferro-form is explained by the rise of the energy levels of the ligand π orbitals caused by the net charge difference on the central iron between the two forms.

The oxidation potential of $Fe^{III}TPP$ (tetraphenyl-porphyrin), one of the model compounds of hemes, in solution has been determined electrochemically,[9] adopting the energy level of the normal hydrogen electrode (NHE) as the standard potential. Neglecting the reorganization energy by solvent, the obtained oxidation potential can be converted to the ionization potential in solution measured by the absolute energy value and then we estimate it to 5.9 eV. This value is in good agreement with the ionization potential, 6.1 eV, of c (O) in solid states. Considering

Table I. Ionization Potentials of Cytochromes (in eV)

	ferri-form (O)	ferro-form (R)	Δ (O−R)
cytochrome c	6.1	5.8	0.3
cytochrome c_3	5.4	4.6	0.8
Δ (c-c_3)	0.7	1.2	

that the porphyrin in c (O) is surrounded by protein, the electronic state of hemes in c (O) is seemed to be similar to those of porphyrins in solution.

In the case of cytochrome c_3, one of multihemo-proteins, four hemes may be located so close to one another (forming a sense of cluster) in a molecule. The fact that the ionization potentials of both c_3(O) and c_3(R) are so small corresponds to this prospect, that is, the electronic interaction among four hemes may enhance the polarization energy in cytochrome c_3. This discussion will be related with unusual properties of c_3(R).[10]

References

* Main parts of this work have been reported in J. Amer. Chem. Soc., 100, 6564 (1978) by K. Kimura, N. Sato, S. Hino, Y. Yagi, and H. Inokuchi.

1) R. W. Henderson and W. A. Rawlinson, "Haematic Enzime", J. E. Falk, R. Lemberg, and R. K. Morton, Ed., Pergamon Press, Elmsford, N. Y., 1961, pp. 370–382.
2) K. Niki, T. Yagi, H. Inokuchi, and K. Kimura, J. Electrochem. Soc., 124, 1889 (1977).
3) S. C. Khandelwal and J. L. Roebber, Chem. Phys. Lett., 34, 355 (1975); B. H. Schechtman and W. E. Spicer, ibid., 2, 207 (1968); J. Berkowitz, J. Chem. Phys., 70, 2819 (1979); S. Kitagawa, I. Morishima, T. Yonezawa, and N. Sato, Inorg. Chem., 18, 1345 (1979).
4) T. Yagi and K. Maruyama, Biochim. Biophys. Acta, 243, 214 (1971).
5) M. Kochi, Y. Harada, T. Hirooka, and H. Inokuchi, Bull. Chem. Soc. Jpn., 43, 2690 (1970).
6) T. Hirooka, K. Tanaka, K. Kuchitsu, M. Fujihira, H. Inokuchi, and Y. Harada, Chem. Phys. Lett., 18, 390 (1973).
7) L. E. Lyons and G. C. Morris, J. Chem. Soc., 1960, 5192.
8) T. Hirooka, M. Kochi, J. Aihara, H. Inokuchi, and Y. Harada, Bull. Chem. Soc. Jpn., 42, 1481 (1969).
9) A. Wolberg and J. Manassen, J. Amer. Chem. Soc., 92, 2982 (1970).
10) K. Kimura, Y. Nakahara, T. Yagi, and H. Inokuchi, J. Chem. Phys., 70, 3317 (1979).

IV—D Chemistry and Physics of Intercalation Compounds of Graphite

A large number of metallic solids are known to be synthesized by the intercalation of various species between the hexagonal sheets of carbon atoms in graphite. Electronic properties of graphite-alkali-metal and graphite-metal-halide intercalation compounds are being studied in relation to their electronic structures by the measurements of the conductivity, the superconductivity, NMR, and the Raman scattering.

IV-D-1 Electrical Conductivity and Superconductivity of Graphite-Alkali-Metal Intercalation Compounds

Mizuka SANO (Univ. of Electro-Communications and

IMS], Hiroo INOKUCHI, Mototada KOBAYASHI*, Shinji KANEIWA*, and Ikuji TSUJIKAWA* (*Kyoto Univ.)

Graphite, a prototype layered solid, can form intercalation compounds with alkali metals, and the compounds thus formed have been reported to be C_8M and $C_{12n}M$ ($n \geq 2$, M=K, Rb, Cs). The distance between graphitic layers expands from 3.36 to 5.33 A, when potassium is intercalated between the layers, and the distance between the K atoms is 4.91 A for the K richest compound, C_8K. This means that large vacancies are newly formed between the layers. Furthermore, C_8M has been reported to be superconductive at low temperatures.[1] We tried to introduce the third component (H_2,[2] benzene,[3] and thiophene in the present work) into these vacancies to observe its effect on the electronic properties of the graphite-alkali compounds.

The basal-plane resistivity of K- and Cs-graphites, synthesized by heating K or Cs with grafoil (Union Carbide Co.), was measured by a four-point technique. The superconducting transition temperature (Tc) of grafoil-K was determined from the temperature dependence of its magnetic susceptibility (χ). Temperatures below 0.32 K were obtained by adiabatic demagnetization of a chromium-potassium alum coolant.[4]

The resistivity of grafoil increased with decreasing temperature from 700×10^{-6} at 300 K to 1440×10^{-6} Ωcm at 80 K. Figure 1a shows the plots of the resistive voltage (V) vs. temperature for C_8K. Hydrogen gas admitted to C_8K at 80 K caused a slight increase in V (Figure 1b). The effect of H_2 on V was reversible in the region up to at least 200 K. C_8K kept in H_2 at 300 K showed a gradual increase in V.
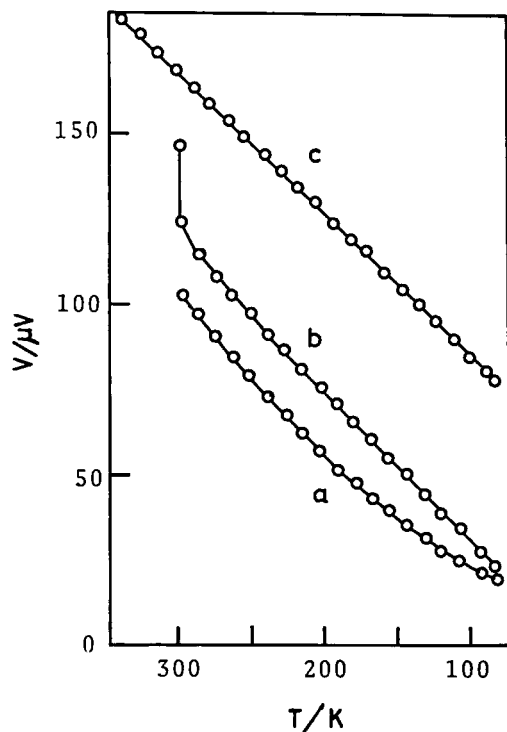

Figure 1. The temperature dependence of resistive voltage for a) C_8K, b) C_8K in hydrogen, and c) C_8K-hydride.
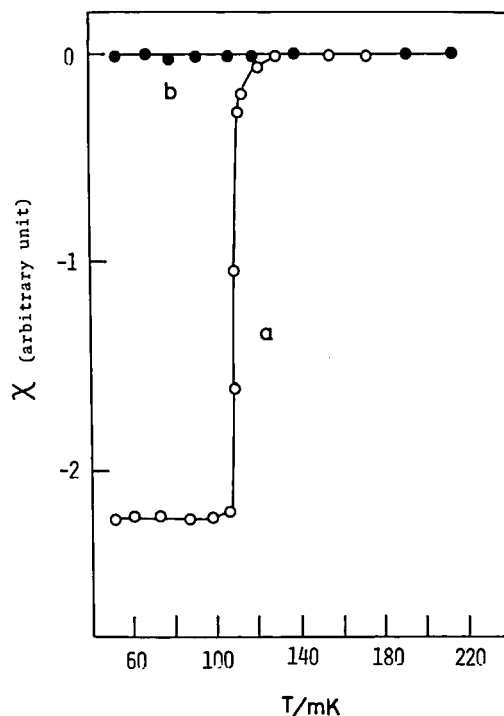

Figure 2. The temperature dependence of magnetic susceptibility for a) $C_{10}K$, and b) C_8K-hydride.

It was found after a week that its color turned blue and the resistivity reached the constant value of 40×10^{-6} from the original value of 23×10^{-6} Ωcm in vacuo at 300 K (Figure 1c). Grafoil-Cs, however, received no influence of H_2 on its resistivity and the change of its color did not occur.

The resistivity for $C_{24}K$ was found to increase to 41×10^{-6}, 60×10^{-6}, and 65×10^{-6} upon the reaction with H_2, benzene, and thiophene, respectively, from the original value of 31×10^{-6} Ωcm in vacuo at 300 K. These intercalation compounds were found to be metallic in character, showing a decrease in resistivity with decreasing temperature.

Upon the reaction with hydrogen, the superconducting transition temperatures for Pd and Th are known to rise from 0 to 4.6, and from 1.37 to 8.35 K, respectively, while T_C for Nb falls from 9.4 to < 1.3K. We therefore measured T_C for grafoil-K. T_C depends on the amount of K intercalated; 0.126 K for $C_{8.6}$ K and 0.108 K for $C_{10}K$ (Figure 2a). The blue compound formed from C_8K with H_2 was found to show no transition above 0.052 K (Figure 2b).

The mechanism for the occurrence of superconductivity in graphite-alkali-metal intercalation compounds has not been elucidated yet, but the increase in resistivity and the decrease in T_C mentioned above can be explained in terms of a decrease in the number of conduction electrons. The number of conduction electrons decreases, if charge transfer takes place from the conducting graphitic layers to hydrogen, forming graphite-alkali-metal-hydride.

References

1) N. B. Hannay, T. H. Geballe, B. T. Matthias, K. Andres, P. Schmidt, and D. MacNair, *Phys. Rev. Lett.*, 14, 225 (1965).
2) Graphite-alkali-metal intercalation compounds possess an H_2–D_2 exchange reaction: H. Inokuchi, N. Wakayama, T. Kondow, and Y. Mori, *J. Chem. Phys.*, 46, 837 (1967).
3) G. Merlé, Ch. Mai, J. Golé, and I. Rashkov, *Carbon*, 15, 243 (1977).
4) M. Kobayashi and I. Tsujikawa, *J. Phys. Soc. Jpn.*, 46, 1945 (1979).

IV-D-2 Raman Scattering from Graphite Intercalated with Iron Chloride

Kentaro OHHASHI *(Kyoto College of Pharmacy)*, Ikuji TSUJIKAWA *(Kyoto Univ. and IMS)*, and Hiroo INOKUCHI

The graphite-metal halide compounds are very popular intercalation compounds. But detailed investigations have been done in recent years, which have brought a great deal of controversies, mainly on their bonding character.[1]

Raman scattering is considered as a useful tool to make clear how the intercalant species are there, that is, their oxidation states, their symmetries etc. can be studied by examining changes in molecular vibrational modes by intercalation. Last year Caswell and Solin published a communication on this.[2]

The intercalation compounds of graphite-$FeCl_3$ were synthesized by vapor phase reaction of highly orientated pyrolytic graphite (HOPG) with vacuum-distilled $FeCl_3$. The conditions for preparing graphite-$FeCl_3$ are the same as in the literature.[3] The 5145 Å line of an Ar ion laser ($\approx$1W) was used as a light source for Raman scattering. The scattered light was observed at the angle of 90° from the incident beam. The samples were mounted so as to be the incident beam inclined by 30° from the c-plane.

Figure 1 shows the Raman spectra for pure graphite and intercalation compound of graphite intercalated with $FeCl_3$ (64 wt%, stage 1). Intercalation compounds of graphite are classified according to their "stage" which is defined as the number of graphitic layers between nearest intercalant layers. The Raman peak at 1582 cm^{-1} of the E_{2g}^2 mode of graphite is replaced by the peaks at 1610 cm^{-1} and 1625 cm^{-1} by intercalation. This result does not agree with that of Caswell and Solin,[2] where the peak appeared at 1626 cm^{-1} in the stage 1 compound while the peak at 1612 cm^{-1} in the stage 2 compound.

The pristine graphite belongs to the D_{6h}^4 space group and has twelve vibrational modes at Γ point, among which three are accoustic ($A_{2u}^1 + E_{1u}^1$), three infrared-active ($A_{2u}^2 + E_{1u}^2$), four Raman-active ($E_{2g}^1 + E_{2g}^2$) and two silent ($B_{2g}^1 + B_{2g}^2$) as shown in Figure 2.

The upshifts of 28 and 43 cm^{-1} as shown in Figure 1 are presumably attributed to intercalation effects on E_{2g}^2 mode at 1582 cm^{-1} in pure graphite. In this mode two carbon atoms in a given layer
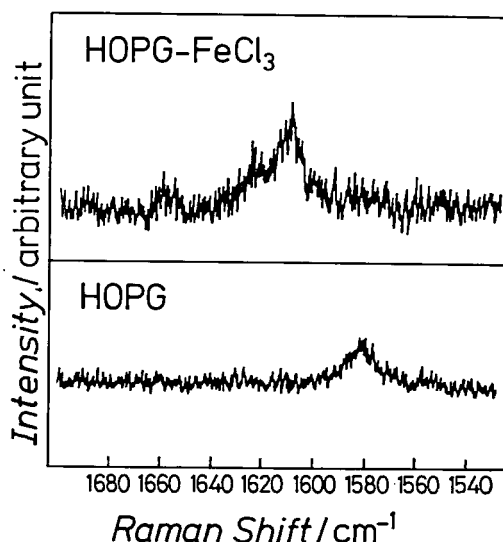

Figure 1. Room temperature Raman spectra of graphite and the intercalation compound of graphite-$FeCl_3$ (64 wt%, stage 1). HOPG refers to highly orientated pyrolytic graphite.

Figure 2. Symmetry species and schematic atomic displacements of the eigenmodes of graphite. Raman and IR activities are indicated in the parentheses by R and IR, respectively. Carbon atoms ● O are in the same layer, other atoms ⊙ ⊕ are in the nearest neighbor layer.

vibrate out of phase in the plane, but its frequency is rather considerably influenced by the neighboring intercalant layers, that will give a key to obtain informations on the bonding character between layers.

We found also one mode at 460 cm^{-1} in the intercalation compound of graphite-$FeCl_3$ (stage 1), which might be an intercalant mode. Further studies will be necessary to analyze the intercalant mode, which may give straightforwardly informations about chemical bonding in this compound.

We are attempting to synthesize intercalation

compounds of graphite-metal halides with several metal oxidation states and stage numbers, in order to study their Raman scattering.

References

1) K. Ohhashi and I. Tsujikawa, *Tanso* (in Japanese) No. 95, 154 (1978).
2) N. Caswell and S. A. Solin, *Solid State Commun.*, 27, 961 (1978).
3) K. Ohhashi, T. Shinjo, T. Takada, and I. Tsujikawa, *J. Phys. (Paris) Colloq.*, C-2 40, 269 (1979).

IV—E Studies of Ion-Molecule Reactions by a Threshold Electron-Secondary Ion Coincidence Technique

Recently it has generally been agreed that a complete understanding of a chemical reaction — this is one of the main goals of chemistry — requires knowledge of the microscopic rate constant for evolution of a system in a single reactant quantum state (translational, rotational, vibrational, and electronic) to a single product quantum state. In neutral-neutral reactions, the access to this "state-to-state" rate constant has been made possible by the advent of new techniques, such as molecular beams and lasers, which prepare and probe these states. Ion-molecule reactions, on the other hand, afford different approaches toward this microscopic rate constants since ions can readily be prepared in various internal states in the initial ionization processes, such as photoionization, and the emitted photoelectrons provide information on the distribution among these states.

In order to contribute toward this common goal of chemistry, we are studying state-selected ion-molecule reactions by the use of a technique which utilizes threshold electron-secondary ion coincidence. The technique allows direct measurements of $k(i,v)$, namely, the reaction rate constant as a function of internal and translational energies of the reactants. Distinct from previous methods for studying state-selected reactions, this technique has versatility which promises a wide variety of future studies to be made.

IV-E-1 Vibrational and Translational Energy Dependence of the Reaction Cross Section for $H_2^+ + H_2 \rightarrow H_3^+ + H$

Inosuke KOYANO and Kenichiro TANAKA

[*J. Chem. Phys.* 69, 3422 (1978)]

The first application of the threshold electron-secondary ion coincidence technique to the reaction

$$H_2^+(v) + H_2 \rightarrow H_3^+ + H \tag{1}$$

has been reported in the previous Reviwe.[1] The vibrational energy dependence of the reaction cross section was examined for vibrational states v=0—3 of the reactant ion at two different collision energies. It was found that while the cross section decreased with increasing vibrational quantum number at both collision energies, the decreasing trend was much less prominent for the higher collision energy than for the lower collision energy.

As a continuation of this work, we have performed more detailed investigation of reaction (1), covering a wider range of collision energies and also going up to v=5 in the case of the lowest collision energy. Much longer accumulation times than before were utilized in the present study, especially for the secondary ions, in order to improve S/N ratio. The apparatus and the principle of operation have been described previously.[2]

Figure 1 summarizes the results obtained at three different average collision energies $\bar{E}_{cm}$ (indicated in the figure). As can be seen from the figure, it has clearly been shown that the rather sharp decrease in
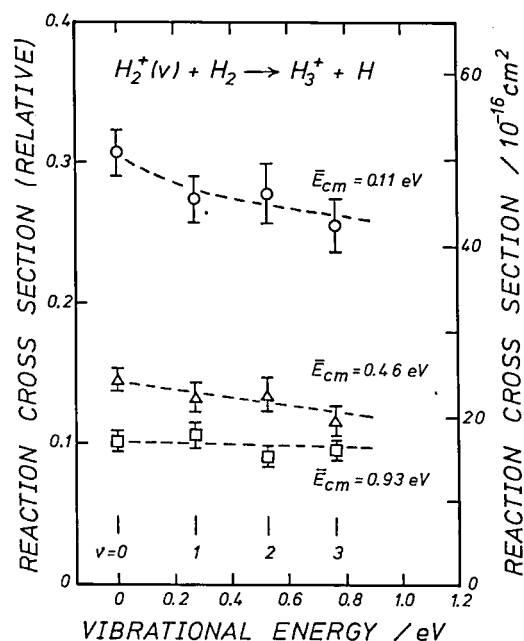
Figure 1. Cross section for the reaction H_2^+ (v) $+ H_2 \rightarrow H_3^+$ $+ H$ as a function of vibrational energy of H_2^+, obtained at three different average collision energies indicated.

the cross section (with increasing vibrational quantum number) observed at the lowest collision energy becomes less and less prominent as collision energy increases, and finally the cross section becomes almost independent of the vibrational quantum number at the highest collision energy studied.

It has been suggested that there is an increases in the reaction cross section from v=3 to v=4 at thermal collision energies.[3] In order to test this point, we
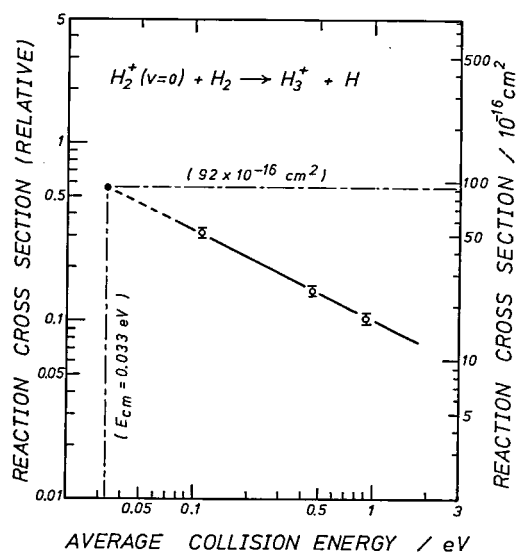
Figure 2. Cross section for the reaction H_2^+ (v=0) + H_2 → H_3^+ + H, plotted as a function of the average collision energy ($\overline{E}_{cm}$).

other vibrational states do not obey this equation so well is evident from the different vibrational energy dependences for different collision energies shown in Figure 1. However, there are no *a priori* reasons that the v=0 reactants should and other reactants should not obey the Langevin equation, since the Langevin theory has nothing to do with the structure or internal energy of reactants. The meaning of this finding remains still to be investigated.

The decrease in the cross section at low collision energies and its variation with collision energy have not yet been interpreted satisfactorily. A phase space theoretical explanation based on the intermediate complex model[4] requires re-examination, since recent diatomics-in-molecules calculation of the potential energy surfaces for the H_4^+ system and other experimental evidences all indicate that there is no potential minimum along the reaction coordinate of H_2^+ + H_2.[5] A view which involves a transition between the ground state and the first excited state potential surfaces[6] may also require re-examination since only the trapezoidal configuration of approach is taken into account there. We are now investigating other possibilities one of which involves a vibrational energy dependent repulsion at long distances of approach.

have extended our measurement at the lowest collision energy (0.11 eV, CM) to include the vibrational states up to v=5. The result indicated that there is no such increase in the region up to v=5.

The collision energy dependence of ion-molecule cross sections is usually discussed in terms of the Langevin equation. However there has been no examination of this equation with state selected cross sections. Thus it is very interesting to find in the present study that the v=0 results best obey this equation, namely the $\overline{E}_{cm}^{-1/2}$ dependence of cross section, as shown in Figure 2. That the results for

References

1) I. Koyano and K. Tanaka, *IMS Ann. Rev.*, 74 (1978).
2) K. Tanaka and I. Koyano, *IMS Ann. Rev.*, 73 (1978).
3) A. J. Yencha, A. Munzer and A. Niehaus, *Abstract of Papers, XI ICPEAC*, Kyoto, (1979), p. 902
4) W. A. Chupka, M. E. Russell and K. Refaey, *J. Chem. Phys.*, 48, 1518 (1968).
5) J. R. Stine and J. T. Muckerman, *J. Chem. Phys.*, 68, 185 (1978).
6) J. R. Krenos, K. K. Lehmann, J. C. Tully, P. M. Hierl and G. P. Smith, *Chem. Phys.*, 16, 109 (1976).

IV—F Photoionization Processes in Small Molecules

Two techniques have generally been used for the study of molecular photoionization processes, i.e., measurements of photoionization efficiency curves (PIEC) and photoelectron spectra (PES). While PIEC yields much valuable information on the ionization processes and energy levels of ions and neutral molecules, difficulty is often encountered with this technique when autoionization obscures the step structure of the curve. In such a situation, we often resort to PES which provides precise locations of ionic states and transition probabilities to these states. However, ionic states that can be studied by the ordinary (constant wavelength) PES are largely limited to the states which combine with the ground state of the parent molecule with favorable Franck-Condon factors.

Another type of photoelectron spectroscopy is threshold electron spectroscopy which uses a variable wavelength light source and detects only the zero kinetic energy photoelectrons (threshold electrons). In this method, ionic states which are not favored by direct ionization are often observed through autoionization, since threshold electrons are produced if an autoionizing state has the same energy as one of the ionic states and the autoionizing transition between them is allowed by selection rules.

Thus it is evident that both of these complementary techniques are necessary for a complete study of photoionization. In this project, we are studying photoionization processes in small molecules by simultaneous measurements of photoionization efficiency curves and threshold electron spectra. So far, H_2, N_2, O_2, and CO have been studied.

102

IV-F-1 Photoionization Efficiency Curve and Threshold Electron Spectrum of CO

Kenichiro TANAKA and Inosuke KOYANO

As one of the extensive studies on photoionization processes in small molecules, we have investigated the photoionization efficiency curve (PIEC) and threshold electron spectrum (TES) of carbon monoxide. The apparatus used was exactly the same as that reported previously[1] except that the resolution of the threshold electron analyzer was improved and the apparent resolution of threshold electron spectra of about 14 meV FWHM (as determined by the $^2P_{1/2}$ peak of Ar) was now attained. Mass-analyzed CO^+ ions and threshold electrons were measured simultaneously at 0.1 Å intervals with 40 seconds signal accumulation time at each point.

Figure 1 shows the whole spectra of the PIEC (top) and the TES (bottom) obtained. Positions of various Rydberg (autoionizing) states as obtained by spectroscopy are also shown in the PIEC, and the locations of vibrational levels in the $X^2\Sigma^+$, $A^2\Pi$, and $B^2\Sigma^+$ states of CO^+ also taken from a compilation of spectroscopic data[2] are indicated in the TES. An enlarged drawing of a part of the spectra is shown in Figure 2 (top and middle) to emphasize the doublet nature of the $A^2\Pi$ peaks. The shape and position of
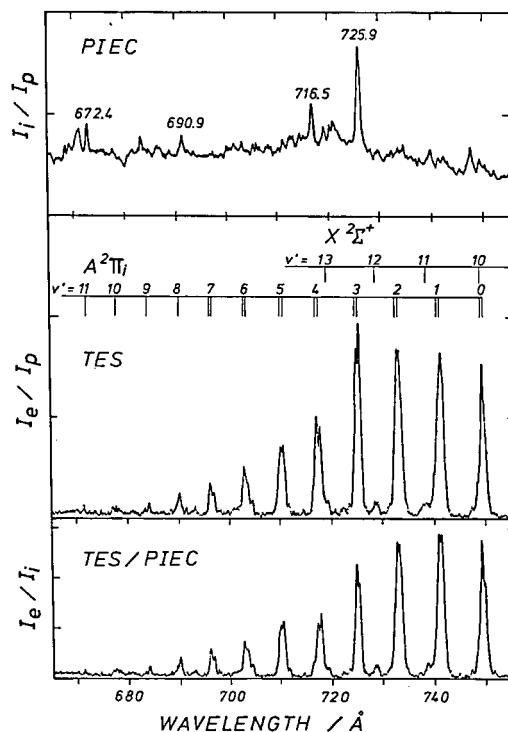

Figure 2. Photoionization efficiency curve (PIEC) and threshold electron spectrum (TES) of CO in the CO^+ $A^2\Pi_i$ region, showing double peaks due to the spin-orbit interaction. Also shown is the ratio of the two spectra (TES/PIEC).
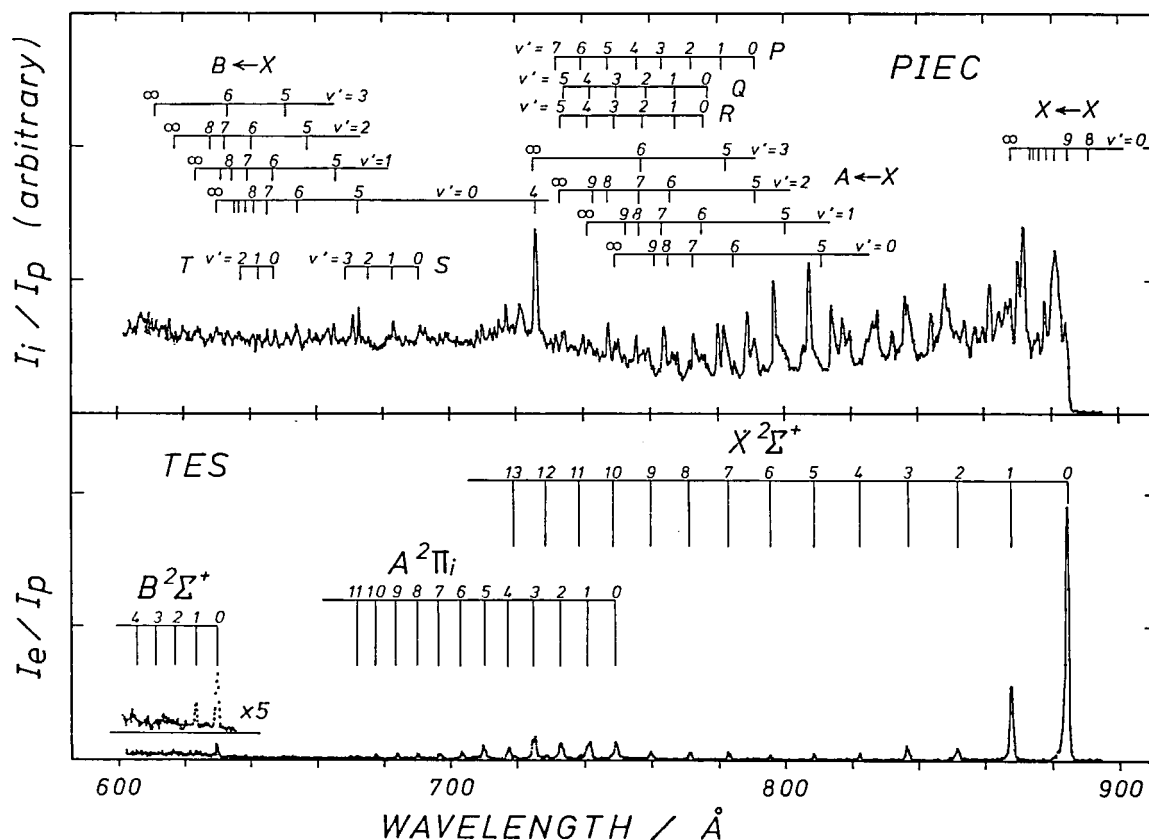

Figure 1. Photoionization efficiency curve (PIEC) and threshold electron spectrum (TES) of CO between 600 - 900 Å.

a TES peak are strongly affected by the occurrence of autoionization peaks at or near the relevant threshold. Thus the plot of the ratio of the threshold electron intensity to the ion intensity often gives more accurate threshold energy of each ionic state. Such a plot (TES/PIEC) is also shown in Figure 2 (bottom).

From the TES in Figure 1, several prominent features can be seen. First of all, all the vibrational levels up to v'=13 have been observed for the $X^2\Sigma^+$ ground state, in contrast with only two levels that can be observed in the HeI PES (v'=0 and 1). This indicates, as discussed in the introductory section of this project, that at least one autoionizing state is exactly overlapped on these ionic levels, and that the autoionizing transitions between these two overlapping levels are favored by selection rules. The threshold energy values for these 14 vibrational levels have been determined within our experimental accuracy of ± 12 meV.

In the transition to the $A^2\Pi_i$ state, the Franck-Condon factors have appreciable values up to v'=11, and thus the TES gave almost the same information as the HeI PES as long as the number and rough positions of the vibrational levels were concerned. However, the intensity distribution of the TES was different from that expected from the Franck-Condon factors and this again yielded information on the autoionizing states. In addition, the doublet structure due to spin-orbit splitting has been observed in our TES for almost all levels of the $A^2\Pi_i$ state. The average energy separation of these doublet peaks has been determined as 10 ± 7 meV, which is to be compared with the spectroscopic value of 14.6 meV.[1]

References
1) K. Tanaka and I. Koyano, IMS Ann. Rev., 75 (1978).
2) P. H. Krupenie, Natl. Stand. Ref. Data Ser. — Natl. Bur. Stand., 5, (1966).

IV—G Studies of Formation and Destruction Mechanisms of Interstellar Molecules

Recent discoveries of a large variety of molecules, including complex organic ones, in interstellar space of our galaxy stimulated not only astrophysicists but also chemists to wonder and investigate how these molecules were formed under the physical conditions prevailing in interstellar space. Among several mechanisms which have been proposed, the gas-phase and grain surface molecular synthesis models are most intriguing to chemists. The only promising gas phase models are those involving ion-molecule reactions, since rates of most neutral reactions are not sufficiently large at interstellar temperatures because of activation energies required.

In this project, we are carrying out non-steady-state calculations of the abundance of these molecules based on an ion-molecule reaction model. Emphasis is placed on the extension of previous calculations to include molecules with more than five atoms and to predict abundance of molecules which have not yet been detected because of the lack of dipole moment.
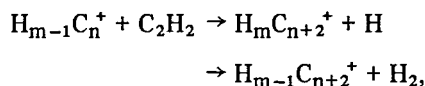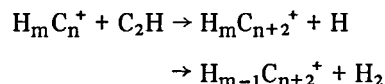
IV-G-1 Formation of HC_nN (n = 3,5,7,9) molecules in Dense Interstellar Clouds by Ion-Molecule Reactions.

Kenichiro TANAKA, Hideo YAMAZAKI (Tokyo Institute of Technology) and Inosuke KOYANO

The recent detections of the n=5,7, and 9 members of the HC_nN series of compounds (cyanopolyyne) in interstellar clouds have prompted us to examine whether the existence of these species can be explained by a simple extension of our gas phase ion-molecule reaction model.[1] For this purpose, 20 new species (10 neutrals and 10 ions) and 34 new reactions (24 rearrangement and 10 ion-electron recombination reactions) were added to our previous model of 71 species and 204 reactions, and coupled differential equations were solved time-dependently. New species added are C_4H, C_4H_2, C_6H, C_6H_2, C_8H, C_8H_2, HC_3N, HC_5N, HC_7N, HC_9N, $C_4H_2^+$, $C_4H_3^+$, $C_6H_2^+$, $C_6H_3^+$, $C_8H_2^+$, $C_8H_3^+$, $H_2C_3N^+$, $H_2C_5N^+$, $H_2C_7N^+$, and $H_2C_9N^+$.

As a first try, successive C-C bond formation was assumed to be achieved in the ion by the reactions with the most abundant neutrals C_2H and C_2H_2:

$$H_mC_n^+ + C_2H \rightarrow H_mC_{n+2}^+ + H$$

$$\rightarrow H_{m-1}C_{n+2}^+ + H_2$$

$$H_{m-1}C_n^+ + C_2H_2 \rightarrow H_mC_{n+2}^+ + H$$

$$\rightarrow H_{m-1}C_{n+2}^+ + H_2,$$

where n=2,4, and 6, and m=2 for n=2 and 3 for n=4 and 6. C-N bond formation was accomplished by the ion-molecule reactions

$$C_{n-1}H_2^+ + HCN \rightarrow H_2C_nN^+ + H$$

$$C_{n-1}H_3^+ + HCN \rightarrow H_2C_nN^+ + H_2$$
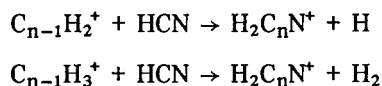
where n=3,5,7, and 9. Neutral cyanopolyynes HC_nN were then formed by the dissociative recombination reactions

$$H_2C_nN^+ + e \rightarrow HC_nN + H.$$
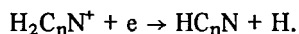
Bond formation in the ion is always in competition

with neutralization and the outcome of this competition determines the relative abundances of the ions and the neutral products. Thus the neutralization reactions of hydrocarbon ions

$$C_nH_2^+ + e \rightarrow C_nH + H$$

$$C_nH_3^+ + e \rightarrow C_nH_2 + H$$
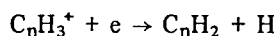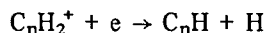
where n=4,6, and 8, were also included in the scheme.

As no experimental data exist on the rate constants of these reactions, Langevin rate constants were used for all of the rearrangement-type reactions with appropriate branching ratios. Rate constants for the electron-ion recombination reactions were set to be 1×10^{-6} cm^{3}s^{-1}.

Calculations are preliminary so far. However, the results showed that gas phase ion-molecule reactions are indeed capable of synthesizing reasonable amount of cyanopolyynes in the time scale of $10^6 \sim 10^8$ years. The density relation $[HC_7N]/[HC_9N] \sim [HC_5N]/[HC_7N] \sim 4$ as observed in Heiles' cloud 2 was not obtained in the present calculation, however.

Refinement of the model and the method of calculations, as well as re-evaluation of the rate constants is in progress.

Reference

1) I. Koyano, K. Tanaka and H. Yamazaki, *IMS Ann. Rev.*, 77 (1978).

IV—H Vacuum UV Photoelectron Spectroscopy of Molecules

In gas-phase photoelectron spectroscopy, the ionization potential is an information obtained from the abscissa of a photoelectron spectrum, while its ordinate gives us information of photoelectron intensity which is closely associated with partial photoionization cross section and photoelectron angular distribution. In vacuum uv photoelectron spectroscopy, it has recently been possible to carry out quantitative intensity measurements of molecular photoelectron spectra. The photoelectron intensity data should be important for studying the processes of photoionization.

IV-H-1 Quantitative Measurements of Photoionization Cross Section of Simple Organic Compounds by Gas-Phase HeI (58.4 nm) Photoelectron Spectroscopy

Yohji ACHIBA, Tomoko YAMAZAKI *(Hokkaido Univ.)*, Shunji KATSUMATA *(Hokkaido Univ.)*, Noriyoshi KAKUTA, and Katsumi KIMURA

In spite of a great number of publications of HeI photoelectron spectra, quantitative nature of the photoelectron spectroscopy is still weak compared with other spectroscopies, for instance, optical absorption spectroscopy. Except for a small number of simple compounds, relative intensities among different molecular species have not been studied. The relative photoelectron intensity from molecule to molecule should be important from the analytical point of view as well as the theoretical point of view. Absolute values of photoionization cross section are of cource more important rather than the relative values especially from the theoretical point of view.

Previously, we have proposed an experimental method of determination of photoionization cross sections by means of vacuum uv photoelectron spectroscopy.[1] In this method, we use a mixture of two gases, a standard and a sample to be studied, to determine the relative peak height and band area. A careful correction should be made for the mole fraction of the binary mixture in the ionization chamber of our spectrometer by measuring gas pressure with two different gauges, one of which is

an MKS Baratron gauge and the other is a Pirani gauge that is sensitive to the type of gas. Another important correction should also be made for the electron collecting efficiency of our spectrometer. This has been done on the basis of Samson's method.[2] Figure 1 shows our scheme of determination of the partial photoionization cross section by the photoelectron spectroscopy.

In the present work we have determined the partial photoionization cross sections (σ) of π electrons at 58.4 nm photons for several typical unsaturated hydrocarbons using HeI photoelectron spectroscopy. Measurements of photoelectron band intensity were carried out with a transmission-corrected electron analyzer, by using a binary mixture of the compound studied and molecular nitrogen as a standard gas whose σ value is already known. In each case, the relative area of the ionization band
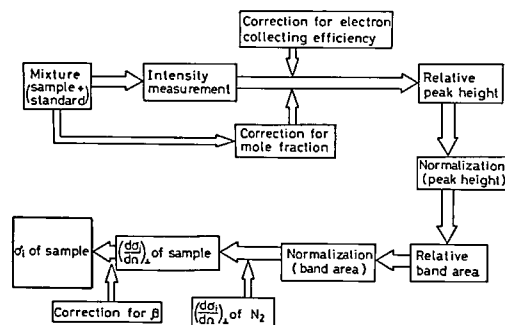

Figure 1. Flowchart for determination of relative and absolute photoionization cross section.

Table I. Partial Photoionization Cross of π Electrons in Unsaturated Hydrocarbons

Compound	σ(Mb)
$HC\equiv CH$	12.2 ± 0.6
$HC\equiv CCH_3$	12.3 ± 0.6
$H_2C=CH_2$	5.7 ± 0.5
$H_2C=CHCH_3$	5.8 ± 0.4
$H_2C=CH-CH=CH_2$	5.2 ± 0.4
Benzene	9.4 ± 0.9

Figure 1. Experimental β values at 58.4 and 30.4 nm and Manson's theoretical curve.[2] The β values obtained here for the $^2B_1$, $^2A_1$ and $^2B_2$ ionic states of H_2O are indicated by O, $\triangle$ and $\square$, respectively.

associated with the π-electron ionization was obtained with respect to the first ionization band of N_2, and relative band area was then converted to the corresponding σ value on the basis of $\sigma = 8.4$ Mb reported by Samson for the first band of N_2.

Table I summarizes the partial photoionization cross sections for the first π bands of the unsaturated compounds. From Table I the following tentative conclusions have been deduced. 1) The effect of methyl substitution is small. 2) The σ value (per one π orbital) of acetylene is slightly larger than that of ethylene. 3) The σ value (per one π orbital) decreases in the order of ethylene, butadiene and benzene.

References

1) K. Kimura, Y. Achiba, M. Morishita and T. Yamazaki, *J. Electron Spectrosc.*, **15**, 269 (1979).
2) J. A. R. Samson and J. L. Gardner, *J. Electron Spectrosc.*, **8**, 35 (1976).
3) J. A. R. Samson, G. N. Haddad and J. L. Gardner, *J. Phys. B*, **10**, 1749 (1977).

IV-H-2 Photoelectron Angular Distribution of Gaseous Compounds at 58.4 and 30.4 nm

Shunji KATSUMATA *(Hokkaido Univ.)*, Yohji ACHIBA and Katsumi KIMURA

The photoelectron angular distribution of free molecules for an unpolarized radiation is given by[1]

$$I(\theta) \propto 1 + (1/2)\beta[(3/2)\sin^2\theta - 1]$$

where $I(\theta)$ is the photoelectron intensity, θ is the angle between the incoming photon and the outgoing photoelectron, and β is the asymmetry parameter ranging from -1 to $+2$, depending upon the photon energy.

Our photoelectron angular distribution studies of gaseous compounds have been carried out for two purposes, one of which is to examine the difference in the asymmetry parameter (β) between HeI (58.4 nm) and HeII (30.4 nm) resonance sources for several simple compounds (H_2, N_2, O_2, H_2O, CO_2, CS_2), and the other is to study the chemical shift of β in the ionization bands associated with out-of-plane chlorine nonbonding orbitals in dichloroethylenes (*cis*, *trans*, and *iso*).
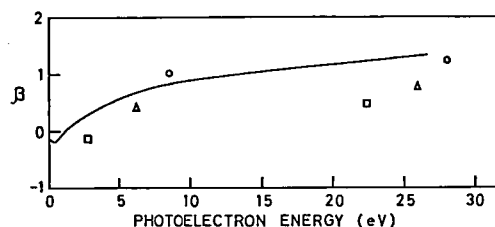
HeI and HeII photoelectron angular distribution measurements were carried out with a spectrometer, Model ADES-400 (VG Scientific Ltd.) in Institute of Applied Electricity, Hokkaido University. Each value of β has been obtained from a set of two photoelectron bands at 90° and 135°

For H_2O, CO_2 and CS_2, it has been concluded that on going from HeI to HeII radiation the energy dependence of β for the nonbonding orbitals of the triatomic molecules is similar to that obtained theoretically by Manson[2] for the corresponding atomic p shells. In Figure 1, the experimental β values are compared with a theoretical curve of Manson.[2] For N_2, it has been found that there is essentially no difference in β between two vibrational peaks ($v' = 0$ and 1) of the first band in the HeII spectrum, whereas in the HeI spectrum an anomalous variation is observed in β between the two peaks, as originally indicated by Carlson.[3] A preliminary report of our β values of N_2, O_2, CO_2 and CS_2 at 58.4 and 30.4 nm has been published elsewhere,[4] and a more detail report including H_2O is published elsewhere.[5]

For H_2 it has been found that there is a little variation of β with photon energy between HeI and HeII radiation, as recently suggested theoretically by Itikawa.[6]

Concerning the photoelectron bands associated with the out-of-plane chlorine nonbonding orbitals, $n(Cl)_+$ in dichloroethylenes, we have found that the β values of the $n(Cl)_-$ orbital is higher than that of the $n(Cl)_+$ orbital which interacts with the $\pi(C=C)$ orbital. The orbital assignments of the HeI photoelectron spectra have been reinvestigated on the basis of the β values obtained here.

References

1) T. A. Carlson and A. E. Jonas, *J. Chem. Phys.*, **55**, 4913 (1971).
2) S. T. Manson, *J. Electron Spectrosc.*, **1**, 413 (1972/73); **2**, 482 (1973).
3) T. A. Carlson, *Chem. Phys. Lett.*, **9**, 23 (1971).
4) S. Katsumata and K. Kimura, *Japan J. Appl. Phys., Supplement* **17-2**, 252 (1978).
5) S. Katsumata, Y. Achiba and K. Kimura, *J. Electron Spectrosc.*, **17**, 229 (1979).
6) Y. Itikawa, *Chem. Phys.*, **30**, 109 (1978); *Chem. Phys. Lett.*, **62**, 261 (1979).

RESEARCH ACTIVITIES V

Division of Applied Molecular Science

Various steps of breakthrough in molecular science have been achieved either by invention of a new methodology based on a physical principle or by discovery of new materials. The research in the division aims at developing new findings and methodologies in molecular science to be adapted for researches in adjoining fields of science. At the same time, introduction of new materials and reactions of interest to theoreticians, spectroscopists and solid state physicists is eagerly desired.

Physical organic chemistry is one of the main themes of this laboratory. Syntheses of molecules of theoretical interest, photochemistry of aromatic compounds to give well-defined intermediates, and structural and dynamical studies by multi-nuclear NMR have been actively carried out. Preparation and structural studies of novel coordination compounds are another subject of this laboratory. UV and CD spectroscopy as well as X-ray crystallography are effectively employed.

V—A   Syntheses and Physico-chemical Properties of Bridged Aromatic Compounds

We are interested in elucidating the structural and electronic factors intimately related to development of particular solid state physical properties such as photoconductivity and superconductivity in order to design these properties at molecular levels. One of possible approaches is to simulate the crystal and electronic structures of the known compounds which exhibit such properties. Attempts have been made to synthesize a series of compounds which incorporate aromatic rings in the three dimensional framework.

Triptycene and cyclophane derivatives made of the donor and acceptor rings are a couple of examples. As a continuation of the work on an intramolecular triptycene quinhydrone which exhibited an interesting charge-transfer and electrochemical behavior, we have examined two internal quinhydrones derived from triptycene triquinone. Irradiation of triptycene derivatives gave a novel condensed aromatic ring.

V-A-1   Intramolecular Triptycene Quinhydrones. III. Two Quinhydrones Derived from 9,10-Dihydro-9,10 [1',2'] benzenoanthracene-1,4,5,8,11,14-hexaone

Hiizu IWAMURA, Takahiko OOSUMI (Ehime Univ. and IMS) and Fumio TODA (Ehime Univ.)

Effects of geometry and conformation on the charge transfer and exciplex interactions have been the subject of extensive studies. Efforts have so far been directed towards the design of most favorable situations. A series of [2.2]-paracyclophane quinhydrones by Staab, et al.,[1] are one of the most successful examples. In a previous paper,[2] we offered the other extreme case; the π-donor and acceptor rings are apparently under unfavorable circumstances, and yet show a surprisingly strong interaction in 1. In order to see the electronic effect of the third ring on the donor-acceptor interaction in 1, intramolecular quinhydrones Q_2H and QH_2 derived from title compound Q_3 have now been examined.

The Diels-Alder reaction of 1,4,5,8-tetraacetoxyanthracene with p-benzoquinone followed by standard

reactions gave triptycene trihydroquinone H_3 which was then oxidized to give triptycene triquinone Q_3. When H_3 and Q_3 were mixed in a polar solvent, intramolecular quinhydrones Q_2H and QH_2 were gradually formed as monitored by ^1H NMR (see Table I). Q_2H was favored over QH_2 in equilibrium expressed by equation 1. The $[Q_2H]/[QH_2]$ value of 1.94 at 20°C in DMSO-d_6, for example, decreased to 1.18 at 60°C.

The electronic spectra of the above equilibrium mixture were analyzed to give the values in Table II for the CT absorption. Thus the CT bands in Q_2H are shifted to the longer wave length than in QH_2, showing again the stronger internal interaction in the former quinhydrone. All the results are in harmony with our previous proposal;[2] through-bond $\sigma(C-C)$-π interaction between the H and Q rings (2) has now been exalted by introduction of the electron-demanding third ring in the triptycene framework.

Reference
1) W. Rebafka and H. A. Staab, Angew, Chem., Internat. Ed., 12, 776 (1973); 13, 203 (1974).
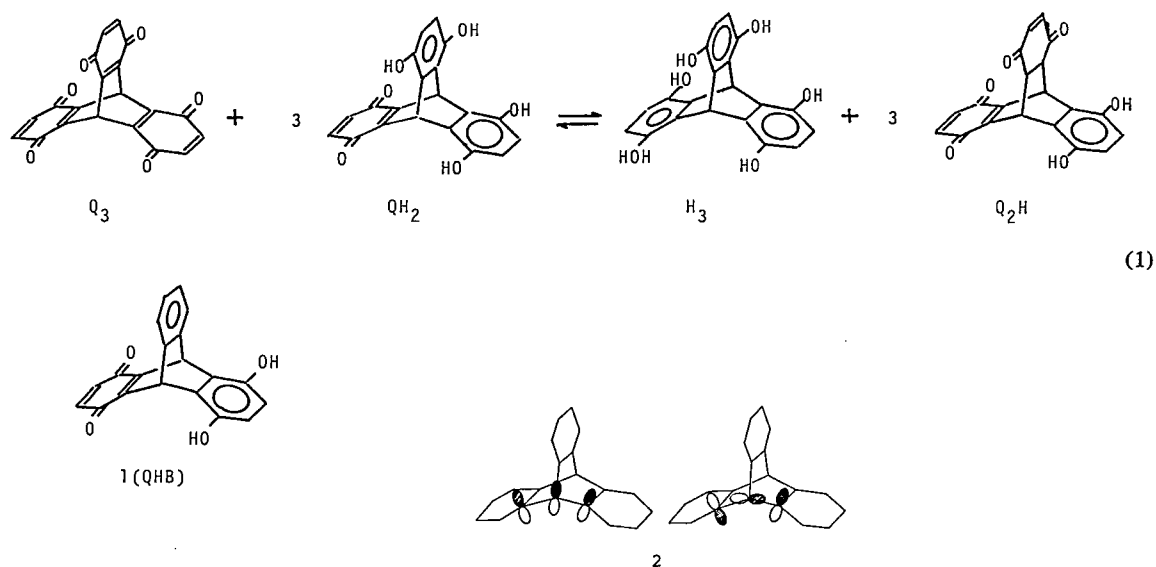2) H. Iwamura and K. Makino, J. Chem. Soc., Chem. Commun., 720 (1978).

Figure 1.

Table I. ^{1}H NMR Chemical Shift Data for the Internal Triptycene Quinhydrones

Compound	Bridgehead	H-Ring	Q-Ring	B-Ring		OH
Q_2H			6.69 (2)	—		
QH_2			6.73 (4)	—		
Q_3	6.13 (2)	—	6.79 (6)	—		
H_3	6.37 (2)	6.26 (2)	—			
QHB	6.03 (2)	6.36 (2)	6.70 (2)	$\begin{Bmatrix}6.90-7.15\\7.35-7.60\end{Bmatrix}$	(4)	8.98 (2)
Q_2B	5.99 (2)	—	6.76 (2)	$\begin{Bmatrix}7.00-7.25\\7.45-7.70\end{Bmatrix}$	(4)	—
H_2B	6.09 (2)	6.29 (4)	—	$\begin{Bmatrix}6.85-7.10\\7.20-7.45\end{Bmatrix}$	(4)	8.66 (4)
QB_2	5.88 (2)	—	6.76 (2)	$\begin{Bmatrix}6.90-7.15\\7.40-7.65\end{Bmatrix}$	(8)	—
HB_2	5.83 (2)	6.37 (2)		$\begin{Bmatrix}6.89-7.06\\7.40-7.46\end{Bmatrix}$	(8)	8.82 (2)

in DMSO-d_6 at 35°C referenced to internal TMS. Number of protons in parentheses.

Table II. Charge-transfer Bands (in DMSO) due to Triptycene Quinhydrones

Compound	λ_{max}	log ϵ	λ_{max}	log ϵ
QHB	430	2.63	500	2.32
QH_2	440	2.98	520	2.72
Q_2H	500	2.47	640	2.1

V-A-2 Syntheses of Multi-layered Charge Transfer Cyclophanes

Yoshiteru SAKATA (Univ. of Osaka and IMS)

Triple- and quadruple-layered CT cyclophanes (eg., 1–3) have been prepared to investigate the behavior of the inner benzene rings, which are sandwiched by a donor and an acceptor.
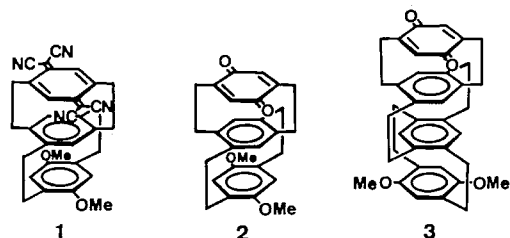
From the CT band maxima of a series of multi-layered cyclophanes (1:λ_{max} 640 nm; ϵ 1880. 2: λ_{max} 436; ϵ 1780),[1] it has been shown that the substituent effect of dimethoxy groups on CT transitions is largest for the second ring faced to the acceptor, moderate for the third ring, and smallest for the fourth ring. Therefore it is concluded that

in a series of multi-layered CT cyclophanes the CT stabilization is affected slightly by relatively weak and decreasing π-basicity of the third and fourth rings.

Reference
1) H. Tatemitsu, B. Natsume, M. Yoshida, Y. Sakata, and S. Misumi, Tetrahedron Lett., 3459 (1978).

V-A-3 A Dibenzo(Harfner's Hydrocarbon), Benz[a] indeno[1,2,3-cd] azulene

Yuzo KAWADA, Hideyuki TUKADA (Univ. of Tokyo), and Hiizu IWAMURA

Photoisomer 1 of triptycene undergoes thermal isomerization in protic solvents to give 8,12b-dihydro-benz[a]aceanthrylene 2.[1] A unique norcaradiene structure in 1 suggests that, when position 7 is substituted with a moderate leaving group as in 4, a novel condensed aromatic ring 5 would be formed.

The idea was born out by irradiation of 1-methyl-thio-(X = SCH₃) and 1-phenoxy-(X = OPh) triptycenes 6 which should afford 4. When a 2 mM solution of 6a in cyclohexane was irradiated with a low pressure mercury lamp in an immersion apparatus, a 79% consumption of the starting material was effected in 2 h. The mixture was separated by chromatography on the Lobar column to give 5 in 28% yield together with 3 (15%) and 7a (7.5%). The structure of 5 was shown by its NMR spectra. ¹H NMR (CDCl₃) δ 7.40 (2H, t), 7.71 (2H, t), 7.8–8.1 (4H, m) and 8.3–8.5 (4H, m). ¹³C NMR (CDCl₃) δ 120.0, 122.8, 123.2, 123.6, 129.4 (quaternary), 130.3, 131.0, 138.1 (quaternary), 138.4, 139.8 and 141.0. The hydrocarbon was obtained similarly from irradiation of 6b.

$\underline{6}$ $\underline{a}$ (X = SCH₃) $\underline{b}$ (X = OPh) $\underline{7}$
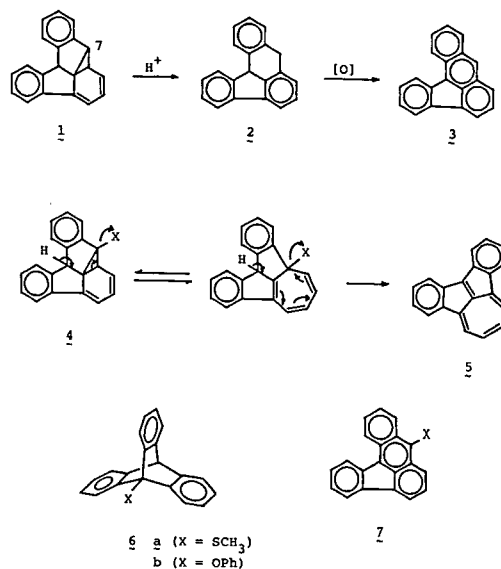
The pentacyclic compound 5 corresponds structurally to a dibenzo derivative of the less stable isomer of the Hafner's hydrocarbons,[2] and yet was found to be very stable under ambient conditions. The stability will be rationalized in terms of the added two benzene rings which replaced the bonds with highest double bond character in the parent tricyclic hydrocarbon.

A donor property of 5 is under scrutiny.

References
1) H. Iwamura and K. Yoshimura, J. Am. Chem. Soc., 96, 2652 (1974); H. Iwamura and H. Tukada, Tetrahedron Lett., 3451 (1978).
2) K. Hafner and J. Schneider, Ann., 624, 37 (1959); K. Hafner, K.-P. Meinhardt, and W. Richarz, Angew. Chem., Internat. Edit., 13, 204 (1974).

V—B Structural and Kinetic Studies by Means of NMR of Other Nuclei

NMR studies of nuclei other than ¹H, ¹³C, ¹⁹F and ³¹P have been actively carried out in these laboratories. This year special emphasis was paid on ¹⁷O in natural abundance.

The first observation of ¹⁷O nuclear magnetic resonance signals was reported as early as in 1951. Chemical shifts of more than one hundred organic compounds with relatively small molecular weight were documented by Christ et al. in 1961. Wider applications of the ¹⁷O NMR technique have since been hampered both by a low natural abundance (0.037%) and by an appreciable electric quadrupole moment ($Q = -2.6 \times 10^{-26}$ cm²) which effects line broadening of ¹⁷O signals. Recent advances in FT-NMR instrumentation together with rf units with a frequency synthesizer and probe heads with a tunable preamplifier have made observation of ¹⁷O NMR routinely available on samples with ¹⁷O isotope in natural abundance. In view of an important role of oxygen-containing functions in chemistry, establishment of a useful ¹⁷O NMR shifts vs. structure correlation is indispensable.

We have first optimized the experimental conditions for the FT measurements and obtained ¹⁷O chemical shifts of a variety of dicoordinated oxygen functions. The ¹⁷O chemical shifts which cover a range as large as several hundred ppm are primarily governed by the sum of electronegativity of the first atoms or groups attached to the central oxygen. The downfield shift due to β-methyl groups in alcohols and ethers is in parallel with decrease in their ionization potentials, demonstrating the importance of the paramagnetic screening term in the ¹⁷O shifts of these compounds. Diamagnetic shift due to γ-carbons and -oxygens has also been disclosed.

The ¹⁷O NMR studies were then extended to the substituent effects on the anisole derivatives. The usefulness of ¹⁷O NMR as a structural probe was demonstrated not only in typical organic substrates (e.g., oxiranes) but also in organometallic compounds, tungsten carbonyls.

V-B-1 ^{17}O NMR of Dicoordinated Oxygen Functions

Tadashi SUGAWARA, Yuzo KAWADA, Morimatsu KATOH, and Hiizu IWAMURA

Fourier transform ^{17}O NMR spectra have been measured for a number of alcohols, ethers, acetals, formates, acetates, and esters of inorganic acids in natural abundance at 10.8 MHz. The experimental conditions were optimized as follows. For a 8000 Hz spectral width, 320 data points in the time-domain spectra were used, the Fourier number being kept at 16384. The number of transients accumulated with a 90° pulse and an acquisition time of 0.02 s was in the range 10^4–10^5 to get spectra of reasonable S/N ratios. When a longer acquisition time (AT) of 0.1 s was employed, the number of data points (DP) increased to 1600 according to equation DP = 2 AT·SW (SW is a spectral width). The measurement under these conditions was found to be worse with respect to the S/N of spectra, not only because it required the accumulation time five times longer than the previous one to get the same sum of the number of transients, but also because it sampled mostly noise signals after the free induction signals practically decayed at $5T_1$(<0.02 s). The ^{17}O shifts and half-band-widths did not differ at all from those obtained under the standard conditions. Since quadrupole relaxation of ^{17}O nuclei is rapid, the use of long delay times between the end of each rf pulse and the beginning of data collection is not in principle necessary. Chemical shifts were measured as frequency shifts from the rf synthesizer frequency (10.782000 MHz) and expressed in ppm relative to the oxygen of water which resonated at 10.78321 MHz when measured in a capillary tube placed concentrically within a sample tube of 10 mm o.d. Chemical shifts are accurate to ± 1 ppm.

The ^{17}O chemical shifts have a wide range of a thousand ppm. This is quite large in reference to 10 ppm and 200 ppm of ^{1}H and ^{13}C shift ranges, respectively, of ordinary organic compounds and shows that ^{17}O NMR can be most informative as a structural prove. The water molecule has the oxygen atom which resonates at one of the highest field region and the resonance for the central oxygen atom of ozone appears at the extreme down field. Other data on the oxygens attached to various kinds of elements are scattered in-between. Changes in the oxygen-17 chemical shifts appear to be due primarily to alterations in the electron density at oxygen caused by changes in the electronegativity of α-atoms attached to the central oxygen atom. As illustrated by an approximately linear correlation in Figure 1, downfield shift is produced as more electronegative atoms are introduced. The line has a slope of about 270 ppm/electronegativity unit which is about six times as steep as those obtained by similar plots of the ^{13}C shifts.[1]
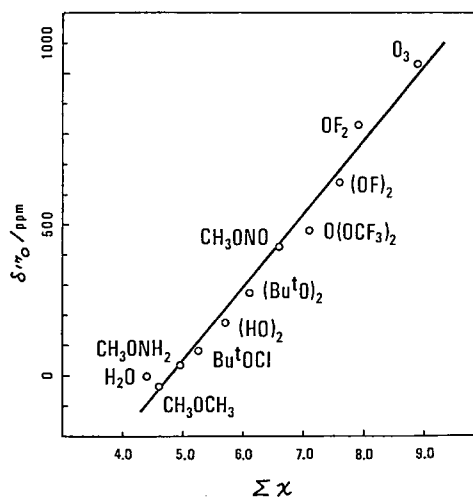
A reasonably smooth correlation is found in the

Figure 1. Plots of ^{17}O NMR shifts vs. the sum of the electronegativities for dicoordinated oxygen compounds. Electronegativities which are group values where relevant are from ref. 2.
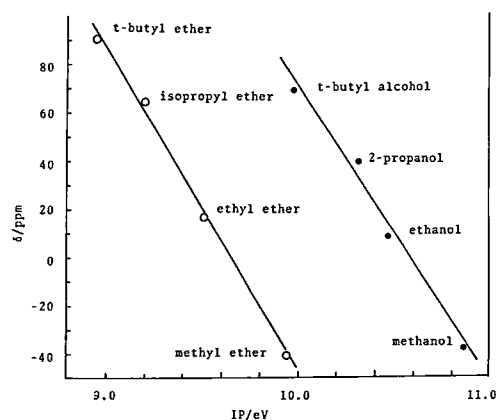
Figure 2. Plots of ^{17}O chemical shifts vs. the adiabatic ionization potentials (from ref. 3) of alcohols and ethers.

^{17}O chemical shifts vs. the ionization potentials plots both for alcohols and ethers as shown in Figure 2. The correlation will demonstrate that the energy levels of the oxygen n-electrons are more sensitive to the structural changes in the alkyl groups than the terminating orbital levels of oxygen and that the effective excitation energy ΔE gets smaller on going from methyl through ethyl and isopropyl to tert-butyl groups. The paramagnetic contribution to the total screening constant is concluded to be important in simple alcohols and ethers.

References

1) P. C. Lauterbur, Ann. N. Y. Acad. Sci., 70, 841 (1958); J. B. Lambert, D. A. Netzel, H. Sun, and K. K. Lilianstrom, J. Am. Chem. Soc., 98, 3778 (1976).
2) J. Hinze and H. H. Jaffe, J. Am. Chem. Soc., 84, 540 (1962); J. Hinze, M. A. Whitehead, and H. H. Jaffe, ibid., 85, 148 (1963); J. E. Huheey, J. Phys. Chem., 69, 3284 (1965); J. R. Van Wazer and J. H. Lecher, "Topics in Phosphorus Chemistry," Vol. 5, Chapt. 3, Interscience, New York, 1967.

3) B. J. Cocksey, H. H. D. Eland, and C. J. Danby, *J. Chem. Soc. (B)*, 790 (1971); F. Broglim, E. Heilbronner, J. Wirz, E. Kloster-Jensen, R. G. Bergman, K. P. C. Vollhardt, and A. J. Ashe III, *Helv. Chim. Acta*, 58, 2620 (1975).

V-B-2 ^{17}O Nuclear Magnetic Resonance Studies. V. ^{17}O Shieldings of Some Substituted Anisoles

Morimatsu KATOH, Tadashi SUGAWARA, Yuzo KAWADA, and Hiizu IWAMURA

Proton nuclear magnetic resonance studies have shown that methoxyl proton shifts are linearly related to the Hammett σ parameter.[1] A similar dependence albeit less pronounced of methoxyl ^{13}C shifts on the nuclear substitution has been reported.[2] In order to investigate the effects of nuclear substitution on the methoxyl oxygen shielding, we have now measured the ^{17}O NMR shifts of sixteen anisoles.

It is apparent from the observed data collected in Table I that the oxygen shifts are highly sensitive to meta and para substitution on the ring; they cover a rather wide total range of 30 ppm. When electron-withdrawing groups are introduced in the aromatic ring of anisoles, the shielding at the oxygen nucleus decreases through the conjugative electron release from the oxygen to the ring. Electron-donating groups increase the ^{17}O shielding of anisoles. A plot of the methoxyl oxygen shifts *versus* the Hammett σ^- values reveals a good linear correlation between the two parameters ($\rho = 16.2$ ppm, correlation coefficient r of 0.963). Analyses of the data according to the Yukawa-Tsuno equation, $\Delta\delta = \rho\{\sigma^\circ + \gamma(\sigma^- - \sigma^\circ)\}$, give the following values: $\rho = 17.2$ ppm and $\gamma = 0.881$.[3] A quantitative measure of the resonance interaction of the methoxyl group with para substituents is thus obtained. These results may be compared with the Hammett σ dependence of the methoxyl hydrogen ($\rho = 0.24$ ppm)[1] and carbon chemical shifts.[2]

Decrease of shielding with the increasing electron-withdrawal observed here should be explained by increase in the mean inverse cube of the 2p electron radius $<r^{-3}>_{oxygen}$ and/or in the orbital terms $[Q_{AA} + \sum_{B \neq A} Q_{AB}]$ in the Karplus-Pople expression of the paramagnetic screening (Eq. 1).[4] Decreasing charge density at the

$$\sigma^A_p = -\frac{e^2\hbar^2 <r^{-3}>}{2m^2c^2(\Delta E)} [Q_{AA} + \sum_{B \neq A} (Q_{AB})] \quad (1)$$

oxygen is expected to lead to a contraction of the 2p orbitals and thereby an increase in the paramagnetic screening. The observed ^{17}O chemical shifts are linearly correlated with the π-electron densities at the oxygen (2040 ppm/π-electron, r = 0.993) or with the π-bond orders between the oxygen and the aromatic carbon attached to it (4770 ppm/π-bond

Table I. ^{17}O NMR Shifts of para and meta Substituted Anisoles

Substituent	δ^{17}O/ppm	π-Bond Order $\times 10^2$	π-Electron Density b
p-NH$_2$	139^a	4.03	1.905
p-OCH$_3$	141	4.16	1.902
p-C(CH$_3$)$_3$	147		
p-CH$_3$	147	4.32	1.899
p-F	148	4.27	1.900
H	151	4.36	1.898
p-Cl			
p-Br	154		
p-CF$_3$	157		
p-CN	163	4.49	1.894
p-NO$_2$	170	4.72	1.888
m-NH$_2$	149		
m-Cl	154		
m-Br	155		
m-F	156		
m-NO$_2$	166		

a subtract 103 ppm from the shift values to convert them into the data referenced to external H$_2$O.

b The π-electron densities and π-bond orders were calculated by the CNDO/2 methods with the aid of the program No. 141 of QCPE on a HITAC M-180 system of this Institute. Molecular geometries employed for the framework of anisoles were basically those reported for 4,4'-anisoin and the standard bond lengths and angles were used otherwise.

order, r = 0.974) calculated by the CNDO/2 methods. The former values should be compared with 10 ppm and 160 ppm per π-electron shifts in ^{1}H and ^{13}C NMR, respectively.

The trend observed here for the anisoles is just the opposite to that of the oxygen nuclei of the aliphatic ethers in which the more electron-donating tertiary alkyl ethers are deshielded compared to less electron-donating primary alkyl ethers.[5] Whreas the change in the effective excitation energy ΔE in Eq. 1 was a dominant factor in the paramagnetic screening there,[5] both the n- and π^*-levels would be affected simultaneously by the ring substituents in the anisoles, leaving the effect of ΔE term less obvious.

We conclude that one of the most direct experimental evidence for the dependence of the electron density about the methoxyl oxygen nucleus on the ring substituents was obtained by the ^{17}O NMR shifts. Namely, the conjugative electron release from the oxygen of anisoles is about 90% of that in phenols.

References

1) C. Heathcick, *Can. J. Chem.*, 40, 1865 (1962).
2) K. S. Dhami and J. B. Stothers, *Can. J. Chem.*, 44, 2855 (1966).
3) Y. Tsuno, T. Ibata, and Y. Yukawa, *Bull. Chem. Soc. Japan*, 32, 960 (1959); Y. Yukawa, Y. Tsuno, and M. Sawada, *ibid.*, 39, 2274 (1966).
4) M. Karplus and J. A. Pople, *J. Chem. Phys.*, 38, 2803 (1963).
5) T. Sugawara, Y. Kawada, and H. Iwamura, *Chem. Lett.*, 1978, 1371; T. Sugawara, Y. Kawada, M. Katoh, and H. Iwamura, *Bull. Chem. Soc. Japan*, in press; C. Delseth and J. -P. Kintzinger, *Helv. Chim. Acta*, 61, 1327 (1978).

V-B-3 ^{17}O NMR Chemical Shifts *versus* Structure Relationships in Oxiranes

Hiizu IWAMURA, Tadashi SUGAWARA, Yuzo KAWADA, Kazuo TORI *(Shionogi Research Lab.)*, Ryonosuke MUNEYUKI *(Shionogi Research Lab.)* and Ryoji NOYORI *(Nagoya Univ.)*

We have shown that ^{17}O chemical shifts covering a more than 1000 ppm range are explained in terms of empirical rules which are in principle quite similar to those used to interpret ^{13}C NMR data. In order to demonstrate the usefulness of ^{17}O NMR as a structural probe of more subtle changes in structure and chemical bonding, we have now examined a series of oxiranes. The FT-experimental conditions on a Varian FT-80A spectrometer (10.78 MHz) were as follows: pulse width; 35 μs, acquisition time; 0.02 s, spectral width; 8000 Hz, number of transients; 10^6-10^7, Fourier number; 16384. The spectra were generally obtained at 34–36°C on pure samples made in these laboratories and dissolved in chloroform-d in a sample tube of 10 mm o.d.

Just as in ^{1}H and ^{13}C NMR of cyclopropanes, oxiranes, and aziridines, the oxygen nuclei of oxiranes

are most highly shielded among the ether family. Introduction of methyl groups to the three-membered ring leads to a gradual downfield shift as shown in Table 1: a 33 ppm downfield shift by one methyl group (1 → 3) and 59, 63, and 66 ppm shifts by two methyl groups (14, 15 and 16 relative to 1, respectively). The third methyl group appears to induce a downfield shift of 25 ppm (10 → 18). The resonance shift of tetramethyloxirane 21 is 47, 43, and 40 ppm downfield from those of dimethyloxiranes 14, 15 and 16, respectively. Thus, whereas the effects of polysubstitution are levelling off, there still holds an approximate additivity; one methyl group has the effect of inducing a ca. 30 ppm downfield shift. The value can be compared with 9.4 ppm of the β-methyl parameter in the additivity rule for the ^{13}C chemical shifts of alkanes.[1]

An upfield shift of ^{17}O resonance in norbornene *exo*-oxide 4 by 18 ppm relative to cyclohexene oxide 10 can be ascribed to the γ-effect. A similar but diminished amount of the effect is already evident in the corresponding cyclopropane derivatives as summarized in Figure 1. The steric γ-effect of an *exo*-cyclopropane ring on the methano-bridge carbon has been pointed out by the present authors;[2] the ^{13}C shift values of the tricyclic hydrocarbons are smaller

Table I. ^{17}O Chemical Shifts of Typical Oxiranes and ^{13}C Chemical Shift Data for the Methylene Carbons of Structurally Related Cyclopropanes.

| Oxirane	No.	δ_{17_O}	δ_{13_C}	Oxirane	No.	δ_{17_O}	δ_{13_C}
ethylene oxide	1	-49	-3.8	cycloheptene oxide	12	4	
1,2-butylene oxide	2	-18		cyclooctene oxide	13	9	
propylene oxide	3	-16	6.0	isobutylene oxide	14	10	14.1
norbornene *exo*-oxide	4	-15	1.2	*cis*-2-butene oxide	15	14	
epichlorohydrin	5	-14		*trans*-2-butene oxide	16	17	
cyclopentene oxide	6	-8	5.8	benzonorbornadiene *exo*-oxide	17	37.5	14.9
1,4-dihydronaphthalene oxide	7	-8	3.0	1-methylcyclohexene oxide	18	28	
styrene oxide	8	-6	9.1	α-piene oxide	19	34	
cycloocta-1,5-diene dioxide	9	2		norbornadiene *exo-oxide*	20	53	19.2
cyclohexene oxide	10	3	10.5	2,3-dimethyl-2-butene oxide	21	57	
cyclohexa-1,4-diene oxide	11	1	6.5				
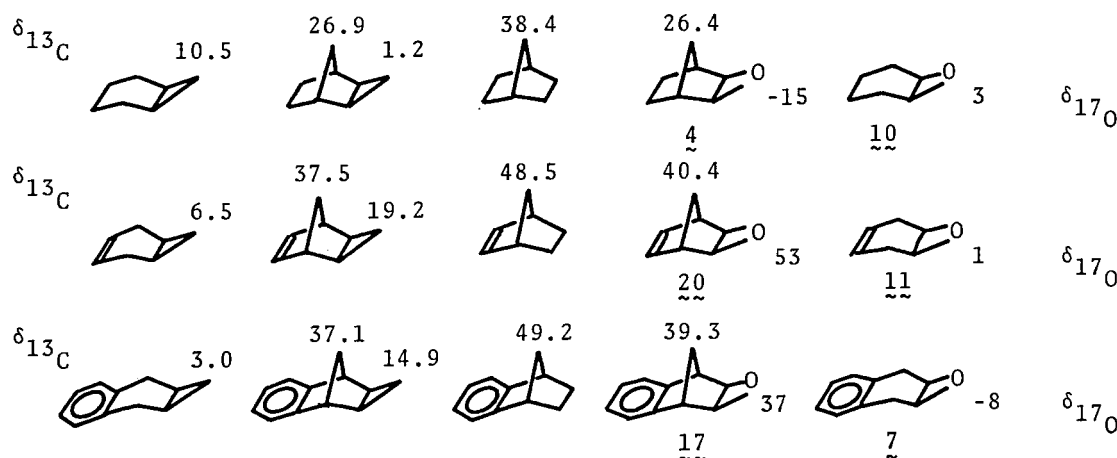
Figure 1. The γ-effects on ^{13}C and ^{17}O chemical shifts.

by 11.5, 11.0, and 12.1 ppm than those of norbornane, norbornene, and benzonorbornene, respectively (Figure 1). Similar γ-effects in ^{13}C shifts due to an exo-oxirane ring are obtained as reported: $\Delta\delta$ of -12.0, -8.1, and -9.9 ppm for 4, 20, and 17, respectively. It can be regarded as the counteraction of this γ-effect which is observed for the ^{17}O shift of 4 and described above.

The downfield ^{17}O shifts by 52 and 45 ppm in 20 and 17 relative to 11 and 7, respectively, and ^{13}C shifts by 12.7 and 11.9 ppm of the cyclopropane methylene in the corresponding tricyclohydrocarbons are unusual and may require some orbital interactions as follows to be taken into account. Just as through-space interaction between the π-orbitals in norbornadiene,[3] a significant overlap is expected between the π-orbital and the Walsh orbital of the oxirane ring beneath the carbon skeleton of norbornadiene exo-oxide 20. The π^* level of the ethylenic moiety mixes with the antibonding Walsh orbital to effect lowering of the π^* orbital (see Figure 2). As a result, an effective n→π^* excitation energy ΔE in Eq. 1 decreases and the paramagnetic screening will increase to give a downfield shift.

$$\sigma_p^A = -\frac{e^2\hbar^2<r^{-3}>}{2m^2c^2(\Delta E)}[Q_{AA} + \sum_{B\neq A}Q_{AB}]\qquad(1)$$

References

1) E. G. Paul and D. M. Grant, *J. Am. Chem. Soc.*, 85, 1701 (1963); D. M. Grant and E. G. Paul, *ibid.*, 86, 2984 (1964).
2) K. Tori, M. Ueyama, T. Tsuji, H. Matsumura, H. Tanida, H. Iwamura, K. Kushida, T. Nishida, and S. Satoh,

Tetrahedron Lett., 327 (1974); A. K. Cheng and J. B. Stothers, *Org. Magn. Reson.*, 9, 355 (1977).
3) R. Hoffmann, *Accounts Chem. Res.*, 4, 1 (1971).

V-B-4 NMR Studies on the Chemical Bonding in Some Tungsten Carbonyls LW (CO)$_5$. ^{17}O Chemical Shifts and One-bond Spin Coupling $^1J(^{183}W-^{13}C)$

Yuzo KAWADA, Tadashi SUGAWARA, and Hiizu IWAMURA

Metal carbonyl compounds of group VIb are the subject of great interest in many facets of chemistry.[1] In elucidating the structures of these compounds and the nature of the metal-to-ligand bonding therein, a number of modern spectroscopic methods have been employed with moderate to great success. As far as NMR spectroscopy is concerned, ^{13}C chemical shifts in the carbonyl group are not necessarily sensitive to variation in ligands. Spin-spin coupling constants are considered to be informative of the metal-to-ligand bonding as exemplified by $^1J(M-C)$ and $^2J(M-C-H)$ values in M = Pt, Hg, Pb and etc., but only a limited number of examples have so far been given for elements of the VIb family.

We have carried out the NMR measurements of ^{17}O chemical shifts and one-bond $^{183}W-^{13}C$ coupling constants for a series of LW (CO)$_5$ in which all nuclides are in natural abundance, and have found that the two NMR parameters serve as a more versatile and sensitive structural probe for metal carbonyls.

Experimental

^{17}O *Chemical Shifts.* The measurements were made on a Varian FT-80A spectrometer at 10.782 MHz. A 200–300 mg sample of the tungsten carbonyl was dissolved in 1.5 ml of CDCl$_3$ or CD$_3$CN which also provided the deuterium signal for the internal lock. The number of transients accumulated with a 90° pulse and an acquisition time of 0.03–0.05 s was in the range 10^4–10^5 to get spectra of reasonable S/N ratios. Chemical shifts were measured as frequency shifts from the synthesizer frequency and expressed in ppm relative to the oxygen of water.

$^1J(^{183}W-^{13}C)$. Coupling constants were read from the satellites of the carbonyl carbon signals obtained on a sample with added Cr(acac)$_3$(ca. 30 mg).

Materials. All the tungsten carbonyls employed in this study were prepared from tungsten hexacarbonyl and purified according to the literature.[2]

Results and Discussion

The results are summarized in Table I in which tungsten carbonyl are classified according to the kinds of ligands into five groups: carbenes, phosphines,
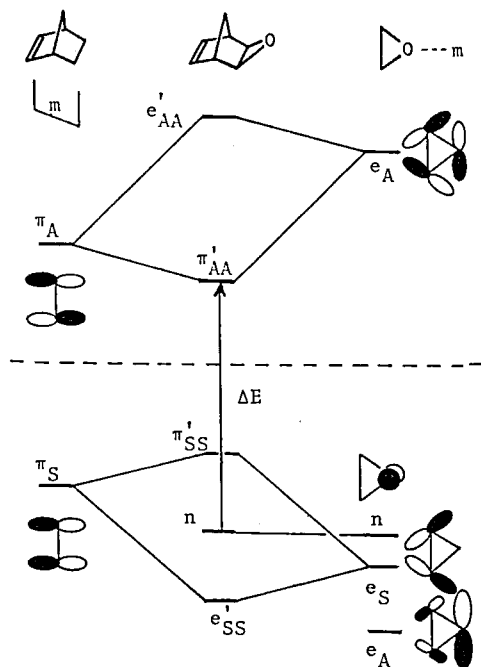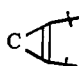

Figure 2. Correlation diagram for the construction of the molecular orbitals of norbornadiene exo-oxide.

Table I. ^{17}O Chemical Shifts and One-bond W-C Coupling Constants for Some Tungsten Carbonyls $W(CO)_5L$

	L	cis	trans	c.g.	cis	trans
I	CO		356.8		124.5	
	CPh$_2$	364.8	452.6	382.4	127.0	102.5
	CPh (OMe)	357.1	388.9	363.5	127.0	115.2
	CPh (OEt)	356.6	387.8	362.8	127.0	116.2
	CMe (OMe)	355.4	386.7	361.7	126.8	116.5
	CPh (NH$_2$)	352.0	372.5	356.1	126.9	124.8
	C⟨ ⟩	350.6	367.6	354.1	125.7	133.0
II	PCl$_3$	355.8	371.8	359.0	127.5	139.2
	P (OMe)$_3$	353.7	359.0	354.8	124.6	139.0
	PBu$_3$	354.1	354.1	354.1	124.4	142.1
	PPh$_3$	353.6	353.6+	353.6	126.5	143.4
III	PPh$_3$	353.6	353.6+		126.5	143.4
	AsPh$_3$		354.4		126.5	155.9
	SbPh$_3$		356.7		125.0	161.8
	BiPh$_3$		358.2		126.2	174.8
IV	Cl$^-$NEt$_4^+$		341.2		128.0	165.6
	Br$^-$NEt$_4^+$		342.1		127.5	171.5
	I$^-$ NEt$_4^+$		347.5		126.8	177.4
V	Pyridine		347.1		131.9	150.2
	Piperidine		346.1		131.6	150.0
	NH$_3$		346.4		129.0	153.2

I – III in CDCl$_3$, IV, V in CD$_3$CN
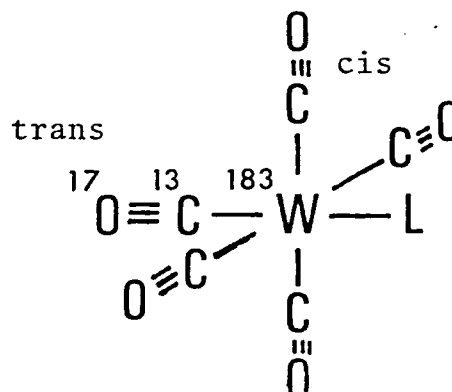
group Va triphenyls, halides, and amines. Firstly it is noted that the ^{17}O resonances of tungsten carbonyls have reasonably sharp peaks (half-band widths of 25—30 Hz) compared to that (100—300 Hz) in usual organic compounds of similar molecular weight. This is presumably due to the more or less spherical structure of the metal carbonyls and the resultant slow relaxation rate which is dominated by the inter-action between the quadrupole moment of ^{17}O and the electric field gradient. Spin-lattice relaxation times are still short enough to allow short acquisition times which enable us to accumulate a large number of transients in a limited time.[3] Secondly we point out that in nine examples resonances for the cis- and trans-carbonyl oxygens were observed as separate signals. Carbonyl groups trans to carbene and phosphine ligands have a range of shifts as large as 100 ppm. Thirdly, spin couplings of ^{183}W with the carbonyl carbon trans to ligands have a range of 75 Hz.

The data in Table I show that the carbonyl oxygens get more shielded and the one-bond spin coupling increases steadily along the series from diphenylcarbene to ammonia. The order of increasing ^{17}O shielding follows one's intuitive ideas about the σ-donor/π-acceptor value of a ligand in the trans position, and can be rationalized in terms of the reduced paramagnetic

^{17}O $\begin{cases} \text{less shielded in } ^+O \equiv C\text{-}W^- = L \\ \qquad \text{(small σ-donor/π-acceptor)} \\ \text{more shielded in } O = C = W^-\text{-}L^+ \\ \qquad \text{(large σ-donor/π-acceptor)} \end{cases}$

screening. Either increased charge density or n-π* excitation energy at the oxygen should be contribut-ing.[4] Backdonation from the tungsten to the carbonyl group induced by the trans ligand with high σ-donor/π-acceptor value will be responsible for the

increased bond strength and the spin-spin coupling of W-C(=O).[5]

We conclude that ^{17}O chemical shifts and $^1J(M-^{13}C)$ will be highly useful in elucidating the chemical bonding in metal carbonyls with a wide variety of ligands.

References

1) C. P. Casey, *CHEMTECH*, 378 (1979).

2) E. A. Abel, I. S. Butler, and G. Reid, *J. Chem. Soc.*, 1963, 2068; T. A. Magee, G. M. Matthews, T. S. Wang, and J. H. Wotiz, *J. Am. Chem. Soc.*, 83, 3200 (1961); D. J. Cardin, B. Cetinkaya, and M. E. Lappert, *Chem. Rev.*, 72, 575 (1972).

3) A. Abragam, "The Principles of Nuclear Magnetism", Oxford Univ. Press, London p. 314 (1961).

4) M. Karplus and J. A. Pople, *J. Chem. Phys.*, 38, 2803 (1963).

5) J. A. Pople and K. P. Santry, *Mol. Phys.*, 8, 1 (1964).

V—C Spin-state Variations among Nickel(II) Complexes Containing Macrocyclic Ligands

Nickel (II) ion forms with macrocyclic tetradentate ligands (L) a number of complexes of the type $NiLX_2$, X = an anion or solvent, which either are diamagnetic or have a triplet ground state. Changes from paramagnetism to diamagnetism and *vice versa* are often brought about by apparently trivial changes in the macrocyclic ligands, anions, and/or solvents. In some cases, the paramagnetic and diamagnetic forms of the same compound can be isolated. We are investigating the behavior of such systems in solutions and in solid states.

V-C-1 The Crystal and Molecular Structure of High- and Low-Spin Nickel (II) Complexes Containing the Macrocyclic Ligand, 5,5,7R(S), 12, 12, 14S(R)-Hexamethyl-1,4,8,11-tetraaza-cyclotetradecane.

Koshiro TORIUMI and Tasuku ITO

[Published partly in *Chem. Lett.*, 1395 (1979)]

Nickel (II) chloride forms with the title macrocyclic ligand (hereafter abbreviated as *meso*-Me$_6$[14] aneN$_4$) complexes of the types [Ni (*meso*-Me$_6$[14] aneN$_4$)] Cl$_2$·2H$_2$O and [NiCl$_2$ (*meso*-Me$_6$[14] aneN$_4$)].[1] The electronic spectra and the magnetic properties of these complexes have revealed that the orange dihydrate, [Ni (*meso*-Me$_6$[14] aneN$_4$)] Cl$_2$· 2H$_2$O, is a square-planar four coordinate complex having a singlet ground state, whereas the violet anhydride [NiCl$_2$(*meso*-Me$_6$[14] aneN$_4$)] is a pseudo-octahedral six coordinate complex having a triplet ground state.[1] Our recent study revealed that the solid, orange diamagnetic dihydrate is converted upon heating to violet paramagnetic anhydride [NiCl$_2$ (*meso*-Me$_6$[14] aneN$_4$)]. Conversely, the solid, violet, paramagnetic anhydrous complex readily revert to [Ni(*meso*-Me$_6$[14] aneN$_4$)] Cl$_2$ · 2H$_2$O when moisture is available. Of particular interest is the fact that two molecules of water are taken up to produce a diamagnetic nickel (II) complex. Taken up water molecules do not coordinate to a nickel (II) ion in the dihydrate, although water has considerable co-ordinating ability compared with chloride ion. In an attempt to determine the role played by water to produce a diamagnetic nickel (II) ion, the structural investigation of [Ni(*meso*-Me$_6$[14] aneN$_4$)] Cl$_2$·2H$_2$O (1) by the single crystal X-ray diffraction method has been carried out. The structural investigation of the anhydrous dichloro-complex (chloroform solvate,

[NiCl$_2$(*meso*-Me$_6$[14] aneN$_4$)] · 2CHCl$_3$)(2)has also been performed in order to establish the change in the structures of the singlet and triplet forms. For comparison, the crystal structure analysis of the fluoro-analogue, [NiF$_2$(*meso*-Me$_6$[14] aneN$_4$)] ·5H$_2$O (3), has also been carried out.

Crystal data. (1) : space group $P\bar{1}$, $a = 8.833(1)$, $b = 8.721(1), c = 8.212(1)$ Å, $\alpha = 86.79(1), \beta = 100.41$ (1), $\gamma = 118.61(1)°$, and $Z = 1$; (2) : space group $P\bar{1}$, $a = 9.656(2), b = 11.253(3), c = 6.781(1)$ Å, $\alpha = 93.98$ (2), $\beta = 91.29(2), \gamma = 90.32(2)°$, and $Z = 1$; (3) : space group $P\bar{1}$, $a = 11.185(2)$, $b = 13.364(3)$, $c = 8.890(1)$, $\alpha = 83.17(2), \beta = 104.94(1), \gamma = 113.00(1)°$, and $Z = 2$.

The structures were solved by the heavy atom method and refined to give R-values of 0.031, 0.047 and 0.031 for (1), (2) and (3), respectively. Perspective drawings of the complexes are shown in Figure 1.

In the orange compound (1), the nickel (II) atom is surrounded by four secondary nitrogen atoms of the macrocyclic ligand, yeilding a square-planar, diamagnetic nickel (II) complex. The chloride ions and the oxygen atoms of water of crystallization are not located near the fifth and sixth coordination site but are situated just above and below the amine nitrogen atoms with respect to the coordination plane. There appear to be four hydrogen bonds of importance in the structure, N(1)-H--Cl [3.261(2) Å], N(2)-H--O [2.948(3) Å], O-H--Cl [3.149(2) Å], and O-H--Cl' [3.175(2) Å]. The hydrogen bond networks are tight and strong enough to prevent the coordination of the water molecules and chloride ions, yielding thereby a diamagnetic nickel (II) complex.

In the violet chloroform solvate (2), the two axial coordination site are occupied by two chloride ions with the Ni - Cl bond distance of 2.562(1) Å, and the Ni - Cl bond is tilted 8° from the normal to the NiN$_4$ plane, giving a distorted octahedral geometry.

A point of particular interest is the correspondence of the Ni - N bond lengths with the spin state of the nickel (II) ion. In the diamagnetic complex (1) the
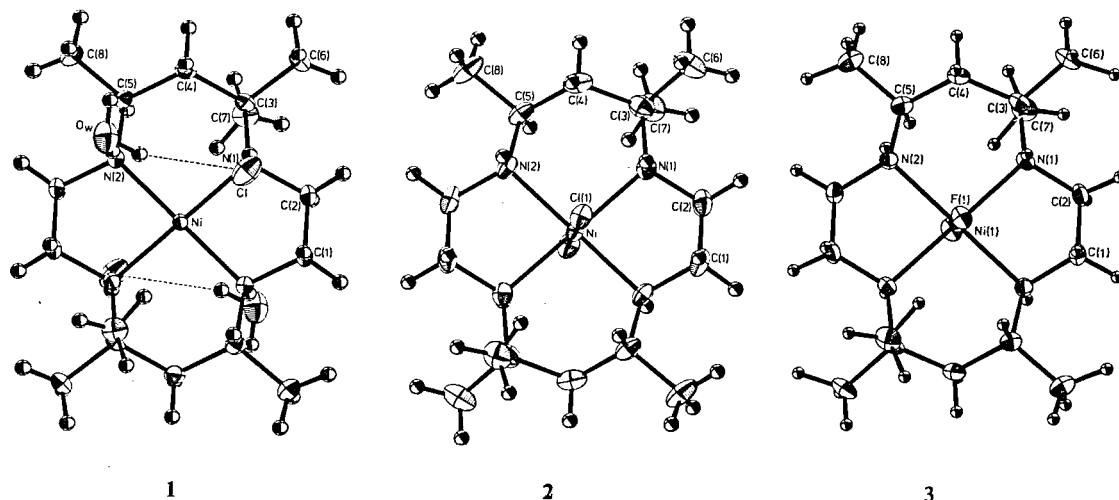
Figure 1. Perspective view of [Ni (meso-Me$_6$[14]aneN$_4$)] · 2H$_2$O (1), [NiCl$_2$(meso-Me$_6$[14]aneN$_4$)] · 2CHCl$_3$ (2), and [NiF$_2$(meso-Me$_6$[14]aneN$_4$)] · 5H$_2$O (3).

Ni - N bond length is 1.959(1) Å while in the para-magnetic complex (2) the Ni - N bond length is 2.081(2) Å. These distances are typical of those found in high- and low-spin nickel (II) complexes with four nitrogen donors.[2] The difference in the Ni - N bond lengths causes the change in the in-plane ligand field strength and produces the spin-state variation of the nickel (II) complexes with the same ligand.

In the compound (3), fluoride ions coordinate to the nickel (II) ion even in the hydrate to give a pseudo-octahedral structure. The average bond distances of Ni - N and Ni - F are 2.090(1) and 2.087 (1) Å, respectively.

In each compound, the macrocyclic ligand adopts the most stable conformation : the six-membered rings take the chair form with the C(5) - CH$_3$ bonds in equatorial positions; the five-membered rings are in the gauche conformation. As a whole, the con-formations of the macrocyclic ligand in these three compounds are not much different.

References

1) D. H. Busch, Adv. Chem. Ser., 62, 616 (1967).
2) S. W. Hawkinson and E. B. Fleischer, Inorg. Chem., 8 2402 (1969).

## V-C-2 A Kinetic Study on the Singlet-triplet Spin-state Equilibrium of the 5,5,7R(S),12, 12, 14R(S)-Hexamethyl-1S(R), 4S(R), 8S(R), 11S(R)-tetraazacyclotetradecanenickel(II) Ion and Dimethylsulfoxide System

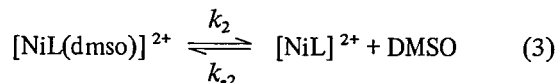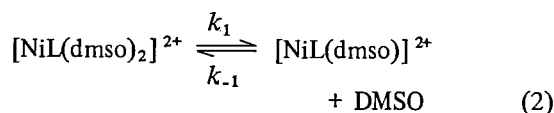Tasuku ITO (IMS and Hokkaido Univ.), Yukiyasu ENDO*, Noboru YOSHIDA*, and Masatoshi FUJIMOTO* (*Hokkaido Univ.)

The perchlorate salt of the title complex ion,

[NiL]$^{2+}$, dissolves in DMSO to give an equilibrium mixture of a singlet, square-planar species, [NiL]$^{2+}$, and a triplet, pseudo-octahedral species, [NiL (dmso)$_2$]$^{2+}$, where L denotes the title macrocyclic ligand. The kinetic study on the spin-state equili-brium in acidified H$_2$O-DMSO mixed solutions,

$$[NiL]^{2+} + 2DMSO \rightleftharpoons [NiL(dmso)_2]^{2+} \quad (1)$$
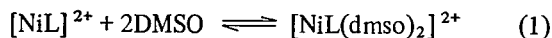
has been carried out by a temperature-jump method. A Union-Giken co-axial cable temperature-jump apparatus Model RA-105 was used. The kinetic data were obtained under pseudo-first-order conditions using an excess of DMSO. A single relaxation signal was observed in $10^{-3} - 10^{-4}$ s region. The relaxation time, τ, was independent of the concentration of the complex, whereas it depended on the concentra-tion of DMSO. The kinetic data were interpreted in terms of a stepwise mechanism,

$$[NiL(dmso)_2]^{2+} \underset{k_{-1}}{\overset{k_1}{\rightleftharpoons}} [NiL(dmso)]^{2+} + DMSO \quad (2)$$

$$[NiL(dmso)]^{2+} \underset{k_{-2}}{\overset{k_2}{\rightleftharpoons}} [NiL]^{2+} + DMSO \quad (3)$$

where reaction 3 equilibrates slowly as compared with reaction 2. The relaxation time, τ, can be expressed as

$$\tau^{-1} [DMSO]^{-1} = k_{-2} + (k_2 K_1 / [DMSO]^2) \quad (4)$$

where $K_1 = k_1/k_{-1}$. The plot of τ^{-1} [DMSO]$^{-1}$ against [DMSO]$^{-2}$ gave a straight line. The values of $k_2 K_1$ and k_{-2} were determined from the slope and the intercept of the straight line to be 1.1×10^4 and 1.3×10^4 mol dm^{-3} s^{-1}, and 70 and 80 mol^{-1}dm^6 s^{-1} at 18.6 and 23.6°C, respectively. Equilibrium constants $k_{-2}/K_1 k_2$ for reaction 1 were calculated from the kinetic data, i.e., the ratio of the intercept

to the slope to be 6.4×10^{-3} and 6.2×10^{-3} mol^{-2} dm^6 at 18.6 and 23.6°C, respectiveiy. These values

are in agreement with the equilibrium constant determined spectrally (5.7×10^{-3} mol^{-2} dm^6 at 25°C).

V—D The Absolute Configuration of (−)589-Tris(acetylacetonato)-germanium(IV) Ion, (−)589-[Ge(acac)3]+

Tasuku ITO, Koshiro TORIUMI, Fumio UENO *(Tohoku Univ.)*,
and Kazuo SAITO *(Tohoku Univ.)*

Absolute configurations of bis- or tris-chelated dissymmetric metal complexes containing unsaturated organic ligands have been deduced from the pattern of the major circular dichroism (CD) bands associated with the absorptions due to the π - π^* transitions of the ligands. This approach is based on the exciton CD theory.[1] It is desirable to confirm the validity of the exciton approach to the determination of the absolute configurations of metal complexes by an X-ray analysis. For this purpose, transition metal complexes are not adequate, since the CD spectra of transition metal complexes in the accessible region are usually associated not only with the absorptions due to the ligands π - π^* transitions but also with those due to the d - d transitions of metal ions and metal-ligand charge transfer transitions. The three types of the electronic excitation in a coordination compound are generally not discrete, having small frequency separations and not small mixing energies. On the other hand, in the exciton approximation, it is assumed that there is no electron-exchange between a ligand and a metal ion or between the individual ligands of the complexes. We have selected for the present purpose (−)589-tris(acetylacetonato)-germanium(IV) perchlorate, (−)589-[Ge(acac)3](ClO4), which was recently resolved into the optical isomer.[2] This complex would be most suitable, since the electronic absorption bands of this complex in the accessible region are only due to the single π - π^* transition of the ligand acac⁻ and the complications that arise in transition metal complexes are not present. The electronic and CD spectra of (−)589-[Ge(acac)3](ClO4) show the expected exciton pattern,[2] indicating that the absolute configuration is Δ.

The structure of (−)589-[Ge(acac)3](ClO4) was solved by the heavy atom method and refine to give an R-value of 0.044 for the 2142 independent reflexions collected by a Rigaku automated four circle diffractometer AFC-5 with graphite mono-chromated Mo Kα radiation ($\lambda = 0.7107$ Å). Crystal data : Trigonal, $P3_1$; $a = 11.592(1)$, $c = 12.983(3)$ Å; $U = 1510.9(4)$ Å^3; $Z = 3$; $D_m = 1.56$, $D_x = 1.55$ g cm^{-3}; μ(Mo Kα) = 17.93 cm^{-1}. Figure 1 shows a perspective
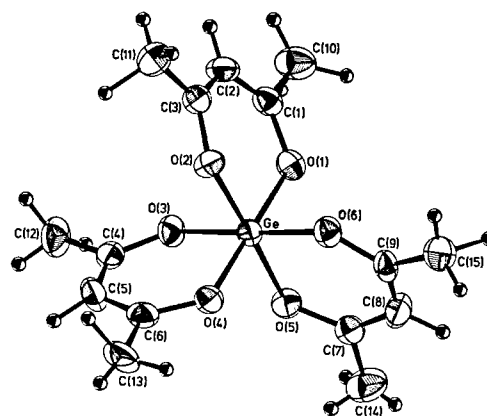

Figure 1. A perspective view of (−)589-[Ge(acac)3]+.

view of (−)589-[Ge(acac)3]+. The germanium atom is surrounded octahedrally by six oxygen atoms of the ligands with average Ge - O distances of 1.870(2) Å. The complex ion illustrated in Figure 1 corresponds to the levorotatory form with respect to Na D line. The three chelate rings present the appearance of right-handed propeller when viewed along the three-fold axis. The absolute configuration can be designated as Δ according to IUPAC convention.

It is concluded that the exciton CD approach to the determination of the absolute configurations of coordination compounds gives a satisfactory result when the electronic structures of the complexes are simple.

References

1) S. F. Mason, *"Fundamental Aspects and Recent Development in Optical Rotatory Dispersion and Circular Dichroism"* ed. by F. Ciardelli and P. Salvadori, Heyden & Son Ltd., London (1971), p. 196.
2) A. Nagasawa and K. Saito, *Bull. Chem. Soc. Jpn.*, **47**, 131 (1974).

117

V—E Molecular Structure and Absolute Configuration of 2,2'-Bis-(diphenylphosphino)-1,1'-binaphthylrhodium(I) complex

Koshiro TORIUMI, Tasuku ITO, and Hidemasa TAKAYA

There has been a great deal of interest in the development of stereoselective asymmetric reactions catalyzed by chiral transition metal complexes. Takaya et al. demonstrated that the Rh(I) complex bearing optically active 2,2'-bis(diphenylphosphino)-1,1'-binaphthyl (1) (hereafter abbreviated to binap) acts as a catalyst for stereoselective hydrogenations of α-acylaminoacrylic acids.[1] This new chiral bis-phosphine ligand was obtained by optical resolution of the corresponding racemic mixture by the use of a chiral palladium complex. The determination of the absolute configuration of this ligand is requisite for the elucidation of the correlation between the catalyst structure and the absolute configuration of the asymmetric hydrogenation products. We have carried out the X-ray crystal structure analysis of $[Rh^I((+)_{589}$-binap) $(nbd)]^+ClO_4^-$ (nbd = norbornadiene), the precursor of the catalyst used in the asymmetric hydrogenations.

The complex $[Rh (binap) (nbd)]^+ClO_4^-$ is dark-red mica-like crystals. Intensities of the reflexions were measured on a Rigaku automated four-circle diffracto-meter, using Cu Kα radiation. A crystal of dimensions 0.34 × 0.32 × 0.32 mm sealed in a Lindemann glass capillary was used for intensity measurement. Of 3503 hkl reflexions within the range $2\theta \le 120°$, 3249 non-zero reflexions were observed. In addition, 1106 hkl reflexions were measured within the range

$2\theta \le 70°$. Corrections were made for Lorentz and polarization, and absorption effects. Decrease in intensity caused by X-irradiation damage was also corrected. Crystal data are: $[RhP_2C_{51}H_{40}]ClO_4$, F.W. = 917.179, orthorhombic, $P2_12_12_1$, $Z = 4$, $a = 11.1035(4)$, $b = 35.238(2)$, $c = 10.8917(4)$ Å, $U = 4261.6(3)$ Å^3, $D_x = 1.430$ g cm^{-3}, $\mu(CuK\alpha) = 49.81$ cm^{-1}. The structure was solved by routine application of the heavy-atom method. Block-diagonal least-squares calculations including hydrogen atoms were carried out, employing a weighting scheme $w = [\sigma^2_{count} + (0.015F_0)^2]^{-1}$. The final R and R_w values were 0.0319 and 0.0414, respectively, for all the 3249 observed reflexions. The absolute configuration was determined by the comparison of the calculated and observed structure amplitudes for Bijvoet pairs.

A perspective drawing of $[Rh ((+)_{589}$-binap$)]^+$ is shown in Figure 1. Rhodium (I) atom has nearly square planar coordination and is surrounded by two phosphorus atoms and two C—C double bonds of norbornadiene which are omitted in Figure 1. The Rh(I) complex has an approximately two-fold axis of rotation through the central Rh atom and a two-fold axis of the binaphthyl group. The absolute configuration of the binaphthyl group is designated as R. The angle between the least-squares planes through the two naphthyl groups is 74.31°. Two phenyl rings B and D orient approximately parallel to naphthyl rings. Some representative interatomic distances and bond angles within the molecule are listed in Table I.

As can be seen from Figure 1, C(26) hydrogen (one of the two ortho hydrogens of the phenyl ring B) and C(40) hydrogen of the phenyl ring D overhang the rhodium atom. Therefore these two hydrogens will exert profound influence on the coordination of the prochiral substrates on the rhodium atom. This causes one face of the olefinic substrates to be preferentially coordinated over the other so as to minimize the steric interactions between these two phenyl rings B and D and bulky vinylic substituents.

1
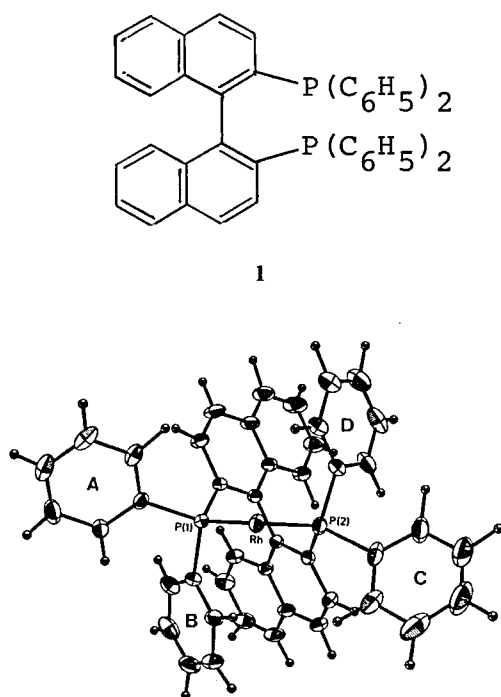
Figure 1. A perspective drawing of $[Rh((+)_{589}$-binap) (nbd)] except norbornadiene.

Table I. Some Interatomic Distances and Bond Angles of $[Rh((+)_{589}$-binap) $(nbd)]^+ClO_4^-$ with their estimated standard Deviations in Parentheses.*)

Rh–P(1)	2.305(1) Å	P(1)–Rh–P(2)	91.82(5)°
Rh–P(2)	2.321(1)		
		Rh–P(1)–C(1)	113.60(16)
P(1)–C(1)	1.836(5)	Rh–P(2)–C(20)	117.88(16)
P(2)–C(20)	1.844(5)		
P(1)–C(21)	1.814(5)	P(1)–C(1)–C(10)	122.99(35)
P(1)–C(27)	1.828(5)	P(2)–C(20)–C(11)	120.84(36)
P(2)–C(33)	1.831(6)		
P(2)–C(39)	1.810(6)	C(1)–C(10)–C(11)	123.72(44)
		C(20)–C(11)–C(10)	123.25(42)

*) See Figure 2 for atom numbering.

118

Such estimation of the steric interactions can interprete the stereochemical courses of the asymmetric hydrogenation of α-acylaminocinnamic acids.[1]

Reference
1) H. Takaya, T. Souchi, A. Yasuda, and R. Noyori, *IMS Ann. Rev.*, 92 (1978).
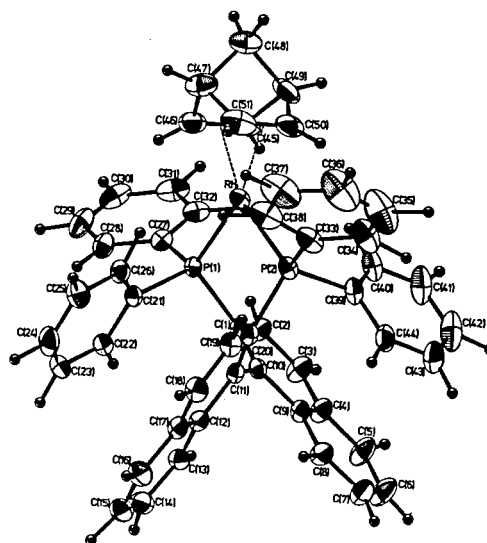
Figure 2. A perspective drawing of [Rh((+)589-binap) (nbd)]+ with atom numbering.

V—F The Crystal Structures of High Spin (298, 150 K) and Low Spin (90 K) States, and Spin Phase Transition Mechanism of a Spin Crossover Complex: Tris(2-picolylamine)ion(II) Chloride Ethanol (1/1)

Yoshihiko SAITO *(Univ. of Tokyo and IMS)*

A cooling device for crystal specimens set on a four-circle diffractometer was constructed as preliminary one to be installed in IMS, as reported in the previous Annual Review.[1] By using this cooling device, the crystal structure of the title compound at 90 K was successfully determined.

The crystals of the title compound undergo a spin phase transition between a high spin state $(t_{2g}^4 e_g^2)$ and a low spin state (t_{2g}^6). They are paramagnetic at room temperature and change to diamagnetic when cooled down.

The crystal structures of [Fe(2-pic)$_3$]Cl$_2$·EtOH in its high spin state (298, 150 K) and low spin state (90 K) were determined by X-ray diffraction. The space group is $P2_1/c$, $Z = 4$ over entire temperature range. At room temperature the cell dimensions are $a = 11.831(3)$, $b = 22.021(4)$, $c = 11.551(3)$ Å, $\beta = 124.28(2)°$, $D_x = 1.329$ g cm^{-3} and at 90 K $a = 11.616(3), b = 21.546(3), c = 11.353(3)$ Å, $\beta = 124.41(2)°$, $D_x = 1.409$ g cm^{-3}. The structures were solved by the heavy atom method and refined to $R = 0.054$, 0.044 and 0.043 (298, 150 and 90 K) based on F. Remarkable changes in Fe-N bond lengths were observed. The average Fe-N bond length in the high spin state (298 K) is 2.195 Å and that in the low spin state (90 K) is 2.013(3) Å. The considerable contraction of the Fe-N$_{(pyr)}$ bond, by as much as 0.2 Å, may be ascribed to back bonding as well as to the change in the spin state. All the amino N atoms of the complex are hydrogen bonded to the chloride ions forming a two-dimensional network parallel to the (100) plane. Solvate ethanol molecules, hydrogen bonded to Cl$^-$, exhibit orientational disorder in the high spin state but regular arrangement in the low spin state. The observed electron density of the ethanol molecules in the high spin state can be most conveniently accounted for if the ethanol molecule with a gauche conformation takes three alternative orientations around the α-carbon atom with different populations. The site with the highest population of 0.43 at 298 K and 0.80 at 150 K is exactly the same as that in the low spin state, where the ethanol molecule occupies regularly.

The structural differences in the two spin states are not only the remarkable changes in Fe-N bond nature in the complex but also the variation of the disorder of the ethanol molecules. When the temperature is lowered in the high spin region, the orientationally disordered ethanol molecules gradually tend to arrange. regularly. In the temperature around 150 K the spin phase transition begins to take place as the dominant site of disordered ethanol takes 80% occupancy and the ligand field strength may increase with a little shortening of the Fe-N bonds. In other words, the ordering of ethanol molecules seems to act as an initiator to Fe^{2+} spin transition. The complex and ethanol would interact with each other through hydrogen bonds when the spin phase transition and the order-disorder transition of ethanol take place. The interactions between the complexes and that between the complex and order-disorder variation of ethanol molecule through hydrogen bonds seem to cause the cooperative nature of this spin phase transition.

Reference
1) Y. Saito, *IMS Ann. Rev.*, 83 (1978).

V—G Syntheses, Characterizations, and Spectroscopic Properties of Cobalt(III) Complexes Containing Aminophosphine Ligands

Junnosuke FUJITA *(Nagoya Univ. and IMS)* and Kazuo KASHIWABARA *(Nagoya Univ.)*

In contrast to the extensive work on cobalt (III)-ammine complexes, little work has been reported on cobalt (III) complexes containing phosphine ligands, although phosphorus belongs to the same V group element as nitrogen. As a first step of studying cobalt (III)-phosphine complexes, we are preparing cobalt (III) complexes containing aminophosphines of the type, $NH_2CH_2CH_2PR^1R^2$. The presence of the amino group will assist formation of the cobalt (III)-phosphorus bond by chelation, and the aminophosphine is an intermediate ligand between a diamine and a diphosphine. Spectroscopic properties of such aminophosphine complexes will be investigated and compared with those of ammine complexes studied extensively.

RESEARCH ACTIVITIES VI

Computer Center, Instrument Center, Low Temperature Center, Chemical Materials Center, Development Workshop

Computer Center

Three research projects are being carried out at the Computer Center. One is the establishment of the JAMOL3 program system which is designed for ab initio MO calculations of large polyatomic systems. The JAMOL3 program has been registered as a library program of this center.

The second project is theoretical investigations of the electronic structure of metal complexes. Fe-porphines without and with axial ligands, and $[Co(CN)_6]^{3-}$ have been studied by ab initio molecular orbital calculations with basis sets of double zeta quality.

The third is the development of data bases on quantum chemistry. Service of a quantum chemistry literature data base (QCLDB) is available to users of the Computer Center.

VI—A   Production of JAMOL3 Program System for ab initio SCF Calculations of Large Molecules

Hiroshi KASHIWAGI, Shigeru OBARA, Toshikazu TAKADA*,
Fukashi SASAKI*, and Eisaku MIYOSHI* (*Hokkaido Univ.)

The program system JAMOL3, which is a new version of JAMOL2[1], has been completed. JAMOL3 was designed for high-speed computation of ab initio LCAO SCF MO's of large polyatomic systems such as metalloporphyrins. By the use of JAMOL programs one can calculate molecules with C_1, C_s, C_i, C_2, D_2, D_4, C_{2v}, C_{4v}, C_{2h}, D_{2h}, D_{2d}, and O_h symmetries on the basis of either usual contracted Gaussian type orbitals (CGTO) or semiorthogonalized orbitals[2-4]. In the development from JAMOL2 to JAMOL3 the following extensions and improvements were made.

a) Increase of the limit of the number of CGTO's.

b) Improvement of the semiorthogonalized orbital scheme[5] which allows a more effectively elimination of two-electron integrals than the old scheme.

c) Speed-up of the molecular integral calculation.

d) Adoption of a new algorithm for the transformation of two-electron integrals from the CGTO basis to the symmetry orbital basis[6].

e) Adapting the data input for the use of TSS terminals.

In Table I timing data of the SCF MO calculation of Co-porphine[7] by JAMOL2 and those of Fe-porphine by JAMOL3 are presented. The used basis set of Fe-porphine is shown in Table II, which is almost same as that of Co-porphine. The total number of CGTO's is 194. The remarkable improvement in the computational speed is obvious from Table I.

One can perform ab initio MO calculations with large basis sets as shown in the following sections. By the development of JAMOL3 a huge number of polyatomic systems have become objects of the ab initio MO computation.

Table I. Comparison of CPU time.

Program	JAMOL2	JAMOL3
Molecule	Co-porphine	Fe-porphine
Computer	FACOM 230-75	HITAC M-180
Center	Hokkaido Univ.	IMS
Speed ratio	1	~1.4

Step	CPU time (hours)	
Transformation matrices One-electron integrals	0.25	0.17
Two-electron integrals (symmetry orbital basis)	9.95	1.95
Supermatrices	0.28	0.30
SCF iteration for a state	~0.27	~0.17
Total	10.75	2.59

Table II. Basis set of Fe-porphine.

atom	GTO	CGTO
Fe	(12s 8p 5d)	[8s 6p 2d]
N	(7s 3p)	[3s 2p]
C	(7s 3p)	[2s 1p][a]
H	(3s)	[1s][a]

a Scale factors which were optimized for ethylene are used.

References

1) H. Kashiwagi, T. Takada, E. Miyoshi, and S. Obara, Library Program Manual of Hokkaido University Computing Center, No. 1 and No. 2 (1977).

2) H. Kashiwagi and F. Sasaki, *Int. J. Quant. Chem., Symp.* 7, 515 (1973).
3) H. Kashiwagi, *Int. J. Quant. Chem.*, 10, 135 (1976).
4) H. Kashiwagi and T. Takada, *Int. J. Quant. Chem.*, 12, 449 (1977).

5) Y. Osanai and H. Kashiwagi, *Int. J. Quant. Chem.*, in press.
6) T. Takada and F. Sasaki, to be published.
7) H. Kashiwagi, T. Takada, S. Obara, E. Miyoshi, and K. Ohno, *Int. J. Quant. Chem.*, 14, 13 (1978).

VI—B Theoretical Investigations of Metalloporphyrins and Inorganic Complexes by the Ab Initio SCF MO Method

In general, metal complexes are interesting polyatomic systems because of their complicated electronic structure and because of their catalytic action. Heme and chlorophyll are prominently important as active centers of energy conversion processes in living bodies. In this project the electronic structure and the mechanism of the energy- and charge-transfer are studied for metal complexes with the ab initio molecular orbital method.

VI-B-1 Ab Initio SCF MO Calculations of Fe-Porphine with a Double Zeta Basis Set

Hiroshi KASHIWAGI and Shigeru OBARA
(Hokkaido Univ. and IMS)

Ab initio LCAO SCF MO calculations of Fe-porphine have been performed with three hundreds of contracted Gaussian type orbitals (CGTO) by the use of the JAMOL3 program mentioned in the previous section VI-A. One of the purposes of this large scale computation is to obtain fundamental wavefunctions which would serve as the standard when one wish to carry out MO calculations on more complex metalloporphyrins with an less extensive basis set.

The molecule is assumed to be planar and to have the D_{4h} symmetry as illustrated in Figure 1[1]. The used basis set is a double zeta set which is shown in Table I. The original primitive GTO's were optimized to construct very accurate Hartree-Fock wavefunctions of related atoms[2-3]. Since the basis set consists of 300 CGTO's, the total number of two-electron integrals is about one billion by a simple account. This enormous number is reduced to about 8 millions by utilizing the molecular symmetry and by adopting the scheme based on semiorthogonalized orbitals[4-5].
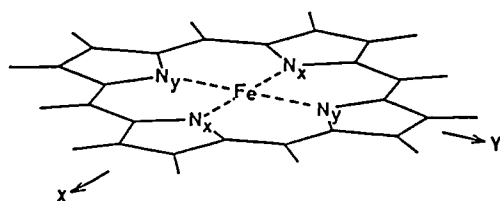

Figure 1. Geometry of Fe-porphine (D_{4h})

Table I. Double zeta basis set of Fe-porphine

atom	GTO		CGTO
Fe	(14s 11p 5d)	2)	[8s 6p 2d]
N	(8s 4p)	3)	[4s 2p]
C	(8s 4p)	3)	[4s 2p]
H	(4s)	3)	[2s]

The timing data are shown in Table II on the HITAC M-180 computer at the Center.

SCF wavefunctions are obtained for several low-, intermediate-, and high-spin states and for π-cation states. The formal occupation number of the d-shell and total energies are shown in Table III. Among them some of results on the lowest intermediate-spin state $^3A_{2g}$ $(d_{xy})^2$ $(d_{xz})^1$ $(d_{yz})^1$ $(d_z{}^2)^2$ are presented as an example. Calculated orbital energies of MO's which include a considerable amount of d-components are in the range from -11 eV to -15 eV. Unpaired electrons in the e_g open shell are very localized at d_{xz} and d_{yz} orbitals. By Mulliken's population analysis 98.7% of unpaired electrons are at the ion atom, while 0.1, 0.8, and 0.3% are at nitrogens, α-carbons, and β-carbons, respectively. The highest occupied orbital is $1a_{1u}$ which is localized at carbon atoms of pyrrole rings. It is higher than the $5a_{2u}$ orbital by 0.53 eV as shown in Table IV. The calculated ionization potentials are also shown in Table IV with observed data obtained from the photo-

Table II. CPU time of the computation of Fe-porphine on HITAC M-180 computer at IMS Computer Center.

Transformation matrices One-electron integrals	0.49 hours
Two-electron integrals (symmetry orbital basis)	5.39
Supermatrices	3.22
SCF iteration for a state	0.67
Total	9.77

Table III. SCF energy of Fe-porphine.

state	d_{xy}	d_π	d_{z^2}	$d_{x^2-y^2}$	E (a.u.)
$^1A_{1g}$	2	4	0	0	−2243.6697
$^3B_{2g}$	1	4	1	0	.6991
^3E_g	2	3	1	0	.7215
$^3A_{2g}$	2	2	2	0	.7351
$^5B_{2g}$	2	2	1	1	.7681
^5E_g	1	3	1	1	.7694
$^5A_{1g}$	1	2	2	1	.7802
$^4A_{2u}$		$(^3A_{2g}-1a_{1u})^+$			.5151
$^4A_{1u}$		$(^3A_{2g}-5a_{2u})^+$			.4979

electron experiment by Kitagawa and Morishima (Kyoto Univ.). The agreement between the calculated and observed values is surprisingly good.

References

1) J. P. Collman, J. L. Hoard, N. Kim, G. Lang, and C. A. Reed, *J. Amer. Chem. Soc.*, 97, 2676 (1975).
2) S. Huzinaga, *J. Chem. Phys.*, 66, 4245 (1977).
3) F. B. Van Duijneveldt, IBM Technical Research Report, RJ945 (1971).
4) H. Kashiwagi and T. Takada, *Int. J. Quant. Chem.*, 12, 449 (1977).
5) Y. Osanai and H. Kashiwagi, *Int. J. Quant. Chem.*, in press.

VI-B-2 The Electronic Structure of Fe (II) Porphine (Pyridine) (CO)

Shigeru OBARA *(IMS graduate student 1978—79 from Hokkaido Univ.)* and Hiroshi KASHIWAGI

Iron porphyrins catalize many reactions in biological systems. In these reactions the change of the oxidation state and the spin state of iron atom is a fundamentally important process. In order to elucidate the electronic structures of the iron complexes and the reaction mechanism, many experimental and theoretical investigations have been made. We have carried out ab initio LCAO MO SCF calculations on Fe(II) P(Py) (CO) to study its electronic structure and nature of iron-ligand bonds.

In figure 1 the assumed geometry of FeP(Py) (CO) is shown. Bond lengths of Fe-CO, Fe-N (porphine) and Fe-N (pyridine) are 1.77, 2.02 and 2.10 Å, respectively. Pyridine is assumed to be on the xz-plane. In order to describe the electron distribution at the
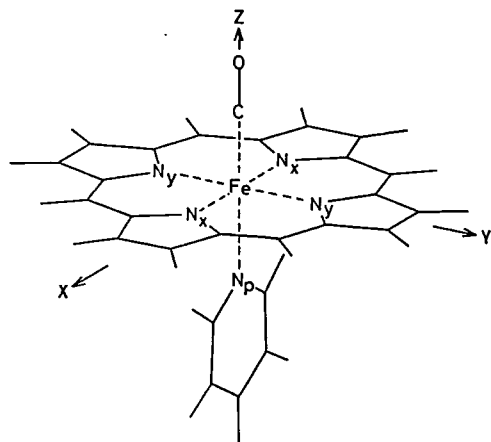

Figure 1. Assumed geometry of FeP (Py) (CO).

Table I. Gross and Overlap Populations of the Ground State $^1A_1$ of FeP (Py) (CO).

gross populations				
Fe	s	6.22	CO	
	p_x	3.95		
	p_y	3.96		
	p_z	4.01		
	d_{z^2}	0.22	σ	9.75
	d_{xz}	1.90	π_x	2.11
	d_{yz}	1.90	π_y	2.11
	d_{xy}	1.97		
	$d_{x^2-y^2}$	0.16		
porphine	σ	135.70		
	π	26.02		
pyridine	σ	36.02		
	π	6.02		

overlap populations						
		$\sigma(CO)$	$\pi_x(CO)$	$\pi_y(CO)$	$\sigma(Py)$	$\pi(Py)$
Fe	s	0.11	—	—	0.01	—
	p	-0.02	-0.03	-0.03	-0.16	-0.02
	d	0.12	0.05	0.05	0.04	0.00
porphine		-0.24	0.04	0.04	-0.07	0.00

ligand bonds precisely, a double zeta basis set is used for ion AO's and for valence orbitals of the carbonyl group and nitrogens. For the other AO's single zeta sets are used. The total number of CGTO's is 241. The integral approximation based on semiorthogonalised orbitals is applied in the calculation. The values of thresholds of $|S_{ij}|$ and (ij|ij) are 0.0001 and 0.000001 a.u., respectively. An error of the total energy caused by the approximation is estimated to be less than 0.001 a.u.

In Table I gross and overlap populations of the ground state $^1A_1(d_{xy})^2(d_{xz})^2(d_{yz})^2$ of FeP (Py) (CO) are given. The increase of electrons in the d_{z^2} orbital of Fe is almost equal to the decrease of σ-electrons of the CO group, while the decrease of electrons in the d_{xz} and d_{yz} orbitals is close to the increase of π-electrons of the CO group. This indicates what is called σ-donation and π-back-donation. The relation between Fe and CO is bonding from the view point of the overlap population. On the other hand the electron transfer from iron to pyridine is very small. The overlap population indicates that the ligand bond is slightly antibonding.

In the Fe-porphine with the D_{4h} symmetry the highest occupied orbital is a_{1u} and the second one is a_{2u}. In the case of FeP (Py) (CO) their order is changed. Though both of them are pure π-orbitals of the porphine ring, the a_{1u} orbital consists of $2p_\pi$ AO's at α- and β-carbons of pyrrole, while the a_{2u} orbital has $2p_\pi$ components of nitrogen atoms. By the coordination of CO and pyridine the energy of a_{2u} is pushed up, while the energy the a_{1u} orbital remains unchanged. Analyses of absorption spectra, ionization potentials, and Mössbauer spectra will be made on this complex and related compounds.

VI-B-3 The Theoretical Study on the Ionization of [Co (CN)$_6$]$^{3-}$

Mitsuru SANO*, Yasuyo HATANO*, Hiroshi KASHIWAGI, and Hideo YAMATERA* *(*Nagoya Univ.)*

The electronic structures of hexacyanometalates, [M (CN)$_6$]$^{3-}$ or [M (CN)$_6$]$^{4-}$, are of interest from both experimental and theoretical points of view. These ions are the simplest of typical symmetrical complexes in which the electron π-back-donation from the metal d$_\pi$ to the ligand 2p$_\pi$ orbitals possibly takes place.

We report a preliminary analysis of the d$_\pi$ energy level position of an ab initio calculation for the [Co (CN)$_6$]$^{3-}$ ion. The present calculation is of the SCF LCAO MO type using a basis set of Gaussian functions. The calculation was carried out by using program packages called JAMOL 2 and JAMOL 3.

Figure 1 shows the outer-shell orbital energy levels of [Co (CN)$_6$]$^{3-}$ and CN$^-$. The CN$^-$ MO energies are in the order, $4\sigma < 1\pi < 5\sigma$. The orbital energy sequence of [Co (CN)$_6$]$^{3-}$ is

$$d_\pi (1t_{2g}) < \sigma (CN^-) < \pi (CN^-).$$

This order is opposite to that found in the XPS experiments. The ΔSCF results for the same complex are given in Figure 2. The ΔSCF value is the difference between the ground state energy and the hole state energy obtained in the open shell SCF calculation. The highest level is the $1t_{2g}$ MO, which consists mainly of metal d$_\pi$ orbitals. The level order from the ΔSCF calculation is
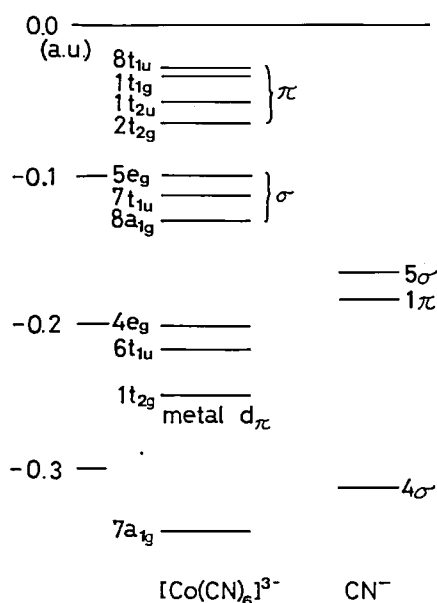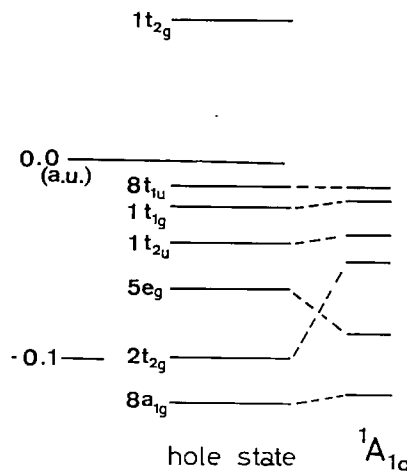
$$\sigma (CN^-) < \pi (CN^-) < d_\pi.$$

Figure 2. SCF energies of hole states (origine is the energy of the ground state $^1A_{1g}$) and orbital energies of the $^1A_{1g}$ states.

This order is consistent with the XPS results.

Figure 3 shows the map of the electron-density difference between the $^1A_{1g}$ ground state and the lowest $^2T_{2g}$ hole state with a hole in the d$_{xy}$ orbital of the metal. The solid lines show the regions where the electron density has been decreased, while the broken lines indicate the regions of increased electron density. This map demonstrates that the ionization of a metal d$_\pi$ electron is accompanied by the transfer of ligand σ electron density to the metal d$_\sigma$ orbital, resulting in partial cancellation of the effect of ionization on the metal core. This orbital relaxation explains why the low-lying $1t_{2g}$ electron is most easily ionized. The $1t_{2g}$ ionization in effect removes an electron from the carbon atoms, not from the cobalt atom.
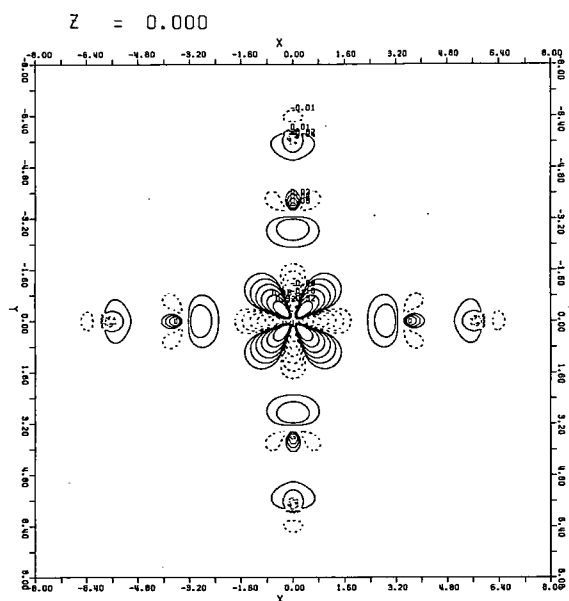

Figure 1. Orbital energy levels of [Co (CN)$_6$]$^{3-}$ and CN$^-$.

Figure 3. The electron-density difference map between the ground state $^1A_{1g}$ and the hole state $^2T_{2g}$.

VI—C QCDB—Quantum Chemistry Data Base

Kimio OHNO *(Hokkaido Univ.)*, Yoshihiro OSAMURA *(Osaka City Univ.)*, Shinichi YAMABE *(Nara Univ. of Education)*, Fumihiko HIROTA *(Shizuoka Univ.)*, Haruo HOSOYA *(Ochanomizu Univ.)*, Suehiro IWATA *(Institute of Physical and Chemical Research)*, Shigeru OBARA, Hiroshi KASHI-WAGI, Keiji MOROKUMA, Masahumi TOGASHI *(Hokkaido Univ.)*, and Kiyoshi TANAKA *(Hokkaido Univ.)*

The following three projects of data bases on quantum chemistry have planned. They are data bases of literatures, numerical data, and programs which are called QCLDB, QCNDB, and QCPDB, respectively. Here we will report on QCLDB, as its first version has been completed.

With a flood of ab initio calculations published in many journals, theorists as well as experimentalists often have a difficult time in finding a correct reference. Richards' famous book series is useful, but one has to wait several years for the latest version to come out. Recognizing the need for a frequently updated and easily accessible literature data base, we have initiated this QCLDB project.

Literatures contained are restricted to those concerning ab initio computations of atomic and molecular electronic structure. Approximately 1200 literatures published in 1977 and 1978 have been collected from twelve internationally well-known core journals.

A compound and/or author name can be used as a key to find a literature. Computational methods, basis sets and calculated properties are also listed. A processing program has been written in PL/I. Service of QCLDB is currently available at the computer of the Center. Although only preliminary at this stage, we have already found QCLDB quite useful and plan to continue our efforts towards this direction.

Instrument Center

In this Center, the reaction mechanism of hydrogenase, the enzyme catalyzing the isotope exchange reaction of hydrogen, the conversion of two modifications of ortho- and parahydrogen and the reduction of cytochrome c_3, is being studied. Physiological functions of hydrogenase and cytochrome c_3 in microorganisms are also investigated.

Electron transport phenomena in hemoproteins and also simple proteins are being investigated in solid phase by d. c. electrical conductivity measurement. The study of the electrode reaction of cytochrome c_3 is carried out by the use of various electrochemical techniques.

The Center is also carrying out the study of molecular geometry in the excited state in solution which is one of the fascinating problems in spectroscopy. In this research, we attempt to investigate the structural change of electronic spectra due to orientational difference and distortion of molecules in solution.

VI—D Pseudopotential in Metals and Ions

Keisaku KIMURA

The usefulness of a pseudopotential method in the field of solid state physics is well documented[1]. It has been also applied to atoms and ions[2]. The empirical relation between ionic and metallic radii is shown in Figure 1. It is striking that the metallic radius is only dependent on the ionic radius irrespective of its difference in core charge z. This relation is empirically represented as

$$R_a = 2\sqrt{R_i} \qquad (1).$$

We will show that there exist a simple analytic expression between ionic radii and metallic radii based on pseudopotential.

The potential of metal ion in the Wigner-Seitz cell is approximated by the pseudopotential as shown in Figure 2. The real potential V is chopped out at the core radius R_C to remove the nodes of oscillating core wave functions. The well depth A_0 is usually chosen so as to fit correct scattering properties. The total energy of electron gas in atomic units ($e = m = \hbar = 1$) per atom is propounded[3] as

$$U_0 = z(1.105/r_s^2) - z(0.458/r_s) + zU_c(r_s)$$

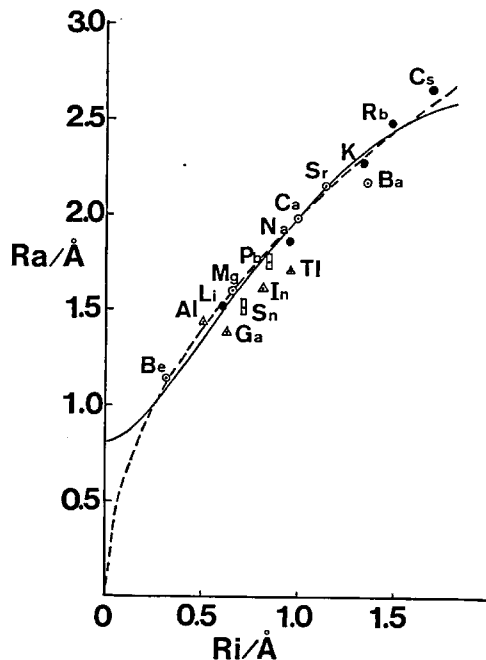$$- (0.9z^2/R_a) + (3z^2/2R_a)(R_c/R_a)^2$$

$$- A_0 z(R_c/R_a)^3 \qquad (2).$$

Figure 1. Metallic radii R_a and ionic radii R_i for I, II, III and IV elements. Solid line is theoretical and broken one is empirical curves. $\bigcirc$: I, $\odot$: II, $\triangle$: III, $\square$: IV group elements.
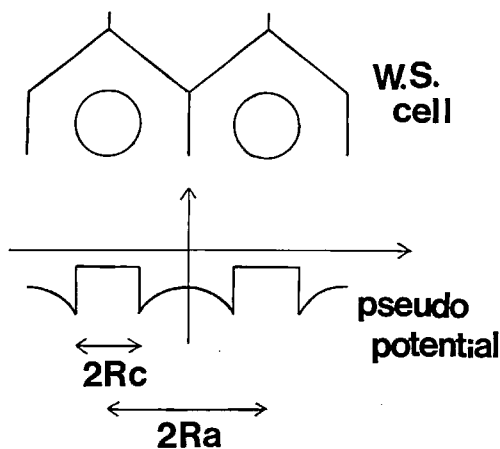

Figure 2. Schematic view of pseudopotential and ion sphere of radius R_c inside the Wigner-Seitz cell.

where $r_s = z^{-1/3} \cdot R_a$. Equation (2) may be differentiated so as to find the equilibrium metallic radius R_a giving the minium U_0.

The exact representation of eq (2) differentiated by R_a is a cubic form which derives no simple relation between R_c and R_a. Within the range of metallic densities, the correlation energy U_c varies slowly with density r_s and in the limit of high densities, it also varies slowly as $0.0622 \ln r_s$. We shall drop out this term in a first approximation. The differentiation of eq (2) with respect to R_a gives

$$R_a^2 - A \cdot R_a + B \cdot (C \cdot R_c - 1) R_c^2 = 0 \qquad (3).$$

$$A = \frac{2.21 \cdot z^{2/3}}{0.9z + 0.458z^{1/3}}, \ B = \frac{9/2 \cdot z}{0.9z + 0.458z^{1/3}},$$

$$C = \frac{2A_0}{3z} \qquad (4).$$

Coefficients A and B are nearly constant for z = 1~4 such as A = 1.45 ± 0.15, and B = 3.7 ± 0.4 though they are a function of z strictly speaking. In addition, the C term falls in the range 0.2~0.3 for many metals of z = 1~4 after values given by Animalu and Heine. Therefore we regard A and B as constant 1.45 and 3.7 respectively and C is merely a fitting parameter. R_c can be repaced by R_i, because the cancellation theorem makes it possible to approximate the core radius to ionic radius as stated by Ashcroft. The solution of eq (3) is

$$R_a = \frac{1}{2} \ [A + \sqrt{A^2 - 4B(CR_i - 1) R_i^2} \ ] \qquad (5).$$

The solid curve in Figure 1 is calculated from eq (5) with C = 0.18.

If we can further omit the first term in eq (2) as a second approximation, the solution becomes much simpler. The solution thus becomes

$$R_i^3 - \frac{R_i^2}{C} + \frac{R_a^2}{BC} = 0 \qquad (6).$$

The root of this cubic equation is approximated by a crossing point of a straight line which passes the two maxima of the function (6), and of abscissa. The solution is simplified as

$$R_a = \sqrt{\frac{2B}{9C}} \cdot R_i \qquad (7).$$

which derives $R_a = 2.1\sqrt{R_i}$ with B = 3.7 and C = 0.18. The empirical relation was thus derived.

Despite its simplicity, both first and second approximations successfully coincided with experimental values. It is interesting to compare the limitting case of R_i which equals to zero (just corresponds to a point core potential model) in both approximations. In a simplest case, R_a reachs to zero when R_i decreases. On the other hand, R_a remains finite when R_1 is zero in the first approximation. The difference between both approximations comes from the contribution of the electron kinetic energy. The pressure of electron gas pushes away the respective nucleus. Thus the R_a value at a point core potential corresponds to that of metallic hydrogen.

References

1) M. L. Cohen and V. Heine, Solid State Physics, 24, (1970)
2) B. J. Austin and V. Heine, J. Chem. Phys. 45, 928 (1966).
3) V. Heine and D. Weaire, Solid State Physics. 24, 262 (1970).

VI—E   Reaction Mechanism of Hydrogenase and Cytochrome c_3

Hydrogenase catalyzes o—p hydrogen conversion, H_2-D_2 hydrogen exchange reaction and electron transfer between hydrogen and cytochrome c_3. Hydrogenase is active not only in solution but also in dry state. Thus we can observe the reaction by Mössbauer spectroscopy which is effective only in dry state. The optical absorption measurement also reveals that cytochrome c_3 is reduced in dry state under the action of hydrogenase. Comparing these observations, we can deduce the characteristic feature of solid state reaction of hydrogenase. In solution, the reduction of cytochrome c_3 both by hydrogenase and electrodes is very fast. This fast electron transfer between different species was found to have a relation to the function of cytochrome c_3 in organisms.

VI-E-1   An Antihemoglobin Type Substrate Saturation Curve in Cytochrome c_3

Keisaku KIMURA, Hiroo INOKUCHI, Katsumi NIKI
(Yokohama National Univ.), and Tatsuhiko YAGI
(Shizuoka Univ.)

Cytochrome c_3 has four hemes in a single peptide chain. The four-heme structure implies an allosteric nature of this protein. Is it unlikely that cytochrome c_3 is an allosteric protein, although it is a monomer portein ? The allosteric character of cytochrome c_3 was suggested by the authers to explain its electric conductivity behaviour[1]. Potentiometric observation shows the apparent number of electrons involved in the electrode reaction in the Nernst equation is less than unity[2], which also supports this proposal.

Figure 1 shows the Nernst plots of the ferri- and ferrocytochrome c_3 system at pH 7.0, 25°C, where C_O and C_R are the concentrations of the heme in ferri- and ferro-form, respectively. The formal potential, -0.528 V (-0.287 V vs NHE) and the Nernst slope, 93 mV, are the same as the previous one[2].
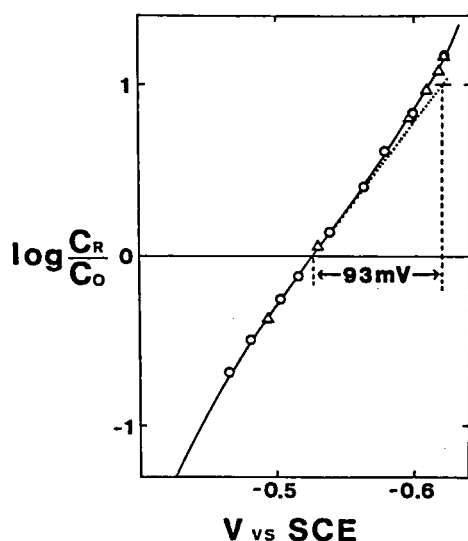
The apparent number of electrons involved in the electrode reaction in the Nernst equation was found to be 0.65. It is noticeable that the plots slightly deviate from a straight line with a solpe of 93 mV in the potential region beyond -0.58 V. The reason for the apparent number n being less than unity in cytochrome c_3, was explained in terms of the spacing of the standard potentials. The total potential spreading was reported to be about 120 mV from potentiometric and voltammetric results.

When we limit ourselves, for the sake of simplicity, to the case where the standard potentials are equally spaced and four hemes in cytochrome c_3 are successively reduced by four-step reversible one-electron reaction, the Nernst slope of 93 mV is explained by the spacing of -40 mV. The observed plots fall on the calculated curve as shown in Figure 1.

When the spacing of the standard potentials, ΔE_0, is negative, the potential field working on an external charge is repulsive, on the other hand, it is attractive

Figure 1. Equilibrium plots of the ferri- and ferrocytochrome c_3 in 0.033 M sodium phosphate buffer at pH 7.0, 25°C with a trace amount of hydrogenase. The solid line is a calculated curve.
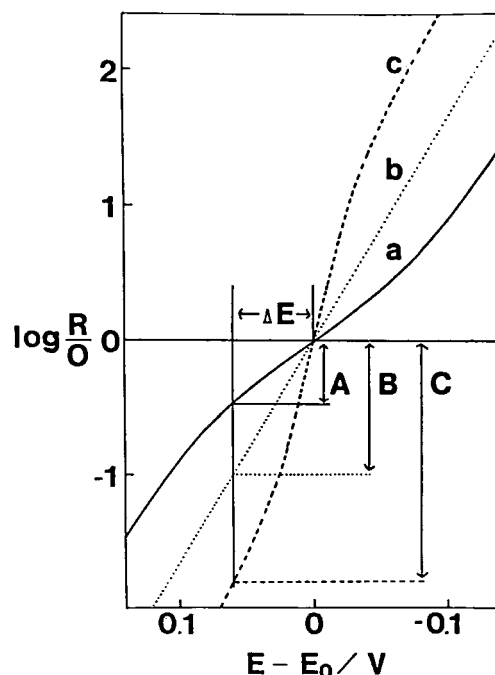

Figure 2. Equilibrium curves of cytochrome c_3 with different n. a) $n < 1$, repulsive interactionj b) $n = 1$; c) $n > 1$, attractive interaction. The concentration change due to a given potential difference, ΔE, increases A, B, and C in this order.

127

in the positive case. Figure 2 shows three typical Nernst curves with $n < 1$, $=1$ and $n > 1$, respectively. One can easily recognize from the Figure that the change in log (R/O) is the largest for $n > 1$ and the smallest for $n < 1$. Therefore it is said that the attractive interaction enhances the external effect (perturbation), while the repulsive interaction reduces it. Recall the case of hemoglobin in which the attractive heme-heme interaction enhances the affinity of hemoglobin toward the oxygen. Cytochrome c_3 is thus an example of antihemoglobin type.

Our electrochemical measurements show that the internal electron exchange is not so fast but the exchange with other species is very fast. These characteristics of cytochrome c_3, together with the fact that this cytochrome exists in soluble fraction in cytosol, suggest the role of this protein as an redox scavenger or an electron buffer.

This function is reminiscent of that of a leucocyte in blood, although they differ in their structure and in the complexity of their reactions. Upon drastic changes in the redox conditions, followed by invasion of oxidant or reductant into a cell, cytochrome c_3 attacks these redox species. This will lead to only a small change in the concentration ratio of ferri- and ferrocytochrome c_3 on account of the allosteric properties of cytochrome c_3. Therefore, the influence of the invader on the metabolic function in this bacterium will be minimized.

Cytochrome c_3 seems to be one of the most skillful architectures in the world to retain the homeostasis of life. The molecular device such as cytochrome c_3 must be essential to prokaryotes having no cell organelle. From recent phylogenetic researches, the origin of *Desulfovibrio* species goes back to 3×10^9 years ago. Cytochrome c_3 might be a precursor of such skillful molecular devices.

References

1) K. Kimura, Y. Nakahara, T. Yagi, H. Inokuchi, *J. Chem. Phys.*, **70**, 3317 (1979).
2) K. Niki, T. Yagi, H. Inokuchi, & K. Kimura, *J. Am. Chem. Soc.*, **101**, 3335 (1979).

VI-E-2 Kinetics of Cytochrome c_3 Reduction with Hydrogenase Studied by Mössbauer Effect

Megumi UTUNO *(The Univ. of Tokyo)*, Keisaku KIMURA, Kazuo ONO *(The Univ. of Tokyo)*, Tatsuhiko YAGI *(Shizuoka Univ.)*, and Hiroo INOKUCHI

Hydrogenase is still active in solid phase as well as in solution.[1] It catalyzes H_2 - D_2 equilibration, o-p hydrogen conversion and cytochrome c_3 reduction with molecular hydrogen in the solid state. Mössbauer spectroscopy, effective only in the solid state, is very useful to confirm an electron transfer in solid phase.

^{57}Fe enriched cytochrome c_3 was prepared and purified from *D. vulgaris*. The specimen was enriched

to about 60% evaluated from Mössbauer absorption measurement. An atmospheric pressure of hydrogen gas was introduced after complete evacuation. The time course of the reaction was traced by Mössbauer spectroscopy at room temperature as shown in Figure 1. Each spectrum is a superposition of two doublets, outside of which is that of ferri-form, whose intensity gradually decreases with time.

The concentration ratio of ferri- to ferro-form was determined by the ratio of the spectrum area of ferri- to ferro-form, a_3/a_2. The plot of $\ln a_3$ vs. time is linear, as shown in Figure 2. A time differential equation of ferri-form rate is described follows

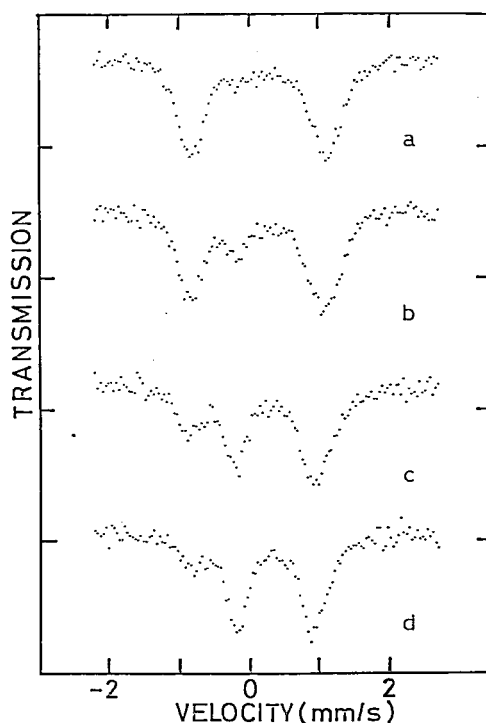Figure 1. Mössbauer spectra of cytochrome c_3 in the time course of reduction. a) 0 s b) 8.4×10^3 s c) 2.7×10^4 s d) 3.7×10^4 s, after beginning of the reduction.
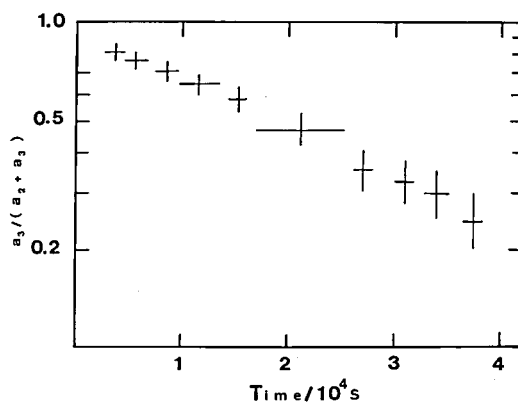

Figure 2. Log plot of the concentration ratio of ferri-form as function of time.

$$da_3/dt = -ka_3$$

in which k is the rate constant which equals to 3.2 $\times 10^{-5}$ s^{-1}. The oxidation of cytochrome c_3 deposited sample with atmospheric oxygen was roughly fitted to the first order law, and the rate constant was also calculated to be about 2.5 $\times 10^{-6}$ s^{-1}. To investigate the reduction process in this system, three kinds of rate determining steps may be considered: self diffusion of cytochrome c_3 molecule, diffusion of electron or proton and enzymic reaction. The possibility of the first case can be ruled out by the following consideration. The oxidation with oxygen is controlled by a diffusion of oxygen molecule because oxidized reaction is much faster than it, as confirmed in aqueous solution. The self diffusion of cytochrome c_3 will be slower than the oxygen diffusion on the substrate. The reducing reaction on that system is much faster than the oxidation, then the former is not controlled by the self diffusion.

In the second case, the electrons will be spread out spherically starting from each hydrogenase mole-cule, and the rate of the reduction will be proportional to the surface area of this sphere, then the rate of the reduction gradually increases with time. In other words, $d^2a_3/dt^2 > 0$ and $d^2a_3/dt^2 < 0$. The fact that the equation $d^2a_3/dt^2 > 0$ was obtained experimentally rejects the possibility of the second case and suggests that it is the third case.

Taking into account of a large excess of cytochrome c_3 in this system, most of the cytochrome c_3 cannot be neighbouring to the hydrogenase molecule and so, cannot be directly effected by the catalytic action of the hydrogenase. Therefore, the reducing reaction of cytochrome c_3 indicates that intra and intermolecular transfer of electrons exist in that molecule. By the present experiment, the direct electron transfer between cytochrome c_3 molecules in solid phase was confirmed.

References

1) K. Kimura, A. Suzuki, H. Inokuchi and T. Tagi, *Biochim. Biophys, Acta,* 567, 96 (1979).

## VI—F Electron Transport Properties of Cytochrome c_3

The electron transport of proteins in the solid state has been reported by numerous investigators with an interest in the carrier transport in biological systems. We have already reported the electron transport in respiratory proteins by means of the electrical conductivity measurement. The difference in the electrical conductivity was found between the film of hemoprotein and that of simple proteins with no heme as a prostheric group as well as the ferri- and ferroform of hemoprotein. Further investigation was made in respect to the role of heme in cytochrome c_3, a member of multihemoproteins. Electrochemical techniques are also being applied to cytochromes in order to clarify the electron transfer character of heme on the electrode surface.

VI-F-1 Electrical Conduction of Hemoprotein in the solid phase: Anhydrous Cytochrome c_3 Film

Keisaku KIMURA, Yusuke NAKAHARA *(Tech. Coll. of Miyakonojo)*, Tatsuhiko YAGI *(Shizuoka Univ.)*, and Hiroo INOKUCHI

Cytochrome c_3 is an electron carrier in the respiratory chain of *D. vulgaris.* This molecules is known to have 4 hemes and is undergone the oxidoreduction by the action of hydrogenase.

ferricyt $c_3(Fe^{3+})$ + 2H$_2$

$\longleftrightarrow$ ferrocyt $c_3(Fe^{2+})$ + 4H$^+$ (1)
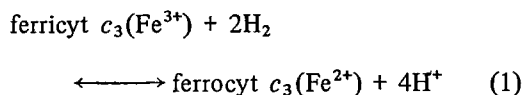
The d.c. conductivity was measured in an atmosphere of hydrogen gas as a surface type. Figure 1 shows the logarithm of the resistivity against the reciprocal of the absolute temperature as a function of hydrogen pressure. Below a hydrogen pressure of 16 Torr, the temperature dependence shows a semiconductive
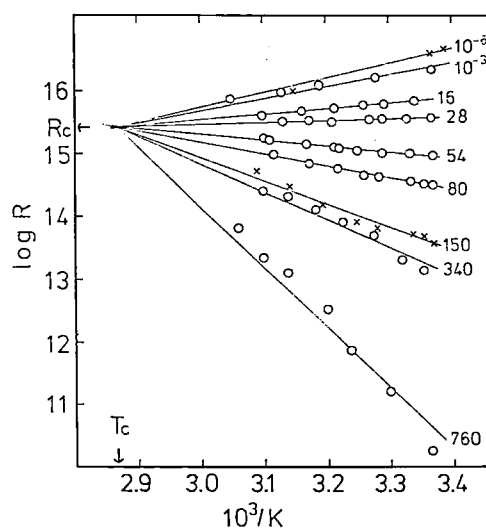

Figure 1. The temperature dependence of resistance as function of hydrogen partial pressure.
The figures on the right side of straight line represent a hydrogen pressure in Torr.

character with a positive activation energy, but above 54 Torr, a negative dependence was observed. These findings are represented by the following empirical equation,

$$\log R - 15.4 = \alpha \left(\frac{10^3}{T} - 2.86 \right) \quad (2)$$

where α is a function of the pressure and is related to the apparent activation energy E.

The pressure dependence of α is represented as follows

$$\alpha = -6.6 \log P/P_0 - 8.8 \quad (3)$$

From these equations, we derive the temperature dependence of the resistivity to be

$$R = 4.1 \times 1.0^{40} \cdot (P/P_0)^{19 - E_1/RT}$$
$$\cdot e^{-E_2/RT} \quad (4)$$

where R is the gas constant, $E_1 = 13$ kcal, and $E_2 = 41$ kcal.

To explain the empirical expression given in Eq. 4, we will introduce semiconductor band treatment and also the Hill equation for allosteric proteins. The empirical Hill equation is represented as

$$Y = \frac{K(P/P_0)^n}{1 + K(P/P_0)^n} \quad (5)$$

in which Y is the ratio of saturation, K is constant and n is the parameter related to the heme-heme interaction. Y is also given by $n(R)$ and $n(O)$, the number of ferro- and ferricytochrome c_3, respectively. Therefore, the phenomenological constant K is now connected with the equilibrium constant between ferri- and ferro-species as follows

$$K(P/P_0)^n = 1/K_e \quad (6)$$

Then the number of ferrocytochrome c_3 molecules are obtained as

$$n(R) = n_0 \cdot K(P/P_0)^n / [1 + K(P/P_0)^n] . \quad (7)$$

Suppose that ferrocytochrome c_3 (Fe^{2+} central ion in porphyrin) has a donor character, with the gap between conduction bond and donor level narrower than the thermal energy, as is shown in Figure 2. At room temperature, all of the donors are excited thermally, so that the resistivity is simply given as

$$\rho = 1/n(R)e\mu \quad (8)$$

where e is the electron charge and μ is the mobility. Combining these equations, we obtain
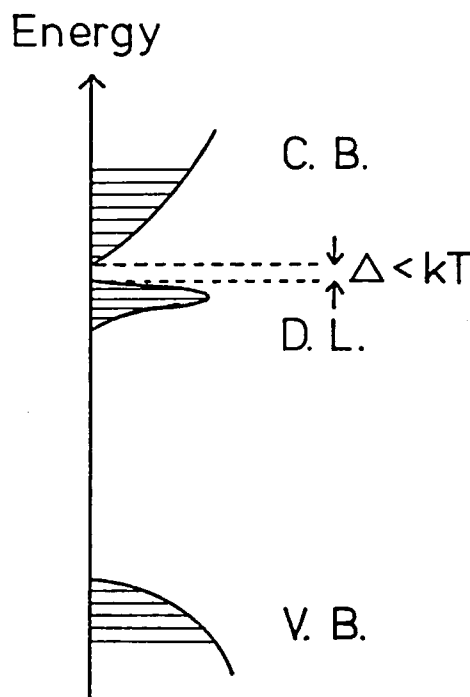
$$\rho = K^{-1}(P/P_0)^{-n}/n_0 e\mu \quad (9)$$

Figure 2. The shematic diagram of density of state of cytochrome c_3 CB, conduction band; DL, donor level; VB, valence band. The gap between CB and DL is presumed to be nallower than the thermal energy kT.

an expression of the same form as the empirical equation. The temperature dependence of the resistivity is obtained by differentiating the logarithm of ρ with respect to the reciprocal of temperature

$$E_R = \frac{d\ln\rho}{d(1/T)} = \frac{d\ln K_e}{d(1/T)} = -\Delta G$$

The experimental value of E_R ($= -E_2$ in eq. 4) is 41 kcal; on the other hand $-\Delta G$ is -40 kcal/mol.

Cytochrome c_3 has 4 hemes in a molecule, so that the hemes in cytochrome c_3 are expected to be situated relatively close to each other. We thus expect the π electron orbitals of the porphyrin rings to overlap each other. The delocalization of π electrons among the hemes may help to increase the conduction in solids.

Here we have to point out that we could not obtain the intrinsic conduction of fully reduced cytochrome c_3 because a small fraction of cytochrome c_3 remained in the ferri-form, due to an unfavorable equilibrium at room temperature. The temperature dependence of conductivity was controlled by the chemical equilibration, therefore we would expect to have the conductivity of the reduced form at low temperature. We also expect a high conductivity for fully reduced cytochrome c_3 even at low temperature. The conductivity measurement of fully reduced cytochrome c_3 at low temperature is now in progress.

VI-F-2 Electrical Conductivity of Solid State Proteins; Simple Proteins and Cytochrome c_3 Anhydrous Film

Yusuke NAKAHARA *(Tech. Coll. of Miyakonojo)*, Keisaku KIMURA, Hiroo INOKUCHI, and Tatsuhiko YAGI *(Shizuoka Univ.)*

We have found[1] that there was a large difference in the resistivity between ferricytochrome c and ferrocytochrome c which was attributable to the electronic state of central metal ion. It is thus important to compare the electrical conductivity of cytochrome c with other hemoproteins having the same molecular weights in order to reveal the effect of heme on the conduction mechanism.

Cytochrome c is a globular hemoprotein with a molecular weight (M_r) of about 12500. Lysozyme $(M_r) = 14600$, ribonuclease $(M_r = 13700)$, trypsin $(M_r) = 23800$, and myoglobin $(M_r = 17000)$ were chosen as reference globular proteins. As a multi-hemoprotein, the electrical conductivity of cytochrome c_3 $(M_r = 14000)$ was measured as well. The film casting method was employed to prepare sample films. The d. c. conductivity of a ferrocytochrome c_3 film was measured in an atmosphere of dry hydrogen gas under 100 V applied voltage. The distance between electrodes was 2 mm. The temperature dependence of the conductivity was measured with successively raising the temperature at a rate of 0.1 - 0.03 K/s after the sample was held at 203 K for 5 minutes. The conductivity of ferricytochrome c_3, on the other hand, was measured in an atmosphere of nitrogen gas. The conductivities of lysozyme, ribonuclease, trypsin and myoglobin were also measured in a dry nitrogen atmosphere in the range from 283 to 343 K, with 500 V applied voltage after heat and evacuation cycles.

The electrical resistivity of simple proteins was so high that the electric current was not observed in the range from 283 to 343 K: The resistivities of these proteins were higher than 10^{14} Ω cm. Table I collects the electrical conductivity data of several protein solids. The ferri-forms of both cytochromes have a similar resistivity in magnitude at room temperature. On the other hand, very drastic difference appeared in the resistivity of the ferro-form. At 268 K, the electrical resistivity of ferrocytochrome c_3 was only 57 Ω cm, which corresponded to that of Ge.

The contribution of heme to the electrical conduction of biological materials is clear because the polypeptide chain itself is an electrical insulator whose resistivity exceeds 10^{14} Ω cm. On the other hand, the resistivity of one hemoprotein keeps about $10^9 - 10^{11}$ Ω cm. Eley and Spivey, in their pioneer work of 1960, could not find the difference in conductivity of hemoprotein from that of simple proteins. The reason may be accounted for by the inadequacy of sample preparations, i.e., application of high temperature, and high pressure which may lead to denaturation of protein.

Taking into acount of the size of porphyrin, 1.3 nm in diameter, the distance is small enough to cause the overlapping of π electrons. Electrochemical measurement of the reduction of cytochrome c_3 on a mercury electrode[2] also suggests that some parts of hemes are exposed to the protein surface and/or the electrons tunnel through a peptide residue.

References

1) Y. Nakahara, K. Kimura and H. Inokuchi, *Chem. Phys. Lett.*, 47, 251 (1977).
2) K. Niki, T. Yagi, H. Inokuchi and K. Kimura, *J. Am. Chem. Soc.*, 101, 3335 (1979).

Table I.

Materials	Activation energy $\Delta E/J\cdot mol^{-1}$	Resistivity $\rho(303K)/\Omega cm$	ρ_0/Ω cm
Lysozyme	——	$>10^{14}$	——
Ribonuclease	——	$>5 \times 10^{14}$	——
Trypsin	——	$>10^{14}$	——
Myoglobin	1.5×10^4	3.6×10^{10}	1.2×10^8
Cytochrome c			
oxid	1.3×10^5	6.1×10^{16} [a]	1.6×10^{-5}
oxid	1.1×10^5 (343–373K)	4.8×10^{15} [a]	2.5×10^{-3}
	5.8×10^4 (313–343K)		
oxid	5.8×10^4 (323–358K)	3.1×10^{11} [a]	4.0×10^1
red	5.8×10^4 (283–333K)	3.1×10^9	4.0×10^{-1}
Cytochrome c_3			
oxid	1.6×10^5 (293–343K)	2.3×10^{12}	5.4×10^{-16}
red	3.7×10^5 (233–268K)	5.7×10^1 [b]	2.5×10^{-70}

a The resistivity at 303 K by the extrapolation with ΔE and ρ_0
b Value at 268 K (T_M)

VI-F-3 Electrochemical Behavior of Cytochrome c_3 Desulfovibrio vulgaris, strain Miyazaki, on Mercury Electrode

Katsumi NIKI *(Yokohama Nat. Univ.)*, Tatsuhiko YAGI *(Shizuoka Univ.)* Hiroo INOKUCHI and Keisaku KIMURA

It has been demonstrated[1] that cytochrome c_3 is electrochemically active and interacts directly with a glassy carbon electrode as an electron carrier. In our previous work[2], we found that the electron transfer reaction of cytochrome c_3 is reversible at the mercury electrode surface, which is the first instance of observing a reversible electrode reaction for a heme protein. In this work, we have further examined the electrode behavior of cytochrome c_3 at mercury electrode by pulse and differential pulse polarography, cyclic voltammetry, and potentiometry. The apparent formal potential which is the mean redox potentials of the four individual hemes in the molecule, is found to be $-(0.528 \pm 0.001)$V.

Cytochrome c_3 produced a single well-defined reduction wave with a small preceding wave at the dropping mercury electrode as shown in Figure 1. The half wave potential is -0.527 V (-0.286 V vs. NHE) and the plot of log $[i/(i_{dc} - i)]$ vs. electrode potential produces a straight line with an inverse slope of 0.085 V from which the apparent number of electrons involved in the electron transfer step is calculated to be less than unity, where i is the cathodic current for the reduction of ferri-form at a given potential and i_{dc} is the cathodic limiting current. The electron transfer reaction rate between cytochrome c_3 and the dropping mercury electrode is too fast to be determined within the time window of the pulse polarographic measurements. The diffusion coefficients of ferri- and ferrocytochrome c_3 calculated from the pulse polarographic data were 0.94×10^{-6} and 0.71×10^{-6} cm^2 s^{-1}, respectively.

The differential pulse polarogram of ferricytochrome c_3 is shown in Figure 2. The polarogram is almost symmetrical with respect to the potential axis at the peak current, -0.522 V. The ratio of the peak
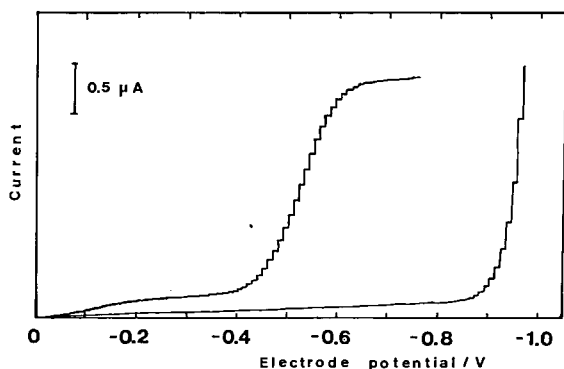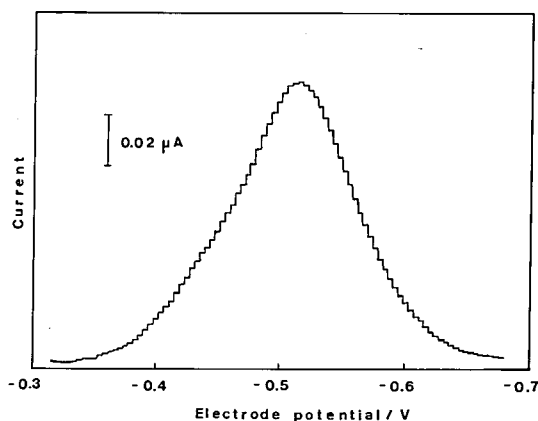

Figure 2. Differential pulse polarogram for the reduction of ferricytochrome c_3.

current of the differential pulse polarogram to the limiting current of the normal pulse polarogram is 0.0714, which indicates that the apparent number of electrons involved in the electrode process, n_{app}, is 0.74. The half-peak width is 118 mV from which n_{app} is also calculated to be 0.76, while the values of n_{app} calculated from the potentiometric slope and the logarithmic plot of the pulse polarogram were 0.64 and 0.70, respectively. All of these values are in good agreement.

Pulse polarographic, scan-reversal pulse polarographic and linear potential sweep voltammetric results indicate that the electrode reaction of ferri- and ferrocytochrome c_3 at mercury electrode is reversible and controlled by the diffusion of the protein molecule from the bulk of the solution to the electrode surface. The electron transfer reaction rate of cytochrome c_3 is too fast to be determined by the present techniques and the rate constant is presumably the order of 0.1 cm s^{-1} or greater.

A multistep very fast electron transfer reaction has to be postulated to explain pulse polarographic, differential pulse polarographic, potentiometric, and voltammetric results. The over-all electrode reaction of cytochrome c_3 is expressed as

$$\text{ferricyt } c_3 + 4 \text{ e} \longleftrightarrow \text{ferrocyt } c_3$$
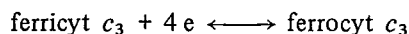
A large Nernst slope, 93 mV, in the potentiometric measurement can be explained by assuming that the electrode reaction is four one-electron steps. The equally spaced four standard potentials with -40 mV spacing generates a Nernst slope of about 90 mV over the c_O/c_R values from 0.2 to 5.0. The simulations were made for the cases where the standard potentials of four hemes were spaced unequally. The differential pulse polarogram simulated from a model with unequally spaced standard potentials (about -50, -20, and -40 mV) is in good agreement with the observed one.

Figure 1. Normal Pulse polarogram of the reduction of ferricytochrome c_3.

References

1) T. Yagi, M. Goto, K. Nakano, K. Kimura, and H.Inokuchi, *J. Biochem. (Tokyo)*, **78**, 443 (1975).
2) K. Niki, T. Yagi, H. Inokuchi, and K. Kimura, *J. Electrochem. Soc.*, **124**, 1889 (1977).

VI—G   Distortion of Molecular Structure by Solvent and
Appearance of Forbidden Bands in Phosphorescence

Toshiro MURAO and Tohru AZUMI *(Tohoku Univ.)*

In lower paraffin matrices, phosphorescence spectra of anthraquinone have sharp and well resolved structures at low temperatures. In all solvents except one, its phosphorescence spectra have no g-type vibrational band as expected from symmetry, and are well explained by the D_{2h} molecular structure. In pentane, the phosphorescence has some totally symmetric vibrational bands, indicating the distortion of the molecule to b_{3u} direction (normal to molecular plane) by solvent effect. Because of experimental difficulty, the molecular orientation in mixed crystals are not known. Now we attempted to calculate how the molecule is oriented in mixed crystals, and which direction the molecule distorts.

Nonbonded interatomic potential energy between atom i in a solute molecule and atom j in a solvent molecule is given by the equation,

$$E_{ij} = -A_{ij}r_{ij} + B_{ij}exp \, (-C_{ij}r_{ij})$$

where A_{ij}, B_{ij} and C_{ij} are parameters determined by the pair of atoms, and r_{ij} is an interatomic ditance.

We have calculated them in three solvents, i.e., pentane, hexane and octane. In hexane and octane, phosphorescence spectra have no g-type vibrational band and are well explained by the D_{2h} molecular structure. The crystal system of hexane and octane is triclinic, the space group is $P\bar{1}$, and a unit cell has a single molecule, while that of pentane is orthorhombic, the space group is Pbcn, and a unit cell has four molecules.

Orientation of anthraquinone in solvents is determined by repulsive interatomic interaction rather than attractive one, especially between hydrogen and carbonyl oxygen atoms in the solute molecule and hydrogen atoms in solvent molecules.

In each solvent, two minimal points of nonbonded energy exist, and these results well coincide with the fact that there are two main phosphorescent sites in each solvent.

One of insertion modes of anthraquinone in pentane is peculiar compared with those in other solvents. According to Figure 1, in this matrix planar anthraquinone molecule is sandwiched in between pentane arrays, and hydrogen atoms and carbonyl oxygen atoms are very close to hydrogen atoms in pentane. Under these conditions, force field to out-of-molecular plane must be large, and hydrogen and oxygen atoms in solute molecule should have trend of distortion to out-of-molecular plane. This conclusion corresponds to the experimental results.

References

1) T. Murao and T. Azumi, *J. Chem. Phys.,* 70, 4460 (1979).
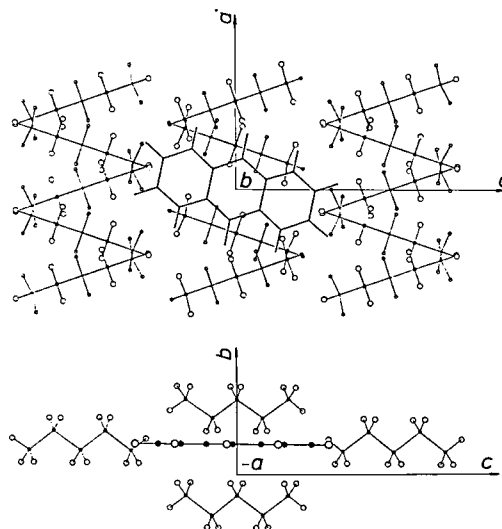2) T. Murao and T. Azumi, *J. Chem. Phys.,* in press.

Figure 1. Orientation of anthraquinone molecule in pentane mixed crystal.

Low Temperature Center

Low Temperature Center develops cryogenic techniques in close cooperation with research divisions and other centers. We are preparing a calorimeter and also an instrument of AC magnetic susceptibility measurement which are operated in the temperature region between liquid helium and room temperatures. In addition, we investigate the solid state properties of polyvalence and mixed valence compounds, which are conductive or exhibit metal-insulator transitions, through the measurements of electrical conductivity, specific heat and magnetic susceptibiiity.

VI—H Electrical, Magnetic and Thermal Properties of the Partially Oxidized Derivative of Magnus Green Salt

Toshiaki ENOKI, Ikuji TSUJIKAWA *(Kyoto Univ. and IMS)*, Ryozo KUBOTA *(Kyoto Univ.)*, and Hanako KOBAYASHI *(Kyoto Univ.)*

Recently, one-dimensional metallic compounds with mixed valence such as KCP $(K_2Pt(CN)_4Br_{0.3} \cdot nH_2O)$ and KOP $(K_{1.6}Pt(C_2O_4)_2 \cdot nH_2O)$ have been studied vigorously in connection with the existence of superconduction. These compounds show the Peierls transition and the charge density wave. The partially oxidized derivative of Magnus Green Salts (MGSPOS) with the formula $Pt_6(NH_3)_{10}Cl_{10}(HSO_4)_4$ is one of the mixed valence one-dimensional metallic compounds originating from the coexistence of two valence states, Pt^{+2} and Pt^{+4} and its averaged oxidation number is +2.33. We have investigated this compound by measurements of electrical conductivity, magnetic susceptibility and heat capacity between liquid helium and room temperatures. The powdered MGSPOS is obtained from Magnus Green Salt $Pt(NH_3)_4 \cdot PtCl_4$, through the oxidation with H_2SO_4 and O_2. Results

of the X-ray powder pattern are consistent with a chain structure proposed by Gitzel et al.[1]. The electrical conductivity[2] shows a sharp peak between 190 and 220 K with the peak value extending over $10^{-1} \sim 10^{-4}\,\Omega^{-1}\,cm^{-1}$ depending on applied samples. The semiconducting phase below the temperature of conductivity peak has the gap energy $E_g \sim 0.03$ eV. In some of our samples, another transition from semiconductor to metal takes place on cooling at about 250 K. Thermal analysis shows that the transition at about 200 K from low temperature side is exothermic, while that at about 250 K is endothermic. Moreover, in this analysis, a weak transition appears at about 140 K, which behaves as a glassy transition. In order to examine these transitions more precisely, we have measured the specific heat of the sample. Figures 1 and 2 show the specific heats obtained by AC calorimetry between about 100 and 300 K. As the temperature rises, the specific heat has a broad peak between 210 and 230 K, the shape of which depends on the rate of the temperature change. On the other hand, it shows no anomaly when the temperature falls down. The specimen dependence appears in the result of the specific heat as well as the electrical conductivity.

We are attempting to synthesize single crystals of MGSPOS with several methods of oxidation and the crystal growth in a silica gel, with the purpose of understanding its conductive property more clearly.
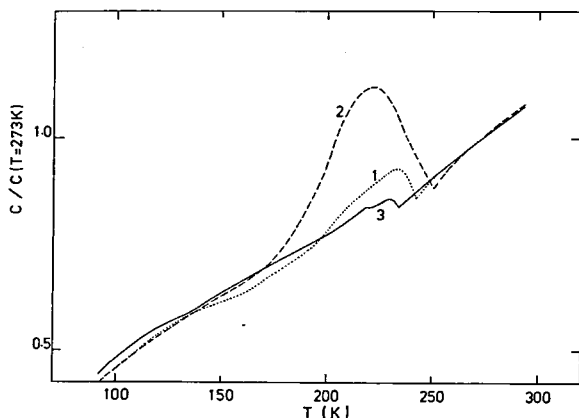

Figure 1. Specific heat of MGSPOS at the rising of the temperature. The rates of the temperature change are as follows; (1) 0.38 K/min; (2) 1.27 K/min; (3) 0.16 K/min.
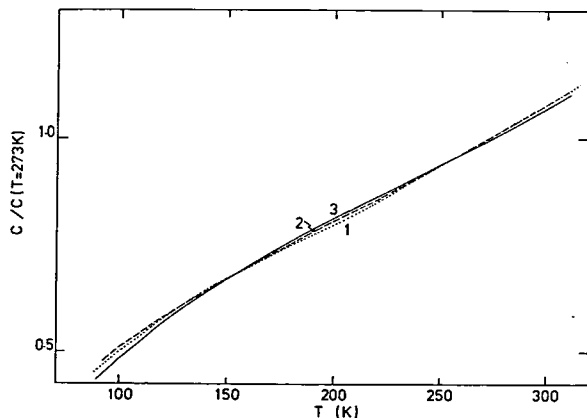
Figure 2. Specific heat of MGSPOS at the falling of the temperature. The rates of the temperature change are as follows; (1) 1.72 K/min; (2) 0.63 K/min; (3) 0.11 K/min.

References

1) W. Gitzel, H. J. Keller, H. H. Rupp, and K. Seibold, Z. Naturforsch 27b, 365 (1972).
2) I. Tsujikawa, R. Kubota, T. Enoki, S. Miyajima, and H. Kobayashi, J. Phys. Soc. Japan 43, 1459 (1977).

VI-I Thermometry by AC Method

Toshiaki ENOKI

AC calorimetry is an appropriate method to measure the specific heat of small size samples. There are many materials, the specific heats of which have not been measured by a usual adiabatic calorimeter because they cannot be propared in an enough amount. We prepared an AC calorimeter in order to investigate the specific heat of samples which are below about 100 mg in the temperature region between about 10 K and room temperature. Figure 1 shows the specific heat of the grafoil (artificial graphite sheet). We are measuring the specific heat

Figure 1. Specific heat of grafoil. The sample weight is 1.18 mg.

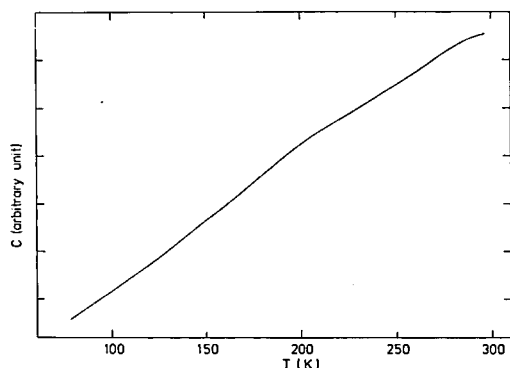of aromatic alkali metal charge transfer complexes and biological substances such as proteins. Furthermore, we are planning to study the occlusion behavior of hydrogen in the charge transfer compounds by AC calorimetry under a regulated atomosphere of hydrogen.

Chemical Materials Center

We have been preparing some condensed aromatics in highly pure states with the purpose of investigating the correlation between their structures and physicochemical properties such as photoconductivity. We have also been studying on the synthesis of new chiral phosphine ligands effective for transition metal catalyzed asymmetric synthesis. Efforts have also been devoted to developing new selective chemical transformations promoted by infrared lasers.

VI—J   Photoconductive Properties of Organic Solids.
Preparation of Highly Pure Condensed Aromatic Compounds

Kinko KOYANO *(Aichi Univ. of Education)*, Arata YASUDA, Hidemasa TAKAYA, Naoki SATO, and Hiroo INOKUCHI

The physical and chemical properties of condensed aromatic compounds have been a subject of continued interests for many years. Although some highly pure condensed aromatics have been prepared and their physicochemical properties investigated, preparations of such samples are in general of great difficulty because of their poor solubility in organic solvents and also of their high melting point. The present study was initiated in order to establish the procedures for obtaining some highly pure condensed aromatics such as pyranthrone, flavanthrone, pyranthrene, and flavanthrene and also to investigate the

correlation between their structures and physicochemical properties such as photoconductivity. Synthesis of flavanthrene (2) was carried out according to the reported procedure starting from flavanthrone (1) (eq. 1).[1] Extraction of 2 with 1,2,4-trichlorobenzene from the black crystalline mass gave, after evaporation of the solvent, crude flavanthrene in 51% yield as dark red crystals, which decomposed at around 410°C. Several recrystallization from 1,2,4-trichlorobenzene followed by sublimation at 300°C (2 × 10^{-7} torr) or a combination of recrystallization from 1,2,4-trichlorobenzene and silica gel chromato-

$$Zn, \quad ZnCl_2 \cdot xH_2O$$
$$NaCl \longrightarrow$$

(1)

1   2

135
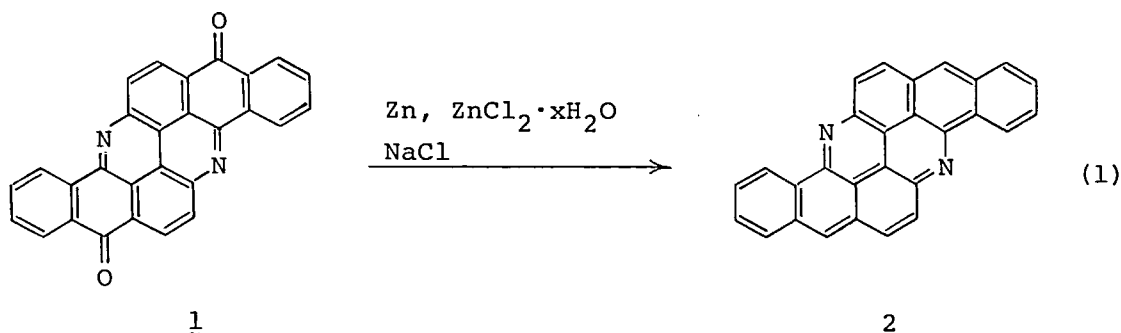
graphy eluted by chloroform gave a pure sample of 2. Mass spectrum of 2 exhibited the molecular ion peak at m/e 378. Homogeneity of the sample was confirmed by analyses by absorption and emission spectra and by high performance liquid chromatography (JAPAN Anal. Ind. Co., LC-08, JAIGEL-1H and 2H columns in series, chloroform, 17 recycles). Differential scanning calorimetry revealed that the melting point of the sample is 396.4°C (lit.[1] 386–388°C). Above 400°C sublimation occurred accompanied by considerable decomposition. Investigation of the purity of the sample by fluorescence lifetime and the measurements of physicochemical properties are underway.

Reference

1) J. Aoki, *Bull. Chem. Soc. Jpn.*, 41, 1017 (1968).

VI-K Synthesis of a New Chiral Phosphine Ligand and its Use in Rh (I)-Catalyzed Asymmetric Hydrogenation of α-Amidoacrylic Acids.

Arata YASUDA, Hidemasa TAKAYA, and Ryozi NOYORI *(Nagoya Univ.)*

We have been studying on the synthesis of new chiral phosphine ligands and their use in transition metal catalyzed asymmetric transformations. We have already prepared racemic 2,2'-bis-(diphenylphosphino)-1,1'-binaphthyl (1) (hereafter abbreviated to BINAP). Optically active samples were obtained by optical resolution by the use of a chiral palladium complex. The absolute configuration of BINAP was determined by x-ray chrystallography (see section V-E in research activities). Further investigation of the catalytic asymmetric hydrogenations of prochiral α-benzoylaminocinnamic acids and their methyl esters were carried out in the presence of Rh (I) complex bearing (R)-1 as the chiral ligand. The results are

(R) – (+) – 1
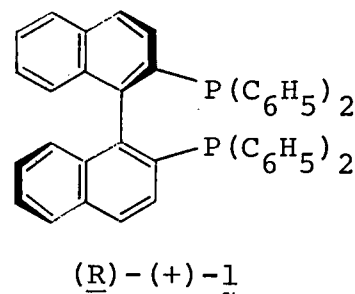
listed in Table I. Although optical purity of the products are still unsatisfactory, some improvements in optical yields were attained in the asymmetric hydrogenation of (Z)-olefins. The mechanism of the asymmetric hydrogenation and the structures of the intermediates are under investigation.

References

1) H. Takaya, T. Souchi, A. Yasuda, and R. Noyori, *IMS Ann. Rev.*, 92 (1978).

VI-L Studies on the New Selective Chemical Transformations Promoted by Infrared Lasers

Hidemasa TAKAYA, Arata YASUDA, and Masashi YAMAKAWA *(Nagoya Univ.)*

In view of the unique characteristics of laser such as monochromaticity, tunability, and high density of the light, chemical reactions induced by laser have been a subject of great interest. The use of infrared lasers may have a number of advantages over conventional thermal methods. For example, selective heating of the starting infrared absorbing materials is possible without competitive thermal reactions of the products. We have installed LUMONICS 203 instrument, a pulsed CO_2 TEA laser equipped with a diffraction grating. Methylenecyclopropanes are well

Table I. Asymmetric Hydrogenation of α-Benzoylaminocinnamic Acid Derivatives in the Presence of $[Rh (binap) (nbd)]^+ ClO_4^-$.[a]

Substrate	Configuration of BINAP	Solvent	Product		
			Yield, %	% e, e	Configuration
C6H5, H >C=C< NHCOC6H5, COOH	R	C_2H_5OH[b]	99	56	S
C6H5, H >C=C< COOH, NHCOC6H5	R	THF	94	53	R
C6H5, H >C=C< NHCOC6H5, COOCH3	R	CH_3OH	92	37	S
C6H5, H >C=C< COOCH3, NHCOC6H5	R	CH_3OH	95	15	S

[a] Hydrogenations were carried out with 1 mmol of substrate and 0.01 mmol of $[Rh (binap) (nbd)]^+ ClO_4^-$ in the specified solvent (15 mL) at the hydrogen pressure of 5 atm (35°C, 12 h).
[b] Triethylamine (1 mmol) was added.

known as one of the degenerate molecules and their thermal and photochemical behaviors have been extensively studied. We have been investigating the infrared laser-promoted isomerization of methylene-cyclopropanes with the purpose of elucidating the mechanism of the isomerization and the effects of the infrared wavelength on the efficiency of the reactions.

Development Workshop

The present activity contributes to the development of two instruments, which are a high power laser and a synchrotron light source.

Since the last year, a visible and infrared laser of picosecond with large tunability using the optical parametric effect has been constructed and its application as a light source for an optical excitation and detection of pulsed electron paramagnetic resonance has been developed.

At the beginning of this year, the design study of the synchrotron light source, UVSOR (ultraviolet synchrotron orbital radiation) was started. UVSOR is a 600 MeV electron storage ring dedicated for optical research, the injector of which is a 600 MeV synchrotron. A preliminary test of the ultrahigh vacuum system is now in progress besides the design study.

VI—M Development of an Intense Widely Tunable Light Source System Using the Optical Parametric Effect

Yoshihiro TAKAGI and Keitaro YOSHIHARA

Picosecond, intense and widely tunable coherent light sources are extremely useful in the fields of photophysics, photochemistry and photobiology.

We have developed a visible and infrared (420 nm-4μ) light source system due to the optical parametric oscillation and amplification (OPOA) pumped by the fundamental, third harmonics or fourth harmonics of a mode-locked YAG laser. Single crystals of ADP or KD*P (99% deuterated) and $LiNbO_3$ were used for the visible and infrared OPOA, respectively. In all cases the two-crystal configuration was used for the purpose of spectral filtering and amplification. Experimental conditions and results are summarized in Table I.

This system is to be assembled as the picosecond measurement systems for emission or absorption spectra in photo-induced chemical reactions. (See the section of LARGE SCALE RESEARCH EQUIP-MENTS).

Table I. Experimental conditions and results on OPOA in ADP, KD*P and $LiNbO_3$.

crystal	excitation wavelength	phase match condition	tuning range	average output power	conversion efficiency	spectral width
ADP	266 nm	temperature	420–700 nm	20 μJ	5%	1–5 Å
KD*P	355 nm	angle	450–630 nm, 810 nm–1.7 μ	100 μJ	5%	2–5 Å
$LiNbO_3$	1064 nm	angle	1.4–4 μ	5 mJ	10%	50 cm^{-1}

RESEARCH FACILITIES

There are five research facilities, i.e., Computer Center, Low Temperature Center, Instrument Center, Chemical Materials Center, and Development Workshop for supporting the research activities in the Divisions of IMS. A certain number of technical associates and technicians as well as scientific staff are assigned to each facility. Upon request of the scientists of IMS, they carry out works in their own specialized fields. The scientific staff of the research facilities also carry out their own research and development in close collaboration with other scientific members of IMS. Most of the instruments installed in the research facilities are in principle open to domestic scientists.

Computer Center

The Computer Center began its computational services in January 1979. The computer system consists of two HITAC M-180 computers with an overall processing capacity of more than 8 million instructions per second. The processor uses 32 bit words and is essentially IBM-compatible at both the hardware and software levels. It has 8 mega byte main memory, 7150 mega byte disk memory and other common I/O devices. The computer is used not only by the research staff of IMS but also by the staff at the nearby National Institutes as well as by scientists outside the Institute in the related fields. The present numbers of project groups and users are 122 and 245, respectively. In the first three months of service, 40000 jobs have been processed with 1300 hours of the CPU time. One of the most important projects of the Computer Center in 1979 is the development of a consolidated computer system which runs without an operator. The hadrware consists of many sensors (smoke, heat, water, temperature, humidity, and earthquake), alarm systems, and automatic fire extinguishers. The software returns preassigned responses to operator calls from the system. The system sends alarms and terminates itself, airconditioners and the power supply in the emergency. It can also automatically stop the operation or freeze running jobs when preassigned conditions are satisfied. The system now provides an uninterrupted, unmanned week long service.

Another important project is the establishment of a program library for molecular science. Many programs are now being developed anew or converted from other computer centers. All of the QCPE programs has been obtained and will be attained on the continued basis. An arrangement is being made to introduce programs supported by the National Resource for Computation in Chemistry at Berkeley, Calif. The library management software has been completed, with which users can search on their TSS terminal whereabouts and guides of wanted programs.

The center has recently begun its new service of QCLDB (Quantum Chemistry Literature Data Base), a file of references of ab initio molecular orbital calculations. For details, see section VI-C of the Computer Center research activities.

Main Console and CPU

TSS-Terminal Room

Low Temperature Center

Low Temperature Center supplies coolants such as liquid nitrogen and liquid helium. The staff of this center also develops new cryogenic techniques in close cooperation with research divisions and other centers.

The center building (1430 m², 2 stories and 1 basement) was completed in March 1979. It consists of three machine rooms, ten laboratories, a machine shop and also a control room for a helium liquefaction and recovery system. The floor and the walls of the machine rooms for compressors and Kinney vacuum pumps were separated from the rest of the building to avoid the propagation of mechanical vibrations of the heavy machines.

The laboratories are to be equipped with spectroscopic, magnetic and calorimetric instruments for low temperature measurements. Seven laboratories are located at basement in order to keep a well regulated environment. Especially, one of them is the shielded room where the attenuation rate of electromagnetic disturbance is 80 eB. One can use two Kinney vacuum pumps in the laboratories when he experiments below 4.2 K.

A helium liquefier (CTI-1410) with capacity of 40 l/h started running and this center is supplying liquid helium to research groups.

Main laboratory building and research facilities are equipped with the recovery pipings for helium gas. Helium gas used by experiments is recovered to Low Temperature Center and purified up to 99.99% purity.

The flowsheet of the helium liquefaction system is as follows:
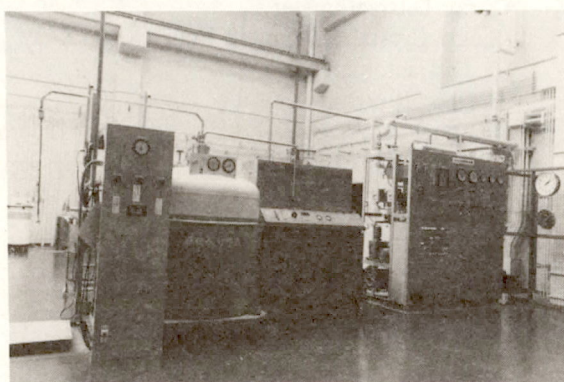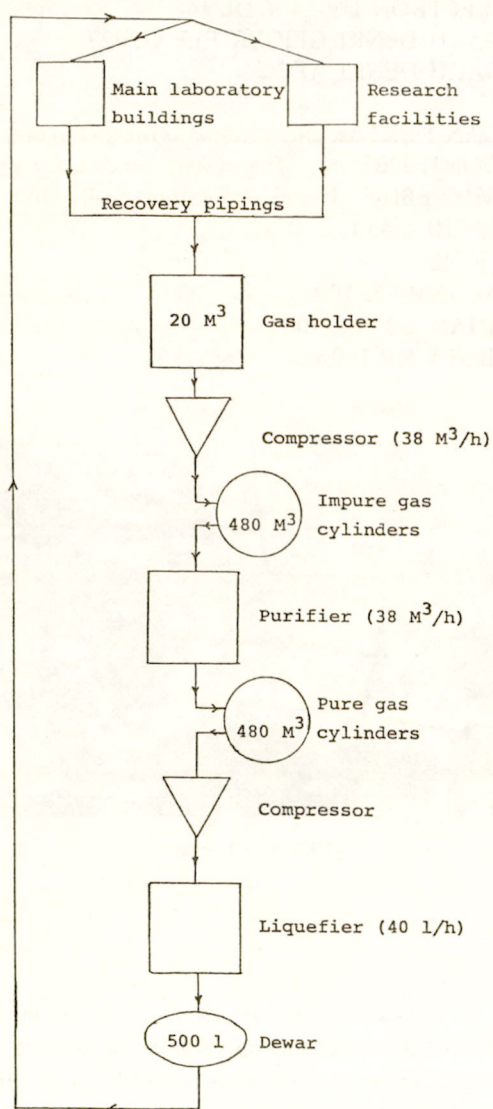
Helium liquefier and purifier

Major equipments are:

Helium liquefier	CTI 1410
Helium purifier	OSAKA SANSO UℓO-1394-5
Cold converter of liquid nitrogen	OSAKA SANSO CO-3
Helium leak detector	ULVAC DLMS-33
Rare gas purifier	BOC MK-3
Optical measurement cryostat	OXFORD CF-240

Main laboratory buildings — Research facilities — Recovery pipings — 20 M³ Gas holder — Compressor (38 M³/h) — 480 M³ Impure gas cylinders — Purifier (38 M³/h) — 480 M³ Pure gas cylinders — Compressor — Liquefier (40 l/h) — 500 l Dewar

139

Instrument Center

The Instrument Center is equipped with instruments for general use as listed below. The Center also lends out electronic and optical instruments, such as oscilloscopes, lock in amplifiers, integrators, function generators, electrometers, power supplies, recorders, single and double monochromators.

The staffs operate these instruments as well as develope new instrumental techniques. The Center had many visiting research scientists and graduate students from universities amount to the total man-days of 245 in the fiscal year of 1978.

The major instruments installed are as follows:

Spectrophotometer	CARY 17
Dual-wavelength Spectrophotometer	HITACHI 556
Fourier-Transform IR Spectrophotometer	JEOL JIR-10
Automatic Recording Spectropolarimeter	JASCO J-40C
Corrected Recording Spectrofluorophotometer	SHIMADZU RF-502
1-Meter VUV Scanning Monochromator	GCA MCPHERSON 225
Photoelectron Spectrometer	PERKIN ELMER PS-18
Laser-Raman Spectrophotometer	JEOL JRS-400T
Nanosecond Spectrometer	APPLIED PHOTOPHYSICS SP-3X+ORTEC
Argon Ion Laser	SPECTRA-PHYSICS 164-05
Helium-Neon Laser	SPECTRA-PHYSICS 125A
CW Dye Laser	SPECTRA-PHYSICS 375-90
Pulsed Dye Laser	MOLECTRON UV-24 + DL 14
X-ray Diffractometer	RIGAKU DENKI GEIGER FLEX 2027
Single Crystal Automatic Four Circle X-ray Diffractometer	RIGAKU DENKI AFC-5
Surface Roughness Tester	SLOAN DEKTAK
Thermal Analyzer	DUPONT 990
High Vacuum Evaporator	ULVAC EBH-6
Scanning Electron Microscope	HITACHI S-450
Magnetic Balance	OXFORD
Fourier-Transform NMR Spectrometer	JEOL JNM-FX 100
ESR Spectrometer	VARIAN E-112/E-900
High Speed Refrigerated Centrifuge	KUBOTA KR-180A

Single Crystal Automatic Four Circle X-ray Diffractometer
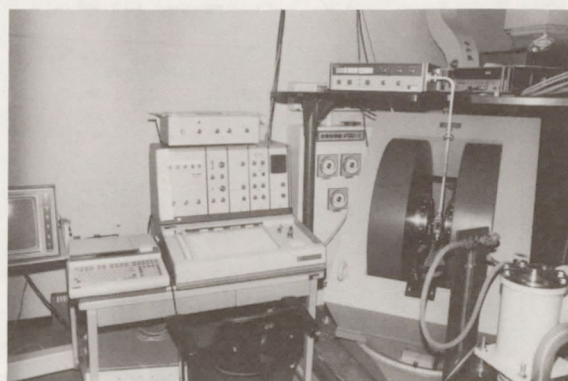
ESR Spectrometer

Chemical Materials Center

The chemical materials center plays an important role in the preparation of chemical substances in IMS. The scientists and technicians of this facility carry out works on synthesis and purification of organic and inorganic compounds and preparation of single crystals. They develop new synthetic procedures to obtain interesting substances in pure forms and in large quantities. They also carry out their own research on

synthesis of new interesting chemicals, developments of new selective chemical transformations, elucidation of reaction mechanisms, and application of new methodologies to analysis of materials (see Research Activities VI-J~L). They participate in taking charge of and disposition of waste chemicals and solvents. The Center building was completed in March 1978. Piping works were completed and laboratory apparatuses were sufficiently equipped. The stockroom stores more than five hundred chemicals and solvents. Hot water enough for experiments is supplied by solar energy collectors equipped on the roof of the building.

Major equipments are:

Gas Chromatograph-Mass Spectrometer	JEOL JMS D300 equipped with EI, CI, and FD ion sources, and JMA-2000 mass data analysis system
NMR Spectrometer	Varian EM-390
High Performance Liquid Chromatographs	JASCO TRI ROTAR and JASCO FAMILIC-100
Inert Atomosphere Glove Box	Vacuum Atmospheres Co. MO-40-2V DRI-TRAIN
CO_2 TEA Laser	LUMONICS 203
Infrared Spectrometer	Hitachi 295
Instrument for Crystal Growth	Assembled in IMS
Analytical Gaschromatograph	Ohkura 701
Preparative Gaschromatograph	Shimadzu GC-6A
Automatic Waste Fluid Disposition Apparatus	Yanaco YWT-1
Plarimeter	JASCO DIP-4
Zone Refiners	Shibayama SS-960 and Instruments Assembled in IMS
Freeze Dryer	RFS-5000
Autoclave	Nitto Koatsu (500 ml) equipped with automatic temperature controller
Automatic Laboratory Washer	Miele G-19LG
Ultrasonic Cleaner	Kokusai Denki UO600FA-UT50A
Bath Cooler	NESLAB CryoCool CC-100 equipped with temperature controller
Low Temperature Room	SANYO ($4°C$, 3.3 m^2)
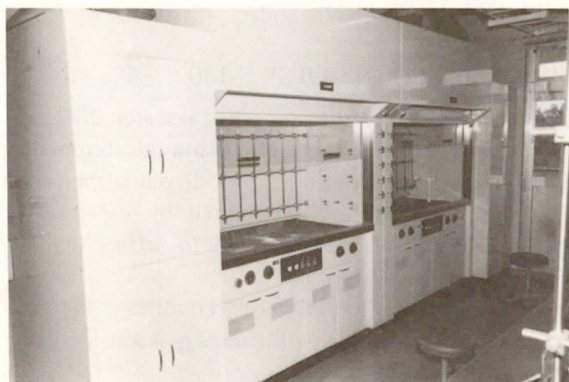
Hoods for organic and inorganic synthesis
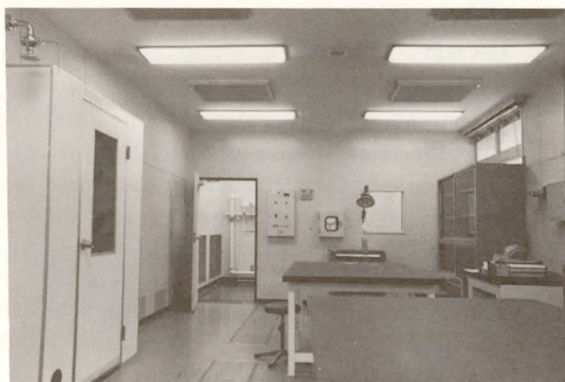
The clean rooms of class 10000 (this side) and class 100 (the inner part)

Development Workshop

Development Workshop is expected to play a unique and important role in research activities at IMS. It designs and constructs instruments based on IMS's own ideas. It also improves existing research equipments. Technicians are making interplay with scientific staff members to support activities of the Workshop. Technical meetings are regularly held twice a year, which provide opportunities for technicians to exchange information and to discuss technical problems with those from other institutes and universities.

Development Workshop consists of machine shop, electronic shop, and glass-blowing shop.

1) Machine Shop

The facilities constructed or to be constructed at IMS include high-vacuum apparatus, lasers, microwave

spectrometers as well as various types of equipments operated at the liquid-helium temperature. All these are of high performance and thus require very fine engineering to prepare their parts. Therefore, in addition to lathes, fraises, drilling machines, and grinders of common use we have installed the following special machines:

(i) NC Lathe (OKUMA TEKKOSHO LS-N). This computer-controlled lathe has been used to prepare microwave lenses with spherical and/or paraboloidal surfaces, made of Teflon, TPX, or metals. It also prepared spherical collectors for electron spectroscopy. None of these parts can be constructed with a normal lathe. The electronic shop develops microcomputer facilities to feed tapes in the NC lathe.

(ii) Spark erosion machine (MAKINO SODICK GP-20L). This has been used to make a 50 mm diameter stainless steel cylinder of 0.025 mm thickness, which is to support an optical window in a low-temperature apparatus. It has also been used to drill a very fine slit (0.04 mm wide and 30 mm long).

(iii) Electron-beam welder (NEC EBW). This can weld tightly two different kinds of metals (e.g. copper and stainless steel). This welding eliminates possible leakage in a vacuum apparatus operated at a very low temperature, especially in those parts that suffer from frequent changes of temperature. We can use a beam of 10 mA accelerated at a voltage of 150 kV under the pressure of 5×10^{-2} Pa or less. The maximum beam power is 1.5 kW.

(iv) Helium/nitrogen leak detector (ULVAC DLM 33). This detects a leakage in an ultra-high vacuum apparatus as small as $3 \times 10^{-9} \ell$ Pa/s. It may even detect the nitrogen gas. This machine consists of a detector combined with a vacuum system designed by the Machine Shop. It is equipped with a microcomputer that automatically eliminates backgrounds and noise signals.

2) Electronic Shop

The major instruments installed are:

Oscilloscope	TEKTRONICS 7904 (500 MHz)
Oscilloscope	TEKTRONICS 475 (200 MHz)
Storage oscilloscope	HEWLETT PACKARD 1741A (100 MHz)
Sampling oscilloscope	IWATSU SAS-610B (12.4 GHz)
Spectrum analyzer	TAKEDA RIKEN 4110M (200 Hz-1.3 GHz)
Frequency counter	TAKEDA RIKEN 5502C ($\leqq 1.4$ GHz)
Lock-in amp	PAR 124
Boxcar integrator	PAR 162
LCR meter	HEWLETT PACKARD 4262A
Teletype	CASIO 502
Minicomputer system	NIHON MINICON ECLIPSE S-130

The Electronic Shop has designed and constructed the following devices by the request of research divisions:

(i) A High-Precision Wavelength Meter for Infrared Diode Laser. The instrument is a Michelson interferometer; fringes for IR diode laser and He-Ne laser (used as a reference) beams, produced by motor-driven corner cube reflectors, are simultaneously counted, and the wavelength of IR laser is thus determined by the ratio of frequencies with the precision of 1-0.1 ppm. The Mechanical Shop has also contributed to setting up this instrument. (Cf. II-C-2)

(ii) A Data Processing System for a Magnetic Balance. This system makes experimental conditions for measurements from 1.5 K to 200 K programmable with access from a key board. A graphic display is also available for data accumulation and processing.

(iii) A Micro-computer Controlled Picture Analyzer for a Picosecond Streak Camera. This system digitizes video signals from a SIT camera and stores them on a 16 kB RAM. A monitor TV attached graphically displays the signals after calibration. As an example picosecond behavior of fluorescent spectra emitted from laser-excited chemical species are being observed under the condition of a single event.

3) Glass-blowing Shop

We have installed the following machines:

Glass Lathe	RIKEN SEIKO RGL-4DLH (max. diameter of the glass pipe: 20 mm)
Spot Welder	NIPPON AVIOTRONICS NW-29 DS (100 W)
Water Welder	FUJI BUSSAN S51-4 (oxygen/hydrogen evolving rate: 170 ℓ/h)
Glass Grinder	SANWA DIAMOND SDK 20-B (diamond disk 300 mmϕ with an angle holder)
Ultrasonic Microboring Machine	CHO-OMPA KOGYO UM-2-7B

Ultrasonic Soldering Machine   ASAHI GLASS SUNBONDER USM-II

The Shop has constructed, among others, high vacuum glass apparatus and laser tubes.
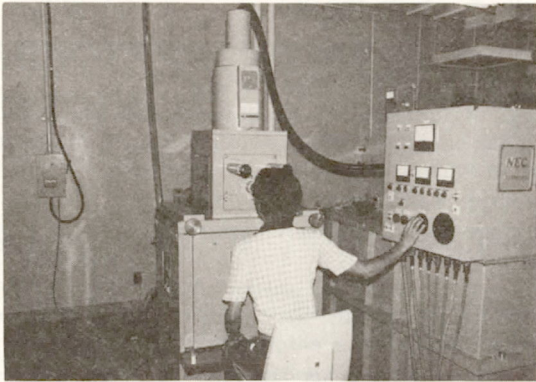
Machine Shop

Glass-blowing Shop

Electronic Shop

LARGE SCALE RESEARCH EQUIPMENTS

1) Time-Resolved Spectroscopy

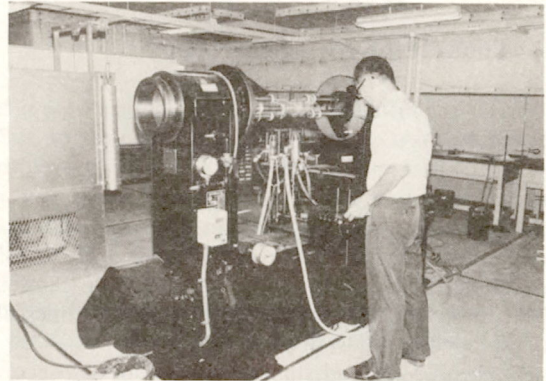After the installment and construction of the pico-second Nd:YAG laser during the fiscal year of 1976 ~1977 (IMS Annual Review 1978), we improved the laser as indicated in 1-a) and 1-b). These improvements were necessary for transient absorption spectroscopy and for developing the picosecond continuously tunable laser described in 2). A system for transient absorption spectroscopy in the picosecond timescale is developed and described in 1-c).

1-a) High power and stable operation of picosecond Nd:YAG laser system

In order to widely apply picosecond laser spectroscopy, it is preferable to obtain as much wavelengths and as high power as possible. Conversions of wavelength are usually made by various kinds of non-linear processes. Thus stable operations of laser oscillation and amplification are required.

Since optical damages of laser rods and optical components limit output power of amplifications and various frequency conversion processes, a special attention was paid on a spatial uniformity of intensity in a laser beam. The laser beam of our oscillator was controlled perfectly to TEM_{00} mode without having an aperture inside the cavity. After passing a single pulse selector and the first amplifier, the cross section of the beam became elliptical. A spatial filter with a 0.8 mm pinhole generates a nearly gaussian beam. Soft apertures are required to avoid Frenel reflection by laser rods. Dye decouplers between the oscillator and amplifiers and between the second and third amplifiers stabilized effectively the energy of the final output. We obtained an average power of

(a)

(c)

(b)

(d)
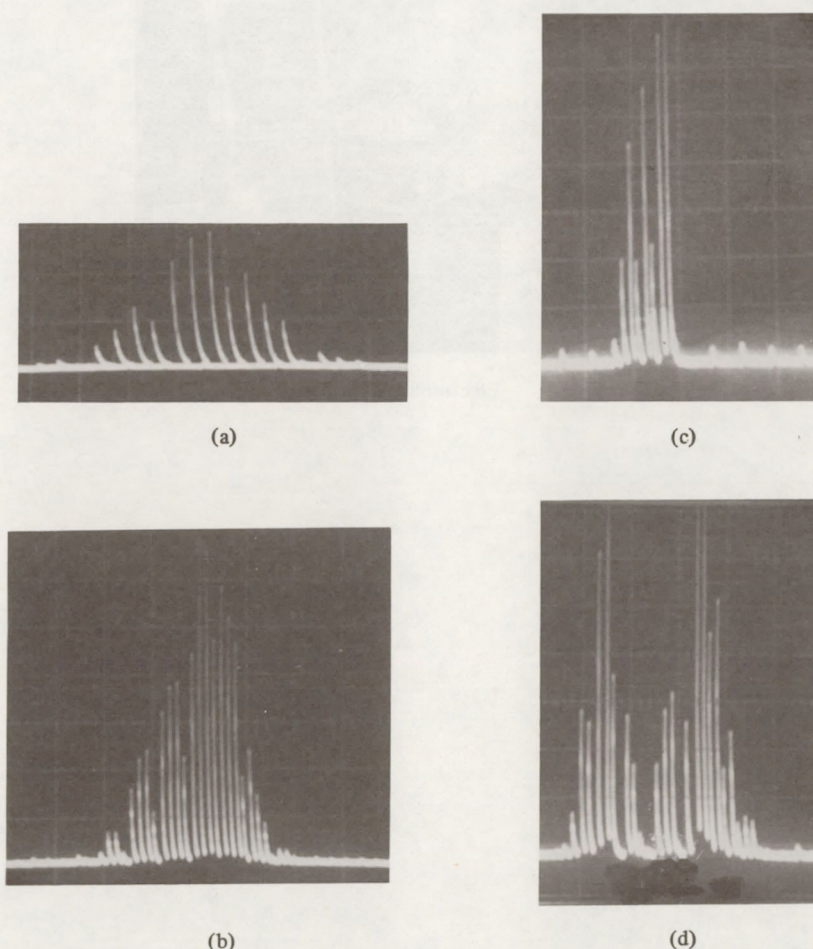
Figure 1. Spectra of the laser output at various conditions. The combination of a 0.8 m double monochromator and a Si-diode array detector was used (0.25 Å/line). a) output from the oscillator λ=1.064 μm, half width $\Delta\lambda \sim 1.7$Å, b) output after three stage amplifer (50 mJ), $\Delta\lambda \sim 3$Å, c) after a second harmonic generator λ=532 nm (input energy to SHG≈40 mJ/cm^2), d) after the SHG at higher input energy (70 mJ/cm^2).

100 mJ/pulse at 2 Hz without an optical damage for more than half a year.

1-b) High conversion efficiency from 2ω to 4ω

For the second harmonic generation from 2ω to 4ω under a high power condition ($\gtrsim 1\,\mathrm{GW/cm^2}$) we have tested several kinds of crystals including KDP, ADP, RDP, and KD*P. Among them we found a KD*P with crystal lengths of $\lesssim 1$ cm gave the best performance. The conversion efficiency for 4ω generation in this crystal decreases to one half at the following conditions; 1) $1.8°\mathrm{C/cm}$ ambient temperature around $22.0°\mathrm{C}$, 2) ~ 3 mrad/cm divergence of the input laser beam, and 3) 1 Å/cm wavelength tolerance. Since our laser is working at the highest power level, the wavelength tolerance gives the most severe problem. The accumulated phase-retardation effect in the laser beam is estimated to be $\sim 4\pi$. This induces selfphase modulation, and then the spectral width of the laser beam becomes 3 Å from the original 1.7 Å at the oscillator. The actual measurements were made with a combination of a 0.8 m double monochromator and a Si detector array, as shown in Figure 1a) and 1b). The width is 3 times of the torelance wavelength in the 1 cm KD*P crystal.

At higher power input ($\gtrsim 2\,\mathrm{GW}$) parametric back reaction occurs. This effect is shown in Figure 1c and 1d. In Figure 1d the central part of the spectrum is nearly missing. If we adjust the angle of the crystal properly at a lower power range, the conversion efficiency from 2ω to 4ω decreases considerably.

The results indicates that the self-phase mudulation is very important in the picosecond YAG laser and the input energy to non-linear crystals should be kept below ~ 1 GW/cm². The two photon absorption of 4ω by nonlinear crystals also restricts the conversion efficiency. This effect becomes important at longer crystals than 1.5 cm at the input energy level more than 4 mJ.

The damage thresholds of KDP and KD*P are highest in the nonlinear crystals we have tested, however KD*P has lower absorption coefficient of the two photon absorption than that of KDP. We achieved up to 3 mJ of 4ω (266 nm) starting from ~ 100 mJ of ω (1.064 µm).

1-c) Picosecond time-resolved absorption spectroscopy

Akira NAMIKI, Minoru SUMITANI, Nobuaki NAKASHIMA, and Keitaro YOSHIHARA
[*Oyo Butsuri (Appl. Phys.)* (in Japanese), **48**, 88 (1979)]

The entire system for picosecond time-resolved absorption spectroscopy is shown in Figure 2. The actinic light for the photolysis is second (532 nm), third (355 nm), or fouth (266 nm) harmonic of the fundamental (1064 nm). The monitor light is a picosecond continuum from D_2O, CCl_4, or BK7 glass excited by the fundamental. The continuum light is split into two halves by a half mirror and served as a sample (I) and reference (I_0) light to make a double-beam optical system. The monitor beams are
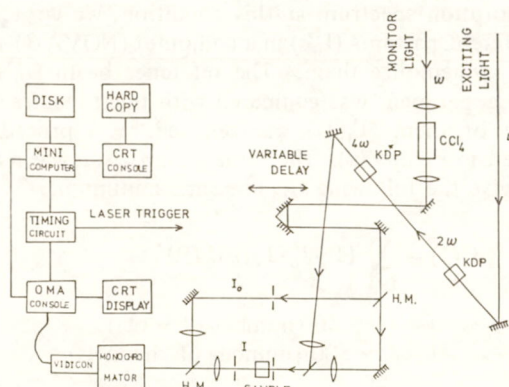

Figure 2. Total measurement system for time-resolved absorption spectroscopy with a mode-locked picosecond Nd:YAG laser.

introduced into a PAR optical multichannel analyzer (OMA) through a monochromator. The frame scanning is made in every 32.8 ms and one scan is divided into 512 channels (scan time per channel is 64 µs). The first 12 channels (768 µs) are used for the various controls in OMA and not used for the actual processing of the optical signals. In order to coincide the scanning of the spectrum and shooting the laser, we have to use one of these 12 channels. Since the laser oscillates after 10 ms delay from a trigger, the scan signal was delayed by about 20 ms and the actual scan was made during the middle of the second frame scan from the original trigger. An appropriate filter circuit is added to avoid a false operation by a noise.
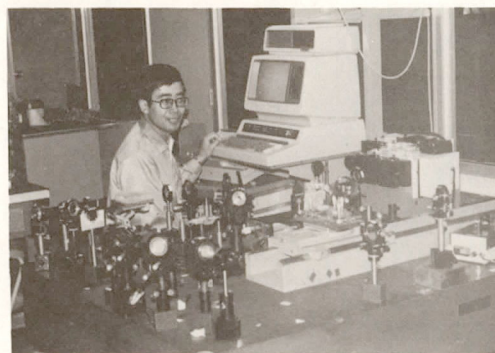
Picosecond time-resolved spectrometer

The OMA is used either with a two or one dimensional mode. In order to take a transient absorption with one pulse (for the case of precious biological materials etc.), it is necessary to measure I and I_0 at the same experiment. The I and I_0 are focused on the upper and lower part of the OMA detector with a minimum mutual interference.

The picosecond continuum spectrum differs shots by shots at the present experimental conditions and gives a few different typical patterns. Besides this, two beams for reference and sample are also slightly different each other. In order to obtain better

absorption spectrum at this condition, we wrote 10 different patterns (I_0^r's) in a computer (NOVA 3) and let it memolize them. The reference beam (I_0') at the experiment was compared with these spectra and one of them ($I_0^r(J)$) was selected by a procedure given in Figure 3a). The actual comparison was made to give the following Q(J) became minimum,

$$Q(J) = \sum_{i=1}^{500} (1 - I_0^r(J, i)/I_0'(i))^2$$

$$J = 1 \sim 10 \text{ (number of shots)}$$
$$i = 1 \sim 500 \text{ (number of channels)}$$

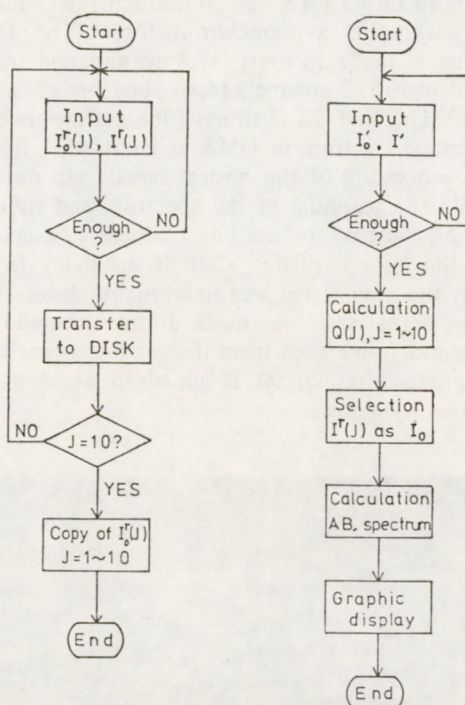When the $I_0^r(J)$ was determined, the corresponding $I^r(J)$, which was also stored in a disc, was used as a true reference spectrum (I_0). A further procedure in calculating the absorption spectrum is shown in Figure 3b).

Transient absorption spectra obtained with this method are shown in Figure 4a) and b). The spectra are the $S_n \leftarrow S_1$ absorption of cis- and trans-stilbene at 77K. Novel features of these spectra are given elsewhere.

2) Picosecond Continuously Tunable Laser from UV to IR

The recent innovation of the high power laser technology and non-linear optics made it possible to develope a tunable laser for a wide wavelength region. Picosecond lasers are particularly suitable for this purpose since the peak damage thresholds of non-linear materials are high for ps pulses. Among various methods of tuning the pumping laser we apply the second harmonic generation, mixing of different wavelengths, and optical parametric oscillations (OPO) on non-linear crystals and the induced Raman scattering by a pressurized hydrogen gas.

The fundamental pumping source is the passively mode-locked Nd^{3+}:YAG laser and 6 stage amplifier systems (photo). Spatial filters and soft apertures

Figure 3. Basic flow charts for the absorption measurements with the two-dimensional mode of OMA. .

Picosecond continuously tunable laser
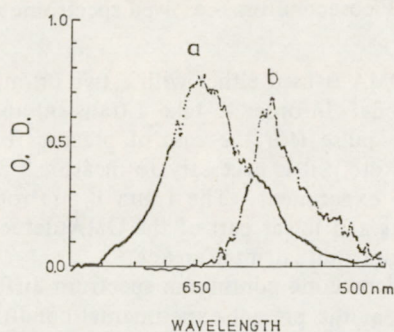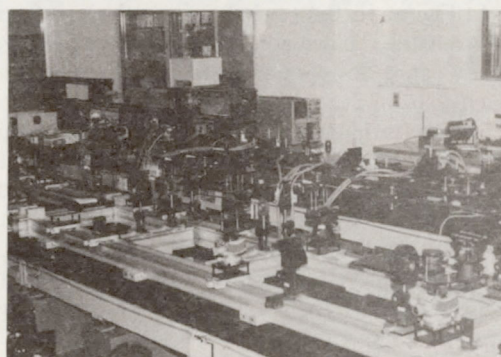

Figure 4. Absorption spectra of excited stilbene at 77K obtained with the two dimensional mode of OMA. a: cis-stilbene, b: trans-stilbene.

are set to maintain the proper quality of the laser beam during the amplifications. A block diagram of the laser system is shown in Figure 1. The visible output will be obtained by OPO of the fourth harmonic (4ω) on an ADP crystal. A small portion of the output corn is selected and amplified by a second crystal. The spectral purity is improved by a selected amplification. The beam is led to a dye amplifier and ethalon system.

The tunable infra-red light is obtained by OPO of ω on a $LiNbO_3$ crystal and amplified by a second crystal. The tuning of the wavelength will be made by tilting the oscillator and amplifier crystals which are controlled by a microcomputer The beam is introduced to a pressurized hydrogen gas cell. A continuously tunable light up to $\sim 13 \mu m$ will be obtained by coherent Raman mixing in H_2. Instruments for the spectroscopic studies will be provided.

A sub-picosecond dye laser which is excited by an Ar ion laser is also under construction (photo).

146
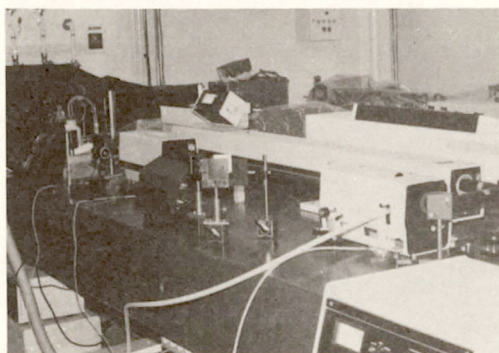
Sub-picosecond dye laser

2-a) Picosecond Optical Parametric Oscillation and Amplification in Visible and IR region

We have been developing Optical Parametric Oscillation and Amplification (OPOA) as an intense picosecond tunable light source for investigations of chemical reactions at IMS. In this section we report the results and the present situation of the experiments on visible and IR OPOA.

2-a-1) Visible OPOA

For visible OPOA, we used cascaded ADP crystals (50 × 10 × 10 mm, 90°z-cut), which were excited by

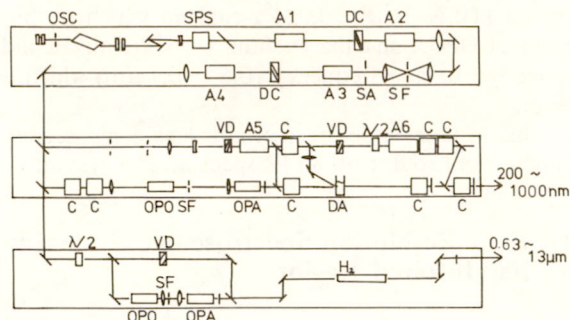**Figure 1.** A block diagram of the picosecond continuously tunable laser from UV to IR. OSC: Nd^{3+}:YAG oscillator; SPS: single pulse selector; A 1 ~ 6: Nd^{3+}:YAG amplifiers; DC: dye cells; SF: spatial filters; SA: soft aperture; VD: variable delay prisms; C: non-linear crystals for frequency conversion; $\lambda/2$: halfwave rotator; OPO: optical parametric oscillator; OPA: optical parametric amplifier; DA: dye amplifier; H_2: induced Raman cell.
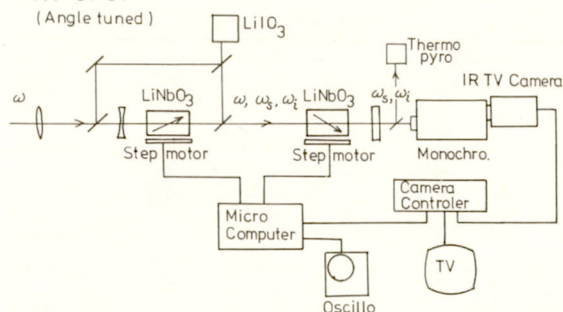

a
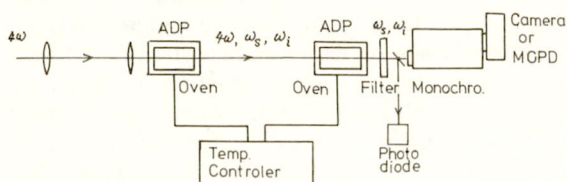
b

Figure 2. Arrangements for the optical parametric oscilla- and amplification and amplification (OPOA).
a) visible OPOA (420 ~ 700 nm).
b) IR OPOA (1.4 ~ 4 μm).

the fourth harmonic (266 nm, 0.5 mJ, 30 psec) of mode-locked single-pulse YAG laser. Output wavelength in the range of 420 ~ 720 nm was controlled by temperature tuning. The temperature of the two crystals was controlled to be equal and was stabilized to ±0.01°C, which corresponds to the stability of the output wavelength of about 0.5 Å at 600 nm. In Figure 2-a), the first crystal acts as an optical parametric oscillator. The average overall output power was 50 μJ and the spectral width was dependent considerably on the output wavelength: 10 Å at λ_i = 600 nm and increased to several tens angstroms near the degenerate wavelength. The divergence of an output beam was about 20 mrad. The central portion of the output beam which is collinear with the pumping beam was amplified and spectrum narrowed through the second ADP. The output power was about 20 μJ with the spectral width of 2 Å almost in all wavelength range.

The OPOA using ADP can cover the whole visible wavelength region (Figure 3a) and have a merit of no walk-off effect. However, the scan rate of the output wavelength was very slow because of the slow response of the temperature variation. We are testing another type of OPOA using a KD*P crystal. We use the combination of cascaded KD*P crystals (40 × 15 × 15 mm, 58°z-cut, type-II) for OPOA and third harmonic (355 nm, 5 mJ, 30 psec) of the mode-locked single pulse YAG laser for an excitation. KD*P crystals will be automatically angle-tuned by means of step motors controlled by a microcomputer. The advantages of this system are as follows: i) it has high scanning rate of wavelength. ii) wide output wavelength range is obtainable (450 nm ~ 1.7 μm) as shown in Figure 4b. iii) a higher output power is expected by the use of strong pumping beam (3rd harmonic of YAG laser), compared with the case of OPOA with ADP.

2-a-2) IR OPOA

We are also testing OPOA in the IR region (1.4 ~ 4 μm) using cascaded $LiNbO_3$ crystals (25 × 10 × 10 mm, 47°z-cut) as shown in Figure 3-c). The crystals were used in the angle-tuned condition at

ADP OPO.

a

LiNbO₃ OPO.

c

Figure 3. Tuning curves of the OPO
c) Angle tuning curve of the IR OPO in LiNbO₃.
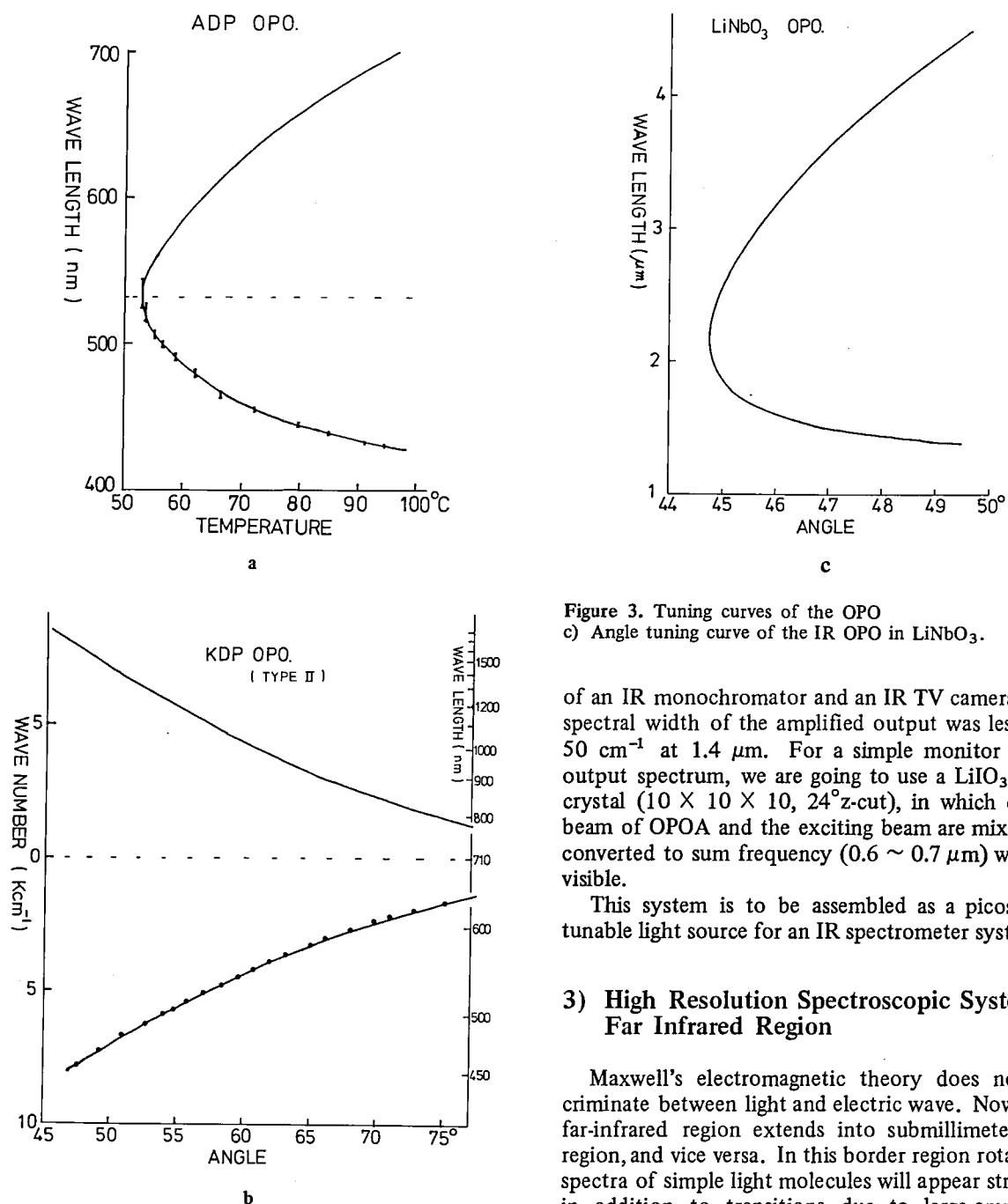
KDP OPO.
(TYPE Ⅱ)

b

Figure 3. Tuning curves of the OPO.
a) Temperature tuning curve of the visible OPO in ADP with the experimental data plots.
b) Angle tuning curve of the visible and infrared OPO in KDP and the experimental data plots in KD*P.

room temperature and were excited by the fundamental of the mode-locked YAG laser ($1.06\,\mu$m, 50 mJ, 30 psec). The amplified output power measured by a thermopyro detector was 5 mJ at maximum which corresponds to 10% of conversion efficiency. No damage was observed in LiNbO₃ for the excitation power density of about 5 GW/cm². Output spectrum was observed by the combination

of an IR monochromator and an IR TV camera. The spectral width of the amplified output was less than 50 cm^{-1} at 1.4 μm. For a simple monitor of the output spectrum, we are going to use a LiIO₃ single crystal (10 × 10 × 10, 24°z-cut), in which output beam of OPOA and the exciting beam are mixed and converted to sum frequency (0.6 $\sim$ 0.7 μm) which is visible.

This system is to be assembled as a picosecond tunable light source for an IR spectrometer system.

3) High Resolution Spectroscopic System in Far Infrared Region

Maxwell's electromagnetic theory does not discriminate between light and electric wave. Nowadays far-infrared region extends into submillimeter-wave region, and vice versa. In this border region rotational spectra of simple light molecules will appear strongly, in addition to transitions due to large-amplitude motions such as internal rotation, ring puckering, and inversion. Unfortunately spectroscopic technique in the region under consideration has been much less developed, compared with that in other regions, because each of generation, transmission, and detection of radiation here is accompanied with greater difficulties. However, remarkable progress has recently been made on design and construction of light sources in this region. A few years ago we had only H₂O, D₂O, HCN, and DCN lasers each of which emits very limited number of lines in far-infrared region for spectroscopic use. Recently CO₂ laser pumped far-infrared lasers have been developed, which use molecules absorbing CO₂ laser light as lasing gases;

methanol, formic acid, and hydrazine are such examples. At present a few hundreds of lines are available for spectroscopic studies in far-infrared region. We can determine their frequencies by mixing them with harmonics of klystrons on high-speed far-infrared detectors. In fact, many of them have been measured precisely. On the other hand, technology for manufacturing mm-wave klystrons and backward wave oscillators (BWO) has made good progress; a Russian BWO reaches up to 1,100 GHz with an output power of more than 100 μW..

The present Large Scale Research Equipment (LSRE) will be set up mainly to observe rotational spectra of unstable molecules, free radicals, and molecular ions which are small in size, but of fumdamental importance in molecular science and other related fields. One of the greatest advantages to work in the far-infrared and submm-wave region is that absorption coefficients of rotational spectra are proportional to square or cube of transition frequencies. Because far-infrared lasers are fixed in frequency, they will be used as light sources for far-infrared laser magnetic resonance (LMR) spectroscopy. Therefore the present LSRE will consist of two parts: a far-infrared LMR spectrometer and a mm and submm-wave spectrometer.

3-a) Far-infrared LMR spectrometer.

Figure 1(a) shows a block diagram of the spectrometer. A CO_2 laser with the maximum output of a few ten watts excites a lasing gas contained in a White type cell. The cell is placed in a far-infrared laser cavity formed by two concave mirrors, one of which can be displaced by a micrometer so as to set the laser cavity at the top of the gain curve. The far-infrared laser cavity also contains a sample cell, which is separated from the White cell by a polyethylene or polypropylene thin film set at the Brewster angle and is under magnetic field varying from zero to 14 kG. A part of far-infrared radiation comes out through a small hole of a concave mirror attached to one end of the sample cell and is detected by an InSb detector cooled to liquid He temperature. A small portion of the detected signal after amplified by a preamplifier is fed to a stabilizer which delivers a DC signal to a PZT attached to an end mirror of the pumping CO_2 laser to set the CO_2 laser frequency so as to maximize the far-infrared laser output. A grating placed at the other end of the CO_2 laser cavity selects an appropriate laser line.

Rotational spectra of paramagnetic species in the sample cell may be scanned by changing magnetic field delivered by an electromagnet. The signal will normally be observed as a decrease in the far-infrared laser output (i.e. absorption). To increase the sensitivity an AC field of 100 kHz will be superimposed on the DC field, and the signal demodulated by a phase sensitive detector will appear as a first derivative on a strip-chart recorder.

3-b) mm- and submm-wave spectrometer.

A microwave spectrometer already set up in the Division of Molecular Structure covers the frequency region up to 180 GHz (1.67 mm). The present LSRE is to extend this coverage up to 250 GHz (1.2 mm) mainly using a series of OKI klystrons, and also to cover 285–315 GHz (1.05–0.95 mm) by a French BWO called carcinotron. Frequency measurement devices, phase-lock systems, and other mm- and submm-wave circuitories will be developed.

These new mm- and submm-wave generators will be used mainly as sources of a source-modulation spectrometer, as shown in Figure 1(b), although some attempts to feed their outputs into a Stark cell will be worthwhile. After passing through an absorption cell mm-wave will be detected by an InSb detector cooled by liquid He. The absorption signal will be picked out by a phase-sensitive detector, and stored on a memory of a mini-computer for further processing.
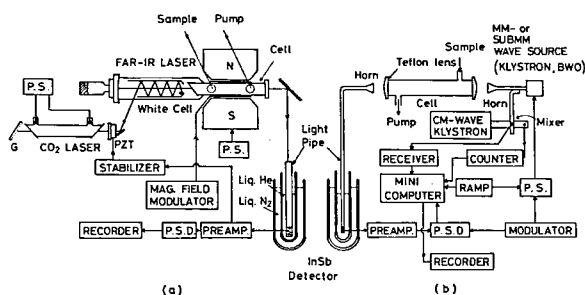

Figure 1.

149

SPECIAL RESEARCH PROJECTS

IMS has two special research projects supported by national funds. Two projects presently in progress under the first five year plan are;

(1) Molecular designing for interesting and useful materials.

(2) Investigation of energy conversion processes at the molecular level.

The projects are being carried out in close collaboration of research divisions and facilities. Collaboration from outside also make important contributions. Research fellows join these projects. Under the program, progress has been made in the following topics:

"Theoretical Studies on Potential Energy Surfaces of Elementary Reaction Processes"

A detailed theoretical investigation of the elementary chemical reaction processes provides a basis both for the energy conversion through chemical reaction and for the molecular designing of useful materials. We have undertaken some molecular orbital studies for this purpose.

The conversion of the reaction energy into the vibrational energy of the product provides a potential for chemical lasers. The HF vibration energy partitioning in the reaction systems $C_2H_5F \rightarrow C_2H_4 + HF$ has been predicted based on the potential energy characteristics along the reaction coordinate (Research Activities I-B-2). The potential energy surface and the dynamics of photoisomerization of polyenes has also been studied. Here the energy is found to transfer from one C=C bond to another in a rather short time interval. (I-C-1 and I-C-2).

Understanding of the mechanism of homogeneous catalysis is an essential ingredient for molecular design of effective catalysts. As the first step toward this goal, we have studied theoretically the nature of interaction between some transition metal ions and ligands. (I-D) The study is being extended for theoretical elucidation of the olefin hydrogenation mechanism reaction catalysed by metal complexes.

"Theory of Electronic Structure on Solid Surfaces and its Catalytic Activities"

Fundamental researches in electronic and molecular processes on solid surfaces are quite important in relation to electrode reactions and heterogeneous catalysis and many other applied fields. A prerequisite of such researches is reliable knowledges of the surface electronic structure and the interaction mechanism between the surface and adparticles. We applied the first principle DV-Xα calculations to various surfaces of metal oxides including MgO, TiO_2, $SrTiO_3$, MeO (Me = Ti, V, Mn, Fe, Co, Ni), ReO_3 and their chemisorption systems. The detailed procedures and the results are presented in section I - F in Research Activities.

Any of the actual molecular processes take place not on the ideal surfaces, but on the real surfaces including surface defects and irregularities. Therefore, we chose as one of the main subjects to study the localised states around various surface defects and to clarify their role on surface molecular processes. It was found that oxygen vacancies often accompany the occupied gap states with the wide range of level position determined by the local atomic configuration on the surface. These defect states take part as the frontier orbital to directly interact with attacking particles or to transfer electrons between the surface and particles.

"Developments of New Selective Organic Reactions Induced by Infrared Lasers"

Studies on the developments of new selective chemical transformations by making the best use of the excellent characteristics of lasers have been started. LUMONICS 203 TEA laser has been installed and several reaction cells suitable for vapor phase reactions were made. In hopes of obtaining thermodynamically unstable molecules from the corresponding more stable starting isomers, investigation of the isomerization of some organic molecules such as methylenecyclopropane derivatives has been carried out. Preparation of highly strained compounds by intramolecular cycloadditions of polyenes is another subject of interests. (See Research Activities IX).

"Novel Polyquinones with a Three-dimensional Molecular Framework"

Strong acceptor molecules have been designed by incorporating the p-benzoquinone chromophore into a series of polytriptycene frameworks. The stepwise increase in the oxidative strength due to through-space and/or through-bond orbital interactions is the subject of theoretical interest. A final cage compound is expected to incorporate donor molecules selectively and to show a number of other interesting properties. Experimental and Results: Triptycene mono- and diquinones, ditriptycene triquinone, and tritriptycene

150

$$n = 1, 2, 3$$
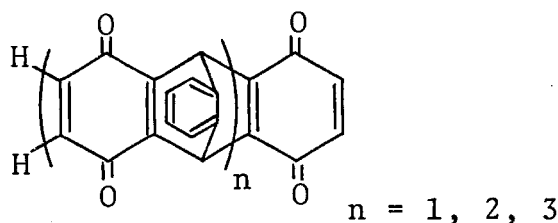
tetraquinones were prepared *via* a series of the Diels-Alder reactions. High performance liquid chromatography on a Japan Analytical Industry Co., Ltd. LC-08 instrument was especially usefull in separating the complex mixtures of each reaction step. The first half-wave potentials (in units of V vs. SCE) of these polyquinones decreased from -0.37 to -0.08 as the number of the quinone ring increased. (See Research Activities V).

"Electronic Characters of Organic Solids Having Interesting Physical and Chemical Properties"

Through the investigation of electronic properties of organic solids by means of the photoelectric measurements, we are studying their electronic structures.

Further, from the photoelectric measurements for highpurity aromatic hydrocarbons, very thin organic polymers, conductive charge transfer complexes including graphite intercalation compounds and also for free radicals, we try to find a principle for molecular design of new compounds having interesting physical and chemical properties.

The photoelectron spectrometer equipped with a temperature control was constructed. In this apparatus, the temperature of the specimen has been controlled from room temperature to liquid nitrogen one, and the controlled range is extending down to liquid helium temperature. The attainable vacuum of the energy analyzer chamber reaches to 10^{-8} Pa. With the observation of the energy distribution curves of the emitted electrons, the structure of the specimen is examined by the LEED/Auger electron optics. (See Research Activities IV).

"The Energy Conversion in Ion-Molecule Reactions"

The purpose of this project was to elucidate the evolution of specific forms of reactant energy and reaction exoergicity of elementary reactions to specific forms of product energy. To pursue this evolution in ion-molecule reactions, reactions of state-selected molecular ions were studied at specified translational energies.

The apparatus "TEPSICO" which has been constructed for this purpose and its performance have been described previously (see IMS *Ann. Rev.* 1978, pp. 73 and 104). This year, a considerable part of effort has been directed to the improvement of this apparatus. The first of the two major improvements is the introduction of an extremely high power pulse generator for exciting helium Hopfield continuum. This increased the incident light intensity by a factor of about 20. The second is the introduction of a minicomputer system which controls the measurements and processes data.

With these improvements, coincidence measurements in systems with small photoionization cross sections and/or small reaction cross sections have been made possible. In addition to completing studies on the reaction $H_2^+(v) + H_2 \rightarrow H_3^+ + H$ (See Research Activities IV-E-1), measurements of the state selected reaction cross sections (relative) for the reaction $CO^+ + D_2 \rightarrow COD^+ + D$ have been initiated.

"Molecular Structure and Chemical Reaction of Highly Excited Atoms and Molecules and of Molecular Ions"

Molecular ions play important roles in chemical reaction and other related fields. However, they are so reactive that little is known about their physical and chemical properties. On the other hand, highly excited atoms and molecules, i.e, those in Rydberg states have recently attracted much attention; they are neutral in charge, but, with an electron in an orbital with a large radius, they may behave in a way similar to molecular ions. The present research project aims at unravelling characteristic properties of molecular ions and also of highly excited atoms and molecules.

An infrared diode laser spectrometer, which has already been installed as a Large Scale Research Equipment, has provided high-resolution vibrational spectra of reactive species including CS, SO, CF, CCl, BO_2, and CH_3. However, unless precise calibration is made for laser wavelength, observed spectra would become much less useful. Therefore, a high-precision wavelength meter has been set up which allows us to determine laser wavelength with a precision of $10^{-3} cm^{-1}$ or better. It has been tested against CO_2 laser lines, the wavelength (and also frequencies) of which have already been precisely measured at NBS (Boulder) and other laboratories. The agreement of the observed wavelengths with literature values is satisfactory, i.e. within $5 \times 10^{-4} cm^{-1}$. This wavelength-meter has already been used to measure spectral lines of molecules mentioned above (See Research Activities II-C-2).

"Molecular Processes of Solar Energy Conversion at Solid Surfaces — Photoelectrode Process and Photocatalysis"

Solar energy conversion into chemical energy and electricity by means of photoelectrode reaction and photocatalysis of semiconductors is being investigated. Photoreduction of methylviologen by using chloro-

phyll, its derivatives, porphines, and organic dyes has been succeeded in. By adding appropriate catalysts such as Pt and Pd to the system, hydrogen was evolved by visible light. Hydrogen evolution by using semiconductor powder such as TiO_2, MoS_2, Cu_2O has been investigated by using a similar method.

The mechanism of O_2 evolution at semiconductor electrode has been investigated by resolving the reaction into several primary steps and evaluating the state density of electron energy of reactive species in solution (H_2O, $\cdot OH$, OH^-). A path to H_2O_2 formation and its catalytic decomposition at the oxide semiconductor surface was suggested to be one of the most probable reaction paths.

In order to clarify the detailed mechanism of photocatalytic reaction on semiconductor surfaces, the dynamic mass technique combined with a pulsed laser has been exploited. By this technique the photocatalytic reaction of CO_2 and H_2O on TiO_2 was investigated. Various photoproducts such as $H\cdot$, CH_4, H_2O_2 and $HCOOH$ have been detected, which indicate the photocatalytic fixation of CO_2 by H_2O and light energy.

Dynamics of photovoltaic effect and charge transfer reaction at semiconductor/electrolyte interface has also been investigated by measuring a transient photocurrent and luminescence caused by illuminating semiconductor surface with a n-sec N_2 or dye laser. (See Research Activities III-D-E).
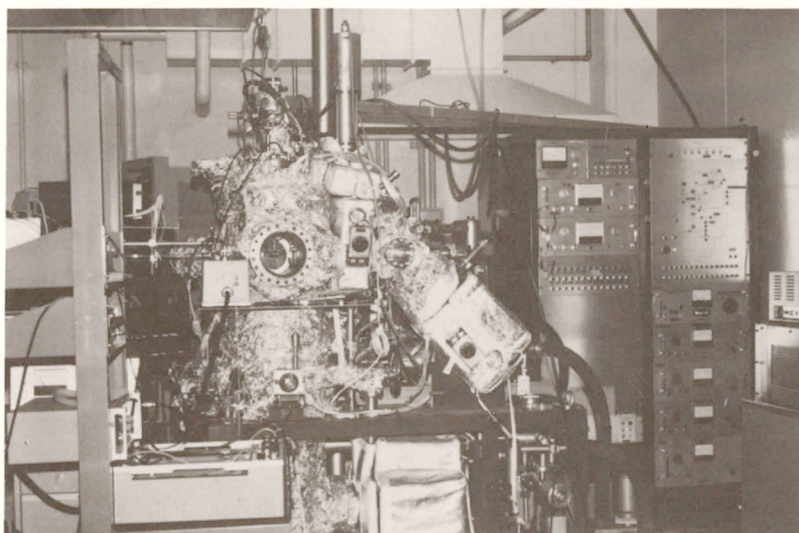
Low temperature ultraviolet photoelectron spectrometer.
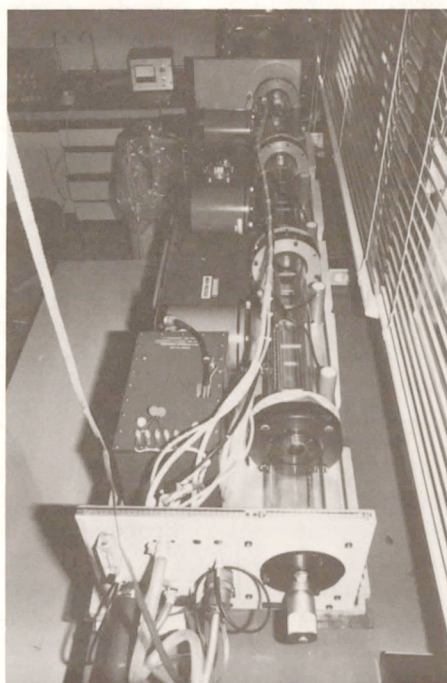
CO_2 Laser (LUMONICS TEA-203-2).

JOINT STUDIES PROGRAM

Large-scale Molecular Orbital Calculations in Molecular Science

Coordinator: **Kimio OHNO** *(Hokkaido Univ.)*

In order to make good use of a powerful computer system newly installed at IMS, strategies and techniques of large-scale theoretical calculations of molecules and solid surfaces were discussed. Two powerful ab initio MO LCAO SCF programs i e. Gaussian 70 and JAMOL3 and a DV-Xα program designed for solid surfaces were the centers of discussion. As the result, powerful improvement and new technical developments were proposed in each of these three programs and some of which were implemented. Actual computations on potential surfaces of various chemical reactions, on metal porphines, Ti_4O_{16}, clusters of Ni were carried out. A careful examination of the results obtained and an analysis of the computational efforts needed are being made and these will serve useful purposes in planning future large-scale theoretical calculations in molecular science. (1978 –9).

Solid State Chemistry of Highly-Photoconductive Compounds: Tetrabenzoperylene and Its Related Hydrocarbons

Coordinators: **Hiroo INOKUCHI** *(Division of Molecular Assemblies)*
Kikujiro ISHII *(Gakushuin Univ.)*
Junji AOKI *(Toho Univ.)*
Satoshi IWASHIMA *(Meisei Univ.)*

After careful purification, very high purity compounds, less than 10^{-6} mole/mole impurity contents, of tetrabenzoperylene and also several nine rings aromatic hydrocarbons, violanthrene A, iso-violanthrene A, violanthrene B, and iso-violanthrene B, were obtained. By means of photoelectron spectroscopic analysis, we are observing their ionization potentials as solids: their values are scattered from 4.82 eV to 5.34 eV widely.

Further, we have started to prepare aza-aromatic hydrocarbons, aza-benzanthrone series, and succeeded to synthesize aza-tetrabenzoperylene. We expect that the introduction of aza-aromatics into the polycyclic ring should give a novel character as compared with polycyclic hydrocarbons. (1978–9)

Developments and Applications of New Spectroscopic Methods Using Tunable, Coherent, and High-Resolution Light Sources

Coordinators: **Eizi HIROTA** *(Division of Molecular Structure)*
Shuji SAITO *(Division of Molecular Structure)*

Tunable lasers (dye lasers in the visible and diode lasers in the infrared) and microwave or rf (from DC to 180 CHz) had become available at IMS. Therefore a special emphasis was given to developments of double resonance techniques, in particular microwave (rf)-optical double resonance (MODR) and microwave (rf)-infrared double resonance (MIDR) K. Takagi (Toyama University) and S. Saito succeeded in observing MODR signals from the excited $\tilde{A}^1A''(100)$ state of HNO. They found that the observed spectra do not fit to the rigid-rotor pattern modified by centrifugal distortion effects, an indication that there are local perturbations possibly of Coriolis type by highly-excited vibrational levels associated with the ground electronic state. M. Takami (IPCR and IMS) observed MIDR signals on NH_3 ν_2 band. A more remarkable result is the detection of rf transitions in the CF_4 ν_3 state. F. Shimizu has contributed much to the design of high-precision wavelength meter for diode lasers. (1978–9)

Molecular Designing and Syntheses of Bridged Aromatic Compounds of Molecular Scientific Interest

Coordinators: **Hiizu IWAMURA** *(Division of Applied Molecular Science)*
Michinori ŌKI *(Univ. of Tokyo)*
Soichi MISUMI *(Osaka Univ.)*

The joint research has been carried out to delineate the strain, deformation and orbital interactions in the aromatic rings which are responsible for a number of interesting properties of bridged aromatic compounds. We have found that the benzene ring deformed out-of-plane to make a boat form is less unstable than the one in a chair form. Experimental evidences in support of the above rule were found by the Osaka group in a number of multi layered cyclophanes. The semiempirical MO energy partitioning analyses have revealed that the general trend derives its origin from a minimal loss of resonance energy at the gunwale of a benzene boat as compared to that at the seat of a chair form.

A number of new triptycene derivatives have been prepared by the Tokyo group to compare the

importance of through-space and throughbond inter-actions between the benzene rings which are held at 120° to each other. A series of intramolecular tripty-cene quinhydrones favored the latter interaction. (1978—9)

Chemisorbed Molecules on Solid Surfaces: Their Structural and Chemical Properties

Coordinator: **Hiroshi TSUBOMURA** *(Osaka Univ.)*

In order to clarify the molecular structure and reactivity of chemisorbed molecules, various methods such as high sensitive reflection spectroscopy, appli-cation of the photon counting method to the electro-nic absorption spectroscopy of very thin molecular assemblies, laser Raman spectroscopy, FTIR spectro-scopy and dye sensitized photocurrent were reviewed by each research group and their application was discussed critically. Special interest was taken in their application to surface phenomena relating catalysis, gas sensors, photocatalytic reactions and photovoltaic effect at semiconductor/electrolyte inter-face. (1978—9)

OKAZAKI CONFERENCES

The Seventh Okazaki Conference

Present Status and Future Trends of High Resolution Molecular Spectroscopy
(September 4–6, 1978)

Organizer: E. Hirota *(IMS)*
Invited Speakers: J. W. C. Johns *(National Research Council of Canada)* and S. G. Kukolich *(Univ. of Arizona)*

High resolution spectroscopy is one of the most fundamental methods widely used in the field of molecular science. This traditional method has recently been improved very much in both resolution and sensitivity, by introducing new techniques such as lasers. The Conference was arranged so as to review the present status of molecular spectroscopy and then to seek out its possible developments in the future. The wavelength regions discussed there extend from rf to the visible. Most spectroscopic results which were presented are obtained using coherent light sources, lasers, microwave, and rf. double resonances of various kinds were proved to be useful to extract information on molecules which is difficult to obtain with a single light source. A few talks were concerned with time-resolved spectroscopy, which elucidated some dynamical behaviors of molecular systems. Special emphasis was given to unstable molecular species with short lifetimes. Laser magnetic resonance spectroscopy was shown to be very efficient for such studies, because of its inherent high sensitivity. Spectra of molecules complicated by internal degrees of freedom, either internal rotation or electron spin and/or orbital motions, were also discussed theoretically.

The Eighth Okazaki Conference

Interactions between Atoms, Molecules and Solid Surfaces
(February 19–21, 1979)

Organizer: K. Morokuma *(IMS)*
Invited Speakers: W. A. Goddard III *(California Inst. of Technology)*, R. P. Messmer *(General Electric, Schenechtady)* and J. C. Tully *(Bell Lab., Murray Hill)*

Thanks largely to the development of new computational techniques and programs, a tremendous advance has been made in the last few years on the detailed theoretical studies of interactions between atoms, molecules and solid surfaces. A large computer system just installed at the IMS Computer Center promises a dramatic upsurge of such studies in Japan.

The Eighth Okazaki Conference 19–21/2/1979

The Conference was intended to bring together scientists of a wide variety of background who are working in the field of molecule (atom)-molecule and molecule (atom)-surface interaction and to survey the present status of the theory in order to attain a perspective view for the future.

Dr. Messmer presented his results of the SW-Xα cluster calculation on the oxygen atom adsorbed on Al and the CO molecule adsorbed on Cu. Dr. Goddard emphasized the importance of calculation of the molecular dissociation energy in the theoretical study of chemisorption. He compared the generalized valence bond approach with an effective core potential favorably to the Xα calculation. A heated discussion arose between the Xα school and the ab initio school over the advantages and disadvantages of both methods. Dr. Tully reported results of generalized Langevin classical trajectory calculation on the dynamics of atom-solid surface collision. A computer-generated movie of the dynamics gave a clear visual insight to the motion of chemisorbed atoms and molecules on the surface. Active discussions have been continued on chemisorption, metal-molecule interactions and the potential energy surfaces of chemical reactions.

The general impression of the Conference was that the theoretical study in the field was indeed in the stage of being able to take an active role in elucidating the mechanism of chemisorption, molecular interactions and chemical reactions.

RESEARCH SYMPOSIA

Intensity of Photoelectron Spectra
(May 26th-27th, 1978)

Organizer: K. KIMURA *(Hokkaido Univ.)*

This Symposium was held to exchange mutual information between theoreticians and experimentalists in the field of photoelectron intensity or photoionization cross section in vacuum uv and x-ray regions. This is the field in which coorporation between theory and experiment is especially important. The recent development of photoelectron spectroscopy has made it possible to produce quantitative photoelectron intensity data associated with the photoionization cross section and the asymmetry parameter of photoelectron distribution. On the other hand, theoretical studies with various qualities have recently been increasing to explain available experimental data for understanding the processes of photoionization. Under these circumstances, discussions were made in the three following topics: (1) on the theory of photoionization cross section, (2) on the intensity of vacuum uv photoelectron spectra in the gaseous and solid states, and (3) on the intensity of x-ray photoelectron spectra in the gaseous and solid states. The Symposium offered a good opportunity to increase mutual understanding between the both groups of theory and experiment.

Symposium on the Production of Hydrogen by Solar Energy Conversion
(June 3rd, 1978)

Organizer: Tatsuhiko YAGI *(Shizuoka Univ.)*

Hydrogen gas is a non-polluting fuel and became spotlighted as a new energy source to be substituted for petroleum, if it could be produced from unlimitedly available water on our planet. There remains a problem of how to afford an energy to decompose water. Biological conversion of the solar energy is one of promising candidates. A family of photosynthetic organisms including green plants, algae and bacteria, synthesize their body constituents by reducing CO_2, the reducing equivalents being supplied from photochemical decomposition of water by means of chloroplast photosystems or similar apparatus thereof.

This symposium was held to discuss on the possibility to develop new devices to trap the reducing equivalents supplied from water for use in reducing protons to produce H_2 by the catalytic action of bacterial hydrogenase. Dr. H. Ochiai (Shimane Univ.) reported on the immobilization of chloroplasts by means of polyvinyl alcohol, and photoanodic current taken out by irradiating the immobilized chloroplast electrode. Dr. J. Yamashita (Osaka Univ.) reported on the photoexcitation and photoanodic current of bacterial chromatophores. Dr. M. Shin (Kobe Univ.) reported on the immobilized ferredoxin and ferredoxin-$NADP^+$ reductase and their characteristics. Dr. T. Yagi reported the stabilization of desulfovibrio hydrogenase, and the separation of an H_2 producing system from an O_2 evolving system by means of enzymic electric cell technique to protect hydrogenase from inhibitory action of O_2 produced by the chloroplast photosystems. Dr. K. Honda (Univ. of Tokyo) proposed the use of a model system consisted of a chlorophyll monolayer spread over an SnO_2 semiconductor electrode in order to construct and analyze a photoenergy conversion system. Dr. Y. Fujita (Okayama Univ.) suggested the photocathodic character of zinc tetraphenylporphyrin coated on a platinum electrode. Dr. T. Matsuura (Kyoto Univ.) explained the mode of action of active oxygen on biological pigments and discussed on the mechanism of decomposition and aging of these important photoreceptor molecules. Finally the attendants discussed on the possibility to construct systems to produce H_2 by means of biophotolysis of water.

Present Situation and Future Prospect in Theoretical and Experimental Studies of Metalloporphyrins
(June 12th-13th, 1978)

Organizers: Hiroshi KOBAYASHI *(Tokyo Inst. of Tech.)* and Hiroshi KASHIWAGI *(IMS)*

Metalloporphyrins play important roles in energy conversion processes in living bodies as various kinds of heme protains and chlorophylls. The electronic structure and the catalytic function of metalloporphyrins are very complicated, because they consist of a central metal, often with d-electrons, a porphyrin ring with a large conjugated π-electron system, and various axial ligands. Therefore, metalloporphyrins are yet important topics of the day in spite of a lot of past investigations. Many theoretical and experimental researchers, especially Dr. Masao Kotani (President, the Science University of Tokyo) attended this symposium. Interesting imformations were reported on the basis of the newest data and instructive discussions were made for the future prospect.

Correlation Studies between Electrical and Optical Properties of Semiconducting Polymers and Molecular Solids
(July 3rd-4th, 1978)

Organizers: Hiroo INOKUCHI *(IMS)* and Naoki SATO *(IMS)*

Extensive studies on electronic transport processes in semiconducting polymers, for instance poly (vinyl-carbazole), polyacetylene, and their charge transfer complexes, have been carried out. On the other hand, the refined works on electronic and optical properties of molecular solids and their complexes have been accumulated. However, the overlapping works between these fields are not so many: Through the discussion of their own research procedures and also of their experimental techniques, we expect to find new progress on both fields.

Studies on Syntheses and Structural Specificity of Novel π-electron Systems
(July 6th-7th, 1978)

Organizer: Tamotsu YOSHINO *(Kyushu Univ.)*

The recent research results of the following titles were reported, and discussed.
1. Synthesis of chiral twisted π-electron systems
   Hiroshi YAMAMOTO (Osaka Univ.)
2. Synthesis of medium rings related to humulene and germacrenes
   Hitosi NOZAKI (Kyoto Univ.)
3. Nonalternant isomers of benzo[a]pyrene
   Ichiro MURATA (Osaka Univ.)
4. Synthesis and structure of novel fulvalenes
   Zenichi YOSHIDA (Kyoto Univ.)
5. Tropoquinones
   Sho ITO (Tohoku Univ.)
6. Bond alternation of conjugated systems
   Jiro TANAKA (Nagoya Univ.)
7. Synthesis of spin labeled aromatic crown ethers and ESR study of their metal complexes
   Kazuhiko ISHIZU (Ehime Univ.)
8. ^{13}C-NMR and CNDO/2 calculation of [2.2]-cyclophanes
   Nobuo MORI (Science Univ. of Tokyo)
9. New water-soluble heterocyclophanes
   Iwao TABUSHI (Kyoto Univ.)
10. Charge-transfer cyclophanes
    Soichi MISUMI (Osaka Univ.)
11. Synthesis of paracyclophanes with an unsaturated bridge by cycloaddition
    Takashi TSUJI (Hokkaido Univ.)
12. Synthesis and properties of multibridged ferro-cenophanes
    Hiroshi YAMAKAWA (Science Univ. of Tokyo)
13. Intraannular cycloaddition products of [3.3]-cyclophane
    Takahiko INAZU (Kyushu Univ.)

14. A suggestion from a physical chemist to synthetic organic chemists
    Noboru MATAGA (Osaka Univ.)
   The research symposium and a social gathering were attended by 28 persons, and closed successfully.

Molecular Approaches to the Characterization of Solid Surface Reaction
(September 7th-9th, 1978)

Organizer: K. TAMARU *(Univ. of Tokyo)*

The purpose of this conference is to discuss about the following subjects.
1) Design of new surfaces——artificial surface, modified surface, reactivity of these surfaces.
2) Photocatalysis and photoelectrode process——interaction of light with solid surface.
3) Development of new technique for surface characterization.
   More than 50 scientists from the fields of surface physics, electrochemistry and catalysis, both theoreticians and experimentalists, discussed above interdisciplinary subjects.

Molecular Processes on Solid Surfaces
(November 8th-9th, 1978)

Organizers: Hideo AKAMATU *(IMS)*, Tadayoshi SAKATA *(IMS)*, and Masaru TSUKADA *(IMS)*

In this symposium it was aimed at to survey the rapidly progressing present status in the study of molecular processes on surfaces from wide aspects. Though the title covers vast research fields ranging from the solid state physics to electrochemistry and catalyses, the problems are highlighted in which real interdisciplinary coorperations are called for. The topics of the symposium includes theory of solid surface and chemisorption, structure and catalytic properties of real surfaces, chemical decoration for the design of surface reactivity and solar energy conversion by means of solid surfaces. Prof. H. Gerischer at Fritz-Harber Institute der Max Planck Gesellschaft reviewed the charge transfer reaction on solid surfaces and talked the photo-decomposition mechanism of semiconductors.

Seminar on Ion-Molecule Reaction Studies with Recently Developed Instruments
(December 8th-9th, 1978)

Organizer: Takaaki TAMURA *(Univ. of Tokyo)*

The following five themes were represented and discussed.

1. Study of ion behaviors by use of drift tube
   M. Takebe (Tohoku Univ.)
2. Application of plasma-chromatography to ion-molecule reaction study
   S. Rokushika (Kyoto Univ.)
3. Gas-phase reaction study at high temperature by use of molecular beam sampling method
   T. Yamazaki, (Toyota Central Res. Dev. Lab.)
4. Atmospheric pressure ionization mass spectrometry.
   Y.Mitsui (Central Res. Lab., Hitachi Ltd.)
5. Time-resolved atmospheric pressure ionization mass spectrometry with repeated pulses from electron linear accelerator
   S. Matsuoka (Univ. of Tokyo)

Symposium on Molecular Ions: Generation, Reaction, and High Resolution Spectroscopy
(January 24th, 1979)

Organizers: Eizi HIROTA *(IMS)*, and Shuji SAITO *(IMS)*

Simple molecular ions such as H_3^+ H_2^+, H_3O^+ and H_2O^+ play important roles not only in the field of molecular science, but also in many other related fields including chemical reactions, space sciences, and so on. However, because of short lifetimes, little is known about their chemical as well as physical properties. Fortunately Dr. G. Herzberg, a former Counsellor of IMS, visited the Institute. This Symposium was arranged with Dr. Herzberg as a main invited speaker. Participants include not only molecular spectroscopists but also people from reaction kinetics, quantum chemistry, and radioastronomy. Dr. Herzberg gave an impressive talk on emission spectra from highly excited states of H_3 and D_3, which allow us to predict rovibronic transitions of H_3^+ and D_3^+. Professor Koyano (IMS), Dr. Suzuki (Kyoto Univ.), Professor Morimoto (Tokyo Observatory), and Professor Saito (IMS) also contributed very much to understanding the nature of molecular ions.

Thermodynamic and Mechanistic Considerations on Reactions in Solution
(February 27th-28th, 1979)

Organizer: Motoharu TANAKA *(Nagoya Univ.)*

In order to understand chemical reactions involving metal ions, it is essential to study interactions metal ions - solvent, ligand - solvent and metal ions - ligand from the thermodynamic and kinetic point of view. In this Conference, discussions have been actively concentrated on the following topics: hydrolysis of metal ions, reactivity and stability of mixed ligand complexes, dissociation kinetics of metal complexes in different solvents, effect of the bound ligand on the ligand exchange reactions, and reactivity of macrocyclic polyamines and related compounds. The formation of mixed ligand complexes involving amino acids has been discussed in terms of the mechanistic consideration, which enables us to predict quantitatively the formation constant of hundreds of mixed ligand copper(II) complexes. Ligand exchange reactions involving β-diketonato complexes has been the subject of extensive discussion. The reactivity of dimeric copper(II) acetate in acetic acid has been discussed in connection with the exchange rate of acetic acid coordinated at the axial site of dimeric copper(II) acetate.

Solar Energy Conversion. Cooperation between Japan and United States of America in its Fundamental Research Field
(February 25th, 1979)

Organizer: Hiroo INOKUCHI *(IMS)*

Discussion on cooperation study of solar energy conversion between Japan and United States of America has been carried out. In its chemical and physical field, the following research projects were proposed.
(1) The interactions of photons and molecules: Chemistry of electronically excited molecules.
(2) Photochemistry in specific environments
(3) Chemical conversion of photon energy into electrical energy
(4) Electronic energy transfers between molecules
(5) Photochemistry of metal complexes
(6) Organic photochemistry
(7) Photodecomposition of water

The New Techniques for the Investigation of Solid State Properties and the Exploration of the Novel Compounds Having Interesting Physical and Chemical Properties
(March 2nd-3rd, 1979)

Organizers: Hiroo INOKUCHI *(IMS)*, Tasuku ITOH *(IMS)*, and Toshiaki ENOKI *(IMS)*

For development of the study of molecular science, the new theoretical and experimental procedures and also the novel compounds having interesting physical and chemical properties should be searched out. This meeting has been held in order to exchange views and knowledges on material science between chemists and physicists. The present situations and future problems of the representative experimental methods using high magnetic field, newtron diffraction, strage ring radiation, high pressure and low temperature were reported by several physicists from the standpoint of solid state physics. In the meanwhile, chemists introduced various compounds, especially polyvalence and mixed valence metal complex compounds, that had interesting characters from the standpoint of material science. And the structures,

the synthesis, the chemical reactivity, transport phenomena and other solid state properties of these compounds were discussed.

Theoretical and Experimental Approaches to Transition State Structures
(March 5th-6th, 1979)

Organizer: Takashi ANDO *(Osaka Univ.)*

The symposium was designed to get together the organic chemists who are engaged in elucidation of reaction mechanisms by means of experimental approaches and the theoretical chemists who are interested in prediction of the behavior of organic molecules by means of molecular orbital calculations, thereby providing interfacial knowledge for the both to understand the present status of the progress in each field and to discuss common problems by use of common languages. The topics were concentrated on the structure and the behavior of the transition states of organic reactions and related phenomena, e.g., kinetic isotope effects in neighboring group participation and hyperconjugation, MO calculation of elimination and substitution, reaction on sulfur with or without d-orbital participation, carbenes and their sigmatropic rearrangement, MO calculation of photoisomerization of polyenes, reduction with NAD (P)H model compounds, proton transfer from carbon acids, and possible intermediates and stereochemistry of aliphatic nucleophilic substitution.

The symposium was successful in increasing the knowledge obtained or able to be obtained by means of different approaches to the common problems. Continuous efforts for discussion and cooperation with each other must be necessary for further progress in this field.

High-Resolution Spectroscopic System in Far Infrared Region
(March 17th, 1979)

Organizer: Eizi HIROTA *(IMS)*

This symposium serves as one of a series of meetings, which discuss, or make decision on, what sort of large scale research equipments are to be set up at the Institute for Molecular Science. The symposium thus started with report on the present status of three equipments that have already been installed.

An equipment called High-Resolution Spectroscopic System in Far Infrared Region is the fourth large scale research equipment of IMS. It consists of two parts; mm- and submm-wave sources and CO_2 laser-pumped far-infrared lasers. Professor Saito (IMS) explained how to extend the frequency region up to 310 GHz and Dr. Yamada (IMS) presented a plan to set up a far-infrared laser magnetic resonance spectrometer. Participants gave advice and suggestions on these projects.

FOREIGN SCHOLARS

Visitors from abroad play an essential role in research activities and always welcome at IMS. The following is the list of foreign scientists who visited IMS in the past year (Aug. 1978–July 1979). The sign * indicates a visitor invited to attend an Okazaki Conference and † indicates a visitor on the Invited Foreign Scholars Program.

Dr. J. T. Hougen†	NBS	(USA)	July 1978 – Mar. 1979
Dr. W. A. Kreiner	Univ. of Ulm	(Germany)	July – Sept. 1978
Prof. N. Jonathan	Univ. of Southampton	(UK)	Aug. 1978
Dr. J. W. C. Johns*	NRC	(Canada)	Sept. 1978
Prof. S. G. Kukolich*	Univ. of Arizona	(USA)	Sept. 1978
Dr. V. K. Kaushik*	Indian Inst. of Tech.	(India)	Sept. 1978
Dr. E. M. Rowe	Univ. of Wisconsin	(USA)	Sept. 1978
Prof. O. H. Griffith	Univ. of Oregon	(USA)	Sept. 1978
Dr. H. Okabe	NBS	(USA)	Sept. 1978
Prof. B. Pullman	Univ. of Paris	(France)	Nov. 1978
Dr. A. Pullman	Univ. of Paris	(France)	Nov. 1978
Prof. B. Bak	Univ. of Copenhagen	(Denmark)	Nov. 1978
Prof. H. Gerischer	Max-Planck Inst.	(Germany)	Nov. 1978
Prof. K. Schaffner	Max-Planck Inst.	(Germany)	Nov. 1978
Prof. J. D. W. van Voorst	Univ. of Amsterdam	(Netherlands)	Dec. 1978
Prof. H. F. King†	State Univ. of New York	(USA)	Dec. 1978 – Mar. 1979
Prof. L. E. Lyons	Univ. of Queensland	(Australia)	Jan. 1979
Prof. M. Calvin	Univ. of California	(USA)	Jan. 1979
Prof. G. Herzberg	NRC	(Canada)	Jan. 1979
Dr. R. Schinke	Univ. of Kaiserslautern	(Germany)	Jan. 1979
Prof. W. Buth	Stanford Univ.	(USA)	Feb. 1979
Dr. M. Inokuti	Argonne National Lab.	(USA)	Feb. 1979
Prof. W. A. Goddard III*	California Inst. of Tech.	(USA)	Feb. 1979
Dr. R. P. Messmer*	G. E. Corp.	(USA)	Feb. 1979
Dr. J. C. Tully*	Bell Lab.	(USA)	Feb. 1979
Prof. W. J. Orville-Thomas	Salford Univ.	(UK)	April 1979
Dr. T. W. Hänsch	Stanford Univ.	(USA)	April 1979
Prof. C. B. Moore†	Univ. of California	(USA)	May – Aug. 1979
Prof. R. H. Myers	Univ. of New South Wales	(Australia)	June 1979
Prof. R. L. Martin	Monache Univ.	(Australia)	June 1979
Prof. C. Sandorfy	Univ. of Montreal	(Canada)	July 1979

Prof. Herzberg at IMS (Jan. 1979)

AWARDS

The Nishina Memorial Foundation awarded its 24th Memorial Prize to Professor Eizi Hirota for his contributions to

"Investigations of Free Radicals by High-Resolution and High-Sensitivity Spectroscopy."

Prof. Hirota's Scientific Achievement:

In 1963 Prof. Hirota started microwave investigations on free radicals, in collaboration with Dr. T. Amano and others. At that time OH was only a free radical detected by microwave spectroscopy. Although Prof. Hirota's first success on SO lagged behind reports from American laboratories, he added data on the excited vibrational state and also on ^{33}SO and ^{34}SO, using his more sensitive spectrometer. After that Prof. Hirota successively detected ClO, NS, NCO, BrO, and SF. One of the most recent examples is a new radical, FSO, for which almost no spectroscopic data have been reported. These contributions not only have opened a new research area in molecular science, but also are much appreciated in related fields including chemical reaction, astro-

physics, and environmental researches.

A few years ago Prof. Hirota introduced new laser techniques to enlarge capabilities of his research group. He has already successfully applied dye-laser excitation and/or saturation spectroscopy to PH_2 and HSO; for the latter he has established a correct rotational assignment for the $\tilde{A}-\tilde{X}$ band. He has also set up an infrared LMR spectrometer, by which he successfully analyzed vibration-rotation bands of SO in both $X^3\Sigma^-$ and $a^1\Delta$ and of NH_2. Prof. Hirota and his coworkers have thus much contributed to improving and developing spectroscopic methods for free radical studies. Prof. Hirota's contributions have motivated similar researches in other laboratories all over the world.

Dr. Tomoji Kawai received a Chemical Society of Japan Award for Young Chemists in 1979 for his contribution to

"Studies on chemical reactions on the solid surfaces by electron spectroscopy and its application to solar energy conversion."

Dr. Kawai's Scientific Achievement:

Dr. Kawai has made contributions in the elucidation of surface catalytic phenomena by electron spectroscopies and also in the solar energy conversion through photocatalysis and photoelectrode process.

1) Development of high resolution Auger electron spectroscopy and its application to the characterization of adsorbed molecules on the surface.

2) Elucidation of dynamical behaviour of surface reactions through direct observation of the catalyst by electron spectroscopies.

3) Surface composition and catalytic activity studied by energy loss spectroscopy, x-ray photoelectron spectroscopy and uv photoelectron spectroscopy.

4) Dynamics of photoinduced surface reaction on semiconductors by pulsed laser-dynamic mass technique.

5) Photoelectrochemical energy conversion by metal-porphine electrode and its dynamic behaviour studied by pulsed laser.

6) Photocatalytic hydrogen evolution from water by using methylviologen.

LIST OF PUBLICATIONS

M. TSUDA, H. TOUHARA, K. NAKANISHI, K. KITAURA and K. MOROKUMA, "Calorimetric and Molecular Orbital Studies of Hydrogen Bonding between Hydrogen Fluoride and Cyclic Ethers", *J. Am. Chem. Soc.,* **100**, 7189 (1978).

S. YAMABE and K. MOROKUMA, "A Theoretical Study on the Paths of Photodissociation: $CH_2=C=O \rightarrow CH_2 + CO$", *J. Am. Chem. Soc.,* **100**, 7551 (1978).

G. R. PACK, G. H. LOEW, S. YAMABE and K. MOROKUMA, "Comparative Study of Semiempirical Methods for Calculating Interactions between Large Molecules Complex", *Inter. J. Quantum Chem.:* Quantum Biology Symp. **5**, 417–432 (1978).

H. ADACHI, M. TSUKADA and C. SATOKO, "Discrete Variational $X\alpha$ Cluster Calculations. I. Application to Metal Clusters", *J. Phys. Soc. Japan,* **45**, 875 (1978).

C. SATOKO, M. TSUKADA and H. ADACHI, "Discrete Variational $X\alpha$ Cluster Calculations. II. Application to the Surface Electronic Structure of MgO", *J. Phys. Soc. Japan,* **45**, 1333 (1978).

B. D. JOSHI and K. MOROKUMA, "A Theoretical Investigation of the Structure of $(Cl_2F)^+$ and Protonated ClF", *J. Am. Chem. Soc.,* **101**, 1714 (1979).

T. YAMABE, K. YAMASHITA, K. FUKUI and K. MOROKUMA, "Structure of Protonated hioformaldehyde", *Chem. Phys. Lett.,* **63**, 433 (1979).

S. KATO and K. MOROKUMA, "Energy Gradient in a Multi-Configurational SCF Formalism and its Application to Geometry Optimization of Trimethylene Diradicals", *Chem. Phys. Lett.,* **65**, 19 (1979).

A. IMAMURA, M. KODA and S. KATO, "A Molecular Orbital Study of the Chemical Reactivity and Biological Activity of Polycyclic Armatic Hydrocarbon Diolexpoxides in Connection with Bay Region Theory", *Gann.,* **70**, 291 (1979).

T. TANAKA, G. SWISLOW and I. OHMINE, "Phase Separation and Gelation in Gelation Gels", *Phys. Rev. Lett.* **42**, 1556 (1979).

K. KITAURA, C. SATOKO and K. MOROKUMA, "Total Energies of Molecules with the Local Density Functional Approximation and Gaussian Basis Sets", *Chem. Phys. Lett.,* **65**, 2 (1979).

E. HIROTA, S. SAITO, and Y. ENDO, "Second-Order Coriolis Resonance between ν_2 and ν_5 of $^{13}CH_3F$ by Microwave Spectroscopy", *J. Mol. Spectrosc.,* **70**, 469 (1978).

E. HIROTA, "Anharmonic Potential Function and Equilibrium Structure of Methylene Fluoride", *J. Mol. Spectrosc.,* **71**, 145 (1978).

C. YAMADA, K. KAWAGUCHI, and E. HIROTA, "Laser Magnetic Resonance Spectroscopy of SO in the $a^1\Delta$ State with a CO_2 Laser as a Source", *J. Chem. Phys.,* **69**, 1942 (1978).

S. SAITO, "Microwave Spectroscopy of Short-Lived Molecules", *Pure and Appl. Chem.,* **50**, 1239 (1978).

C. YAMADA and E. HIROTA, "Infrared Diode Laser Spectroscopy of Carbon Monosulfide", *J. Mol. Spectrosc.,* **74**, 203 (1979).

E. HIROTA, "Diode Laser Spectroscopy of the ν_6 Band of Methyl Fluoride", *J. Mol. Spectrosc.,* **74**, 209 (1979).

E. HIROTA, "Internal Rotation in Isopropyl Alcohol Studied by Microwave Spectroscopy", *J. Phys. Chem.,* **83**, 1457 (1979).

M. TAKAMI, "Infrared-Microwave Double Resonance of NH_3 Using a Tunable Diode Laser", *Appl. Phys. Lett.,* **34**, 684 (1979).

J. M. MORRIS and K. YOSHIHARA, "Interband transitions in molecular crystals. Triplet—triplet absorptions in ketone crystals," *Molec. Phys.,* **36**, 993 (1978).

A. NAMIKI, N. NAKASHIMA, and K. YOSHIHARA, "Fluorescence quenching due to the electron transfer. Indole—chloromethanes in rigid ethanol glass," *J. Chem. Phys.,* **71**, 925 (1979).

H. KATO and K. YOSHIHARA, "Laser-induced fluorescence, energy transfer, and dissociation of Cs_2," *J. Chem. Phys.,* **71**, 1585 (1979).

A. NAMIKI, M. SUMITANI, N. NAKASHIMA, and K. YOSHIHARA, "Time-resolved absorption spectroscopy with a picosecond laser," *Oyo Butsuri (Appl. Phys.)* (in Japanese), **48**, 784 (1979).

E. KAWAI, K. TANIMURA and T. SAKATA, "Conversion and storage of light energy. Evolution of hydrogen in neutral aqueous solution by a catalytic electrode process", *Chem. Lett.,* 137 (1979).

T. KAWAI, M. TSUKADA, H. ADACHI, C. SATOKO and T. SAKATA, "Electronic Structure of Adsorbed OH^- on the Deffect Site of TiO_2 Surface", *Surface Sci.,* **81**, L640 (1979).

T. SAKATA, T. KAWAI and K. TANIMURA, "The Photovoltaic Effect at the interface between Semiconductor and Electrolyte", *Ber. Bunsenges. Phys. Chem.,* **83**, 486 (1979).

S. HINO, T. HIROOKA, and H. INOKUCHI, "Photoemission from Anthracene and Compounds Containing Anthracene Ring Systems", *Bull. Chem. Soc. Jpn.,* **50**, 620 (1977).

S. HASHIMOTO, K. SEKI, N. SATO, and H. INOKUCHI, "Anisotropic Light Absorption of Oriented Polyethylene in Vacuum Ultraviolet Region", *Rep. Progr. Polym. Phys. Jpn.,* **21**, 375 (1978).

163

S. HASHIMOTO, K. SEKI, N. SATO, and H. INOKUCHI, "The Effect of Elongation on the Absorption Coefficients of Polyethylene in the Vacuum Ultraviolet Region", *Rep. Progr. Polym. Phys. Jpn.*, **21**, 379 (1978).

K. HONMA, I. KOYANO, and I. TANAKA, "The Effect of the Vibrational and Translational Energies of Ionic Reactant on the Reaction $C_3H_4^+ + NH_3 \rightarrow C_3H_3 + NH_4^+$", *Bull. Chem. Soc. Jpn.*, **51**, 1923 (1978).

Keisaku KIMURA, N. SATO, S. HINO, T. YAGI, and H. INOKUCHI, "Ionization Potentials of Ferricytochrome c_3", *J. Am. Chem. Soc.*, **100**, 6564 (1978).

K. TANAKA and I. KOYANO, "Threshold Electron-Secondary Ion Coincidence Technique for the Study of Internal Energy Dependence of Ion-Molecule Reactions", *J. Chem. Phys.*, **69**, 3422 (1978).

S. BANDO, Y. MATSUURA, N. TANAKA, N. YASUOKA, M. KAKUDO, T. YAGI, and H. INOKUCHI, "Crystallographic Data for Cytochrome c_3 from Two Strains of Desulfovivrio vulgaris, Miyazaki", *J. Biochem.*, **86**, 269 (1979).

S. HINO and H. INOKUCHI, "Electron Escape Depths of Organic Solids II. The Energy Dependence of Naphtacene and Perylene Films", *J. Chem. Phys.*, **70**, 1142 (1979).

I. IKEMOTO, Y. SATO, T. SUGANO, N. KOSUGI, H. KURODA, K. ISII, N. SATO, K. SEKI, H. INOCUCHI, T. TAKAHASHI, and Y. HARADA, "Photoelectron Spectroscopy of the Molecular and Solid of 11,11, 12,12-Tetracyanonapthoquinodimethane (TNAP)", *Chem. Phys. Lett.*, **61**, 50 (1979).

Keisaku KIMURA, Y. NAKAHARA, T. YAGI, and H. INOKUCHI, "Electrical Conduction of Hemoprotein in the Solid Phase: Anhydrous Cytochrome c_3 Film", *J. Chem. Phys.*, **70**, 3317 (1979).

Keisaku KIMURA, A. SUZUKI, H. INOKUCHI, and T. YAGI, "Hydrogenase Activity in the Dry State. Isotope Exchange and Reversible Oxidoreduction of Cytochrome c_3", *Biochim. Biophys. Acta*, **567**, 96 (1979).

S. KITAGAWA, I. MORISHIMA, T. YONEZAWA, and N. SATO, "Photoelectron Spectroscopic Study on Metallooctaethylporphyrins", *Inorg. Chem.*, **18**, 1345 (1979).

H. NAKAHARA, K. FUKUDA, and H. INOKUCHI, "Absorption Spectra and Photoemission of Chlorophyll-B Multilayers", *Chem. Lett.*, 453 (1979).

K. NIKI, T. YAGI, H. INOKUCHI, and Keisaku KIMURA, Electrochemical Behavior of Cytochrome c_3 of Desulfovibrio vulgaris, Strain Miyazaki, on Mercury Electrode", *J. Am. Chem. Soc.*, **101**, 3335 (1979).

M. SANO and H. INOKUCHI, "The Conductivity of Graphite-Alkali-Metal-Hydrogen Ternaly Systems". *Chem. Lett.*, 405, (1979).

K. SEKI and H. INOKUCHI, "Photoelectron Spectrum of *l*-Tryptophan in the Gas Phase", *Chem. Phys. Lett.*, **65**, 158 (1979).

T. TAKAHASHI, Y. HARADA, N. SATO, K. SEKI, H. INOKUCHI, and S. FUJISAWA, "Gas and Solid Phase Photoelectron Spectra of 5,6,11,12-Tetraphenylnaphthacene (Rubrene)", *Bull. Chem. Soc. Jpn.*, **52**, 380 (1979).

F. WILLIG, G. FRAHM, W. ENGEL, N. SATO, and K. SEKI, "On the Origin of Photo-Electron-Microscope-Pictures of Organic Samples", *Z. Phys. Chem.* (Frankfult), **112**, 59 (1979).

H. IWAMURA and K. MAKINO, "9,10-Dihydro-9,10[1',2']-benzenoanthracene-5,8-diol-1,4-dione. An Intramolecular Triptycene Quinhydrone", *J. C. S., Chem. Comm.*, 720 (1978).

H. IWAMURA and H. TUKADA, "The Wittig Rearrangement" of α-Alkoxycarbenes Formed by Photorearrangement of 1-Alkoxytriptycenes", *Tetrahedron Lett.*, 3451 (1978).

T. SUGAWARA, Y. KAWADA, and H. IWAMURA, "Oxygen-17 NMR Chemical Shifts of Alcohols, Ethers and Esters", *Chem. Lett.*, 1371 (1978).

M. YAMADA, S. NAKADA, T. ITO, and M. FUJIMOTO, "Complexometric Titrations based on Thermochromism", *Chem. Lett.*, 1153 (1978).

T. ITO and K. TORIUMI, "The Crystal Structure of 7R(S), 14S(R)-5,5,7,12,12,14-Hexamethyl-1,4,8,11-tetraazacyclotetradecanenickel(II) Chloride Dihydrate", *Chem. Lett.*, 1395 (1978).

Y. KAWADA, T. SUGAWARA, and H. IWAMURA, "Oxygen-17 N.M.R. Shifts of Some Tungsten Carbonyl Complexes. A Sensitive Measure of the σ-Donor/π-acceptor Ratio of Ligands", *J. C. S., Chem. Comm.*, 291 (1979).

Y. ENDO, T. ITO, N. YOSHIDA, and M. FUJIMOTO, "A Kinetic Study of the Reaction of the 5,5,7R(S), 12,12,14R(S)-Hexamethyl-1S(R),4S(R),8S(R),11S(R)-tetraazacyclotetradecanenickel(II) Ion and Dimethylsulfoxide Involving a Singlet-Triplet Spin-State Equilibrium", *Chem. Lett.*, 565 (1979).

H. IWAMURA, T. SUGAWARA, and Y. KAWADA, "^{17}O NMR Chemical Shifts Versus Structure Relationships in Oxiranes", *Tetrahedron Lett.*, 3449 (1979).

R. NOYORI, M. YAMAKAWA, and H. TAKAYA, "Evidence for a Trimethylenemethane Complex Intermediate in the Nickel (0) Catalyzed Reaction of Methylenecyclopropane", *Tetrahedron Lett.*, 4823 (1978).

M. WATANABE, and K. NISHIOKA, "Fundamental Absorption in RbF-GsF Solid Solutions", *J. Phys. Soc. Japan*, **45**, 1670 (1978).

M. WATANABE, and K. NISHIOKA, "Absorption Spectra of Li- and Na-Halides in the 5-40 eV Region", *Japan. J. appl. Phys.*, **17**, Suppl. 17-2 201 (1978).

Review Articles and Textbooks

E. HIROTA, "Revolution in Infrared Spectroscopy: Diode Laser", *Gendai Kagaku* (in Japanese), 1978. 11,38.

K. YOSHIHARA, N. NAKASHIMA, A. NAMIKI, M. SUMITANI, Y. TAKAGI, "Picosecond spectroscopy and its application to photochemistry," *Kokagaku* (Photochemistry) (in Japanese) 3, 62 (1979).

J. AIHARA and H. INOKUCHI, "The History of Electron and Electron Spectroscopy", *Kyoritsu Kagaku Library* (in Japanese), 16, Kyoritsu (1978), pp. 1–42.

Y. HARADA and K. SEKI, "UPS", *Kyoritsu Kagaku Library* (in Japanese), 16, Kyoritsu (1978), pp. 166–230.

H. INOKUCHI, Keisaku KIMURA, Y. NAKAHARA, and T. YAGI, "Electron Transfer in Cytochrome c_3", *Kagaku* (in Japanese), 33, 918 (1978).

T. YAGI and H. INOKUCHI, "Activity of Hydrogenase, and Its Application", in "Biological and Chemical Applications of Solar Energy", K. Shibata, A. Imamura, and A. Ikegami Ed., University of Tokyo Press (1978), pp. 45–59.

I. KOYANO, "Chemical Reactions — An Aspect as Atomic and Molecular Processes", *Physics Monthly* (in Japanese), 1, 268 (1979).